Modeling Secondary Organic Aerosol Formation From Emissions of Combustion Sources

Submitted in partial fulfillment of the requirements for

the degree of

Doctor of Philosophy

in

Engineering and Public Policy

Shantanu Hemant Jathar

B.E., Mechanical Engineering, University of Pune
M.S., Mechanical Engineering, University of Minnesota

Carnegie Mellon University
Pittsburgh, PA

August, 2012

Acknowledgements

Simply put, the last four years have been memorable. I have learned a lot from the research at the Center for Atmospheric Particle Studies, the curriculum at Engineering and Public Policy and the interdisciplinary environment at Carnegie Mellon University. I am honored to have been instructed and to have worked and interacted with some extraordinary people without whom the learning process would have been impossible.

I want to offer a heart-felt thank you to my advisors Peter Adams and Allen Robinson for both have been superb teachers, research advisors and mentors. They have helped me improve and in some cases build from scratch, my research, writing and presentation skills. They have been very supportive of all the research and personal choices I have made over time. I will always admire the teaching skills that Peter brought to the classroom and to our office meetings and always be inspired by Allen's burning desire to contribute to science and society.

I would like to thank Neil Donahue for his timely and critical contribution to my thesis work. He has been an inspiration when I have struggled with translating the real world into mathematical equations. I would also like to thank Jane Clougherty for her valuable feedback on my proposal and this thesis. I offer my thanks to Daniel Tkacik, Marissa Miracolo and Tim Gordon for introducing me to the experimental side of things. I would like to thank Albert Presto, Andy May, Ben Murphy, Chris Hennigan, Daniel Tkacik, Kaytlin Henry, Marissa Miracolo, Ngoc Nguyen and Tim Gordon for the instrument help, data and technical expertise offered while working together on various projects.

Over the past four years, I have probably spent as much time with my wife Poorva (who lived in Saint Paul, MN) as I have spent at the airport or in the air (exaggeration). My time in Pittsburgh and this thesis would not have been possible without her constant support and

commitment and her perseverance in handling the long-distance relationship. I would like to thank mom and dad who have been a constant source of inspiration to work harder and aim higher. I also feel indebted to my Aaji (grandmother) whose infectious happiness and care-free spirit serve as my guiding lights for life. I would have been ecstatic if she were with us today and I dedicate this thesis to her memory.

While a significant fraction of my time was spent on the thesis, I must admit that a lot of time was spent in the company of the Mafia. Mafia, unlike the definition that comes to mind, refers to a group of graduate students in Engineering and Public Policy that entered the program in 2008: Brandon/Sarah Mauch, Brinda Thomas, Catherine Izard/Mark Desnoyer, Kelly Klima, Kim Mullins, Kyle Siler-Evans, Emily Fertig, Eric/Rachel Hittinger, Pete Versteeg, Shira Horowitz/Carl Angiolillo, Steve Rose/Lucy Brudnak and Tim Gordon. I feel that I have learnt as many life-lessons from my academic program than I have from the Mafia. Frankly, they have made the time spent in Pittsburgh something that I will treasure forever. Thanks to them I am now a slightly improved runner, biker, squash and tennis player, movie critic, climber, hiker, s'more maker, pronouncer and video-game appreciator.

And finally, I want to thank Tim Gordon for being a great friend with whom I have shared endless discussions on everything from squirrels to jams.

My thesis work was funded by the EPA STAR program through the National Center for Environmental Research (NCER) under grants RD-83337401-0 and R833748 and the US Department of Defense Strategic Environmental Research and Development Program (SERDP) under project WP-1626. I would also like to acknowledge the additional financial support provided by the John and Claire Bertucci Fellowship in 2011.

Abstract

Atmospheric aerosols exert a large influence on the Earth's climate and cause adverse public health effects, reduced visibility and material degradation. Secondary organic aerosol (SOA), defined as the aerosol mass arising from the oxidation products of gas-phase organic species, accounts for a significant fraction of the submicron atmospheric aerosol mass. Yet, there are large uncertainties surrounding the sources, atmospheric evolution and properties of SOA. This thesis combines laboratory experiments, extensive data analysis and global modeling to investigate the contribution of semi-volatile and intermediate volatility organic compounds (SVOC and IVOC) from combustion sources to SOA formation. The goals are to quantify the contribution of these emissions to ambient PM and to evaluate and improve models to simulate its formation.

To create a database for model development and evaluation, a series of smog chamber experiments were conducted on evaporated fuel, which served as surrogates for real-world combustion emissions. Diesel formed the most SOA followed by conventional jet fuel / jet fuel derived from natural gas, gasoline and jet fuel derived from coal. The variability in SOA formation from actual combustion emissions can be partially explained by the composition of the fuel.

Several models were developed and tested along with existing models using SOA data from smog chamber experiments conducted using evaporated fuel (this work, gasoline, fischer-tropschs, jet fuel, diesels) and published data on dilute combustion emissions (aircraft, on- and off-road gasoline, on- and off-road diesel, wood burning, biomass burning). For all of the SOA data, existing models under-predicted SOA formation if SVOC/IVOC were not included.

For the evaporated fuel experiments, when SVOC/IVOC were included predictions using the existing SOA model were brought to within a factor of two of measurements with minor adjustments to model parameterizations. Further, a volatility-only model suggested that differences in the volatility of the precursors were able to explain most of the variability observed in the SOA formation.

For aircraft exhaust, the previous methods to simulate SOA formation from SVOC and IVOC performed poorly. A more physically-realistic modeling framework was developed, which was then used to show that SOA formation from aircraft exhaust was (a) higher for petroleum-based than synthetically derived jet fuel and (b) higher at lower engine loads and vice versa.

All of the SOA data from combustion emissions experiments were used to determine source-specific parameterizations to model SOA formation from SVOC, IVOC and other unspeciated emissions. The new parameterizations were used to investigate their influence on the OA budget in the United States. Combustion sources were estimated to emit about 2.61 Tg yr^{-1} of SVOC, IVOC and other unspeciated emissions (sixth of the total anthropogenic organic emissions), which are predicted to double SOA production from combustion sources in the United States.

The contribution of SVOC and IVOC emissions to global SOA formation was assessed using a global climate model. Simulations were performed using a modified version of GISS GCM II'. The modified model predicted that SVOC and IVOC contributed to half of the OA mass in the atmosphere. Their inclusion improved OA model-measurement comparisons for absolute concentrations, POA-SOA split and volatility (gas-particle partitioning) globally suggesting that atmospheric models need to incorporate SOA formation from SVOC and IVOC if they are to reasonably predict the abundance and properties of aerosols.

This thesis demonstrates that SVOC/IVOC and possibly other unspeciated organics emitted by combustion sources are very important precursors of SOA and potentially large contributors to the atmospheric aerosol mass. Models used for research and policy applications need to represent them to improve model-predictions of aerosols on climate and health outcomes. The improved modeling frameworks developed in this dissertation are suitable for implementation into chemical transport models.

Table of Contents

List of Tables

List of Figures

Glossary

AMS	Aerosol Mass Spectrometer
BC	Black Carbon
EC	Elemental Carbon
FT	Fischer-Tropsch
GC-MS	Gas Chromatography Mass Spectrometry
HEPA	High Efficiency Particulate Air
HOA	Hydrocarbon-like Organic Aerosol
HONO	Nitrous Acid
HR-AMS	High Resolution Aerosol Mass Spectrometer
IVOC	Intermediate Volatility Organic Compounds
NEI	National Emissions Inventory
OA	Organic Aerosol
OC	Organic Carbon
OH	Hydroxyl Radical
OOA	Oxygenated Organic Aerosol
PM	Particulate Matter
POA	Primary Organic Aerosol
PTR-MS	Proton Transfer Reaction Mass Spectrometry
Q-AMS	Quadrupole Aerosol Mass Spectrometer
ROC	Remaining Organic Compounds
SOA	Secondary Organic Aerosol
SMPS	Scanning Mobility Particle Sizer
SPECIATE	EPA Database for Emissions Profiles
SVOC	Semi-Volatile Organic Compounds
UCM	Unresolved Complex Mixture
UV	Ultra-Violet
VOC	Volatile Organic Compounds

Chapter 1: Introduction

1.1 Motivation

Atmospheric aerosols or particulate matter, defined as tiny particles suspended in air, play a key role in many ecological and environmental processes. Aerosols absorb and scatter solar radiation and affect the formation, lifetime and precipitation of clouds. The Intergovernmental Panel on Climate Change (IPCC) estimates that aerosols might be masking close to half of the global warming caused by greenhouse agents (IPCC, 2007). Aerosols smaller than 2.5 micron or $PM_{2.5}$ have a large impact on human health. There is ample evidence for their adverse health effects as seen with increases in mortality, and cardio-pulmonary, respiratory and allergic diseases (Bernstein et al., 2004). Every year, exposure to elevated fine PM is suspected to result in 60,000 deaths in the United States alone and about half a million deaths globally (Kaiser, 2005;Nel, 2005). Despite incriminating evidence, there are large gaps in our understanding of the sources, atmospheric evolution and properties of aerosols that are needed to ascertain and eventually mitigate their influence.

Atmospheric aerosols are composed of the following major constituents: organics, elemental carbon, sulfate, nitrate, ammonium, sea salt, dust and metals, all of which have both natural and anthropogenic sources. Of those mentioned, organic aerosol (OA) accounts for about a third of the atmospheric aerosol mass (Zhang et al., 2007;Jimenez et al., 2009). Yet, it remains the least understood because organics (gas+particle) comprises of a mixture of tens of thousands of organic compounds (Goldstein and Galbally, 2007), each with a different set of physical and chemical properties that continuously evolve with changes in gas-particle partitioning and atmospheric oxidation. The complexity has meant that we have limited knowledge about their sources, atmospheric evolution and properties.

Aerosol models are regularly used in both research and regulatory applications to study their climate and human health outcomes with the intention to develop technologies and policies that eventually mitigate those adverse outcomes. Typically, these aerosol models under-predict OA mass concentrations on urban, regional and global scales. The under-prediction can sometimes reach an order of magnitude, especially on global scales and downstream of urban areas during photo-chemically active periods. (Heald et al., 2005;Vutukuru et al., 2006;Johnson et al., 2006;Morris et al., 2006;Dzepina et al., 2009;Dzepina et al., 2010). These models also tend to predict a dominance of directly emitted OA or primary organic aerosol (POA) (Farina et al., 2010) when ambient measurements suggest that OA is dominated by aerosol formed through the oxidation of gas-phase emissions or secondary organic aerosol (SOA) (Zhang et al., 2007;Jimenez et al., 2009). The poor model performance has made it very hard to evaluate the effects of OA on climate and human health.

It is important that models predict the right sources, composition and properties of ambient OA. For example, ambient OA is highly oxygenated and therefore has a higher propensity to uptake water and affect cloud formation, both of which have a strong influence on aerosol's radiative forcing on climate. Hence, an effort to accurately simulate global OA formation should help reduce the large uncertainty in the aerosol radiative forcing reported by the IPCC (IPCC, 2007). To protect human health and the environment, the Clean Air Act has required the Environmental Protection Agency to set National Ambient Air Quality Standards for $PM_{2.5}$ and other pollutants. Recently, the EPA reported that according to the standards revised in 2006, 17 million people in the United States lived in counties that were not in compliance for $PM_{2.5}$ (EPA, 2012). OA might need to be controlled to bring $PM_{2.5}$ mass levels into attainment, especially in counties like Los Angeles that are not in compliance (EPA, 2012) and where $PM_{2.5}$

is dominated by OA (Sardar et al., 2005). Additionally, there is considerable uncertainty in understanding the mechanism or fraction of $PM_{2.5}$ that affects human health. Hence, a regulation simply based on $PM_{2.5}$ mass (as in the United States) may be inefficient and possibly ineffective. A preliminary step in designing effective regulation would be to understand the cause and effect relationship better through models that predict the correct source contribution, composition and properties of $PM_{2.5}$.

As defined earlier, SOA is the OA mass arising from the oxidation of gas-phase organic species. Until recently, SOA formation was believed to be dominated by the first-generation oxidation products of high-flux volatile organic compounds (VOC) such as terpenes and single-ring aromatics. SOA formed from speciated VOCs is defined as traditional SOA (T-SOA) and is explicitly accounted for in most SOA models. However, a potential shortcoming is that these traditional SOA models might be missing a group of SOA precursors, particularly from combustion sources. Recent laboratory experiments show that combustion emissions when photo-oxidized form substantial SOA mass, greatly in excess of what can be explained by traditional SOA models (Robinson et al., 2007;Grieshop et al., 2009;Miracolo et al., 2011;Miracolo et al., submitted). Similarly, field studies show that SOA formation measured downwind of urban areas or large combustion sources is under-predicted by traditional SOA models (Hodzic et al., 2010;Dzepina et al., 2009;Volkamer et al., 2006). Robinson et al. (2007) proposed that a significant part of the unexplained SOA stemmed from the oxidation of low-volatility organic vapors; they have been defined by Donahue et al. (2009) as semi-volatile and intermediate volatility organic compounds (SVOC and IVOC). Fundamentally, SVOC/IVOC form SOA in the same manner as VOCs; oxidation adds functional groups to the organic molecule, which reduces the volatility (vapor pressure) of the product and leads to condensation

into the particle phase. However, the lower initial volatility of SVOC/IVOC means that they can have higher SOA yields than VOCs (Lim and Ziemann, 2009;Presto et al., 2010). Donahue et al. (2009) defined SOA from SVOC/IVOC as non-traditional SOA (NT-SOA).

A key attribute of SVOC/IVOC is that they are hard to measure and even harder to speciate with traditional gas chromatography (GC) techniques (Schauer et al., 1999, 2002). The problem is fundamentally caused by the number of isomers growing exponentially with carbon number; these isomers co-elute from the GC-column (Goldstein and Galbally, 2007). Since the molecular identity of the vast majority of SVOC/IVOC cannot be ascertained, SOA formation from these compounds cannot be investigated or modeled in the same manner as T-SOA formed from speciated VOCs (benzene, alpha-pinene, and others). Instead, models that represent SOA formation from SVOC/IVOC have been based on the volatility of the emissions and their transformation in volatility space (Robinson et al., 2007;Dzepina et al., 2009;Murphy and Pandis, 2009;Pye and Seinfeld, 2010).

SVOC/IVOC could be important SOA precursors and therefore influential in determining the abundance and properties of atmospheric aerosols that impact climate and public health. However, there are large uncertainties surrounding the sources and transformation of SVOC/IVOC in the atmosphere. .

1.2 Objectives

The objectives of this thesis are to develop methods to represent NT-SOA formation from SVOC/IVOC in models using laboratory experiments and quantify their influence on the formation and properties of SOA in the atmosphere on local, regional and global scales.

The first objective of this thesis is to develop methods to represent NT-SOA formation from SVOC/IVOC in OA models. This work is primarily motivated by the absence of well-constrained mechanisms and parameters to model NT-SOA formation. The existing mechanisms are either conservatively developed from first principles or built on a handful of experimental data from a single combustion source. The mechanisms use the same parameters for different combustion sources assuming that different sources have similar potentials to form NT-SOA. This work aims to use laboratory experiments conducted in this work and elsewhere to develop realistic methods to model NT-SOA formation from the oxidation of SVOC/IVOC emissions arising from different combustion sources. At the same time, this work also tries to test, integrate and improve the entire SOA model.

The second objective of this thesis is to conduct laboratory experiments specifically designed to provide additional data to accomplish the first objective. SOA data for combustion sources are needed for use in the first objective. However, only a few datasets are available since SOA experiments on combustion emissions are complicated and expensive to run. This work addresses that need by conducting laboratory experiments on reasonable surrogates for real combustion emissions that are simpler, easy to characterize and cheaper to run.

The third objective of this thesis is estimate the influence SVOC/IVOC exert on the abundance and properties of ambient OA on a regional and global scale. Contemporary models do not perform well in predicting the concentrations and properties of OA on a global scale. Although regional models perform slightly better, they could be deficient in predicting the source apportionment of OA. This work intends to use the mechanisms and parameters developed as part of the earlier objectives to model NT-SOA formation from SVOC/IVOC using a simplified model for the United States and a global climate model for the world.

1.3 Outline

Each chapter in this thesis maps to one of the objectives mentioned above. Below, we provide a brief overview for each chapter.

In chapter 2, we employ the volatility-based method proposed by Robinson et al. (2007) to model NT-SOA formation from SVOC/IVOC. The NT-SOA model is built inside an existing OA model coupled to a climate model. Predictions from the climate model are used to determine the influence of SVOC/IVOC on the global OA budget. Predictions are also used to evaluate the model by comparing model-predictions of OA mass and properties to measurements made across the globe.

In chapter 3, we use SOA data collected from two field campaigns to test existing methods and build new methods to represent NT-SOA formation from SVOC/IVOC. The SOA data consist of several smog chamber experiments conducted on emissions from two different aircraft engines run at different engine loads with two types of fuel.

In chapter 4, we conduct smog chamber experiments on evaporated fuels to quantify the formation and properties of SOA arising from them. The data are compared against SOA formation from emissions of engines that use those fuels and the comparison is used to examine how fuel composition can influence SOA formation from engine exhaust.

In chapter 5, the SOA data collected in chapter 4 are used to test different SOA models. The objective is to assess how well a model is able to capture SOA formation as a function of the precursor's volatility and/or molecular structure.

In chapter 6, we use data from several campaigns where SOA formation was measured from emissions of different combustion sources. The data are used to develop a source-resolved

parameterization to model NT-SOA. Next, the parameterizations are used in a model to identify the influence of NT-SOA and also the contribution of different sources to the OA budget in the United States.

In chapter 7, we summarize the key findings from this thesis, make recommendations to policy-makers interested in aerosol research and address future work.

1.4 References

Bernstein, J. A., Alexis, N., Barnes, C., Bernstein, I. L., Bernstein, J. A., Nel, A., Peden, D., Diaz-Sanchez, D., Tarlo, S. M., and Williams, P. B.: Health effects of air pollution, The Journal of Allergy and Clinical Immunology, 114, 1116-1123, 2004.

Dzepina, K., Volkamer, R., Madronich, S., Tulet, P., Ulbrich, I., Zhang, Q., Cappa, C., Ziemann, P., and Jimenez, J.: Evaluation of recently-proposed secondary organic aerosol models for a case study in mexico city, Atmospheric Chemistry and Physics, 9, 5681-5709, doi:10.5194/acp-9-5681-2009, 2009.

Dzepina, K., Cappa, C. D., Volkamer, R. M., Madronich, S., DeCarlo, P. F., Zaveri, R. A., and Jimenez, J. L.: Modeling the multiday evolution and aging of secondary organic aerosol during milagro 2006, Environmental Science & Technology, 45, 3496-3503, doi: 10.1021/es103186f, 2010.

EPA: Our nation's air: Status and trends through 2010, Environmental Protection Agency, 2012.

Farina, S. C., Adams, P. J., and Pandis, S. N.: Modeling global secondary organic aerosol formation and processing with the volatility basis set: Implications for anthropogenic secondary organic aerosol, Journal of Geophysical Research, 115, D09202, doi:10.1029/2009JD013046, 2010.

Goldstein, A. H., and Galbally, I. E.: Known and unexplored organic constituents in the earth's atmosphere, Environmental Science & Technology, 41, 1514-1521, doi:10.1021/es072476p, 2007.

Grieshop, A., Donahue, N., and Robinson, A.: Laboratory investigation of photochemical oxidation of organic aerosol from wood fires 2: Analysis of aerosol mass spectrometer data, Atmospheric Chemistry and Physics, 9, 2227-2240, 2009.

Heald, C. L., Jacob, D. J., Park, R. J., Russell, L. M., Huebert, B. J., Seinfeld, J. H., Liao, H., and Weber, R. J.: A large organic aerosol source in the free troposphere missing from current models, Geophys. Res. Lett., 32, doi:10.1029/2005GL023831, 2005.

Hodzic, A., Jimenez, J., Madronich, S., Canagaratna, M., DeCarlo, P., Kleinman, L., and Fast, J.: Modeling organic aerosols in a megacity: Potential contribution of semi-volatile and intermediate volatility primary organic compounds to secondary organic aerosol formation, Atmospheric Chemistry and Physics, 10, 5491-5514, doi:10.5194/acp-10-5491-2010, 2010.

IPCC, W.: Climate change 2007: The physical science basis, Summary for Policy Makers, Contribution of Working Group I to the Fourth Assessment Report of the Intergovernmental Panel on Climate Change, 2007.

Jimenez, J., Canagaratna, M., Donahue, N., Prevot, A., Zhang, Q., Kroll, J., DeCarlo, P., Allan, J., Coe, H., Ng, N., and others: Evolution of organic aerosols in the atmosphere, Science, 326, 1525, 2009.

Johnson, D., Utembe, S. R., Jenkin, M. E., Derwent, R. G., Hayman, G. D., Alfarra, M. R., Coe, H., and McFiggans, G.: Simulating regional scale secondary organic aerosol formation during the torch 2003 campaign in the southern uk, Atmos. Chem. Phys., 6, 403-418, 2006.

Kaiser, J.: Mounting evidence indicts fine-particle pollution, Science, 307, 1858-1861, 2005.

Lim, Y. B., and Ziemann, P. J.: Chemistry of secondary organic aerosol formation from oh radical-initiated reactions of linear, branched, and cyclic alkanes in the presence of no x, Aerosol Science and Technology, 43, 604-619, 2009.

Miracolo, M., Hennigan, C., Ranjan, M., Nguyen, N., Gordon, T., Lipsky, E., Presto, A., Donahue, N., and Robinson, A.: Secondary aerosol formation from photochemical aging of aircraft exhaust in a smog chamber, Atmos. Chem. Phys, 11, 4135-4147, doi:10.5194/acp-11-4135-2011, 2011.

Miracolo, M. A., Drozd, G. T., Jathar, S. H., Presto, A. A., Lipsky, E. M., Corporan, E., and Robinson, A. L.: Fuel composition and secondary organic aerosol formation: Gas-turbine exhaust and alternative aviation fuels, Environmental Science & Technology, submitted.

Morris, R. E., Koo, B., Guenther, A., Yarwood, G., McNally, D., Tesche, T. W., Tonnesen, G., Boylan, J., and Brewer, P.: Model sensitivity evaluation for organic carbon using two multi-pollutant air quality models that simulate regional haze in the southeastern united states, Atmos. Environ., 40, 4960-4972, 2006.

Murphy, B., and Pandis, S.: Simulating the formation of semivolatile primary and secondary organic aerosol in a regional chemical transport model., Environmental science & technology, 43, 4722-4728, doi:10.1021/es803168a, 2009.

Nel, A.: Air pollution-related illness: Effects of particles, Science, 308, 804-806, 2005.

Presto, A. A., Miracolo, M. A., Donahue, N. M., and Robinson, A. L.: Secondary organic aerosol formation from high-no x photo-oxidation of low volatility precursors: N-alkanes, Environmental Science & Technology, 44, 2029-2034, 2010.

Pye, H., and Seinfeld, J.: A global perspective on aerosol from low-volatility organic compounds, Atmos. Chem. Phys, 10, 4377-4401, doi:10.5194/acp-10-4377-2010, 2010.

Robinson, A. L., Donahue, N. M., Shrivastava, M. K., Weitkamp, E. A., Sage, A. M., Grieshop, A. P., Lane, T. E., Pierce, J. R., and Pandis, S. N.: Rethinking organic aerosols: Semivolatile emissions and photochemical aging, Science, 315, 1259-1262, 2007.

Sardar, S. B., Fine, P. M., and Sioutas, C.: Seasonal and spatial variability of the size-resolved chemical composition of particulate matter (pm10) in the los angeles basin, Journal of Geophysical Research, 110, D07S08, 2005.

Schauer, J. J., Kleeman, M. J., Cass, G. R., and Simoneit, B. R. T.: Measurement of emissions from air pollution sources. 2. C1 through c30 organic compounds from medium duty diesel trucks, Environ. Sci. Technol, 33, 1578-1587, 1999.

Schauer, J. J., Kleeman, M. J., Cass, G. R., and Simoneit, B. R. T.: Measurement of emissions from air pollution sources. 5. C1- c32 organic compounds from gasoline-powered motor vehicles, Environ. Sci. Technol, 36, 1169-1180, 2002.

Volkamer, R., Jimenez, J. L., San Martini, F., Dzepina, K., Zhang, Q., Salcedo, D., Molina, L. T., Worsnop, D. R., and Molina, M. J.: Secondary organic aerosol formation from anthropogenic air pollution: Rapid and higher than expected, Geophys. Res. Lett, 33, 17, 2006.

Vutukuru, S., Griffin, R. J., and Dabdub, D.: Simulation and analysis of secondary organic aerosol dynamics in the south coast air basin of california, J. Geophys. Res., 111, doi:10.1029/2005JD006139, 2006.

Zhang, Q., Jimenez, J. L., Canagaratna, M. R., Allan, J. D., Coe, H., Ulbrich, I., Alfarra, M. R., Takami, A., Middlebrook, A. M., Sun, Y. L., Dzepina, K., Dunlea, E., Docherty, K., DeCarlo, P. F., Salcedo, D., Onasch, T., Jayne, J. T., Miyoshi, T., Shimono, A., Hatakeyama, S., Takegawa, N., Kondo, Y., Schneider, J., Drewnick, F., Borrmann, S., Weimer, S., Demerjian, K., Williams, P., Bower, K., Bahreini, R., Cottrell, L., Griffin, R. J., Rautiainen, J., Sun, J. Y., Zhang, Y. M., and Worsnop, D. R.: Ubiquity and dominance of oxygenated species in organic aerosols in anthropogenically-influenced northern hemisphere midlatitudes, Geophys. Res. Lett, 34, L13801, doi:10.1029/2007GL029979, 2007.

Chapter 2: The influence of semi-volatile and reactive primary emissions on the abundance and properties of global organic aerosol*

Abstract

Semi-volatile and reactive primary organic aerosols are modeled on a global scale using the GISS GCM II' "unified" climate model. We employ the volatility basis set framework to simulate emissions, chemical reactions and phase partitioning of primary and secondary organic aerosol (POA and SOA). The model also incorporates the emissions and reactions of intermediate volatility organic compounds (IVOCs) as a source of organic aerosol (OA), one that has been missing in most prior work. Model predictions are evaluated against a broad set of observational constraints including mass concentrations, degree of oxygenation, volatility and isotopic composition. A traditional model that treats POA as non-volatile and non-reactive is also compared to the same set of observations to highlight the progress made in this effort. The revised model predicts a global dominance of SOA and brings the POA/SOA split into better agreement with ambient measurements. This change is due to traditionally defined POA evaporating and the evaporated vapors oxidizing to form non-traditional SOA. IVOCs (traditionally not included in chemical transport models) oxidize to form condensable products that account for a third of total OA, suggesting that global models have been missing a large source of OA. Predictions of the revised model for the SOA fraction at 17 different locations compared much better to observations than predictions from the traditional model. Model-predicted volatility is compared with thermodenuder data collected at three different field

* Originally published as: Jathar, S. H., Farina, S. C., Robinson, A. L., and Adams, P. J.: The influence of semi-volatile and reactive primary emissions on the abundance and properties of global organic aerosol, Atmos. Chem. Phys., 11, 7727-7746, doi:10.5194/acp-11-7727-2011, 2011.

campaigns: FAME-2008, MILAGRO-2006 and SOAR-2005. The revised model predicts the OA volatility much more closely than the traditional model. When compared against monthly averaged OA mass concentrations measured by the IMPROVE network, predictions of both the revised and traditional model lie within a factor of two in summer and mostly within a factor of five during winter. A sensitivity analysis indicates that the winter comparison can be improved either by increasing POA emissions or lowering the volatility of those emissions. Model predictions of the isotopic composition of OA are compared against those computed via a radiocarbon isotope analysis of field samples. The contemporary fraction, on average, is slightly under-predicted (20%) during the summer months but is a factor of two lower during the winter months. We hypothesize that the large wintertime under-prediction of surface OA mass concentrations and the contemporary fraction is due to an under-representation of biofuel (particularly, residential wood burning) emissions in the emission inventory. Overall, the model evaluation highlights the importance of treating POA as semi-volatile and reactive in order to predict accurately the sources, composition and properties of ambient OA.

2.1 Introduction

Atmospheric aerosols play a key role in many ecological and environmental processes. They influence the earth's climate (IPCC, 2007) and have a large impact on public health (Bernstein et al., 2004). Organics account for a significant fraction of the fine atmospheric aerosol mass (Zhang et al., 2007) and hence have been extensively studied using climate models to determine their global impact (Penner et al., 1998;Cooke et al., 1999;Koch, 2001;Chung and Seinfeld, 2002;Park et al., 2003;Park et al., 2006). However, when evaluated against observations, these models usually under-predict surface organic aerosol (OA) mass

concentrations (Liousse et al., 1996;Chung and Seinfeld, 2002;Park et al., 2003;Tsigaridis and Kanakidou, 2003;De Gouw et al., 2005;Heald et al., 2005;Volkamer et al., 2006). For example, Chung and Seinfeld (2002), on average, under-predicted organic carbon (OC) mass concentrations by a factor of 3 to 4. Tsigaridis and Kanakidou (2003) observed a similar under-prediction over rural and marine areas where measured OC mass concentrations were lower than 1 $\mu g\ m^{-3}$. Volkamer et al. (2006) noted that the discrepancy between model predicted secondary OA and observations increased with the photochemical age. Park et al. (2006), however, predicted OA concentrations within a factor of 2 with very little bias. This poor performance makes it difficult to evaluate the effects of OA on global climate and human health.

Previous quantitative evaluations of model performance have mainly focussed on absolute OA mass concentrations and not considered other properties such as chemical composition, volatility and isotopic composition. This has been due to the lack of field measurements and/or the limited prediction capabilities of models. Recently, instruments like the Aerosol Mass Spectrometer (AMS), Particle-Into-Liquid Sampler (PILS) and thermodenuders and techniques like radiocarbon isotope analysis have provided new insight into the sources, composition and reactivity of OA typically unavailable from mass measurements (Weber et al., 2001;Zhang et al., 2005;An et al., 2007;Schichtel et al., 2008). For example, global models tend to predict a dominance of primary organic aerosol (POA) or direct particulate emissions, which have been assumed to be non-volatile and non-reactive (Kanakidou et al., 2005;Jimenez et al., 2009). However, AMS results suggest that atmospheric OA is dominated by secondary organic aerosol or SOA which is aerosol mass formed from the oxidation products of gas-phase organic precursors (Robinson et al., 2007;Zhang et al., 2007). This is one example which points to potentially significant problems with how OA is simulated in global models.

The shortcomings in current OA models may partly be due to their assumption that POA is non-volatile and non-reactive. Recently, various studies have challenged these views (Grieshop et al., 2009a;Grieshop et al., 2009b;Robinson et al., 2007;Huffman et al., 2009). First, they showed that diesel engine, biomass burning and meat cooking POA emissions are semi-volatile, i.e. they contained species that span a large range of vapor pressures that exist in a gas-particle equilibrium as dictated by absorptive partitioning theory (Pankow, 1994). Second, Robinson et al. (2007) argued that certain intermediate volatility organic compounds (IVOCs), capable of forming OA, were missing from emission inventories compiled using conventional techniques. Using source test data, Shrivastava et al. (2008) estimated the missing IVOCs to account for 0.25 to 2.8 times the POA mass measured using conventional filter techniques. Third, smog chamber experiments demonstrated that photooxidation of diesel exhaust and woodsmoke enhanced OA concentrations beyond that predicted by the oxidation of conventional VOC precursors (Grieshop et al., 2009b;Robinson et al., 2007;Miracolo et al., 2010;Sage et al., 2008). It is suspected that semi-volatile and IVOC vapors oxidize to generate additional SOA; this SOA has been recently termed non-traditional SOA (Donahue et al., 2009).

On a regional scale, recent efforts in modeling carbonaceous aerosols have considered the semi-volatile and reactive nature of POA (Robinson et al., 2007;Shrivastava et al., 2008;Murphy and Pandis, 2009). The only study, so far, to have attempted that in a global model is that by Pye and Seinfeld (20110). All of these new models predict a global dominance of SOA and bring the POA/SOA split in better agreement with field measurements. Although they arrive at similar qualitative conclusions, the schemes used to model semi-volatile and reactive POA are not well constrained due to the lack of available experimental data and are therefore very uncertain. In

light of this uncertainty, an important next step is to assess these schemes by evaluating model performance in direct comparison with observations.

In this paper, we model semi-volatile and reactive POA and IVOC emissions using the volatility basis set (VBS) in conjunction with a global climate model. The VBS is an efficient framework for simulating the gas-particle partitioning, dilution and chemical aging of semi-volatile organics. Model performance is evaluated using observations of surface concentration, oxygenation, volatility and isotopic composition.

2.2 Model description

In this work, we use a 'unified' general circulation model (GCM) to simulate global OA. The model is based on the Goddard Institute for Space Studies General Circulation Model II' (GISS GCM II') (Hansen et al., 1983;Rind and Lerner, 1996;Rind et al., 1999) and includes online tropospheric chemistry (Harvard tropospheric O_3-NO_x-hydrocarbon chemical model (Liao et al., 2003)) and aerosol modules (Adams et al., 1999;Chung and Seinfeld, 2002;Liao et al., 2004;Farina et al., 2010). The GCM has a horizontal resolution of 4° latitude by 5° longitude with 9 vertical layers. The simulated period represents a non-specific year near the end of the 20th century. In addition to organics and elemental carbon (soot), the GCM explicitly treats sulfate, nitrate, ammonium, sea salt and mineral dust as described in Liao et al. (2005).

The OA model is based on the work of Farina et al. (2010). Farina et al. (2010) implemented the VBS to simulate the formation and gas-particle partitioning of SOA produced from the oxidation of VOC precursors (isoprene, monoterpenes, sesquiterpenes, alkanes, alkenes and aromatics). In addition, they also used the VBS to model the gas-phase aging of anthropogenic SOA. They assumed that POA was non-volatile and non-reactive and also did not

account for IVOCs. In this paper we modified the model of Farina et al. (2010) to account explicitly for semi-volatile and reactive POA and IVOCs. We use the VBS to describe their emissions, mixing, gas-particle partitioning and aging. The ensuing sections describe in detail the revised OA model.

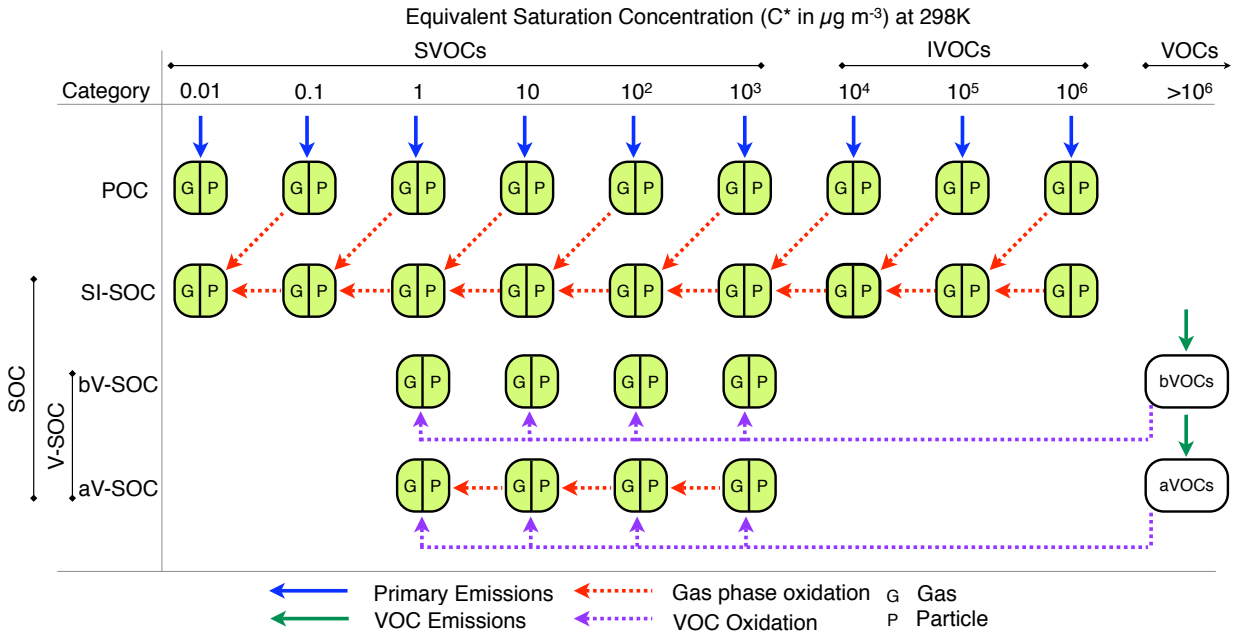

Figure 2.1: Schematic for the volatility basis set (VBS) framework as used in this study. The saturation concentration spectrum is divided into semi-volatile (SVOC, C* = 0.01-10^3 μg m^{-3}) and intermediate volatility (IVOC, C* = 10^4-10^6 μg m^{-3}) organic compounds. VOCs are graphically presented with C*>10^6. bVOCs and aVOCs are biogenic and anthropogenic VOCs respectively. See Sections 2.2.1.1 and 2.2.1.2 for a detailed discussion.

2.2.1 Organic aerosol (OA) modeling

2.2.1.1 Volatility basis set and equilibrium partitioning

The VBS framework describes OA by separating low volatility organics into decadally spaced bins of effective saturation concentration (C*) between 0.01 to 10^6 μg m^{-3} (Figure 2.1) (Donahue et al., 2006). C* (inverse of the Pankow-type partitioning coefficient, K_p) is proportional to the saturation vapor pressure and is a semi-empirical property that describes the gas-particle partitioning of an organic mixture (Pankow, 1994). Each C* 'bin' contains species

that span a range of volatilities, i.e. the 1 μg m-^{3} bin contains species with C* between 0.3 μg m^{-3} and 3 μg m^{-3}. The lowest volatility bin, 0.01 μg m^{-3}, contains all species lower in volatility than 0.03 μg m^{-3}. The C* spectrum is conventionally divided into semi-volatile (SVOC, 0.01-10^{3} μg m^{-3}) and intermediate volatility (IVOC, 10^{4}-10^{6} μg m^{-3}) organic compounds.

Unlike previous models, the revised model explicitly treats the gas-particle partitioning of all low volatility organics. The model assumes ambient OA to exist in an equilibrium between the gas and particle phases as dictated by Raoult's law and that the organics in the particle phase form a pseudo-ideal solution (Pankow, 1994). The partitioning equations are as follows (Donahue et al., 2006):

$$\zeta_i = \left(1 + \frac{C_i^*}{C_{OA}}\right)^{-1} \quad ; \quad C_{OA} = \sum_{i=1}^{N} \zeta_i \times OC_i \tag{2.1}$$

where ζ_i is the fraction of organic mass in volatility bin '*i*' in the particulate phase, C_i^* is the effective saturation concentration of bin '*i*' in μg m^{-3}, C_{OA} is the total particulate OA (POA+SOA) concentration in μg m^{-3}, OC_i is the total organic concentration (gas+particle) in bin '*i*' in μg m^{-3} and *N* is the number of basis set bins. An important uncertainty is whether all components of OA absorb into the same phase as this would affect the value of C_{OA}. Recent experimental evidence on this issue are mixed where some studies indicate a single phase (Asa-Awuku et al., 2009) while others indicate multiple phases (Song et al., 2007). In the absence of conclusive evidence that suggests phase separation for ambient OA, we assume all OA (POA and SOA) to form a single phase. In addition, Shrivastava et al. (2008) found that multiple phases had a very small effect on predicted OA mass concentrations in simulations that treated POA as semi-volatile and reactive.

Shifts in gas-particle partitioning due to changes in temperature are represented using the Clausius-Clapeyron equation (Donahue et al., 2006),

$$C_i^*(T) = C_i^*(T_{ref}) \exp\left[\frac{\Delta H_v}{R}\left(\frac{1}{T_{ref}} - \frac{1}{T}\right)\right]\frac{T_{ref}}{T} \quad (2.2)$$

where T_{ref} is the reference temperature (298 K), ΔH_v is the enthalpy of vaporization and R is the universal gas constant. ΔH_{vap} is an uncertain parameter and therefore simulations are performed to assess the sensitivity of the results to a varying ΔH_{vap}.

2.2.1.2 OA terminology

OA has been traditionally divided into two categories: POA and SOA. POA is organic material directly emitted in the particle phase; it has traditionally been assumed to be non-volatile and non-reactive. SOA is OA formed in the atmosphere from reactions of gaseous precursors; traditional chemical transport models have only accounted for SOA production from very volatile precursors. However, recent research has blurred the distinction between POA and SOA. Hence, it is necessary to revise certain conventionally used terms that are now either obsolete and/or confusing.

Figure 2.2 represents the various classes of OA with the help of a tree diagram. Using the VBS framework, we define primary organic carbon (POC) as the sum of all the emissions that have a C* lower than 10^6 μg m^{-3}. This includes all traditionally defined POA emissions and any IVOC emissions added to the model. We assume that organic emissions with C* higher than 10^6 μg m^{-3} are explicitly accounted as VOC species. As POC is semi-volatile, it dynamically partitions between the gas and particle phases with changes in dilution and temperature. We define POA as the particle phase component of POC and primary organic gas (POG) as the vapor

phase component of POC. We further categorize POC into SVOCs and IVOCs, where SVOCs refer to the gas+particle organic mass in the 0.01 to 1000 μg m^{-3} bins and IVOCs refer to the organic mass in the 10^4 to 10^6 μg m^{-3} bins. The exact boundary between the SVOCs and IVOCs is somewhat artificial; SVOCs exist in both the gas and particle phase while IVOCs exist exclusively as vapors in the atmosphere but are less volatile than VOCs. This distinction is made to examine the influence of IVOCs on the OA budget, an influence that has been explored by only a handful of studies (Shrivastava et al., 2008;Murphy and Pandis, 2009;Farina et al., 2010;Pye and Seinfeld, 2010).

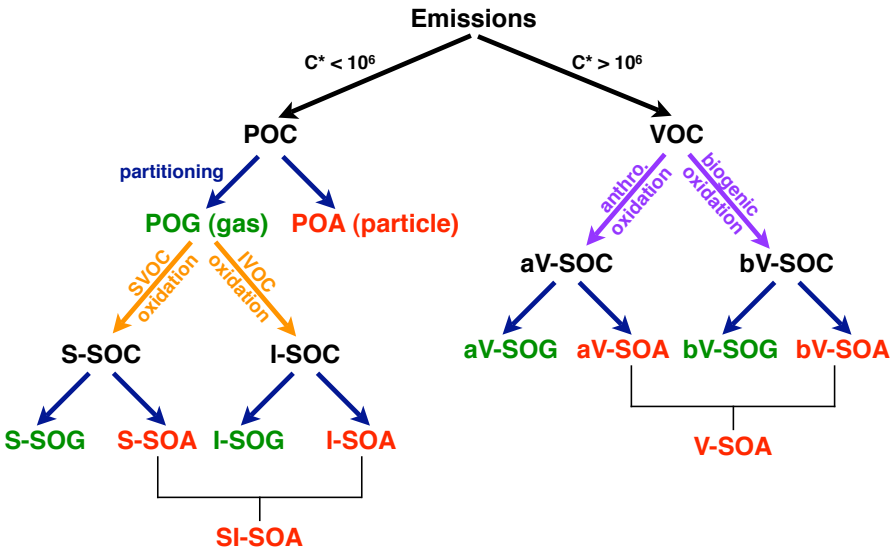

Figure 2.2: Tree diagram of various classes of OA in the revised model.

A key objective of this work is to study the fate of SVOC and IVOC vapors which are believed to oxidize in the atmosphere to form lower volatility products, which condense into the particle phase. In this work, we use terminology used in Tsimpidi et al. (2009) and define S-SOG and S-SOA as the gas and particle phase components arising from the oxidation of SVOC vapors. Similarly, we define I-SOG and I-SOA as the gas and particle phase components arising

from the oxidation of IVOC vapors. SI-SOG is the sum of S-SOG and I-SOG and SI-SOA is the sum of S-SOA and I-SOA. The sum of SI-SOG and SI-SOA is called SI-SOC.

Gas and particle phase products from the oxidation of VOCs are referred as V-SOG and V-SOA respectively, with their sum defined as V-SOC. The traditional abbreviations are prefixed with 'a' to identify the anthropogenic contribution and 'b' for the biogenic contribution. OA, hence, is a sum of POA, SI-SOA and V-SOA while SOA is the sum of SI-SOA and V-SOA.

This VBS framework can efficiently track material from any number of different sources and precursors. However, given the computational resources available and the goals of the paper, the model separately tracks four classes of organics as shown in Figure 2.1: POC, SI-SOC (S-SOC and I-SOC together), aV-SOC and bV-SOC. POC and SI-SOC are tracked using two separate 9 bin VBS while bV-SOC and aV-SOC are tracked using two separate 4 bin VBS (Figure 2.1). The VOC precursors for V-SOC shown in Figure 2.1 are described in detail in Farina et al. (2010).

Table 2.1: Definitions and abbreviations used for classes of OA.

	Publication				
Categories	This work/ Tsimpidi et al. (2009)	Shrivastava (2008)	Murphy and Pandis (2009)	Dzepina et al. (2009)	Dzepina et al. (2010)
Unoxidized POA or fresh POA	POA	POA	FPOA	POA	POA
SOA from SVOCs and IVOCs or non-traditional SOA	S-SOA+ I-SOA= SI-SOA	OPOA	OPOA	NT-SOA	SOA_{SVOC} + SOA_{IVOC}
Biogenic and anthropogenic SOA from VOCs or traditional SOA	bV-SOA, aV-SOA	Biogenic SOA, Anthro. SOA	BSOA, ASOA	T-SOA	Traditional SOA

Other recent papers have also proposed new definitions for different classes of OA. To help the reader, Table 2.1 relates the different types of OA referred to in this paper to those used in recent manuscripts that deal with semi-volatile POC and SOC.

2.2.1.3 POC emissions

To simulate POC, we need to the know the total emissions of low volatility ($C^* < 10^6$ μg m^{-3}) organics and their volatility distribution. However, this information is only known for a very small number of sources. Therefore, we estimate the POC emissions using existing inventories and data from studies of diesel exhaust and woodsmoke to distribute these emissions in volatility space.

Table 2.2: Annual emissions of POC and elemental carbon (EC) by source category

	Annual Emissions ($Tg\,yr^{-1}$)	
Source	POC[a]	EC
Fossil Fuels		
North America (Heald)[b]	1.14	1.35
North America (Bond)[c]	0.66	0.42
Rest of the world (Bond)[c]	3.67	2.62
Bio Fuels		
North America (Heald)[b]	2.04	0.19
North America (Bond)[c]	0.98	0.10
Rest of the world (Bond)[c]	10.7	1.52
Open Burning (GFEDv2)[d]	38.9	2.74
Total (Heald + Bond + GFEDv2)	56.4	8.42
Total (Bond + GFEDv2)	54.9	7.40

[a] Assuming an OM:OC of 1.8, [b] Heald et al. (2005), [c] Bond et al. (2004), [d] Van der Werf et al. (2006).

Table 2.2 lists the annual global emissions of POC and elemental carbon (EC) by source category. The POC emissions are the sum of the traditional POA emissions from existing inventories plus an estimate of the missing IVOC emissions. The combined inventory, representative of emissions for the early 21st century, provides a monthly averaged value for each grid cell.

Traditional particulate matter emission inventories are compiled using emission factors that are determined using quartz and/or teflon filters collected at elevated aerosol concentrations (100-10,000 μg m^{-3}). Hence, these inventories do not capture all of the POC emissions up to C* =10^6 μg m^{-3} (Robinson et al., 2010;Shrivastava et al., 2008). Shrivastava et al. (2008) assumed that traditional emission inventories account for all SVOC emissions but only a fraction of the IVOC emissions. Source test data suggest that the amount of IVOC emissions missing is between 0.25 and 2.8 times the POC emissions measured using a quartz filter (Schauer et al., 1999, 2001, 2002).

For this work, we used the traditional fossil and biofuel POA emissions from Bond et al. (2004), which are not based on a specific year. The open burning emissions are based on GFEDv2 (Van der Werf et al., 2006); they are from 2005 as the annual emissions for that year lie close to the median for the 1997 through 2006 period. Although the Bond et al. (2004) inventory is the most recent for fossil and biofuel combustion emissions, the North American winter-time predictions based on this inventory are a factor of 2 too low when compared to observations (Heald et al., 2006). Therefore, we updated the Bond et al. (2004) North American traditional POA and EC emissions using the Cooke et al. (1999) fossil fuel inventory and the Park et al. (2003) biofuel inventory (Heald et al., 2005). We use an organic-matter-to-organic-carbon ratio of 1.8 to convert the POC emission inventory values from TgC yr^{-1} to Tg yr^{-1} (Turpin and Lim, 2001;El-Zanan et al., 2005;Zhang et al., 2005).

Following the approach of Shrivastava et al. (2008), we assume the SVOC emissions to be completely represented by the traditional emission inventory or 56.4 Tg yr^{-1} and that the IVOC emissions are 1.5 times the traditional emission inventory or 84.6 Tg yr^{-1}.

Pye and Seinfeld (2010) used a different approach to estimate the missing IVOC emissions. They use naphthalene as a surrogate and estimate IVOC emissions to be 27 Tg yr^{-1} which is close to the lower end of the range suggested by the source test data. Given the large uncertainty, simulations are performed to investigate the sensitivity of the predictions to the amount of IVOC emissions.

The revised model requires that the POC emissions are distributed across the VBS. This requires knowing the volatility distribution of the emissions. In this work, we assume that all POC emission sources (fossil fuels, biofuels, open burning) have the same volatility distribution as there are currently inadequate data to perform a more refined analysis (Robinson et al., 2007). This volatility distribution is the same as that determined for diesel exhaust (Robinson et al., 2007) and used by Shrivastava et a. (2008) to predict the evolution of OA in eastern US. In reality, the emissions from each source have a distinct composition of organic species and therefore a unique volatility distribution. However, volatility data are available for very few sources (Robinson et al., 2007;Grieshop et al., 2009b). To address potential uncertainty associated with our assumption we conducted different model simulations using different volatility distributions.

2.2.1.4 Photochemical aging

Organic vapors react with atmospheric oxidants which changes their volatility, gas-particle phase partitioning and hence the amount of OA. This process, within the bounds of the VBS, is termed aging. Here, aging does not include the oxidation of VOCs, which is dealt with explicitly in other parts of the model. In this paper, aging also does not include the microphysical processes (condensation and coagulation) that produce an internally mixed aerosol. Finally, the

model also does not account for any aging due to heterogeneous, aqueous phase and condensed-phase reactions. We recognize that these processes might be important but given the uncertainty, we choose to focus on the gas phase aging of organic vapors.

We use a simple aging mechanism as used in previous studies employing the VBS (Farina et al., 2010;Lane et al., 2008;Shrivastava et al., 2008). The basic scheme is illustrated using red arrows in Figure 2.1. Aging proceeds by a first-order reaction of VBS vapors with OH radicals producing a product that has a C* one order of magnitude lower than its precursor. The vapor concentration after time Δt is given in equation (2.1) where OG_i^t represents the mass of gas-phase organics in bin '*i*' at time *t*, [*OH*] is the OH radical concentration and k_{OH} is the reaction rate constant.

$$OG_i^{t+\Delta t} = OG_i^t exp(-k_{OH}[OH]\Delta t) + OG_{i+1}^t [1 - exp(-k_{OH}[OH]\Delta t)] \quad (2.3)$$

We assume that the oxidation products in the vapor phase continue to age and form even lower volatility products. Although oxidation might result in additional mass being added to the products, we are conservative in our aging scheme and do not add any additional mass. Primary organic vapors or POG and SI-SOG are assumed to age with a reaction rate of 4 x 10^{-11} cm^3 $molecules^{-1}$ s^{-1}, based on the work of Shrivastava et al. (2008).

The aging mechanism used in this work is very different from that of Pye and Seinfeld (2010). They model SVOC aging using a single oxidation step that adds 50% additional mass and assign the aged products a C* value two orders of magnitude lower than the precursors. They model IVOC oxidation by assuming that the SOA forming potential of IVOCs is the same as naphthalene. Therefore, a fundamental difference is that Pye and Seinfeld (2010) assume that the aging process can be captured in a single oxidation step and hence they have a specific C* for their aged products. Our mechanism, in contrast, implicitly assumes that the gas phase aged

products continue to oxidize to form products that steadily move down in C* space. In addition, our lowest VBS C* bin (0.01 μg m^{-3}) is much lower than most of the C*s used by Pye and Seinfeld (2010) to represent their aged products (0.2 and 16.46 μg m^{-3} for SVOCs and 0.0001 and 1.69 μg m^{-3} for IVOCs). Therefore, given time, our aging scheme will tend to form more OA than Pye and Seinfeld (2010) though it is difficult to say which is correct based on available data. Although we know very little about how aging proceeds, we believe it has a large influence on the OA budget and the ability of the model to reproduce observations. To illustrate its influence, we run a simulation where the POC is treated as semi-volatile but not allowed to age.

Farina et al. (2010) assumed that the SOA mass yields for biogenic VOCs represent completed reactions and hence they do not need to be aged. We realize that this is a significant assumption that requires additional study that is outside the scope of this manuscript. However, simple "first guess" aging parameterizations, when applied to biogenic SOA, lead to gross over-predictions in regional models (Lane et al., 2008;Murphy and Pandis, 2009). Hence, as per Farina et al. (2010), the biogenic V-SOG is not allowed to age while the anthropogenic V-SOG is allowed to age with a reaction rate of 4 x 10^{-11} cm^3 $molecules^{-1}$ s^{-1}.

Previous studies that have modeled POA as non-volatile have considered a hydrophobic to hydrophilic conversion of POA, which has been referred to as "aging" without being very precise about what processes were being represented. Although, it was initially meant to represent the evolution of POA from an externally mixed to an internally mixed state (Cooke et al., 1999), it has also been interpreted to represent a heterogeneous oxidation of OA to more hydrophilic products. In either case, "aging" in traditional models is different than "aging" here, which is defined as ongoing oxidation of organics in the vapor phase. Moreover, we argue, based

on the arguments by Kroll et al. (2011), that heterogenous chemistry appears to be a much slower process than the photochemical aging described in this section.

2.2.1.5 Deposition

Gas and particle phase organics are subject to dry and wet deposition. Dry deposition of gas-phase organics is based on the resistance-in-series scheme of Wesley (1989). Particle-phase dry deposition velocities are calculated based on the treatment of sulfate as described in Koch et al. (1999). Wet deposition of gas and particle phase organics are treated separately for large-scale and convective clouds, following the GCM cloud schemes described in Del Genio and Yao (1993) and Del Genio et al. (1996). Dissolved gases and aerosols are scavenged within and below precipitating clouds. The solubility of gases is defined by their effective Henry's law constants and all organic gases are assigned a Henry's law constant of 10^5 M atm^{-1}. It is likely that higher volatility products on account of being less oxygenated have a lower Henry's law constant and vice-versa but in the absence of any robust data, we consider it to be constant across volatility. Also, we do not perform a sensitivity simulation with the Henry's law constant because the effect was previously explored by Farina et al. (2010).

The previous version of the unified model (Farina et al., 2010) divided POA into hydrophobic and hydrophilic categories which had different wet deposition characteristics (Chung and Seinfeld, 2002). By assuming that OA forms a single phase (Section 2.2.1.1), we use the same wet deposition characteristics for all OA and hence avoid this additional categorization all together. Following Chung and Seinfeld (2002), all organic particles are assigned a scavenging efficiency of 80%. Again, it is likely that the scavenging efficiency, just like the

Henry's law constant, is a function of volatility but in the absence of any robust data, we consider it to be constant across volatility.

2.3 Simulations

Multiple simulations were performed to evaluate the performance of the new modeling framework. Each simulation was performed for a one-year period with four months of spin up time to initialize concentration fields. Given the uncertainty in many input variables, we have evaluated the sensitivity of model results to the POC emissions, the POC volatility distribution, IVOC emissions, and the partitioning process. The sensitivity scenarios run in this study are listed in Table 2.3 and briefly described below.

Table 2.3: Overview of simulations

Framework	Name	POA	Aging?	US Inventory	Compared to BASE
Traditional	TRAD	Non-volatile	No	Heald	Non-volatile and non-reactive POA
Revised	BASE	Semi-volatile	Yes	Heald	–
	LOEM	Semi-volatile	Yes	Bond	Lower emissions in North America
	LOVL	Semi-volatile	Yes	Heald	Lower volatility POC
	NOIV	Semi-volatile	Yes	Heald	No IVOCs
	HVAP	Semi-volatile	Yes	Heald	ΔH_{vap} as a function of C^* and T
	NOAG	Semi-volatile	No	Heald	No POC Aging

BASE: This simulation represents our best estimate for all the input parameters. As described previously, fossil and bio fuel emissions of POC are from Heald et al. (2006) for North America and Bond et al. (2004) for the rest of the world and open burning emissions are from GFEDv2 (Van der Werf et al., 2006). All POC sources (fossil fuel, bio fuel, open burning) are treated alike and have the same volatility distribution, shown in Figure 2.3(a). IVOC emissions are assumed to be 1.5 times the published POC emission inventories. To represent the dependence of C_{OA} on

temperature, we use a ΔH_{vap} value of 30 kJ mol^{-1}, a value that has been used by Farina et al. (2010).

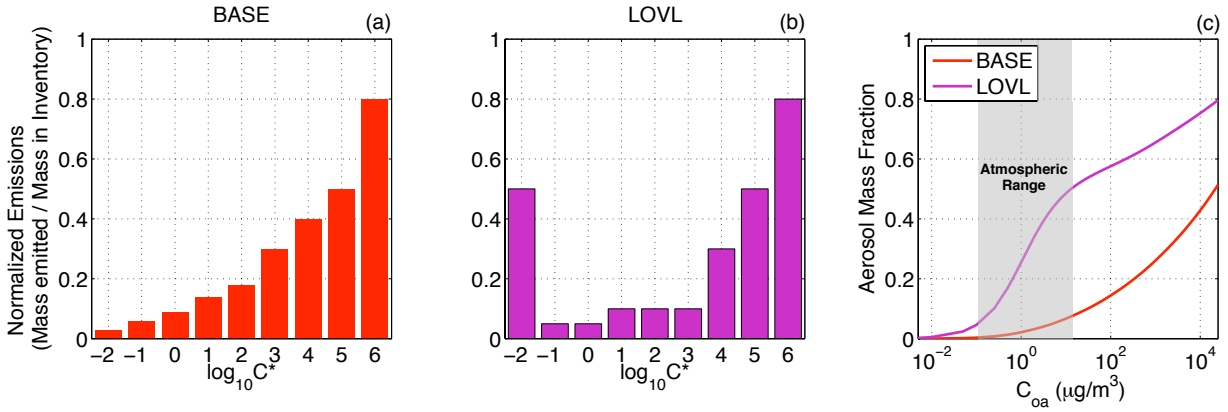

Figure 2.3: Volatility distribution of POC emissions for (a) BASE and (b) LOVL scenarios as a fraction normalized to the POC emission inventory total. Panel (c) shows the change in aerosol mass fraction for the BASE and LOVL volatility distributions as a function of C_{OA} at 298 K. The normalized SVOC emissions fully represent the traditional POC emission inventory and hence sum to 1. The normalized IVOC emissions are 1.5 times the emission inventory and hence sum to 1.5.

TRAD (**TRAD**itional): To compare and quantify the progress made in this research effort, the model is also run in the traditional configuration where we treat POC as non-volatile and non-reactive. This is the same version of the model that Farina et al. (2010) ran except for changes in the POC emission inventory.

LOEM (**LO**w **EM**issions): To investigate the sensitivity of the model to the magnitude of the POC emissions, we run the LOEM scenario that utilizes the Bond et al. (2004) inventory over North America. This reduces the fossil and bio fuel POC emissions over North America by slightly less than 50%.

LOVL (**LO**w **Vo**L**a**tility): To investigate the sensitivity of the model to the volatility distribution of the POC emissions, we employ a low volatility distribution which is constructed by moving

half of the mass in the SVOC bins to the lowest bin without altering the IVOC distribution. Figure 2.3(b) plots the LOVL volatility distribution.

NOIV (**NO IV**ocs): To quantify the contribution of IVOCs to global OA, we run the NOIV scenario where no IVOCs are added to the inventory.

HVAP (**H**eat of **VAP**orization): To quantify the sensitivity of the results to the enthalpy of vaporization, we use the work of Epstein et al. (2010) to describe ΔH_{vap} as a function of C* and temperature. Epstein et al. (2010) propose a much larger and wider range of ΔH_{vap}'s (40-150 kJ mole^{-1}) than used in the BASE case. One needs to exercise caution when interpreting results from the HVAP scenario as yields for SOA formation have been derived using a single value for the heat of vaporization (ΔH_{vap} =30-60 kJ mole^{-1} depending on the study). However, given that most SOA chamber experiments are done quite close to 298 K - the reference temperature for the VBS - using the revised heat of vaporization values will not have a large effect on the SOA mass yields.

NOAG (**NO AG**ing): To investigate the influence of gas-phase POC aging on OA burdens, we run the NOAG scenario where POC is treated as semi-volatile but the vapors are not allowed to age to form SI-SOA.

2.4 Results

2.4.1 Model predictions

2.4.1.1 Surface concentrations

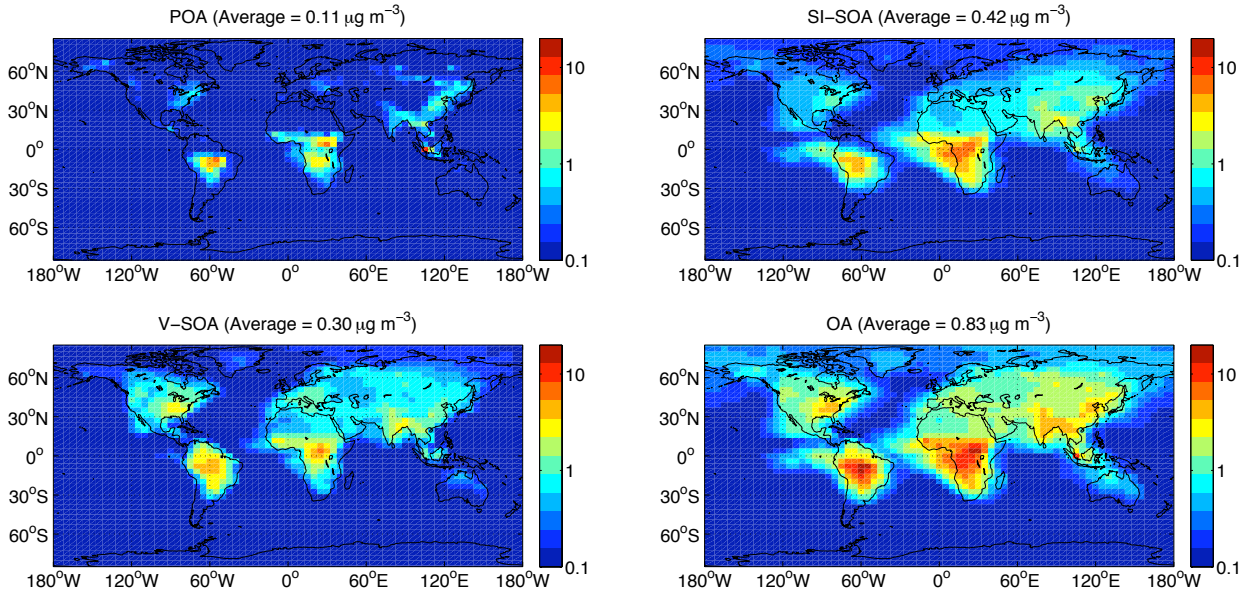

Figure 2.4: Annual-average surface concentrations of POA, SI-SOA, V-SOA and total OA in μg m^{-3} for BASE simulation. Area-weighted surface concentrations are shown in parentheses.

Figure 2.4 plots the annually-averaged global surface mass concentration for POA, SI-SOA, V-SOA and total OA predicted using the BASE model. Their domain-averaged surface mass concentrations are 0.11, 0.42, 0.30 and 0.83 μg m^{-3}, respectively. The highest OA mass concentrations are predicted in the Amazon, Congo and southeast Asian tropical forests. They are due to a combination of biomass burning emissions and SOA formed from biogenic VOCs. Higher OA mass concentrations are also predicted in the northeastern US and parts of India and China where there are substantial fossil and biofuel combustion emissions.

Appreciable amounts of POA are only present in locations where total OA mass concentrations are high (>5 μg m^{-3}), i.e. close to locations with high emissions. However, over most of the modeling domain, OA mass concentrations are low (<5 μg m^{-3}) and most (97%) of the POC evaporates leaving very little directly-emitted organic mass in the particle phase. Therefore, the POA concentrations in the revised model are spatially inhomogeneous. In contrast, the spatial distribution of SI-SOA, which is formed from POC vapors, is more

homogenous and exhibits a well-mixed regional presence. In fact, SI-SOA, although derived from POC emissions, resembles traditional SO or V-SOA in terms of its spatial distribution.

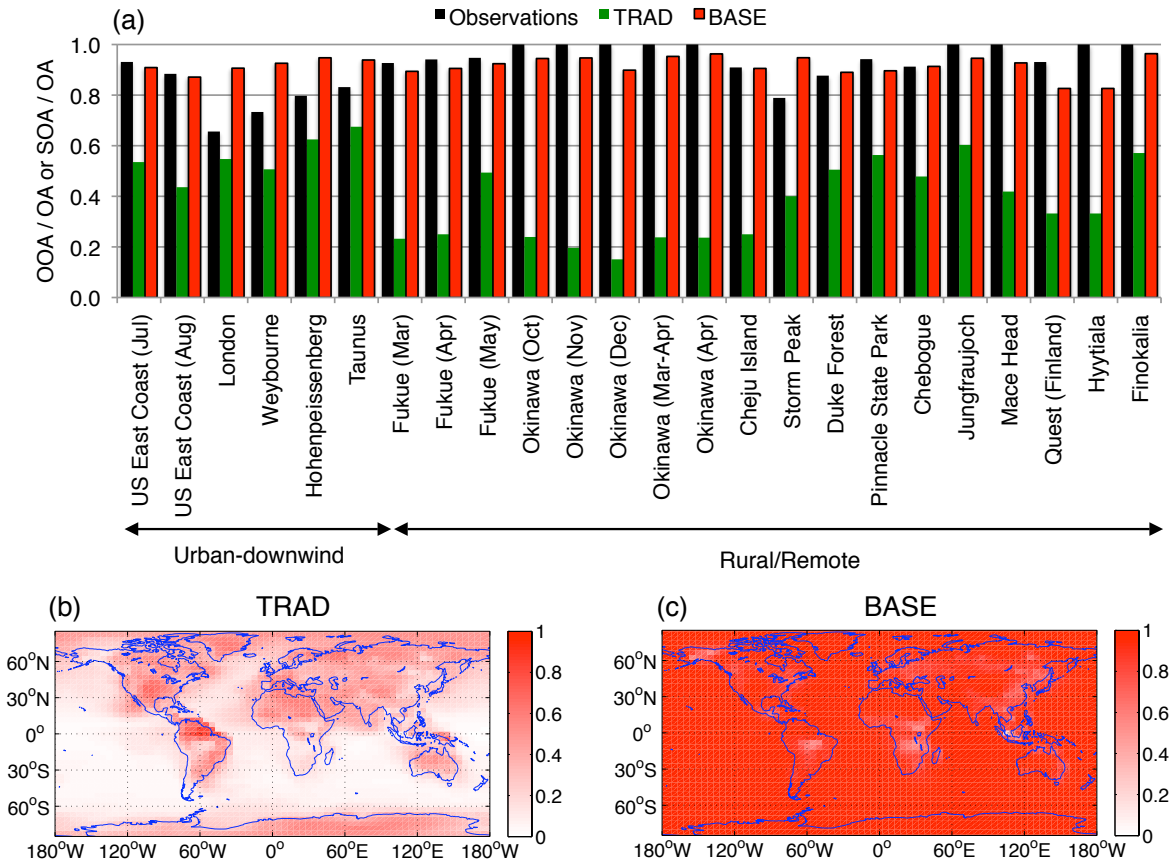

Figure 2.5: (a) Comparison of observed OOA to OA ratios with model results of SOA to OA ratios from the BASE and TRAD scenarios. Model-predicted global distribution of SOA to OA ratio for (b) TRAD and (c) BASE cases. Data in (a) are from Zhang et al. (2007).

In contrast to most previous models, the BASE model predicts a global distribution of OA that is dominated by SOA. To illustrate this, Figure 2.5(b-c) plots the model-predicted global distribution of the SOA-to-OA ratio using annually-averaged values for the TRAD and BASE scenarios. The BASE model consistently predicts a SOA-to-OA ratio of 0.8 or higher for all locations except for the Amazon, Congo, Alaska and east coast of China. In the TRAD case, OA in most locations is predicted to be POA. For example, over land the SOA-to-OA ratio ranges

from 0.4 to 0.7 while over oceans the ratio is close to 0.1. Therefore, the TRAD case predicts a higher SOA fraction near source regions and a lower SOA fraction away from source regions, a trend that is reversed in the BASE case.

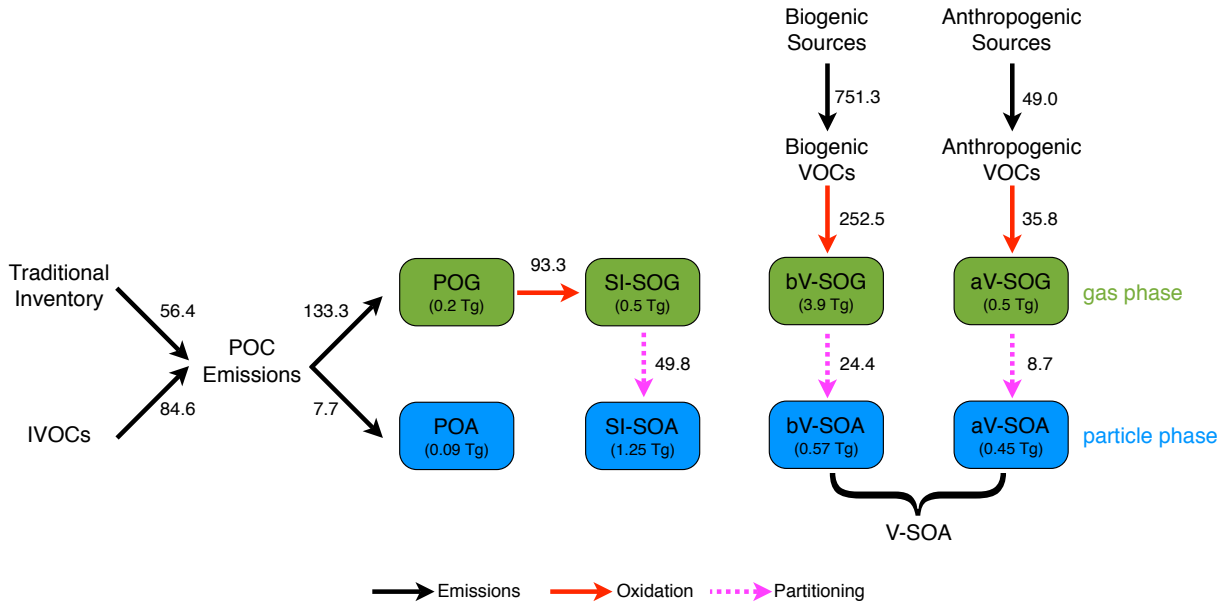

Figure 2.6: Schematic showing annual production (arrows, Tg yr^{-1}) and burdens (textboxes, Tg) for the gas and particle phase classes of organic aerosol predicted by the BASE model.

2.4.1.2 OA budgets

Figure 2.6 presents the breakdown of the overall OA budget . POC emissions, directly and indirectly via chemistry, contribute 57.5 Tg yr^{-1} of OA and traditional VOC oxidation forms 33.1 Tg yr^{-1} of OA to yield a total OA production rate of 90.6 Tg yr^{-1}. Of the 141 Tg yr^{-1} (or 78.3 TgC yr^{-1}) of POC mass emissions, only 7.7 Tg yr^{-1} (5%) partitions into the particle phase, without undergoing chemical reactions, to form POA. The remainder (POG) is chemically transformed in the atmosphere to form lower volatility products, some of which (49.8 Tg yr^{-1}) partitions into the condensed phase to form SI-SOA. SVOC oxidation forms 22.5 Tg yr^{-1} (45%) of SI-SOA which means that slightly less than half of the traditional POC emissions are 'recovered' into the particle phase through the oxidation of SVOC vapors. IVOC oxidation forms

27.3 Tg yr^{-1} (55%) of the SI-SOA and hence contributes to more than half of the SI-SOA and to slightly less than a third (30%) of the total OA formed, making it an important contributor to OA formation.

We can divide the amount of SI-SOA formed by the amount of POG reacted to compute an effective aerosol mass yield of 53%. The yield, when compared at a C_{OA} of 1 μg m^{-3}, is much higher than the aerosol mass yields observed for biogenic VOCs like alpha-pinene (4%) and isoprene (1%) in smog chamber experiments (Farina et al., 2010). However, the yield is similar to those of aromatics like benzene (33%) and naphthalene (66%) (Ng et al., 2007;Chan et al., 2009). Hence, the mechanism used in this work to represent the gas-phase chemistry of POC would be similar to a traditional mechanism, which treated all POC like aromatics.

Table 4 compares the OA burdens for the different sensitivity runs and from previous studies. Across the set of sensitivity runs, the POA and SI-SOA burden, counted together, remains fairly constant (1.34-1.45 Tg) except for the NOIV and NOAG scenarios. This suggests that the OA burden is insensitive to the POC volatility distribution and the ΔH_{vap}. This is because changes in partitioning affected by changes in the volatility distribution and ΔH_{vap} are offset by the low volatility products formed via oxidation of the evaporated vapors. Further, the difference in total OA burden between the BASE and the NOIV scenario (0.89 Tg) highlights the potential contribution that oxidation of IVOCs can have on the global burden (38% of the total). Of this 0.89 Tg, oxidation products of IVOCs contribute 0.73 Tg directly and 0.16 Tg indirectly by providing a larger absorbing phase which shifts the gas-particle partitioning towards the particle phase. In addition, the difference between the BASE and NOAG scenarios (1.56 Tg) emphasizes the large contribution that POC oxidation or "aging" has on the OA burden.

While our estimate for the total OA produced (90.6 Tg yr^{-1}) lies between that of previous studies (63 and 116 Tg yr^{-1}) (Heald et al., 2008;Hoyle et al., 2007;Chung and Seinfeld, 2002;Henze et al., 2008;Pye and Seinfeld, 2010;Kanakidou et al., 2005) a detailed comparison of the burdens predicted by BASE reveal important differences from those predicted with models that treat POA as non-volatile and non-reactive (Chung and Seinfeld, 2002;Liao and Seinfeld, 2005;Koch, 2001;Tsigaridis and Kanakidou, 2003;Farina et al., 2010). The BASE model reduces the POA burden by an order of magnitude compared to those other models, which significantly changes the POA-SOA split. But, if the primary-in-origin OA, i.e. POA and SI-SOA, are considered together, the burden is similar to that predicted by other models. This indicates that the evaporated POC returns back to the condensed phase through the oxidation of SVOC and IVOC vapors to produce roughly the same burden one would predict in a model with non-volatile and non-reactive POA. Although we predict a similar burden, we estimate a very different spatial distribution of OA (Section 2.4.1.1) and a very different extent of oxygenation of OA (Section 2.4.2.2).

The BASE burdens are much closer to the predictions of Pye and Seinfeld (2010) which is the only other global model that accounts for semi-volatile and reactive POC. The BASE model predicts a POA/SOA split of 4/96% while Pye and Seinfeld (2010) predict it to be 2/98%. In comparison, the TRAD model predicts a POA/SOA split of 47/53%. Similarly, the BASE model predicts SI-SOA to account for 53% while Pye and Seinfeld (2010) predict SI-SOA to account for 54% of the total OA burden. Further, the OA burden predicted by BASE also compares well with the burden proposed by Heald et al. (2010).

In this work, we used the model of Farina et al. (2010) to treat SOA formation from VOCs. However, since the simulation of POA and SOA is integrated under the VBS, changes in

handling the POA can influence the V-SOA burden. Across the BASE, LOEM, LOVL and NOIV scenarios, the V-SOA burden does not change significantly. However, there is a two-fold increase in the V-SOA burden in the HVAP scenario due to the enhanced sensitivity of the gas-particle partitioning of biogenic V-SOCs to changes in temperature. Our model does not allow for aging of biogenic V-SOCs, which results in most (90%) of the biogenic V-SOC mass to exist in the gas phase. In the free troposphere, where temperatures are lower, a lot of this gas-phase mass condenses into the particle phase yielding a higher burden in the HVAP scenario. In contrast, anthropogenic V-SOCs, which are allowed to age, account for only 13% of the total gas+particle mass burden with a much lower fraction (50%) in the gas phase. Hence, we do not see a significant shift in the anthropogenic V-SOA burden due to the changes in temperature in the HVAP scenario.

2.4.2 Comparison with field measurements

To evaluate model performance, we compare predictions to a wider set of observations than considered by previous studies. The evaluation considers OA composition, volatility and isotopic composition in addition to surface OA mass concentrations. While total OA concentrations are important in understanding the abundance, the other metrics are useful in identifying the sources, chemistry and composition of ambient OA.

2.4.2.1 Surface OA concentrations

United States: Figure 2.7 shows scatter plots comparing model-predicted total OA mass concentrations from BASE, LOEM, LOVL, HVAP and NOAG with measured values from the

Interagency Monitoring of Protected Visual Environments (IMPROVE) network (IMPROVE, August, 1995). Table 2.5 presents the statistical performance metrics for all the model runs including the TRAD scenario. The IMPROVE network measures PM concentrations across ~200, mostly remote/rural, locations within the United States. Each point on the scatter plot represents a monthly averaged value at a particular grid cell. The IMPROVE network reports OA mass concentrations in µgC m^{-3}. To compare with model predictions they are converted to µg m-3 using a conservative organic-mass-to-organic-carbon ratio of 1.8, based on the work of Turpin and Lim (2001) and Aiken et al. (2008). In Figure 2.7, red points represent the summer months of June, July and August and blue points represent the winter months of December, January and February.

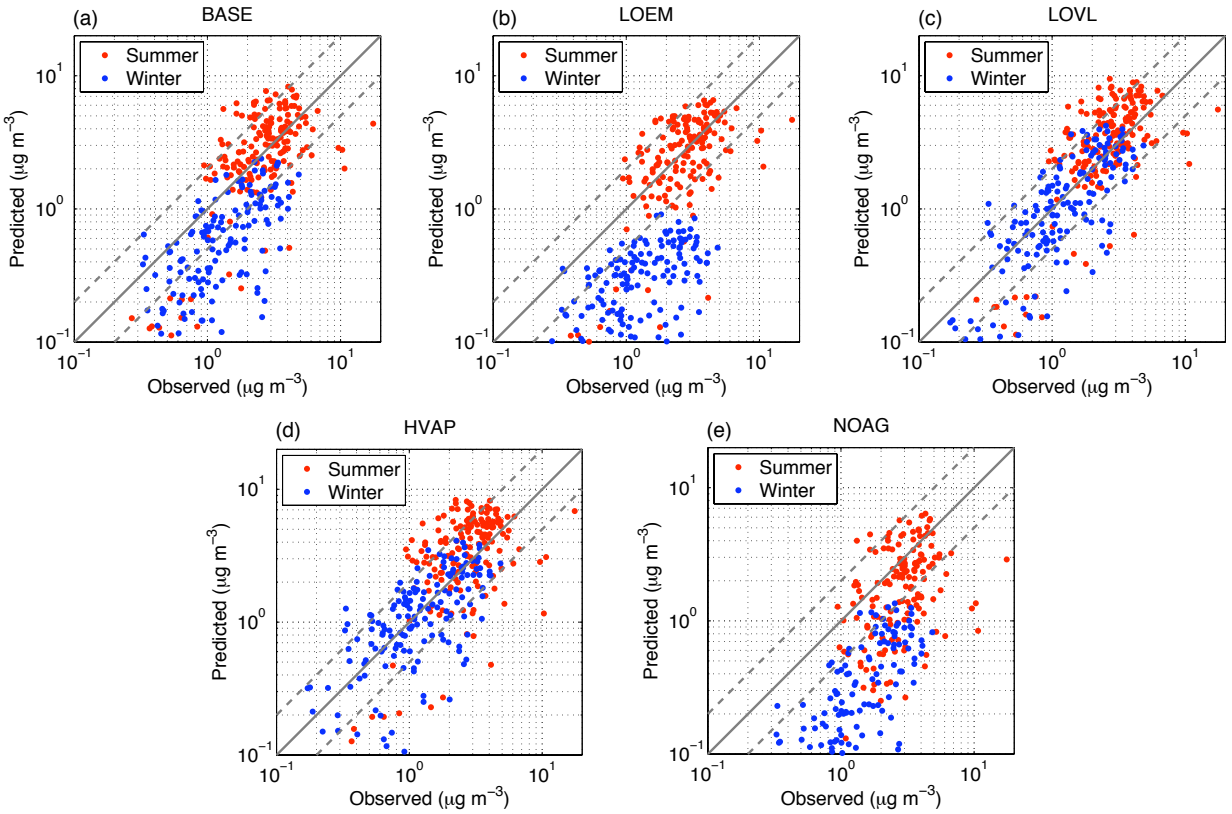

Figure 2.7: Scatter plots comparing model predictions from BASE, LOEM, LOVL, HVAP and NOAG with observations at IMPROVE sites from the 2001 to 2002. Red represents the summer months of June, July and August (JJA) and blue represents the winter months of December,

January and February (DJF). The solid grey line is the 1:1 line and the dashed lines are the 1:2 and 2:1 lines.

We initially compare observations to results from the BASE scenario (Figure 2.7(a)) and then highlight differences amongst the different sensitivity cases. In summer, the BASE predictions for OA mass concentration lie within a factor of 2 of observations with little bias. The winter-time predictions of the BASE model, however, are centered around the 1:2 dashed line with most (83%) predictions lying within a factor of 5.

Statistical metrics of fractional bias and fractional error were calculated to quantitatively evaluate model performance.

$$Fractional\,Bias = \frac{1}{N}\sum_{i=1}^{N}\frac{M-O}{\frac{M+O}{2}} \quad (2.4)$$

$$Fractional\,Error = \frac{1}{N}\sum_{i=1}^{N}\frac{|M-O|}{\frac{M+O}{2}} \quad (2.5)$$

where M are predicted values, O are observed values and N is the sample size.

For the BASE scenario, both the fractional bias and error are smaller in summer than in winter. The TRAD model, in comparison, has similar performance metrics in summer but better metrics in winter than the BASE model. So on an absolute OA mass concentration basis, the TRAD model performs better than the BASE model due to differences in wintertime results. In the BASE model, reduced photochemistry in winter results in reduced aerosol formation through gas-phase oxidation of POC emissions. The TRAD model, on the other hand, predicts higher OA concentrations because none of the POC emissions evaporate. We are not surprised by the performance seen of the TRAD model because Park et al. (2006), using the same emissions inventory and IMPROVE observations, arrived at a similarly good model-measurement

comparison. Park et al. (2006) achieved the better model performance by increasing the fossil and biofuel OC emissions over North America by a factor of ~2.

Figure 2.7(b) indicates that the lower emissions (in the LOEM case) lead to a greater under-prediction during the winter months without significantly changing the summer comparison. This result is consistent with the finding of Heald et al. (2006) that North American winter-time predictions using the Bond et al. (2004) inventory are low when compared to observations. The lower volatility distribution (in the LOVL case) improves winter performance without significantly changing the summer performance. This occurs because the OA emitted from primary organic sources (POA and SI-SOA) accounts for a larger fraction of the winter OA (65%) than the summer OA (30%). Hence, any change in the magnitude or volatility distribution of POC emissions has a bigger influence over the OA mass concentrations in winter than in summer. The HVAP scenario, using a wider range of enthalpy of vaporization values, better reproduces the winter data with a slight over-prediction during the summer. Overall, both the LOVL and HVAP scenarios better predict the absolute OA concentrations than the BASE and LOEM scenarios due to an improved winter-time comparison. Both LOVL and HVAP predict, on an annual basis, a negligible fractional bias and a fractional error of ~50%. Model predictions from the NOAG scenario suggest that the model-measurement comparison worsens as the OA mass concentration decreases. That model does well in polluted locations (high OA mass concentration) presumably because the OA is very close to the source and is still fresh. This implies that as the OA moves away from source regions, there is an enhancement in the OA mass that the NOAG model does not account for. It is clear, when compared to the BASE scenario, that aging the POC emissions is an essential process that needs to be modeled in order to enable a better model-measurement comparison.

Presumably, the wintertime comparison could also be improved by aging biogenic SOA. However, given that biogenic VOC emissions are higher (Guenther et al., 2006) and photochemical processing is stronger in the summer, aging biogenic SOA at the same rate as anthropogenic SOA would influence the summertime IMPROVE comparison much more than the wintertime IMPROVE comparison.

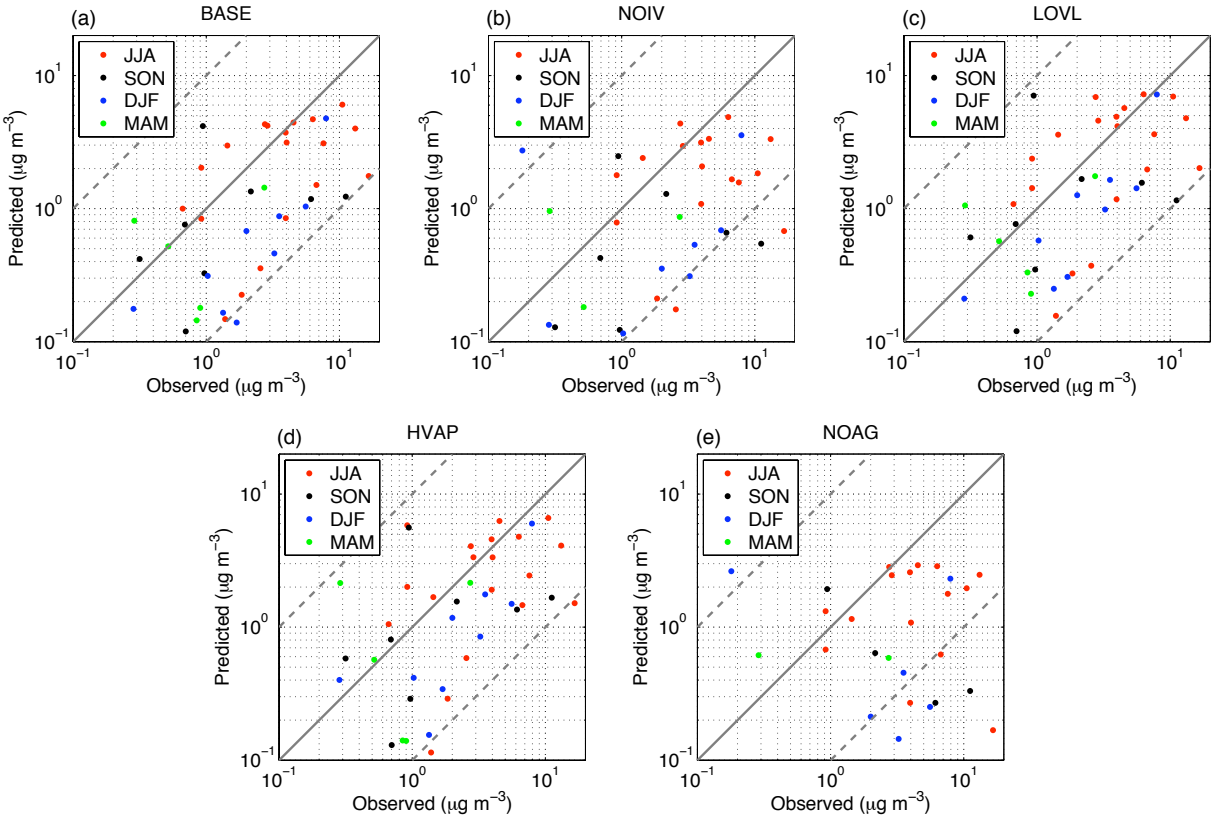

Figure 2.8: Scatter plot comparing model predictions from BASE, LOVL, NOIV, HVAP and NOAG with observed values at rural, remote and marine sites across the globe (Liousse et al., 1996;Chung and Seinfeld, 2002;Zhang et al., 2007). Red represents the months of June, July and August (JJA), black represents the months of September, October and November (SON), blue represents the months of December, January and February (DJF) and green represents the months of March, April and May (MAM) The solid grey line is the 1:1 line and the dashed lines are the 1:10 and 10:1 lines.

Rest of the World: Figure 2.8 shows scatter plots comparing model-predicted OA mass concentrations from BASE, LOVL, NOIV, HVAP and NOAG with observations from across the globe (Liousse et al., 1996;Chung and Seinfeld, 2002;Zhang et al., 2007). The performance in

the summer and winter months across the four comparisons is similar to that shown in Figure 2.7. The scatter, however, is much greater than the IMPROVE comparisons and the predictions sometimes lie an order of magnitude below observations. For example, for the BASE case, the annual fractional bias is -83% and the fractional error is 105%, both much larger than the annual IMPROVE metrics. The large scatter might be due to inconsistent and non-standardized measurement methods used by the different global networks such as differences in artifact correction, carbon analysis method or sampling duration. The IMPROVE network, in contrast, is an integrated effort employing standardized protocols and instruments for measurement, making it a much more consistent dataset to compare against.

2.4.2.2 Oxygenated organic aerosol

Recent work, using aerosol mass spectroscopy and factor analysis, has identified two chemically distinct classes of OA: hydrocarbon-like OA (HOA) and oxygenated OA (OOA) (Zhang et al., 2005). HOA is oxygen depleted OA and is associated with fresh POA emissions; and OOA is oxygen rich OA and is associated with aged OA/SOA and biomass burning (Zhang et al., 2007;Zhang et al., 2005;Robinson et al., 2007;Donahue et al., 2009). Zhang et al. (2007) estimated the fraction of HOA and OOA in OA at numerous locations around the world. We compare those estimates with model predictions assuming HOA to be equivalent to POA and OOA to be a sum of SI-SOA and V-SOA. Based on our discussion in Section 2.2.1.4, for the TRAD model, we consider all non-volatile POA to be "unaged" and therefore as HOA and V-SOA to be OOA.

Figure 2.6(a) compares the observed OOA-to-OA ratio at urban-downwind and rural/remote locations to model predictions of the SOA-to-OA ratio from the TRAD and BASE

models. The comparison deliberately omits urban locations due to the GCM's low spatial resolution. The observations indicate that OOA accounts for a large fraction of ambient OA. The BASE case reproduces more accurately the fraction of OOA with model predictions lying between -21 and +27% of observations. In comparison, the TRAD model, on an average, under-predicts the OOA fraction by a factor of two. To determine the sensitivity of the model predictions to different input parameters, we calculate a concentration-weighted average SOA-to-OA ratio for the urban-downwind and rural/remote location categories for the various sensitivity runs. The sensitivity runs predict a range from 0.79 to 0.93 for the urban-downwind locations and 0.71 to 0.90 for rural/remote locations respectively. The observed average, in comparison, was 0.83 and 0.95. In contrast, the TRAD model-predicted average was 0.56 and 0.45 respectively. This suggests that a high SOA-to-OA ratio that is consistent with observations is an outcome of the revised framework (semi-volatile and reactive POA) and is not sensitive across the range of possible input parameters. Therefore, the revised framework better predicts the high fractional contribution of SOA as reported by field studies.

2.4.2.3 OA volatility

Figure 2.9 compares model-predicted OA volatility to measurements from three different field campaigns: (a) FAME campaign in May-June of 2008 (FAME-2008) at Finokalia, a remote site in the northeast of Crete, Greece, (b) Mexico City campaign in March-April 2006 (MILAGRO-2006) and (c) Riverside campaign in July-August 2005 (SOAR-2005). The OA volatility was measured using thermodenuders and is represented as a thermogram, which is a plot of the OA mass fraction remaining as a function of temperature. The measured thermograms have been corrected for non-equilibrium effects in the thermodenuder using the work of Lee et

al. (2010) for FAME-2008 and the work of Cappa and Jimenez (2010) for MILAGRO-2006. For SOAR-2005, the thermogram has not been corrected for non-equlibrium conditions in the thermodenuder. A thermogram for the model predictions is computed using a simple equilibrium model that changes the OA gas-particle partitioning with temperature based on the Clausius-Clapeyron equation.

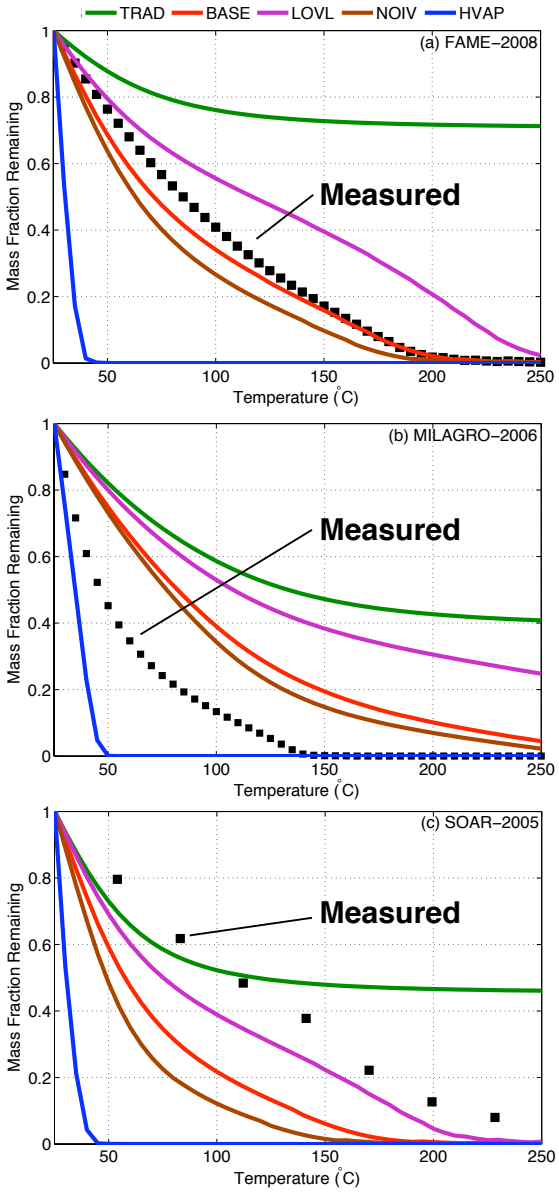

Figure 2.9: Thermograms comparing equilibrium-corrected data from the (a) the FAME-2008 campaign and (b) MILAGRO-2006 campaign with model results. (c) Thermogram comparing raw

measured data from SOAR-2005 with model results. Data are from Lee et al. (2010), Cappa and Jimenez (2010) and Huffman et al. (2009b).

At all three locations, the BASE case predicts the OA volatility better than the TRAD case. The TRAD model, at all locations, predicts a low volatility OA due to a large presence of non-volatile POA that does not evaporate with increase in temperature. The initial decrease in the mass fraction remaining for the TRAD model is due to the evaporation of semi-volatile V-SOC. At higher temperatures, the flat response of the thermogram reflects the remaining POA, which is treated as non-volatile by the TRAD model and does not evaporate at any temperature. Amongst the various sensitivity runs, the NOIV scenario predicts a somewhat more volatile OA while the LOVL predicts a somewhat lower volatility OA; however, these differences are likely to be within the measurement uncertainty. The HVAP case, in contrast, predicts a much higher volatility OA, overpredicting the evaporation of ambient OA with temperature and highlighting the sensitivity of the gas-particle partitioning to ΔH_{vap}. Cappa and Jimenez (2010) also found that Epstein et a. (2010) formulation of ΔH_{vap} produces a much too strong C* sensitivity to temperature.

For the MILAGRO data-set, a possible explanation for a higher observed volatility could be the proximity of the measurement site (T0 supersite) to the urban source region. This means a shorter time for aging and thus a potentially more volatile OA. The model results, on the other hand, are representative of a well-mixed and aged aerosol in a 4° latitude by 5° longitude grid cell. In contrast, FAME-2008 is a better data-set to evaluate the model predictions against because it is isolated from large sources and therefore indicative of OA transported and aged over longer distances. For the SOAR dataset, the BASE scenario predicts a slightly more volatile OA perhaps because the field data is not in equilibrium during measurement.

2.4.2.4 OA isotopic composition

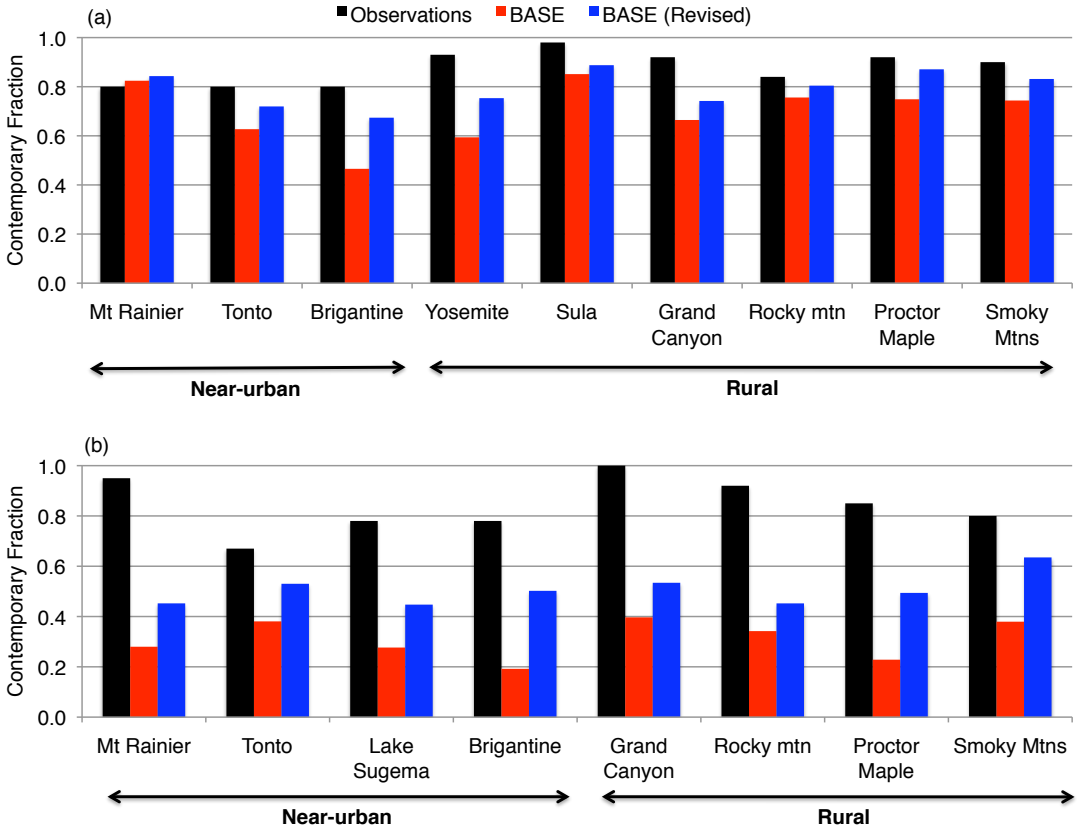

Figure 2.10: Contemporary fraction of OA at IMPROVE sites during the (a) summer and (b) winter months compared with model results from BASE and BASE (Revised). Data are from Schichtel et al. (2008).

The radioactive isotope of carbon (^{14}C) is used to distinguish fossil (coal, gasoline, diesel) and contemporary (wood, agricultural waste, pollen, vegetation) contributions to ambient OA (Szidat, 2009). Schichtel et a. (2008) present the isotopic composition for 12 rural sites collocated with the IMPROVE network. Figure 2.10 shows a comparison between Schichtel et al. (2008) measured contemporary fractions during the (a) summer and (b) winter months and model results from the BASE scenario (all sensitivity runs predict similar results). To calculate the fossil and contemporary fractions, we include both OC and EC. Fossil carbon includes EC, POA and anthropogenic SOA from fossil fuel sources. Contemporary carbon includes EC, POA

and anthropogenic SOA from biofuels and open burning, and biogenic SOA. The emission inventory for VOC precursors of aV-SOA do not allow for separate tracking of fossil and contemporary sources. Hence, we divide aV-SOA into its fossil and contemporary fractions in the same proportion as the total annual fossil and contemporary emissions of anthropogenic VOCs in the US.

For summer, the observed contemporary fractions vary from 0.8 to 1.0, which the BASE model slightly under-predicts (0.62 to 0.85). In winter, the observed contemporary fractions range from 0.67 to 1.0 which are significantly under-predicted by the BASE model (0.35 to 0.55). There are two possible reasons for the shortcoming of the model in predicting the contemporary fraction in winter. First, for the observations, the EC on average, accounts for 15% of the total carbon (TC) in summer and 22% of the TC in winter. In comparison, the BASE model predicts that EC on average, accounts for 22% of the TC in summer and 60% of the TC in winter. Hence, the BASE model predicts the correct EC:TC ratio in the summer but over-predicts EC concentrations in the winter, which are mostly fossil in origin (80% of US EC emissions), at all locations except Mt Rainier (refer to Figure S.1 in supplementary material). Second, the BASE scenario under-predicts OC concentrations in winter, which are mostly contemporary in origin (78% of US OC emissions), at all locations except Grand Canyon. This leads to a larger fossil fraction and a smaller contemporary fraction in winter. Therefore, lower predicted EC concentrations and higher predicted OC concentrations will likely improve wintertime comparisons. To that effect, we take EC concentrations from the LOEM (LOw EMissions) scenario and pair them with OC concentrations from the LOVL (LO VoLatility) scenario to predict the contemporary fraction. This combination, labeled "BASE revised" modestly improves the comparison during the winter months.

It is also possible that the model-predicted contemporary fraction in winter is low because the biogenic SOA, which is all contemporary, is not allowed to age. However, as mentioned in Section 2.4.2.1, this would badly over-predict the summertime OA mass concentration as was seen by Lane et al. (2008) and Murphy and Pandis (2009). Hence, it is not clear whether the aging of biogenic SOA is important in predicting the correct contemporary fraction in winter.

2.5 Discussion and Conclusions

In this work, we develop a global OA model that treats POA as semi-volatile and reactive and incorporates the emissions and oxidation of IVOCs as an additional source of OA. The OA model employs the volatility basis set (VBS) framework to simulate the emissions, chemical reactions and phase partitioning of all OA. Model sensitivity was assessed by varying the POC emissions, volatility distribution and the heat of vaporization.

The BASE version of the revised model predicts an annual OA production rate of 90.6 Tg yr^{-1} and a global burden of 2.37 Tg. In contrast to previous models that treat POA as non-volatile and non-reactive, the revised model predicts that most of OA is SOA, i.e. formed from the oxidation of vapor/gas phase organics. This happens because most of the POA evaporates and reacts with atmospheric oxidants to form low volatility products that condense into the particle phase as SI-SOA. This brings the POA/SOA split predicted by the revised model in better agreement with ambient measurements. This work also emphasizes the importance of oxidation of IVOCs as an additional source of OA. The revised model predicts that they contribute to more than a third of the total OA formed in the atmosphere. This implies that global and regional models that do not account for IVOCs could be under-estimating OA formation by 50%. The

amount of OA arising from IVOC oxidation depends on the magnitude of IVOC emissions and the mechanisms that model its oxidation in the atmosphere both of which remain fairly uncertain. Pye and Seinfeld (2010) use a different method to model IVOC emissions and reactivity, and hence predict a very different (5% compared to our 30%) contribution of IVOCs to the global OA budget. If we wish to determine their true influence, more effort needs to be made to constrain their emissions, concentration and reactivity in the atmosphere.

We evaluated model performance by comparing predictions not only against ambient OA mass concentrations but also against observations that provide insight into the sources, chemistry and properties of OA. These additional observations include degree of oxygenation, volatility and isotopic composition. The revised versions of the model perform much better on all those additional observations than the traditional version of the model. This illustrates that by treating POA as semi-volatile and reactive and accounting for emissions and oxidation of IVOCs, we have improved the model's capability in predicting the sources, chemistry and properties of OA. For example, we are able to predict the degree-of-oxygenation of OA. This has important implications for climate models that determine the effects of aerosols on radiative forcing since oxygenated OA have a higher propensity to uptake water and affect cloud formation. We are also able to predict the volatility of OA which is important in determining its lifetime and fate in the atmosphere.

Amongst the sensitivity runs, the scenario where IVOC emissions are set to zero does reasonably well in predicting the observed degree-of-oxygenation and volatility but significantly under-predicts wintertime OA mass concentrations over the United States. The BASE version performs similar to the no-IVOC version but has a slightly better wintertime performance. The simulation, where we use the parameterization by Epstein et al. (2010) to represent the enthalpy

of vaporization, performs well in predicting the OA mass concentrations over the United States and the degree-of-oxygenation. But, it predicts an ambient OA that has a very high volatility compared to measurements at the FAME, MILAGRO and SOAR field campaigns. The low volatility version of the model, however, performs reasonably well across all three metrics. Given the simulations performed in this work, we could argue that to get model predictions to agree with observations across mass concentrations, degree-of-oxygenation and volatility, the ideal model would need a (1) high IVOC contribution to the OA burden, (2) volatility lower than that of diesel exhaust for POC emissions and (3) a lower sensitivity of the OA to changes in temperature than those proposed by Epstein et al. (2010).

A comparison of OA mass concentrations between the revised model and the IMPROVE network revealed good agreement in the summer months and an under-prediction in the winter months. The sensitivity runs suggest that the comparison during the winter months can be improved, without affecting the summer comparison, by increasing emissions or decreasing the volatility of the POC emissions. The under-prediction of OA mass concentrations and the contemporary fraction in winter lead us to hypothesize that the emission inventory is probably under-representing a contemporary source in winter. To support that argument, Bond et al. (2004) show that about 60% of contained POC emissions in the US are from residential biofuel use and that more than 50% of the uncertainty in those emissions arises from residential wood burning. Hence, it is likely that residential biofuel emissions are under-represented in the emission inventory in winter.

Models that simulate the abundance and properties of OA need to account for the semi-volatile and reactive nature of POA. However, there are currently significant uncertainties in building models that represent that behavior. Future work needs to focus on quantifying the total

POC (vapor+particle) emissions, volatility and atmospheric processing. Further, models that are used to simulate OA need to be evaluated by comparing model predictions with observations of intensive properties that provide clues about their physical and chemical processes: degree of oxygenation, volatility and isotopic composition.

2.6 Supplementary material

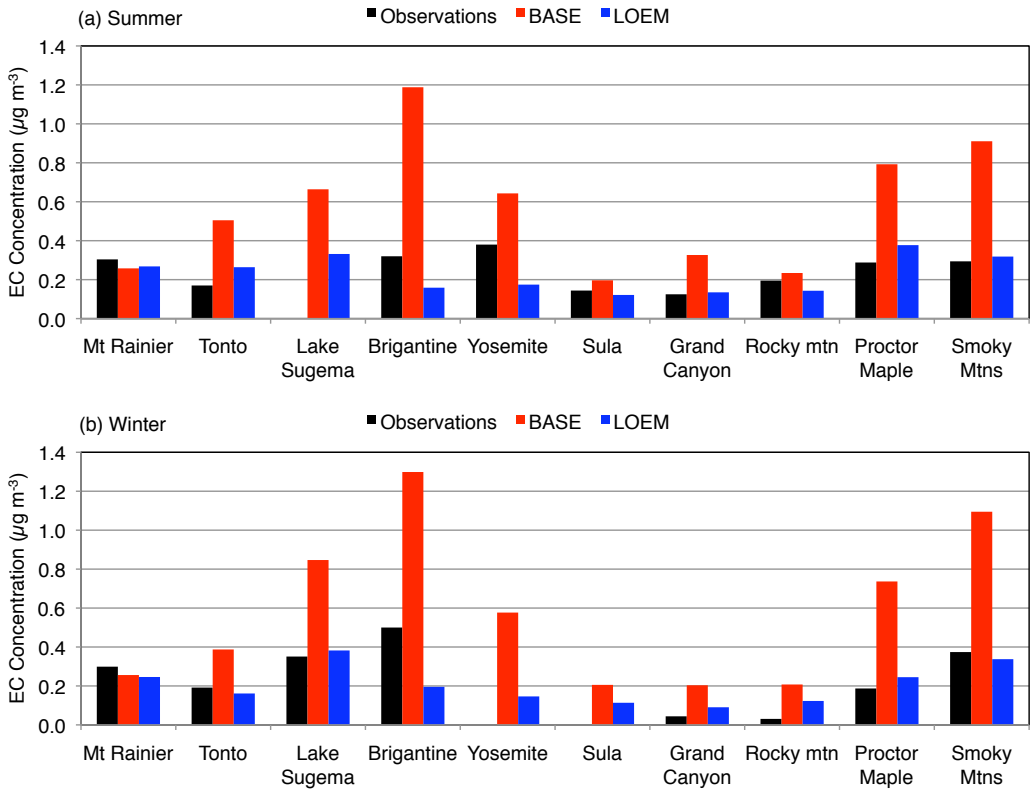

Figure S.1: EC concentrations at IMPROVE sites during the (a) summer and (b) winter months compared with model results from the BASE and LOEM scenarios. Data are from Schichtel et al. (2008).

2.7 Acknowledgements

This work was supported by the EPA STAR program through the National Center for Environmental Research (NCER) under grants RD-83337401-0 and R833748.

2.8 References

Adams, P. J., Seinfeld, J. H., and Koch, D. M.: Global concentrations of tropospheric sulfate, nitrate, and ammonium aerosol simulated in a general circulation model, Journal of Geophysical Research-Atmospheres, 104, 1999.

An, W. J., Pathak, R. K., Lee, B. H., and Pandis, S. N.: Aerosol volatility measurement using an improved thermodenuder: Application to secondary organic aerosol, Journal of Aerosol Science, 38, 305--314, 2007.

Asa-Awuku, A., Miracolo, M., Kroll, J., Robinson, A., and Donahue, N.: Mixing and phase partitioning of primary and secondary organic aerosols, Geophysical Research Letters, 36, L15827, doi:10.1029/2009GL039301, 2009.

Bernstein, J. A., Alexis, N., Barnes, C., Bernstein, I. L., Bernstein, J. A., Nel, A., Peden, D., Diaz-Sanchez, D., Tarlo, S. M., and Williams, P. B.: Health effects of air pollution, The Journal of Allergy and Clinical Immunology, 114, 1116-1123, 2004.

Chan, A. W. H., Kautzman, K. E., Chhabra, P. S., Surratt, J. D., Chan, M. N., Crounse, J. D., Kurten, A., Wennberg, P. O., Flagan, R., and Seinfeld, J. H.: Secondary organic aerosol formation from photooxidation of naphthalene and alkylnaphthalenes: Implications for oxidation of intermediate volatility organic compounds (ivocs), Atmospheric Chemistry and Physics, 9, 3049-3060, 2009.

Chung, S. H., and Seinfeld, J. H.: Global distribution and climate forcing of carbonaceous aerosols, J. Geophys. Res, 107, 4407, 2002.

Cooke, W., Liousse, C., Cachier, H., and Feichter, J.: Construction of a 1 degrees x 1 degrees fossil fuel emission data set for carbonaceous aerosol and implementation and radiative impact in the echam4 model, J. Geophys. Res, 104, 22--137, 1999.

De Gouw, J., Middlebrook, A., Warneke, C., Goldan, P., Kuster, W., Roberts, J., Fehsenfeld, F., Worsnop, D., Canagaratna, M., Pszenny, A., and others: Budget of organic carbon in a polluted atmosphere: Results from the new england air quality study in 2002, J. Geophys. Res, 110, 2005.

Donahue, N., Robinson, A., Stanier, C., and Pandis, S.: Coupled partitioning, dilution, and chemical aging of semivolatile organics, Environ. Sci. Technol, 40, 2635-2643, doi:10.1021/es052297c, 2006.

Donahue, N. M., Robinson, A. L., and Pandis, S. N.: Atmospheric organic particulate matter: From smoke to secondary organic aerosol, Atmospheric Environment, 43, 94--106, 2009.

El-Zanan, H. S., Lowenthal, D. H., Zielinska, B., Chow, J. C., and Kumar, N.: Determination of the organic aerosol mass to organic carbon ratio in improve samples, Chemosphere, 60, 485--496, 2005.

Farina, S. C., Adams, P. J., and Pandis, S. N.: Modeling global secondary organic aerosol formation and processing with the volatility basis set: Implications for anthropogenic secondary

organic aerosol, Journal of Geophysical Research, 115, D09202, doi:10.1029/2009JD013046, 2010.

Grieshop, A., Donahue, N., and Robinson, A.: Laboratory investigation of photochemical oxidation of organic aerosol from wood fires 2: Analysis of aerosol mass spectrometer data, Atmospheric Chemistry and Physics, 9, 2227-2240, 2009a.

Grieshop, A. P., Logue, J. M., Donahue, N. M., and Robinson, A. L.: Laboratory investigation of photochemical oxidation of organic aerosol from wood fires 1: Measurement and simulation of organic aerosol evolution, Atmospheric Chemistry and Physics, 9, 1263-1277, 10.5194/acp-9-1263-2009, 2009b.

Guenther, A., Karl, T., Harley, P., Wiedinmyer, C., Palmer, P., and Geron, C.: Estimates of global terrestrial isoprene emissions using megan (model of emissions of gases and aerosols from nature), Atmospheric Chemistry & Physics, 6, 3181-3210, 2006.

Hansen, J., Russell, G., Rind, D., Stone, P., Lacis, A., Lebedeff, S., Ruedy, R., and Travis, L.: Efficient three-dimensional global models for climate studies: Models i and ii, Monthly Weather Review, 111, 609--662, 1983.

Heald, C., Henze, D., Horowitz, L., Feddema, J., Lamarque, J., Guenther, A., Hess, P., Vitt, F., Seinfeld, J., Goldstein, A., and others: Predicted change in global secondary organic aerosol concentrations in response to future climate, emissions, and land use change, J. Geophys. Res, 113, 2008.

Heald, C. L., Jacob, D. J., Park, R. J., Russell, L. M., Huebert, B. J., Seinfeld, J. H., Liao, H., and Weber, R. J.: A large organic aerosol source in the free troposphere missing from current models, Geophys. Res. Lett, 32, 18, 2005.

Heald, C. L., Jacob, D. J., Turquety, S., Hudman, R. C., Weber, R. J., Sullivan, A. P., Peltier, R. E., Atlas, E. L., De Gouw, J. A., Warneke, C., and others: Concentrations and sources of organic carbon aerosols in the free troposphere over north america, J. Geophys. Res, 111, 2006.

Henze, D., Seinfeld, J., Ng, N., Kroll, J., Fu, T., Jacob, D., and Heald, C.: Global modeling of secondary organic aerosol formation from aromatic hydrocarbons: High- vs. Low-yield pathways, Atmospheric Chemistry and Physics, 8, 2405--2420, 2008.

Hoyle, C., Berntsen, T., Myhre, G., and Isaksen, I.: Secondary organic aerosol in the global aerosol- chemical transport model oslo ctm 2, Atmospheric Chemistry and Physics, 7, 5675--5694, 2007.

Huffman, J., Docherty, K., Mohr, C., Cubison, M., Ulbrich, I., Ziemann, P., Onasch, T., and Jimenez, J.: Chemically-resolved volatility measurements of organic aerosol fom different sources., Environmental science & technology, 43, 5351, 2009.

IMPROVE: Improve data guide, August, 1995.

IPCC, W.: Climate change 2007: The physical science basis, Summary for Policy Makers, Contribution of Working Group I to the Fourth Assessment Report of the Intergovernmental Panel on Climate Change, 2007.

Jimenez, J., Canagaratna, M., Donahue, N., Prevot, A., Zhang, Q., Kroll, J., DeCarlo, P., Allan, J., Coe, H., Ng, N., and others: Evolution of organic aerosols in the atmosphere, Science, 326, 1525, 2009.

Kanakidou, M., Seinfeld, J., Pandis, S., Barnes, I., Dentener, F., Facchini, M., Van Dingenen, R., Ervens, B., Nenes, A., Nielsen, C., and others: Organic aerosol and global climate modelling: A review, Atmospheric Chemistry and Physics, 5, 1053--1123, 2005.

Koch, D.: Transport and direct radiative forcing of carbonaceous, Journal of geophysical research, 106, 20--311, 2001.

Lane, T. E., Donahue, N. M., and Pandis, S. N.: Simulating secondary organic aerosol formation using the volatility basis-set approach in a chemical transport model, Atmospheric Environment, 42, 7439-7451, 2008.

Liao, H., Adams, P. J., Chung, S. H., Seinfeld, J. H., Mickley, L. J., and Jacob, D. J.: Interactions between tropospheric chemistry and aerosols in a unified general circulation model, J. Geophys. Res, 108, 4001, 2003.

Liao, H., Seinfeld, J. H., Adams, P. J., and Mickley, L. J.: Global radiative forcing of coupled tropospheric ozone and aerosols in a unified general circulation model, J. Geophys. Res, 109, 16207, 2004.

Liao, H., and Seinfeld, J. H.: Global impacts of gas-phase chemistryaerosol interactions on direct radiative forcing by anthropogenic aerosols and ozone, J. Geophys. Res, 110, D18208, 2005.

Liousse, C., Penner, J., Chuang, C., Walton, J., Eddleman, H., and Cachier, H.: A global three-dimensional model study of carbonaceous aerosols, Journal of Geophysical Research-Atmospheres, 101, 1996.

Miracolo, M. A., Presto, A. A., Lambe, A. T., Hennigan, C. J., Donahue, N. M., Kroll, J. H., Worsnop, D. R., and Robinson, A. L.: Photo-oxidation of low-volatility organics found in motor vehicle emissions: Production and chemical evolution of organic aerosol mass, Environmental Science & Technology, 16305-16327, 2010.

Murphy, B., and Pandis, S.: Simulating the formation of semivolatile primary and secondary organic aerosol in a regional chemical transport model., Environmental science & technology, 43, 4722-4728, doi:10.1021/es803168a, 2009.

Ng, N., Kroll, J., Chan, A., Chhabra, P., Flagan, R., and Seinfeld, J.: Secondary organic aerosol formation from m-xylene, toluene, and benzene, Atmos. Chem. Phys, 7, 3909-3922, doi:10.5194/acp-7-3909-2007, 2007.

Pankow, J. F.: An absorption model of gas/particle partitioning of organic compounds in the atmosphere, Atmospheric Environment, 28, 185-188, 1994.

Park, R. J., Jacob, D. J., Chin, M., and Martin, R. V.: Sources of carbonaceous aerosols over the united states and implications for natural visibility, J. Geophys. Res, 108, 4355, 2003.

Park, R. J., Jacob, D. J., Kumar, N., and Yantosca, R. M.: Regional visibility statistics in the united states: Natural and transboundary pollution influences, and implications for the regional haze rule, Atmospheric Environment, 40, 5405--5423, 2006.

Penner, J., Chuang, C., and Grant, K.: Climate forcing by carbonaceous and sulfate aerosols, Climate Dynamics, 14, 839--851, 1998.

Pye, H., and Seinfeld, J.: A global perspective on aerosol from low-volatility organic compounds, Atmos. Chem. Phys, 10, 4377-4401, doi:10.5194/acp-10-4377-2010, 2010.

Rind, D., and Lerner, J.: Use of on-line tracers as a diagnostic tool in general circulation model development 1. Horizontal and vertical transport in the troposphere, Journal of Geophysical Research-Atmospheres, 101, 1996.

Rind, D., Lerner, J., Shah, K., and Suozzo, R.: Use of on-line tracers as a diagnostic tool in general circulation model development 2. Transport between the troposphere and stratosphere, Journal of Geophysical Research-Atmospheres, 104, 1999.

Robinson, A. L., Donahue, N. M., Shrivastava, M. K., Weitkamp, E. A., Sage, A. M., Grieshop, A. P., Lane, T. E., Pierce, J. R., and Pandis, S. N.: Rethinking organic aerosols: Semivolatile emissions and photochemical aging, Science, 315, 1259-1262, 2007.

Robinson, A. L., Grieshop, A. P., Donahue, N. M., and Hunt, S. W.: Updating the conceptual model for fine particle mass emissions from combustion systems, Journal of the Air & Waste management association, 60, 1204-1222, 2010.

Sage, A., Weitkamp, E., Robinson, A., and Donahue, N.: Evolving mass spectra of the oxidized component of organic aerosol: Results from aerosol mass spectrometer analyses of aged diesel emissions, Atmospheric Chemistry and Physics, 8, 1139--1152, 2008.

Schauer, J. J., Kleeman, M. J., Cass, G. R., and Simoneit, B. R. T.: Measurement of emissions from air pollution sources. 2. C1 through c30 organic compounds from medium duty diesel trucks, Environ. Sci. Technol, 33, 1578-1587, 1999.

Schauer, J. J., Kleeman, M. J., Cass, G. R., and Simoneit, B. R. T.: Measurement of emissions from air pollution sources. 3. C1- c29 organic compounds from fireplace combustion of wood, Environ. Sci. Technol, 35, 1716--1728, 2001.

Schauer, J. J., Kleeman, M. J., Cass, G. R., and Simoneit, B. R. T.: Measurement of emissions from air pollution sources. 4. C1-c27 organic compounds from cooking with seed oils, Environmental Science & Technology, 36, 567-575, 2002.

Schichtel, B. A., Malm, W. C., Bench, G., Fallon, S., McDade, C. E., Chow, J. C., and Watson, J. G.: Fossil and contemporary fine particulate carbon fractions at 12 rural and urban sites in the united states, J. Geophys. Res, 113, 2008.

Shrivastava, M. K., Lane, T. E., Donahue, N. M., Pandis, S. N., and Robinson, A. L.: Effects of gas particle partitioning and aging of primary emissions on urban and regional organic aerosol concentrations, Journal of Geophysical Research-Atmospheres, 113, D18301, doi:10.1029/2007JD009735, 2008.

Song, C., Zaveri, R., Alexander, M., Thornton, J., Madronich, S., Ortega, J., Zelenyuk, A., Yu, X., Laskin, A., and Maughan, D.: Effect of hydrophobic primary organic aerosols on secondary organic aerosol formation from ozonolysis of a-pinene, Geophysical Research Letters, 34, 2007.

Szidat, S.: Radiocarbon analysis of carbonaceous aerosols: Recent developments, CHIMIA International Journal for Chemistry, 63, 157--161, 2009.

Tsigaridis, K., and Kanakidou, M.: Global modelling of secondary organic aerosol in the troposphere: A sensitivity analysis, Atmos. Chem. Phys, 3, 1849--1869, 2003.

Turpin, B., and Lim, H.: Species contributions to pm2. 5 mass concentrations: Revisiting common assumptions for estimating organic mass, Aerosol Science and Technology, 35, 602--610, 2001.

Van der Werf, G., Randerson, J., Giglio, L., Collatz, G., Kasibhatla, P., and Arellano Jr, A.: Interannual variability in global biomass burning emissions from 1997 to 2004, Atmospheric Chemistry and Physics, 6, 3423--3441, 2006.

Volkamer, R., Jimenez, J. L., San Martini, F., Dzepina, K., Zhang, Q., Salcedo, D., Molina, L. T., Worsnop, D. R., and Molina, M. J.: Secondary organic aerosol formation from anthropogenic air pollution: Rapid and higher than expected, Geophys. Res. Lett, 33, 17, 2006.

Weber, R., Orsini, D., Daun, Y., Lee, Y., Klotz, P., and Brechtel, F.: A particle-into-liquid collector for rapid measurement of aerosol bulk chemical composition, Aerosol Science and Technology, 35, 718--727, 2001.

Zhang, Q., Worsnop, D., Canagaratna, M., and Jimenez, J.: Hydrocarbon-like and oxygenated organic aerosols in pittsburgh: Insights into sources and processes of organic aerosols, Atmos. Chem. Phys, 5, 3289--3311, 2005.

Zhang, Q., Jimenez, J. L., Canagaratna, M. R., Allan, J. D., Coe, H., Ulbrich, I., Alfarra, M. R., Takami, A., Middlebrook, A. M., Sun, Y. L., Dzepina, K., Dunlea, E., Docherty, K., DeCarlo, P. F., Salcedo, D., Onasch, T., Jayne, J. T., Miyoshi, T., Shimono, A., Hatakeyama, S., Takegawa, N., Kondo, Y., Schneider, J., Drewnick, F., Borrmann, S., Weimer, S., Demerjian, K., Williams, P., Bower, K., Bahreini, R., Cottrell, L., Griffin, R. J., Rautiainen, J., Sun, J. Y., Zhang, Y. M., and Worsnop, D. R.: Ubiquity and dominance of oxygenated species in organic aerosols in anthropogenically-influenced northern hemisphere midlatitudes, Geophys. Res. Lett, 34, L13801, doi:10.1029/2007GL029979, 2007.

Chapter 3: Modeling the formation and properties of traditional and non-traditional secondary organic aerosol: Problem formulation and application to aircraft exhaust*

Abstract

We present a methodology to model secondary organic aerosol (SOA) formation from the photo-oxidation of low-volatility organics (semivolatile and intermediate volatile organic compounds). The model is parameterized and tested using SOA data collected during two field campaigns that characterized the atmospheric evolution of dilute gas-turbine engine emissions using a smog chamber. Photo-oxidation formed a significant amount of SOA, much of which cannot be explained based on the emissions of traditional, speciated precursors; we refer to this as non-traditional SOA (NT-SOA). The NT-SOA can be explained by emissions of low-volatility organic vapors measured using sorbents. Since these vapors could not be speciated, we employ a volatility-based approach to model NT-SOA formation. We show that the method proposed by Robinson et al. (2007) is unable to explain the timing of NT-SOA formation because it assumes a very modest reduction in volatility of the precursors with every oxidation reaction. In contrast, a Hybrid method, similar to models of traditional SOA formation, assumes a larger reduction in volatility with each oxidation step and results in a better reproduction of NT-SOA formation. The NT-SOA yields estimated for the low-volatility organic vapor emissions are similar to literature data for large *n*-alkanes and other low-volatility organics. The yields vary with fuel composition (JP8 versus Fischer-Tropsch) and engine load (idle versus non-idle). These

* Originally published as: Jathar, S. H., Miracolo, M. A., Presto, A. A., Adams, P. J., and Robinson, A. L.: Modeling the formation and properties of traditional and non-traditional secondary organic aerosol: problem formulation and application to aircraft exhaust, Atmos. Chem. Phys. Discuss., 12, 9945-9983, doi:10.5194/acpd-12-9945-2012, 2012.

differences are consistent with the expected contribution of high (aromatics and n-alkanes) and low (branched alkanes and oxygenated species) SOA forming species to the exhaust.

3.1 Introduction

Atmospheric aerosols exert a large influence on climate and public health (Bernstein et al., 2004;IPCC, 2007). Secondary organic aerosol (SOA), defined as the organic particulate mass arising from the oxidation products of gas-phase organic species, accounts for a significant fraction of the submicron atmospheric aerosol mass (Zhang et al., 2007). Until recently, SOA formation was believed to be dominated by the first-generation oxidation products of high-flux volatile organic compounds (VOCs) such as terpenes and single-ring aromatics. SOA formed from speciated VOCs is defined as traditional SOA (T-SOA) and is explicitly accounted for in chemical transport models. However, these models systematically under-predict organic aerosol levels (Heald et al., 2005;Vutukuru et al., 2006;Johnson et al., 2006;Morris et al., 2006;Dzepina et al., 2009;Dzepina et al., 2010), especially during photochemically active periods.

Recent laboratory and field studies show that combustion emissions when photo-oxidized form substantial SOA mass, greatly in excess of what can be explained by T-SOA models (Robinson et al., 2007;Grieshop et al., 2009;Hodzic et al., 2010;Miracolo et al., 2011;Miracolo et al., submitted). Robinson et al. (2007) proposed that a significant part of the unexplained SOA stemmed from the oxidation of low-volatility organic vapors, i.e. semi-volatile and intermediate volatility organic compounds (SVOCs and IVOCs). SVOCs refer to the organic mass that have an effective saturation concentration (C*) less 10^3 μg m^{-3} and IVOCs refer to the organic mass that have a C* greater than 10^4 but less than 10^7 μg m^{-3}. In the remainder of this text, we refer to SVOCs and IVOCs together as primary organic carbon (POCs). POCs are co-emitted by

combustion sources but are less volatile than VOCs. However, these emissions are not included in models because the vast majority of them cannot be speciated, they do not contribute significantly to ozone formation, and their measurement requires difficult-to-use sorbents. Fundamentally, POC vapors form SOA in the same manner as VOCs; oxidation adds functional groups to the organic molecule, which reduces the volatility (vapor pressure) of the product and leads to condensation into the particle phase. However, the lower initial volatility of POCs mean that they can have higher SOA yields than VOCs (Lim and Ziemann, 2009;Presto et al., 2010). SOA formed from POC vapors is denoted as non-traditional SOA (NT-SOA).

A key attribute of POC vapors is that the vast majority of the mass cannot be speciated with traditional GC-based techniques (Schauer et al., 1999, 2002). Instead it is classified as an unresolved complex mixture (UCM) that is thought to be dominated by branched and cyclic alkanes (Robinson et al., 2007;Robinson et al., 2010). The problem is fundamentally caused by the number of isomers growing exponentially with carbon number; these isomers co-elute from the GC-column (Goldstein and Galbally, 2007). Since the molecular identity of the vast majority of POC vapors cannot be ascertained, SOA formation from these compounds cannot be investigated or modeled in the same manner as traditional speciated SOA precursors (benzene, alpha-pinene, et al.). Instead, NT-SOA models have been based on the volatility of the emissions and a volatility-based oxidation mechanism (Robinson et al., 2007;Dzepina et al., 2009;Murphy and Pandis, 2009;Jathar et al., 2011).

Robinson et al. (2007) proposed a method (Robinson-2007) for NT-SOA formation in which POC vapors react with the hydroxyl radical (OH) to form products that were one order of magnitude lower in volatility than their precursor. Pye and Seinfeld (2010) proposed a single-step mechanism for SVOCs where the products of oxidation were two orders of magnitude lower

in volatility than the precursor and used SOA-yield data for naphthalene as a surrogate for all IVOCs. Both methods have been implemented in plume, regional and global chemical transport models and are known to close large gaps between observed and predicted SOA concentrations (Shrivastava et al., 2008;Tsimpidi et al., 2009;Dzepina et al., 2010;Pye and Seinfeld, 2010;Jathar et al., 2011).

However, there are several shortcomings with existing methods to model NT-SOA formation. First, the parameters for those methods were based on very limited or no experimental data. For example, the parameters in Robinson et al. (2007) for SVOCs/IVOCs and Pye and Seinfeld (2010) for SVOCs have not been constrained using any laboratory data. Shrivastava et al. (2008) later showed that the parameters used in Robinson et al. (2007) were able to reasonably predict the measured SOA formation from diesel exhaust; it has been assumed that the diesel exhaust parameters can be used to model all emissions (fossil fuel, bio fuel and biomass burning) (Shrivastava et al., 2008;Jathar et al., 2011). Further, Pye and Seinfeld (2010) used naphthalene as a surrogate for IVOCs even when IVOC UCM is thought to be mainly composed of branched and cyclic alkanes (Robinson et al., 2007;Robinson et al., 2010). Second, both methods assumed that each oxidation reaction reduces the volatility of the precursor by one to two orders of magnitude, which is much less than that required to make SOA from VOCs (Kroll and Seinfeld, 2008). Third, the IVOC emissions were not directly measured. For the Robinson-2007 method they were estimated by scaling POA based on the work of Schauer et al. (1999, 2001, 2002); for the Pye and Seinfeld (2010) method they were estimated by scaling naphthalene emissions.

In this paper, we present a new method (Hybrid method) to represent NT-SOA formation from POC vapors. First we present the theoretical framework which is based on the volatility

basis set approach (Donahue et al., 2006) and the work of Pankow (1994) and Odum et al. (1996). Next, the Hybrid method is applied to SOA data from smog chamber experiments conducted on diluted aircraft exhaust. A limitation of smog chamber experiments is that it only captures the atmospheric evolution of the first few generations of oxidation of the precursors and its immediate products. Therefore, we focus on the SOA production from only the first generation of oxidation. Although this work focuses on aircraft exhaust, the techniques described can be applied to develop parameterizations for NT-SOA formation from other combustion sources.

3.2 SOA model formulation

The modeling of both T-SOA and NT-SOA is based on the approach of Pankow (1994) and Odum et al. (1996), which parameterizes smog chamber SOA data using a set of semi-volatile surrogate products. The amount of SOA is defined by the gas-particle partitioning of these surrogate products. While Odum et al. (1996) represented SOA with two surrogate products, more recently, researchers (Hildebrandt et al., 2009;Shakya and Griffin, 2010) have used four or more surrogates expressed using the volatility basis set (VBS) (Donahue et al., 2006). The VBS (Donahue et al., 2006) separates low-volatility organics into logarithmically spaced bins of effective saturation concentration (C*) between 0.01 to 10^7 μg m^{-3} at 298 K. C* (inverse of the Pankow-type partitioning coefficient, K_p) is proportional to the saturation vapor pressure; it is a semi-empirical property that describes the gas-particle partitioning of an organic mixture (Pankow, 1994). The gas-particle partitioning is calculated using absorptive partitioning theory:

$$\zeta_i = \left(1 + \frac{C_i^*}{C_{OA}}\right)^{-1}$$
$$C_{OA} = \sum_{i=1}^{N} \zeta_i \times M_i\big|_{g+p} \qquad (3.1)$$

where, ζ_i is the fraction of mass in volatility bin 'i' in the particulate phase, C_i* is the effective saturation concentration of bin 'i' in μg m^{-3}, C_{OA} is the total particulate OA concentration in μg m^{-3}, $M_i|_{g+p}$ is the total organic concentration (gas+particle) in bin 'i' in μg m^{-3} and N is the number of basis set bins. The volatility basis set (VBS) is used to track the concentration of all low-volatility organics (SOA and POC). Although both the SOA formation and POC can be tracked using single basis set, for this work we use three separate basis sets to separately track different types of material. One VBS tracks the traditional SOA produced from the oxidation of speciated VOC precursors. A second tracks the fresh, unoxidized POC and a third tracks the SOA produced from the oxidation of POC.

T-SOA has traditionally been modeled using a distribution of first-generation, non-reactive surrogate products that were much lower in volatility than their precursor. More recently, multi-generational oxidation of the first-generation products was considered (Lane et al., 2008). Previous work has modeled NT-SOA formation from POC emissions with a simple, volatility-based multi-generational oxidation scheme (Robinson-2007) (Robinson et al., 2007;Shrivastava et al., 2008;Jathar et al., 2011). However, there are two potential shortcomings with this approach for NT-SOA. First, the Robinson-2007 parameterization assumes that each oxidation reaction only reduces the volatility of the precursor by one order of magnitude. However, oxidation reactions form a variety of products with different volatilities; for example the addition of a carbonyl, alcohol, nitrate or acid group creates a product with a volatility approximately 1, 3, 3 or 4 orders of magnitude lower than the precursor (Kroll and Seinfeld,

2008). Therefore, a more realistic NT-SOA parameterization would distribute the products over a set of volatility bins, with some of the bins having much lower volatility than the precursor species (similar to T-SOA models). Second, the Robinson-2007 parameterization assumes the same reduction in volatility for each generation of oxidation. Recent experiments indicate that the reduction in volatility due to oxidation reactions changes as the molecules become more oxygenated and fragmentation (carbon-carbon scission) becomes important (Chacon-Madrid et al., 2010;Chacon-Madrid and Donahue, 2011;Kroll et al., 2011).

To address these shortcomings, we propose that the first generation of NT-SOA production from the oxidation of POCs be treated similar to T-SOA (with precursor specific parameters) and that multi-generational oxidation be treated the same for all SOA. We call this the Hybrid approach, which enables a single, unified framework to be used to model both T-SOA and NT-SOA. We first describe that framework and then its application to develop parameterizations for NT-SOA formation.

The framework can be represented using the following equations:

$$\frac{d[X_j]}{dt} = -k_{Ox,X_j}[Ox][X_j] \quad (3.2)$$

$$\frac{d[M_i|_{g+p}]}{dt} = \underbrace{\sum_j \alpha_{i,j} k_{Ox,X_j}[Ox][X_j]}_{first-generation\ products} + \underbrace{\underbrace{\sum_k^N \beta_{i,k} k_{Ox,M_k}[Ox][M_k|_g]}_{production} - \underbrace{k_{Ox,M_i}[Ox][M_i|_g]}_{loss}}_{multi-generational\ oxidation} \quad (3.3)$$

Equation (3.2) represents the first-generation oxidation of SOA precursors (speciated VOC or POC) where $k_{Ox,Xj}$ is the reaction rate between the oxidant *[Ox]* and SOA precursor [X_j]. The index *j* indicates different precursors, either speciated VOC precursors or volatility bins of the POC distribution. Equation (3.3) tracks the secondary organic material in each VBS bin '*i*'. $M_i|_{g+p}$ is the total gas+particle organic mass in the '*i*'th bin of the VBS; its gas-particle

partitioning is calculated using equation (3.1). The first term in equation (3.3) represents the first-generation products formed in 'i'th bin as a result of the precursor oxidation where $\alpha_{i,j}$ is the mass yield for the first-generation oxidation reaction. The second and third terms in equation (3.3) account for the evolution of material in the VBS due to multi-generational oxidation where we assume that only vapors in the VBS ($M|_g$) react. $\beta_{k,i}$ is the mass yield from multi-generational oxidation reactions in bin 'k' and $k_{Ox,M}$ is the oxidation rate of vapors in the VBS.

To interpret smog chamber data, the framework (equations 3.1-3.3) is implemented in a box model that is comprised of two modules: a T-SOA and a NT-SOA module, both of which are described below. The T-SOA module is based on a standard SOA model (Pankow, 1994;Odum et al., 1996); it uses the speciated VOC emissions and oxidant data to predict the amount of T-SOA that is formed. In the NT-SOA module, the amount of NT-SOA formed is first estimated by subtracting off the predicted T-SOA from the measured SOA. Then, the parameters in equations (3.1-3.3) are determined by fitting the NT-SOA data.

Defining the NT-SOA by difference effectively assumes that the T-SOA module is correct. However, published yields for T-SOA precursors (e.g. toluene) vary by more than a factor of two (Ng et al., 2007;Lane et al., 2008;Hildebrandt et al., 2009). As discussed below, the T-SOA model used for this work is based on upper end of the published data and therefore the difference approach may systematically underestimate NT-SOA.

3.2.1 Traditional SOA (T-SOA)

We define T-SOA as the SOA mass formed through the oxidation of speciated VOC precursors. To simulate T-SOA, X_j in equation (3.2) represents an individual precursor (e.g. benzene, toluene, n-dodecane, or cyclohexane) and OH is assumed to be the only oxidant. We

use the SAPRC 2007 lumping and the mass-yields ($\alpha_{i,j}$ in equation 3.2) proposed by Murphy and Pandis (2010) for all the speciated VOC precursors listed in Table 3.2. The mass yields are at the high end of those reported in the literature; therefore the T-SOA prediction is an upper bound estimate, which, in turn, results in a lower bound estimate for NT-SOA. The lumping and parameters ($k_{Ox,Xj}$ and $\alpha_{i,j}$) for the T-SOA model are provided in Tables S.1 and S.2 (supplementary material). Figure 3.1(a) shows a schematic for the T-SOA model.

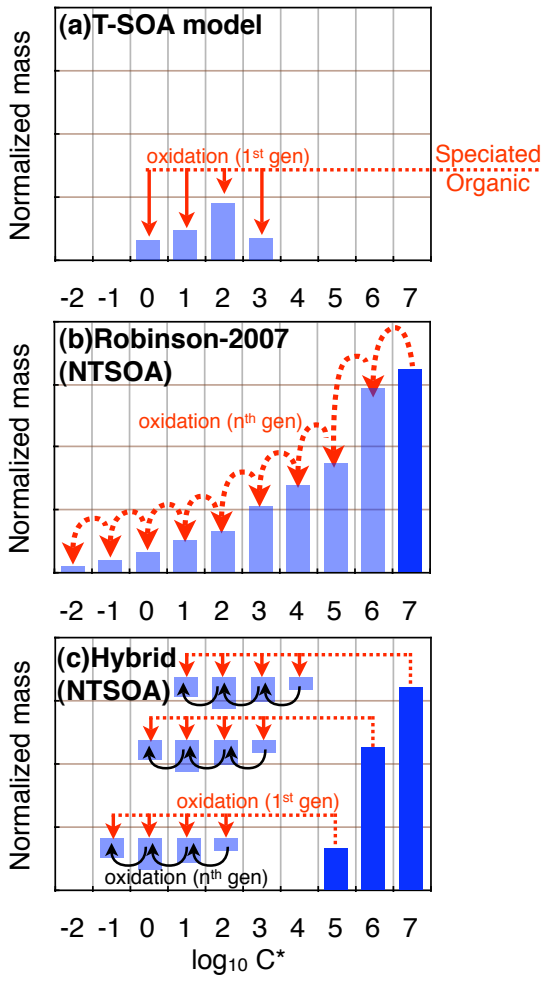

Figure 3.1: Schematics that demonstrate the SOA mechanism for the T-SOA model, Robinson-2007 method and Hybrid method.

To treat multi-generational oxidation of T-SOA, we use the parameterizations recently applied to anthropogenic SOA in regional and global models (Shrivastava et al., 2008;Murphy

and Pandis, 2009;Murphy and Pandis, 2010;Farina et al., 2010;Jathar et al., 2011). Gas-phase mass of the T-SOA products reacts with the OH radical ($k_{Ox,M}$ = 1 x 10^{-11} cm^3 $molecules^{-1}$ s^{-1}) to form a product that is one order of magnitude lower in volatility than the precursor or shifted by one C^* bin relative to the precursor. To account for the addition of oxygen, 7.5% of the precursor's mass is added to the product. Hence, for T-SOA, the $\beta_{i,k}$ in equation (3.3) takes the form:

$$\beta_{i,k} = \begin{cases} +1.075 & if\ k = i+1; \\ 0 & otherwise \end{cases} \quad (3.4)$$

3.2.2 Non-traditional SOA (NT-SOA)

NT-SOA is defined as the SOA mass formed through the oxidation of POC vapors. The mass of NT-SOA is the difference between the measured SOA and the predicted T-SOA. In this section, we present two different approaches to parameterize the NT-SOA formation using the VBS framework (equations 3.1-3.3). The methods differ in whether and how they account for first-generation oxidation and ongoing multi-generational oxidation (see Figure 3.1(b) and (c)).

Robinson-2007 method

Robinson et al. (2007) proposed a simple method to model NT-SOA formation, which uses a single oxidation kernel for all POC oxidation reactions. This method omits a detailed description of the volatility distribution of first-generation products and instead includes only a simple, multi-generational oxidation scheme. The scheme is shown schematically in Figure 3.1(b).

The simplest way to implement this scheme is to place the volatility-resolved POC precursor mass (X_j) directly into the corresponding VBS (M_i) and eliminating equation (3.2) and

the first term in equation (3.3). Similar to the treatment of multi-generational oxidation for T-SOA (Lane et al., 2008), any gas-phase mass in the VBS is reacted with the OH radical to form a product that is in a lower volatility bin than its precursor. For NT-SOA (Robinson-2007), $\beta_{i,k}$ takes the form:

$$\beta_{i,k} = \begin{cases} +(1 + f_{oxy}) & if\ k = i + q; \\ 0 & otherwise \end{cases} \quad (3.5)$$

where, q is the shift in volatility for the product and f_{oxy} is the fraction of oxygen added to the product per reaction.

To simulate NT-SOA formation using the Robinson-2007 method, one must define $k_{Ox,M}$, f_{oxy} and q. Robinson et al. (2007) and Shrivastava et al. (2008) used a $k_{Ox,M}$ of 4 x 10^{-11} cm^3 $molecules^{-1}$ s^{-1}, a f_{oxy} of 0.*075* and a q of *1* based on SOA data for diesel exhaust. Grieshop et al. (2009a) proposed a $k_{OH,M}$ of 4 x 10^{-11} cm^3 $molecules^{-1}$ s^{-1}, a f_{oxy} of 0.*40* a q of *2* based on SOA data for dilute woodsmoke. Dzepina et al. (2009, 2010) and Hodzic et al. (2010) have applied these parameterizations to simulate SOA formation over Mexico City. In addition to evaluating the previously proposed sets of $k_{OH,M}$, f_{oxy} and q values, we also fit the NT-SOA data to determine an optimum set of values for these parameters.

Hybrid method

The Hybrid method is similar to the previously discussed T-SOA model. The first-generation of NT-SOA formation is parameterized by fitting equations (3.1-3.3) to smog chamber data. A generic multigenerational aging scheme is then used for subsequent generations of oxidation. The allows for a more physically realistic treatment of the first-generation oxidation that better represents known effects of photochemical aging on volatility. The Hybrid scheme is shown schematically in Figure 3.1(c).

In the Hybrid scheme, for the first generation of oxidation, the volatility-resolved POC emissions are treated as precursors or as X_j in equation (3.2) and are assumed to react only with the OH radical. We assume that $k_{Ox,Xj}$ is 4 x 10^{-11} cm^3 $molecules^{-1}$ s^{-1} for POCs with a C* < 10^4 $\mu g\ m^{-3}$ and 3x10^{-11} cm^3 $molecules^{-1}$ s^{-1} for POCs with a C* ≥ 10^4 $\mu g\ m^{-3}$ based on reactivity data for alkanes in these volatility ranges (C_{12+} iso-alkanes, C_{10+} cycloalkanes, multi-ring aromatics) (Atkinson and Arey, 2003).

The mass-yield matrix ($\alpha_{i,j}$ in equation 3.3) for the Hybrid method is derived by fitting the NT-SOA data. Since there are ten precursors (C* = 0.01 to 10^7 $\mu g\ m^{-3}$; Table 3.2) and each precursor's products are fit across 4 VBS bins, the Hybrid method potentially requires 40 free parameters (many more than can be constrained with the data). Presto et al. (2010), following the work of Lim and Ziemann (2009), found that for *n*-alkanes, the addition of 2 carbon atoms to an *n*-alkane shifted its corresponding SOA product distribution, on average, by one C* bin or one order of magnitude in C* space. Therefore, we assume the same product distribution arising from each POC precursor, but shifted in volatility space by one order of magnitude. This approach reduces the number of free parameters to four. For instance, if [a_1 b_1 c_1 d_1] represents the mass yield for the precursor C* = 10^6 $\mu g\ m^{-3}$ across C* bins [1 10 100 1000] ($\mu g\ m^{-3}$), the mass-yield matrix $\alpha_{i,j}$ would take the form,

$$\alpha_{i,j} =$$

Precursors: $C^*=10^{-2}$	$C^*=10^{-1}$	$C^*=10^{0}$	$C^*=10^{1}$	$C^*=10^{2}$	$C^*=10^{3}$	$C^*=10^{4}$	$C^*=10^{5}$	$C^*=10^{6}$	$C^*=10^{7}$	Products
a_1	-	-	-	-	-	-	-	-	-	$C^*=10^{-8}$
b_1	a_1	-	-	-	-	-	-	-	-	$C^*=10^{-7}$
c_1	b_1	a_1	-	-	-	-	-	-	-	$C^*=10^{-6}$
d_1	c_1	b_1	a_1	-	-	-	-	-	-	$C^*=10^{-5}$
-	d_1	c_1	b_1	a_1	-	-	-	-	-	$C^*=10^{-4}$
-	-	d_1	c_1	b_1	a_1	-	-	-	-	$C^*=10^{-3}$
-	-	-	d_1	c_1	b_1	a_1	-	-	-	$C^*=10^{-2}$
-	-	-	-	d_1	c_1	b_1	a_1	-	-	$C^*=10^{-1}$
-	-	-	-	-	d_1	c_1	b_1	a_1	-	$C^*=10^{0}$
-	-	-	-	-	-	d_1	c_1	b_1	a_1	$C^*=10^{1}$
-	-	-	-	-	-	-	d_1	c_1	b_1	$C^*=10^{2}$
-	-	-	-	-	-	-	-	d_1	c_1	$C^*=10^{3}$
-	-	-	-	-	-	-	-	-	d_1	$C^*=10^{4}$

(6)

For multi-generational oxidation, we use the same set of parameters used to model the multi-generational oxidation of T-SOA (equation 3.4).

3.3 Experimental data

3.3.1 Overview of experimental methods

The SOA modeling is performed on data from smog chamber experiments conducted on diluted emissions from two different gas-turbine aircraft engines. Here, we provide a brief overview of both field campaigns; further details can be found in Miracolo et al. (2011), Presto et al. (2011), Miracolo et al. (submitted) and Drozd et al. (in prep). The first study investigated SOA formation from dilute emissions from a CFM56-2B gas turbine engine operating on Jet Propellant – 8 (JP8) fuel (Presto et al., 2011;Miracolo et al., 2011) at four different engine loads (4% - ground idle, 7% - idle/taxing, 30% - landing and 85% - takeoff). In the second study, experiments were conducted on dilute emissions from a T63 gas turboshaft engine operating on

JP8, Fischer-Tropsch (FT) and JP8/FT 50:50 blend fuels at idle and cruise loads. On a mass-basis, JP8 consists of 53% straight/cyclic alkanes, 30% branched alkanes and 17% aromatics while FT consists of 88% branched alkanes and 12% cyclic alkanes. The experiments used in this work are listed in Table 3.1, including the naming convention used in the paper.

Table 3.1: List of smog chamber experiments conducted at the 171st Air Refueling Wing in Pittsburgh and Wright-Patterson Air Force Base.

Number	Experiment Name	Engine	Load	Fuel
1	CFM56-JP8-Idle(1)	CFM56-2B	4%	JP8
2	CFM56-JP8-Idle(2)	CFM56-2B	4%	JP8
3	CFM56-JP8-Idle(3)	CFM56-2B	4%	JP8
4	CFM56-JP8-Taxi	CFM56-2B	7%	JP8
5	CFM56-JP8-Landing	CFM56-2B	30%	JP8
6	CFM56-JP8-Takeoff	CFM56-2B	85%	JP8
7	T63-JP8-Idle	T63	Idle	JP8
8	T63-FT-Idle(1)	T63	Idle	FT
9	T63-FT-Idle(2)	T63	Idle	FT
10	T63-Blend-Idle	T63	Idle	JP8:FT Blend
11	T63-JP8-Cruise	T63	Cruise	JP8
12	T63-FT-Cruise	T63	Cruise	FT

Briefly, the experiments involved collecting emissions from about 1-m downstream of the engine exit plane and then transferring them through a heated transfer line into a portable Teflon smog chamber. The emissions were diluted with clean (HEPA- and activated-carbon filter) air to achieve concentration levels in the chamber that were representative of those typically found roughly 100-m downstream of the engine exit plane. The concentrations correspond to a dilution ratio of 50 to 200. To initiate photo-oxidation, the chamber was exposed to natural or artificial sunlight; a suite of instruments tracked the evolution of the gas- and particle-phase pollutants.

We are aware that experimental uncertainty could affect the quality of data from smog chamber experiments and therefore the conclusions from our analysis. The experimental uncertainty can be thought of as that associated with measurements, repeatability and atmospheric relevance. Of the three, the uncertainty in measurements is probably the lowest as the instruments and techniques used to characterize smog chamber data have evolved over the past two decades. In this work, measurement uncertainties are quantified and wherever possible, included in our analysis. Particularly for experiments used in this work, there is slightly more uncertainty associated with repeatability partly because it is too expensive to repeat every experiment and partly because there might be factors that have a larger than anticipated effect on the experiment (ambient temperature, relative humidity, VOC/NOx ratio). The uncertainty was kept to a minimum by undertaking tasks such as cleaning the chamber for 12 hours before use, ensuring a minimum background concentration and running a blank experiment. But the largest uncertainty results from whether our static and controlled experiments are truly representative of the dynamic processes in the atmosphere. Atmospheric relevance was ensured by diluting the emissions and maintaining VOC/NOx ratios to those found in the atmosphere and in some cases exposing the chamber to natural sunlight than artificial UV light.

3.3.2 Overview of PM and SOA data

Figure 3.2 compiles the primary (black carbon and primary organic aerosol or POA) and secondary PM (sulfate and SOA) data from the two field campaigns. Details can be found in Miracolo et al. (2011, 2012). The secondary PM data were measured after three to four hours of oxidation inside the smog chamber. The sum of the measured primary PM emissions and secondary PM formation spans two orders of magnitude (60-3300 mg kg-fuel^{-1}) and is a strong function of the engine type, load and fuel. These variations are discussed in detail in companion

publications (Presto et al., 2011;Miracolo et al., 2011;Miracolo et al., submitted;Presto et al., submitted;Drozd et al., in prep); here the focus is on modeling the SOA formation measured in the smog chamber. Briefly, at the end of every experiment, the wall-loss corrected secondary PM formation exceeded the direct primary PM emissions, by as much as a factor of 75. Further, SOA accounts for more than half of the secondary PM mass (remainder is sulfate) except for in the CFM56-JP8-takeoff and T63-FT-cruise experiments and more than three quarters of the PM mass in the idle experiments. On average, the T63 engine had higher emissions and higher secondary PM formation than the CFM56 engine. Both the SOA formation and precursor emissions decrease substantially with increasing engine load, i.e. idle vs. takeoff and idle vs. cruise.

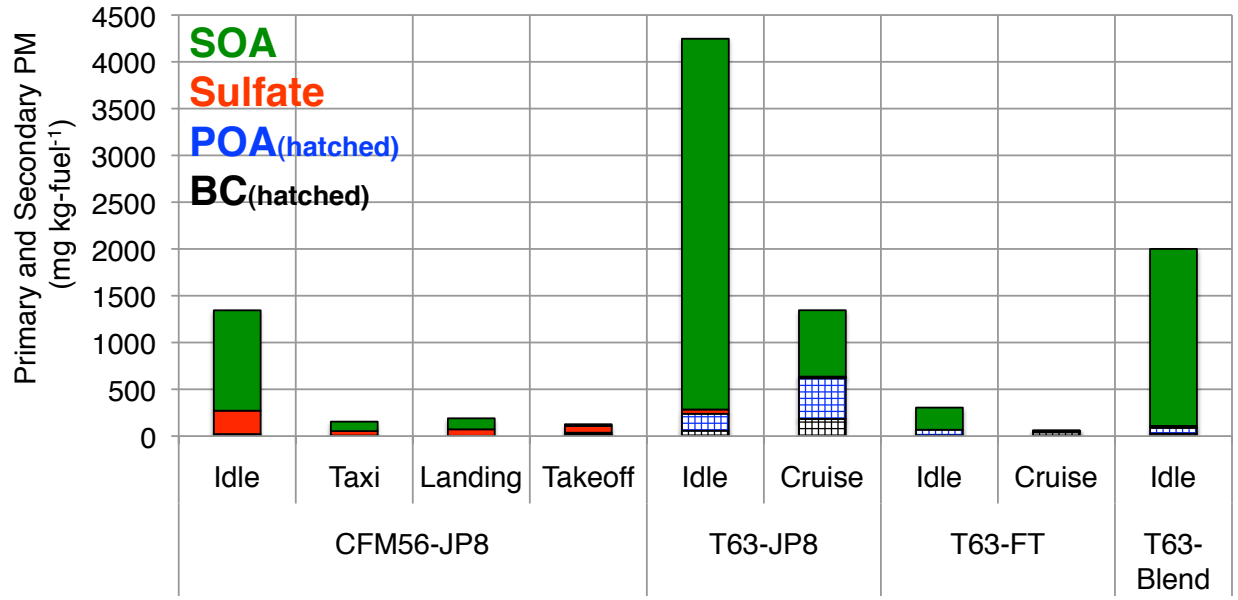

Figure 3.2: Average black carbon, POA, sulfate and SOA from aircraft exhaust across the two field campaigns. CFM56 and T63 are gas turbine engines. JP8 is a petroleum-based aviation fuel, FT is a Fischer-Tropsch fuel derived from coal and Blend is a 50:50 JP8:FT mixture. The results for CFM56-JP8-Idle are the average of three independent experiments and the results for T63-JP8-Idle are the average of two independent experiments. For the repeat experiments, we do not see a large experiment-to-experiment variability. We did not perform a cruise experiment for T63-Blend.

3.3.3 Measured SOA precursors

Simulating SOA formation requires detailed information on SOA precursor concentrations. Table 3.2 reports VOC and POC (IVOC and SVOC) emissions data for the different experiments. The VOC data were measured using SUMMA canisters and analyzed using a GC-MS (Presto et al., 2011). VOC measurements were only made for one of three CFM56-JP8-Idle experiments and the measured VOC emission profile was applied to the other two experiments. For the CFM56-JP8-Taxi and CFM56-JP8-Landing experiments, only a small number of VOCs were measured (Presto et al., 2011) and therefore we estimated emissions of additional VOCs using data from the APEX study (Wey et al., 2006). The VOC emissions at taxi were assumed to be 40% of those at idle and VOC emissions at landing were assumed to be the same as those at takeoff.

Table 3.2: Emission factor (mg kg-fuel^{-1}) for speciated VOCs and POCs for each engine, fuel and engine load.

		CFM56-JP8				T63-JP8		T63-FT		T63-Blend
	Species	**Idle**	**Taxi**	**Landing**	**Takeoff**	**Idle**	**Cruise**	**Idle**	**Cruise**	**Idle**
VOC	1-butene	194.6	58.4	2.2	2.2	388.6	1.2	155.2	1.4	379.3
	1-heptene	61.5	18.5	-	-	0.1	0.0	6.2	0.0	15.0
	1-hexene	81.1	24.3	-	-	-	-	-	-	-
	1-methylcyclohexene	5.2	1.6	-	-	-	-	-	-	-
	1-octene	5.9	1.8	1.2	1.2	-	-	-	-	-
	1-pentene	91.2	27.4	10.8	10.8	79.2	0.0	67.8	0.0	0.0
	1,2-butadiene	6.4	1.9	-	-	1.4	0.0	4.8	0.0	4.7
	1,2-diethylbenzene	10.9	3.3	1.9	1.9	-	-	-	-	-
	1,2,3-trimethylbenzene	47.0	14.1	1.7	1.7	4.1	0.0	10.5	0.0	42.4
	1,2,4-trimethylbenzene	41.9	12.6	7.4	7.4	24.1	0.0	29.7	0.0	155.3
	1,2,4,5-tetramethylbenzene	27.2	8.2	-	-	-	-	-	-	-
	1,3-butadiene	230.3	69.1	-	-	379.0	2.7	75.2	1.3	0.0
	1,3-diethylbenzene	10.2	3.1	1.8	1.8	14.2	1.1	176.4	0.0	162.5
	1,3,5-trimethylbenzene	14.4	4.3	1.0	1.0	15.9	0.0	38.0	0.0	61.8
	1,4-diethylbenzene	46.7	14.0	1.9	1.9	3.6	3.8	73.7	0.0	88.4
	2-ethyltoluene	12.6	3.8	34.2	34.2	15.5	2.8	10.8	0.0	39.7
	2-methyl-1-butene	30.3	9.1	1.0	1.0	50.9	0.0	78.5	0.0	34.5

	2-methyl-1-pentene	10.6	3.2	-	-	5.0	0.0	10.4	0.0	5.3
	2-methyl-2-butene	6.0	1.8	-	-	9.3	0.0	21.2	0.0	31.2
	2-methyl-2-pentene	2.1	0.6	0.6	0.6	-	-	-	-	-
	2-methylheptane	7.1	2.1	-	-	8.6	0.0	5.4	0.0	11.2
	2-methylhexane	6.7	2.0	-	-	29.3	0.0	8.3	0.0	26.1
	2-methylpentane	50.2	15.1	1.0	1.0	-	2.1	11.1	0.0	22.0
	2,2-dimethylbutane	1.5	0.5	-	-	62.7	0.0	19.3	0.0	0.0
	2,3-dimethyl-2-pentene	7.5	2.3	1.0	1.0	14.3	0.0	5.1	0.0	18.7
	2,3-dimethylbutane	2.8	0.8	2.0	2.0	52.4	4.4	15.8	0.0	76.4
	2,3,4-trimethylpentane	5.3	1.6	-	-	8.2	0.0	27.2	0.0	30.8
	2,4-dimethylpentane	-	-	-	-	2.5	0.0	18.8	0.0	24.5
	3-ethyltoluene	15.8	4.7	-	-	8.8	0.5	33.8	0.0	24.5
	3-methyl-1-butene	29.5	8.9	-	-	-	-	-	-	-
	3-methylheptane	5.7	1.7	2.9	2.9	-	0.8	5.8	0.0	5.6
	3-methylhexane	24.5	7.4	-	-	2.5	0.8	9.3	0.0	20.3
	3-methylpentane	12.5	3.8	-	-	4.5	0.0	7.2	0.0	30.7
	4-ethyltoluene	7.7	2.3	3.1	3.1	26.3	0.0	64.4	0.0	85.4
	4-methyl-1-pentene	27.2	8.2	0.7	0.7	-	-	-	-	-
	4-methylheptane	5.6	1.7	1.8	1.8	-	0.0	9.1	0.0	8.9
	a-pinene	6.2	1.9	-	-	16.9	0.8	85.7	0.0	78.6
	acetylene	2858.9	857.7	9.2	9.2	834.9	36.3	839.3	10.9	1080.9
	benzene	232.0	69.6	72.4	72.4	273.2	4.7	123.2	0.7	282.2
	butane	24.8	7.4	29.2	29.2	38.9	0.0	252.3	1.4	366.0
	butylbenzene	8.5	2.6	-	-	5.0	0.5	108.5	0.0	16.9
	c-1,3-dimethylcyclopentane	-	-	-	-	0.7	0.0	11.8	0.0	2.8
	c-2-butene	11.7	3.5	0.9	0.9	14.7	0.5	85.5	1.0	78.9
	c-2-hexene	6.1	1.8	14.4	14.4	17.8	0.0	16.9	0.0	36.7
	c-2-pentene	8.4	2.5	-	-	59.6	0.0	66.9	0.0	45.3
	c-3-hexene	7.2	2.2	-	-	-	-	-	-	-
	cyclohexane	51.9	15.6	-	-	1.5	0.0	57.2	0.0	4.7
	cyclohexene	14.5	4.4	3.7	3.7	4.4	0.0	4.3	0.0	18.2
	cyclopentane	12.6	3.8	1.8	1.8	26.5	0.0	34.1	0.0	18.9
	cyclopentene	95.5	28.7	-	-	1.9	0.0	23.6	0.0	16.0
	cyclopropane	2.9	0.9	-	-	-	-	-	-	-
	decane	2.5	0.8	33.4	33.4	5.3	9.1	173.1	0.0	231.4
	dodecane	108.3	32.5	16.1	16.1	-	-	-	-	-
	ethane	115.5	34.7	83.3	83.3	149.6	26.6	143.7	0.0	158.6
	ethene	77.3	23.2	28.1	28.1	2865.5	49.6	1379.7	8.8	2984.4
	ethylbenzene	3.9	1.2	1.0	1.0	24.1	0.0	59.2	0.0	75.3
	heptane	5.9	1.8	-	-	132.8	0.0	16.3	0.0	114.0

	hexane	15.4	4.6	2.4	2.4	231.9	66.9	26.9	0.0	149.9
	hexylbenzene	16.6	5.0	-	-	-	-	-	-	-
	i-butane	42.7	12.8	42.2	42.2	4.9	0.4	89.5	0.0	0.0
	i-butene	71.7	21.5	5.5	5.5	119.8	0.0	512.3	0.0	425.4
	i-pentane	34.0	10.2	29.9	29.9	0.0	0.0	0.0	0.0	270.7
	isoprene	56.0	16.8	-	-	82.3	0.0	38.6	0.0	5.0
	i-propylbenzene	4.8	1.4	0.8	0.8	8.3	0.0	102.6	0.0	90.5
	limonene/indan	7.9	2.4	-	-	0.0	0.0	0.0	0.0	0.0
	m-xylene	26.4	7.9	1.1	1.1	37.6	0.0	55.5	0.0	7.3
	methylcyclohexane	14.4	4.3	-	-	5.1	0.0	5.8	0.0	15.9
	methylcyclopentane	11.2	3.4	-	-	2.6	0.0	11.8	0.0	14.2
	naphthalene	45.9	13.8	1.6	1.6	-	-	-	-	-
	nonane	36.1	10.8	-	-	112.5	0.0	3.4	0.0	121.3
	o-xylene	5.2	1.6	-	-	24.1	0.0	66.4	0.0	80.9
	octane	7.5	2.3	0.9	0.9	14.9	0.0	3.4	0.0	21.7
	p-xylene	4.8	1.4	3.8	3.8	19.6	1.0	44.4	0.0	95.8
	pentane	12.0	3.6	15.6	15.6	12.3	0.0	60.9	0.0	4.6
	propane	37.4	11.2	32.6	32.6	30.3	0.0	15.5	0.0	13.9
	propene	696.2	208.9	6.3	6.3	1087.8	5.3	1120.6	13.0	1545.6
	propylbenzene	16.6	5.0	1.4	1.4	14.6	0.0	35.3	0.0	38.4
	propyne	72.3	21.7	-	-	84.0	0.7	97.6	0.1	123.3
	sec-butylbenzene	39.4	11.8	1.6	1.6	-	-	-	-	-
	styrene	8.2	2.5	-	-	12.4	0.0	7.5	0.0	24.2
	tetradecane	4.9	1.5	0.9	0.9	-	-	-	-	-
	toluene	84.7	25.4	3.0	3.0	108.5	1.5	34.0	0.3	98.6
	1,3-hexadiene (trans)	6.3	1.9	-	-	7.6	0.0	29.7	0.0	9.1
	t-2-butene	61.0	18.3	4.3	4.3	53.0	1.1	116.8	0.4	108.2
	t-2-hexene	9.5	2.9	-	-	9.9	0.0	13.0	0.0	13.4
	t-2-pentene	15.7	4.7	-	-	102.1	0.0	28.2	0.0	138.4
	tridecane	47.4	14.2	1.9	1.9	-	-	-	-	-
	undecane	93.7	28.1	15.8	15.8	2.2	2.5	45.4	0.0	99.1
POC	$C^* = 10^{-2}$ µg m^{-3}	4.8	1.7	3.2	2.1	31.0	0.3	21.8	3.8	17.6
	$C^* = 10^{-1}$ µg m^{-3}	4.8	2.8	4.4	3.1	48.6	0.5	38.1	6.1	27.6
	$C^* = 10^{0}$ µg m^{-3}	6.4	3.4	4.7	3.8	24.7	0.2	28.7	7.7	18.7
	$C^* = 10^{1}$ µg m^{-3}	4.8	10.6	7.0	4.5	61.8	0.6	76.6	14.0	56.4
	$C^* = 10^{2}$ µg m^{-3}	4.8	23.5	7.0	4.9	85.5	0.8	118.8	3.1	73.6
	$C^* = 10^{3}$ µg m^{-3}	11.2	158.8	16.4	13.4	15.0	0.1	1.8	0.0	8.0
	$C^* = 10^{4}$ µg m^{-3}	25.6	285.1	10.4	8.4	56.2	0.5	9.7	0.0	26.6
	$C^* = 10^{5}$ µg m^{-3}	80.0	34.1	4.0	5.9	984.0	9.4	196.3	12.6	493.3
	$C^* = 10^{6}$ µg m^{-3}	1459.4	39.1	20.0	11.3	4901.3	46.6	3613.6	12.4	3814.1
	$C^* = 10^{7}$ µg m^{-3}	1459.4	0	0	0	4901.3	0	3613.6	0	3814.1

POC emissions were characterized by GC-MS analysis of quartz filter and Tenax TA sorbent tube samples (Presto et al., 2011). Formally, we define POC as the sum of (both speciated and unspeciated) emissions that have a C* lower than or equal to 10^7 μg m^{-3}. Presto et al. (2011) speciated less than 10% of the POC emissions (similar to studies done with other sources (Schauer et al., 1999, 2002)) the remainder was reported as an unresolved complex mixture. To estimate the total mass of POC emissions, Presto et al. (submitted) developed a calibration curve for the UCM mass with fuel and lubricating oil used by the aircraft. The emissions were then distributed into the VBS based on the GC elution time (Presto et al., submitted). Further, they found that the chromatogram for all idle emissions appeared to peak near a C* of 10^6 μg m^{-3} implying that there were considerable emissions of species with a C* greater than 10^6 μg m^{-3} that could not be quantified but were entirely capable of forming SOA. To ensure the inclusion of all low volatility organics that are capable of forming SOA, we assume that the mass of emissions in the C*=10^7 μg m^{-3} bin equals the mass in the C*=10^6 μg m^{-3} bin for all the idle experiments. Table 3.2 reports measured POC emissions as a function of C*.

Figure 3.3 plots the measured SOA and its precursors – POC and VOC– for the different experiments. The VOCs include only those that form SOA based on the SAPRC classification. Apart from the T63-JP8-Cruise experiment, the measured SOA is smaller than the sum of the precursors (POC + VOC). Theoretically, the precursor mass would need to be larger than the SOA mass if we believe that the SOA is a product of gas-phase oxidation of organic emissions. So, it is likely that the precursors in the cruise experiments are mostly oxygenated species and therefore not accounted for in Figure 3.3 because our instrumentation largely targets hydrocarbons and modestly polar species. The POC emissions, on average, are larger than the

speciated SOA precursors and therefore likely to be very important SOA precursors. Most of the POC emissions are IVOCs.

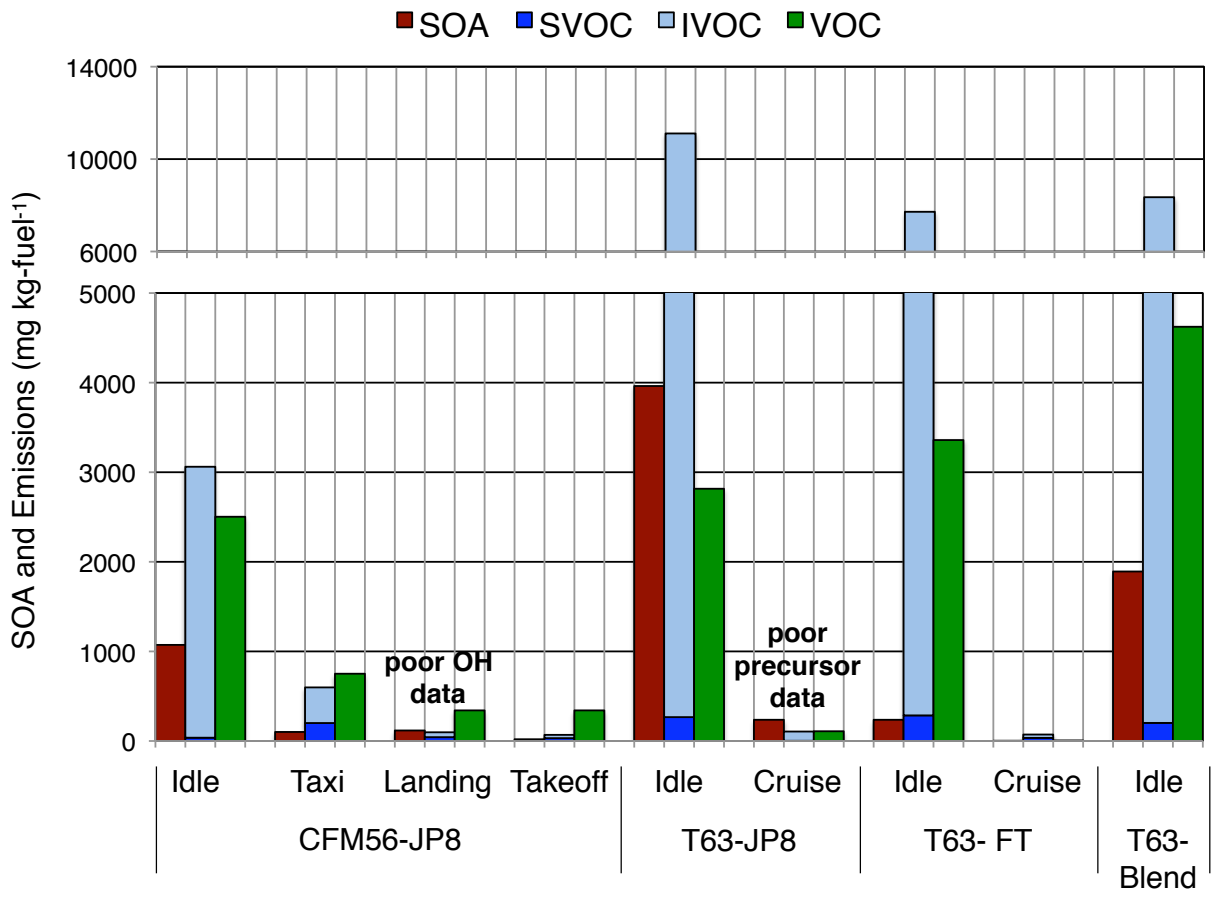

Figure 3.3: Average emission factors for SOA, POC (SVOC and IVOC) and VOC (SOA precursors) across the two field campaigns. The results for T63-JP8-Idle are the average of two independent experiments. We did not perform a cruise experiment for T63-Blend.

3.3.4 Oxidant concentrations

The vast majority of the SOA precursors in aircraft exhaust are saturated species (there are significant unsaturated light VOCs, which do not form SOA); therefore the oxidation chemistry in the smog chamber experiments are largely driven by the hydroxyl radical (OH) and not by ozone. OH concentrations were not directly measured but inferred from the measured decay of organic (e.g. toluene) and inorganic (e.g. SO_2) species. The OH concentration varied with time and was about 10^7 molecules cm^{-3} at the beginning of the experiment and dropped to

10^6 molecules cm^{-3} by the end. For some experiments, we estimated the OH exposure only using high reactivity species ($k_{OH} > 10^{-11}$ cm^3 $molecules^{-1}$ s^{-1}) to reduce uncertainties associated with any bag leakage. Figure S.1 shows the median OH exposure (orange cross) with the standard error of the mean (green bars) calculated for each experiment. The OH exposure ranges from 4 to almost 50 hours of atmospheric oxidation at a typical OH concentration of 10^6 molecules cm^{-3}.

3.4 Results

3.4.1 T-SOA

Model predictions for T-SOA are compared to the measured SOA in Figure 3.4(a). Each point represents a time-averaged value over 100 seconds from an individual experiment. The CFM56 and T63 data are presented in separate panels. The model predicts that aromatics are the most important T-SOA precursors. In order to quantify the model-measurement comparison, we calculate the fractional error:

$$Fractional\ Error = \frac{1}{N}\sum_{i=1}^{N}\frac{|P-M|}{\frac{P+M}{2}} \quad (3.7)$$

where P is the predicted OA, M is the measured OA mass and N is number of data points. Fractional error values are listed in Figure 3.4(a). Except for the CFM56-JP8-Takeoff and T63-FT-Idle experiments, the T-SOA module predicts about half of the measured SOA. We hypothesize that the large unexplained SOA is a direct result of unspeciated POC oxidation and is hereon referred to as NT-SOA.

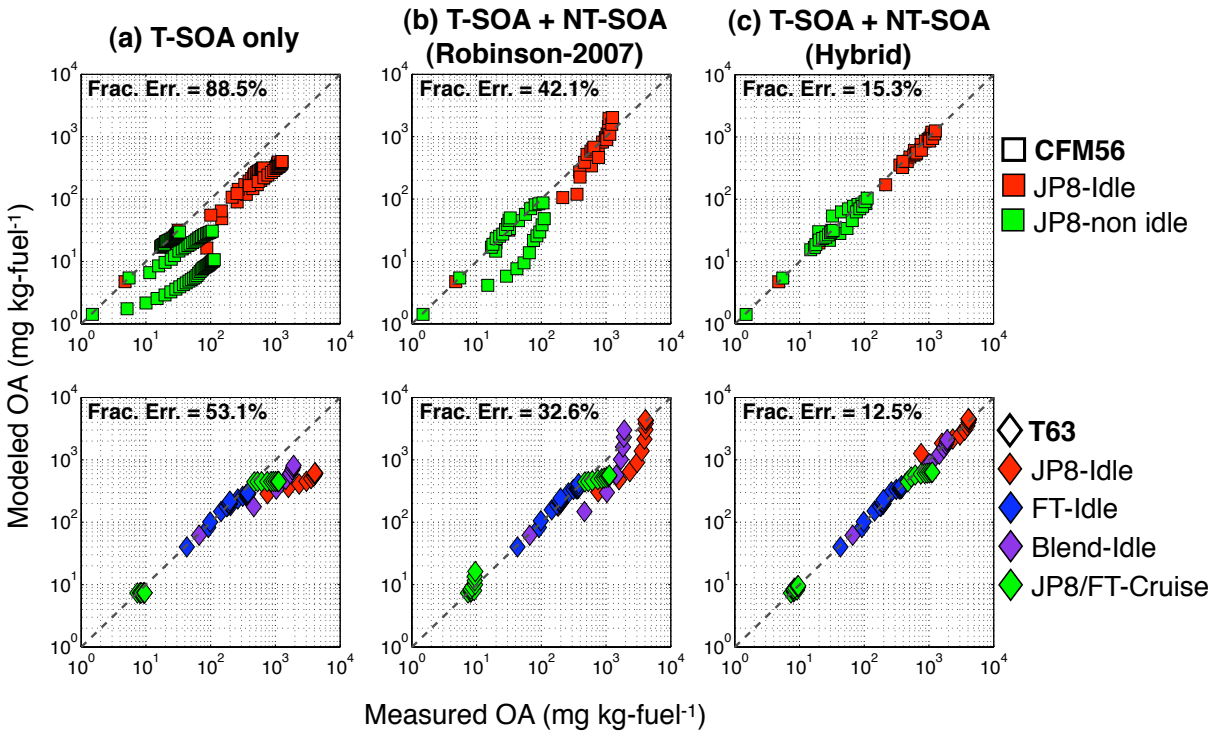

Figure 3.4: Modeled vs measured OA mass for the T-SOA model and two versions of the NT-SOA model (Robinson-2007 and Hybrid). The top row shows experiments done on the CFM56 engine and the bottom row shows experiments done on the T63 engine.

3.4.2 NT-SOA formed versus POC reacted

The NT-SOA is estimated by subtracting the T-SOA prediction from the measured SOA. Except for the T63-FT experiments, NT-SOA accounts for anywhere between 30 and 96% of the SOA measured in the chamber. Although the T-SOA model explains essentially all of the SOA formed in the T63-FT experiments, the mass yields of Murphy and Pandis (2010) are at the high end of those reported in the literature and therefore the T-SOA model may overestimate T-SOA.

Before applying the NT-SOA models, we first evaluate a mass balance between the estimated NT-SOA and the estimated mass of reacted POC. For this calculation, we assume that the POCs with C* < 10^4 μg m^{-3} react with the OH radical with a reactivity of 4 x 10^{-11} cm^3 $molecules^{-1}$ s^{-1} and POCs with C* ≥ 10^4 μg m^{-3} react with the OH radical with a reactivity of 3 x

10^{-11} cm^3 $molecules^{-1}$ s^{-1}. To quantify the mass balance, we calculate an effective NT-SOA yield, which is defined as follows:

$$Effective\ NT-SOA\ Yield = \frac{NT-SOA\ formed}{POC\ reacted} \quad (3.8)$$

Figure 3.5 plots the effective NT-SOA yield as a function of the OA concentration (C_{OA}). There are several important points to make from the plot. First, from a mass balance perspective, the NT-SOA yields are reasonable (i.e. they are less than 1), which means that the amount of NT-SOA formed is less than the amount of POC reacted. Second, the effective NT-SOA yields are similar to published yield data for IVOCs, such as *n*-dodecane and *n*-tridecane (Presto et al., 2010) and large (C_{10+}) branched and cyclic alkanes (Lim and Ziemann, 2009). Figure 3.5 indicates that for the JP8 experiments, the effective NT-SOA yields fall between the measured yields for *n*-dodecane (C_{12}) and *n*-tridecane (C_{13}). This is not surprising since the UCM distribution of both the emissions and unburned fuel peak between C_{11} and C_{15} (Corporan et al., 2011;Presto et al., 2011). Finally more most experiments, the NT-SOA yields increase with increasing C_{OA}, implying that the NT-SOA is semi-volatile, similar to T-SOA formed in smog chamber experiments (Odum et al., 1996).

The effective yields in Figure 3.5 appear to depend on both engine load and fuel composition. First, the idle experiments appear to have higher yields than non-idle experiments. This could be due to differences in precursor composition; the idle POC emissions are comprised of compounds that more efficiently produce SOA than non-idle emissions. If true, then different NT-SOA parameterizations would need to be developed for different engine loads. Alternatively, the higher idle-experiment yields may also be due to partitioning differences (idle experiments were conducted at higher C_{OA}). Second, the NT-SOA yields for JP8-Idle are higher than Blend-Idle which are higher than FT-Idle. Accounting for differences in C_{OA} values, it could be argued

that Blend-Idle yields are an arithmetic average of the JP8-Idle and FT-Idle yields. Miracolo et al. (submitted) showed that the differences in SOA formation between JP8 and FT could mostly be attributed to compositional differences in the fuels. FT is comprised of mainly branched alkanes with low SOA yields versus JP8 which contains much higher yield n-alkanes and aromatics. Therefore, different NT-SOA parameterizations may be needed for different fuel types.

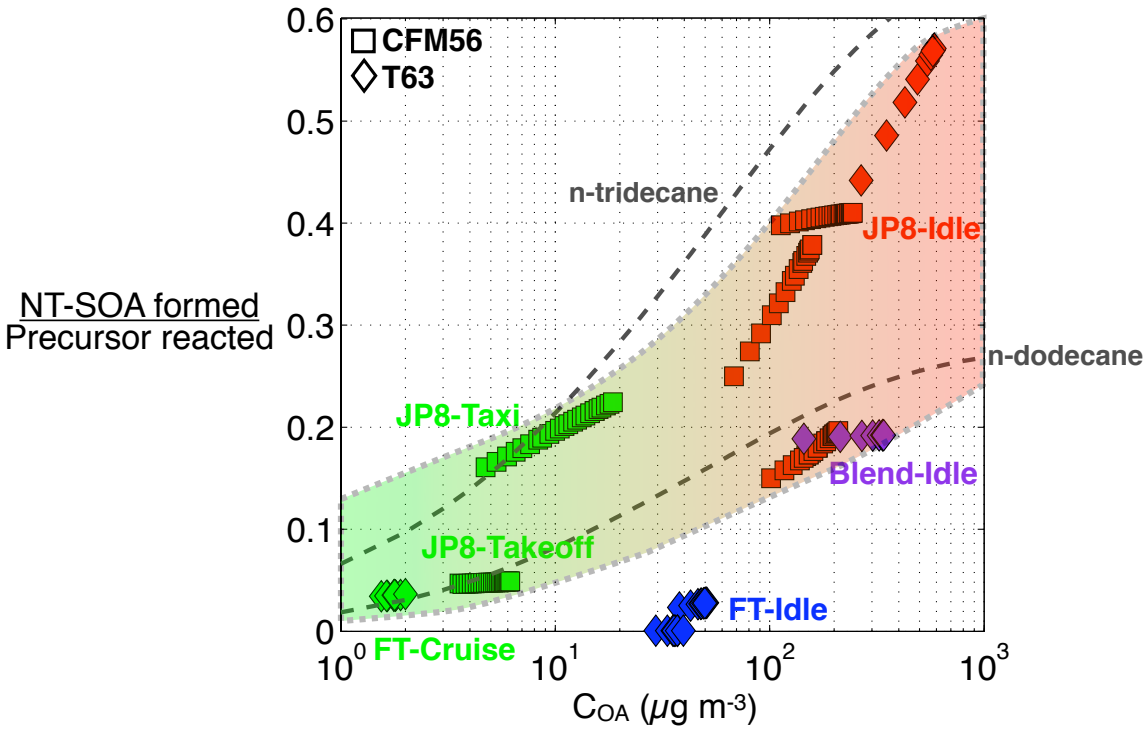

Figure 3.5: NT-SOA yield plotted as a function of COA. For reference, we also include SOA yields for n-dodecane and n-tridecane (dotted grey lines).

3.4.3 Parameterizing NT-SOA formation

In this section we develop parameterizations for NT-SOA formation by fitting the measured SOA production. The goal is to determine an optimum parameter-set for the Robinson-2007 ($k_{OH,M}$, f_{oxy} and q) and Hybrid approaches ($\alpha_{i,j}$; equation 3.5).

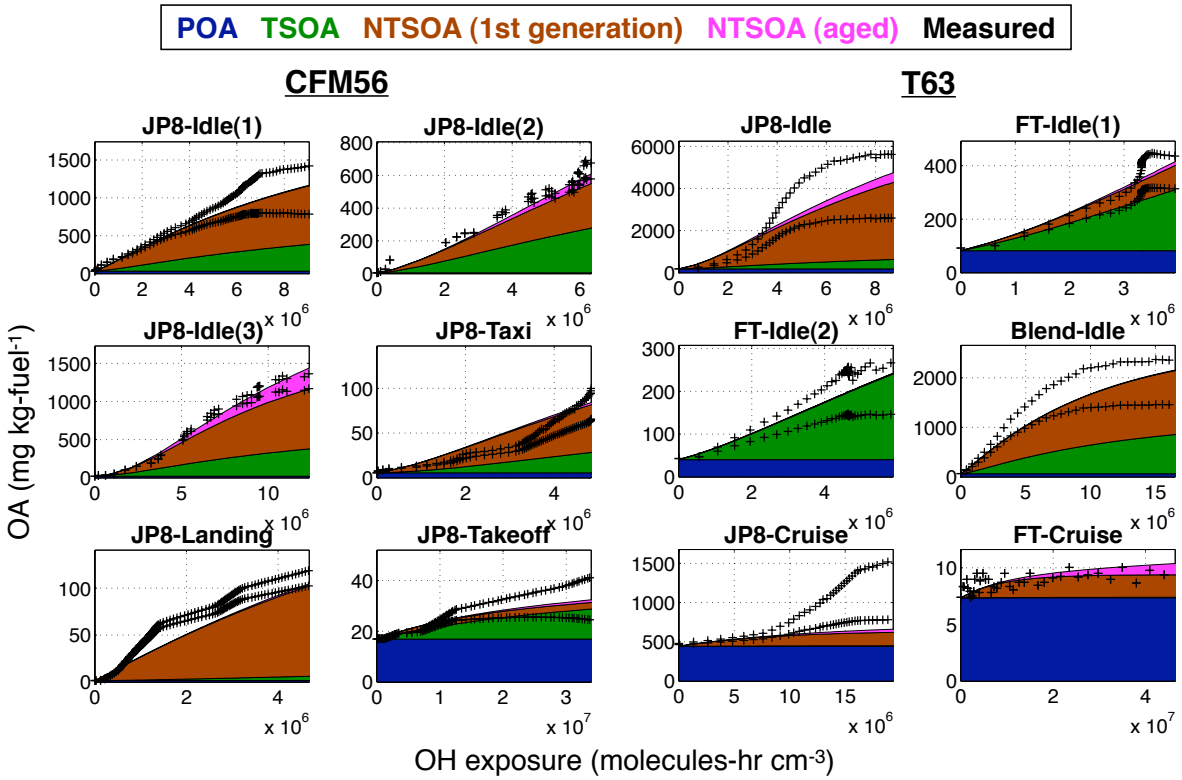

Figure 3.6: Model predictions of OA compared to those measured during the experiment. NT-SOA is predicted using the Hybrid method using best fits for each experiment.

Robinson-2007 method

The Robinson-2007 method, when using the Robinson et al. (2007) and Grieshop et al. (2009) parameter sets, under-predicts the NT-SOA formed during idle-experiments but over-predicts it during non-idle experiments. Therefore, we fit the NT-SOA data to find an optimum parameter set for the Robinson-2007. We considered a wide but realistic range of reaction rates (k_{OH}), fraction of oxygen added to the product per reaction (f_{oxy}) and shift in volatility (q). For k_{OH}, we use a range of 1 to 5 x 10^{-11} cm^3 $molecules^{-1}$ s^{-1} based on Atkinson and Arey (2003). For f_{oxy}, we use a range of 0.05 to 0.4, which corresponds to the addition of 1 to 5 oxygen atoms per generation to a C_{15} alkane. For q, we use a value of either 1 to 2, which corresponds to 1 to 2 orders of magnitude change in the product volatility with each oxidation reaction. Within these

ranges, the optimum set was determined by minimizing the fractional error (equation 3.5) between model predictions and measurements for each experiment.

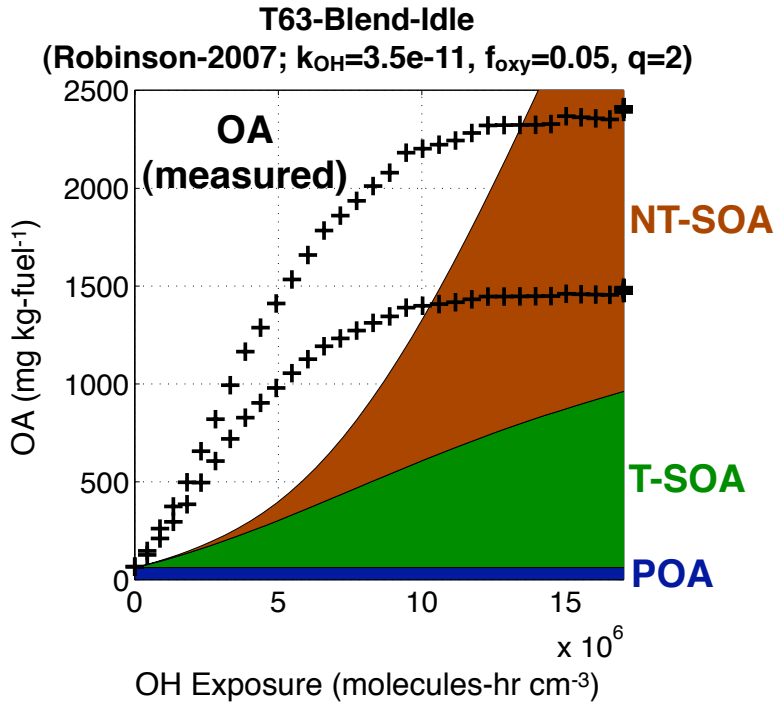

Figure 3.7: Measured OA compared to model predictions using best-fits of the Robinson-2007 method for the T63-Blend-Idle experiment.

For the idle experiments (except for the FT-Idle) an aggressive parameter-set (k_{OH} = 3-5 x 10^{-11} cm^3 $molecules^{-1}$ s^{-1}, f_{oxy} = 0.05-0.4, q = 2) is required to reproduce the SOA data. In comparison, a more modest parameter-set (k_{OH} = 1-3 x 10^{-11} cm^3 $molecules^{-1}$ s^{-1}, f_{oxy} = 0.05-0.3, q = 1) is sufficient to describe the non-idle SOA data. The results are illustrated in Figure 3.4(b), which plots model predictions using the Robinson-2007 method with the best fit for each experiment against the OA measured in the chamber. Compared to predictions from the T-SOA model alone, we see model predictions improve for the CFM56 experiments but only slightly for the T63 experiments. The improvement is quantified by the fractional error values listed in Figure 3.4.

Although an optimum parameter set provides some improvement over the T-SOA model, the Robinson-2007 method cannot reproduce the temporal trend in the data. The measured SOA mass varies linearly or rolls over with OH exposure in the chamber (Figure 3.6). However, the NT-SOA calculated using the Robinson-2007 method shows the opposite trend with little NT-SOA formed initially and significantly more is formed later. This effect is clearly seen for the T63-Blend-Idle case in Figure 3.7. This happens because the Robinson-2007 approach requires several generations of oxidation (a lot of OH exposure) before a large fraction of the products have a C* low enough to partition into the particle phase. The problem is most severe in the idle experiments where almost all of the emissions are IVOCs (Table 3.2). The Robinson-2007 method works for the CFM56-JP8-Taxi and CFM56-JP8-Takeoff experiments primarily because a sizeable fraction of the emissions are already found in lower C* bins (C* = 10^2-10^4 μg m^{-3}; Table 3.2).

The O:C ratio of OA reveals additional problems with the Robinson-2007 method. The O:C of the POA is measured before the oxidation phase of the experiment. For T-SOA, we use the work of Chhabra et al. (2010) to assign the O:C for SOA formed from alkenes and aromatics and the work of Presto et al. (2010) to assign the O:C for SOA formed from alkanes. For NT-SOA, we calculate O:C by explicitly tracking the addition of oxygen per reaction (f_{oxy}). For a few of the experiments, the optimum parameter-set for the Robinson-2007 method predicts a very high O:C ratio (>0.8) of OA. This occurs because precursors have to go through multiple generations of oxidation before they reach a low enough volatility to partition into the particle phase. A consequence of this is that a lot of oxygen is added, with the exact amount depending on the values of f_{oxy} and q. For example, for the optimized parameter-set for the T63-JP8-Idle experiment (k_{OH} = 5 x 10^{-11} cm^3 $molecules^{-1}$ s^{-1}, f_{oxy} = 0.40, q = 2), the O:C of the product would

be close to 1 after only two generations of oxidation versus 0.32 for the measured data. It is clear the Robinson-2007 method with a modest reduction in volatility with each oxidation reaction is unable to reproduce both the temporal dependence of NT-SOA and the O:C of OA.

Hybrid method

We fit the NT-SOA data to determine a set of VBS yields (equation 3.5) for the Hybrid parameterization for each experiment individually. Figure 3.6 plots the time series of measured and predicted OA for each experiment, with the NT-SOA calculated using the best fit for the Hybrid method. The upper and lower bounds of the SOA are presented to indicate experimental uncertainty due to wall-losses (we have not accounted for uncertainty in the T-SOA model). The predicted contribution from the first generation of oxidation of POC is labeled 'NTSOA (1st generation)' and the contribution from multi-generational oxidation is labeled 'NTSOA (aged)'. Figure 3.6 indicates that the multi-generational oxidation -- as defined by equation (3.4) -- contributes negligibly to the SOA mass over the range of oxidant exposures observed in these experiments. Scatter plots of the model versus measurements are shown in Figure 3.4(c). The Hybrid method is able to reproduce the data better than the Robinson-2007 method with significantly lower fractional error.

To compare the Hybrid method fits across different experiments, Figure 3.8 plots the effective NT-SOA yields for select POC precursors as a function of C_{OA} for the JP8 experiments. The effective yield is defined as the SOA formed by each discrete POC precursor divided by the mass of POC precursor reacted. Figure 3.8(a) shows yields for the precursors 10^3 and 10^4 μg m^{-3} and 8(b) shows yields for precursors 10^5, 10^6 and 10^7 μg m^{-3}. For visual clarity, we have excluded points for all POC precursors that contribute less than 15% to the NT-SOA mass. The

lower C* surrogates generally do not contribute much NT-SOA mass because their emissions are either low and/or because very little of their mass exists as vapors and is therefore available for oxidation

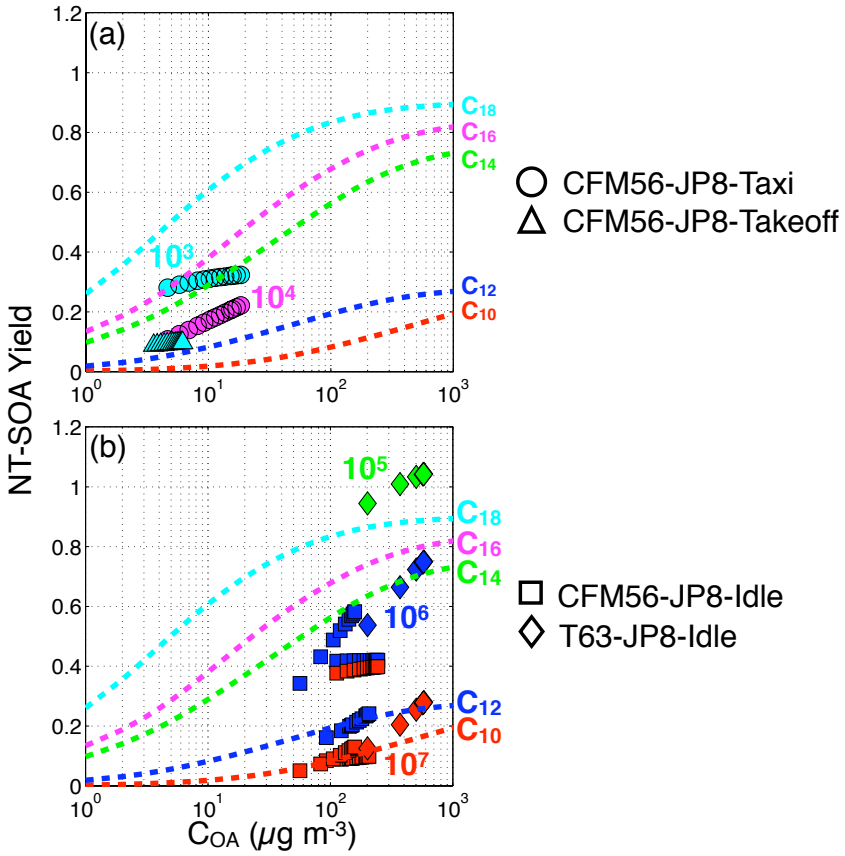

Figure 3.8: SOA yield plotted for POC precursors that contribute more than 15% of NT-SOA mass as a function of COA (symbols). For reference, we also plot SOA yields for n-decane (estimated), n-dodecane, n-tetradecane, n-hexadecane and n-octadecane (estimated) (dotted lines). The different colors connect the symbols to the dotted lines. For example, the SOA yields for the C*=106 µg m-3 bin for all the experiments are plotted with blue squares and the SOA yield for C* equivalent n-dodecane (C12) is plotted with a blue dotted line.

For all of the idle experiments (Figure 3.8(b)), irrespective of the field campaign, almost all of the NT-SOA is produced from oxidation of IVOCs (C* bins: 10^5,10^6 and 10^7 µg m^{-3}). This is expected because 90% of the POC emissions are IVOCs which peak at C*=10^6 µg m^{-3}. These emissions appear to be mostly composed of unburned fuel (Miracolo et al., submitted). In contrast, for the non-idle experiments (Figure 3.8(a)), the NT-SOA arises from less volatile

POCs in 10^3 and 10^4 μg m^{-3} bins. We hypothesize that at higher loads the combustion efficiency is higher and hence the fuel (C* peak of 10^6 or 10^7 μg m^{-3}) might be partially oxidized to form intermediates that have a slightly lower volatility (10^3 or 10^4 μg m^{-3}).

Figure 3.8(a) shows that the effective SOA yields for POCs in the 10^3 and 10^4 μg m^{-3} bins (symbols) are lower than the published yields for *n*-alkanes (Presto et al., 2010) in the same C* range (dashed lines; C_{18} ~ 10^3 μg m^{-3} and C_{16} ~ 10^4 μg m^{-3}). This suggested that the unspeciated POC mass in the 10^3 and 10^4 μg m^{-3} is likely composed of branched and oxygenated compounds which have lower yields than corresponding n-alkanes (Lim and Ziemann, 2009). In comparison, Figure 3.6(b) shows that the SOA yields for POCs in the 10^5, 10^6 and 10^7 μg m^{-3} bins (symbols) are equal or higher than published yields for *n*-alkanes in the same C* range (dashed lines; C_{14} ~ 10^5 μg m^{-3}, C_{12} ~ 10^6 μg m^{-3} and C_{10} ~ 10^7 μg m^{-3}). Therefore, the unspeciated POC mass in the 10^5, 10^6 and 10^7 μg m^{-3} bins is likely composed of cycloalkanes, alkylbenzenes and polycyclic aromatics which have higher yields than n-alkanes (Ng et al., 2007;Hildebrandt et al., 2009). This seems consistent with the emissions in these bins being comprised of unburned fuel when the engine is idling.

3.5 Conclusions and discussion

In this work, we investigated the potential contribution of low-volatility organic vapors to SOA formation from diluted aircraft exhaust. First, we propose that unspeciated low-volatility organic vapors (POC; S/IVOC) are important classes of SOA precursors in aircraft exhaust because speciated VOCs could only account for less than half of the measured SOA. Second, we demonstrated that the method proposed by Robinson et al. (2007) to model NT-SOA formation does not have a large enough volatility shift to reproduce the temporal evolution of the SOA

production. Third, we developed a new method (Hybrid) to model NT-SOA (similar to traditional SOA models) that separated the first generation of oxidation – which was constrained using laboratory data – from future generations of oxidation. To explain the measured data, the first generation of oxidation produces much lower volatility products than the Robinson et al. (2007) approach and therefore provides a realistic representation of chemistry.

In addition to varying with organic aerosol concentration, the NT-SOA yields appear to be a function of both the (a) fuel composition and (b) engine load. This is not surprising since both molecular structure in addition to volatility influences SOA yields (Lim and Ziemann, 2009). For example, the effective NT-SOA yield is highest for JP8 and lowest for FT while the 50:50 blend appears to be an average of JP8 and FT. The JP8 consists mostly of straight/cyclic alkanes (53%) and aromatics (17%), which form more SOA than branched alkanes that mostly constitute FT (88%) (Lim and Ziemann, 2009). The effective NT-SOA yields also appear to be higher for JP8 idle emissions than for JP8 non-idle emissions. Therefore, the NT-SOA yields also appear to depend on engine load, again, presumably due to differences in precursor composition. The idle emissions appear to be comprised of unburned alkanes and aromatic compounds found in the fuel which have higher SOA yields than the non-idle emissions, which appear to be comprised of partially burned fuel. Therefore, different NT-SOA parameterizations may be needed for different fuels and different engine loads.

Table 3.3: VBS yields for POCs for non-idle and idle emissions.

POC C*	Non-Idle Yields					Idle Yields			
	$C^*=10^0$ $\mu g\ m^{-3}$ (a_1)	$C^*=10^1$ $\mu g\ m^{-3}$ (b_1)	$C^*=10^2$ $\mu g\ m^{-3}$ (c_1)	$C^*=10^3$ $\mu g\ m^{-3}$ (d_1)		$C^*=10^0$ $\mu g\ m^{-3}$ (a_1)	$C^*=10^1$ $\mu g\ m^{-3}$ (b_1)	$C^*=10^2$ $\mu g\ m^{-3}$ (c_1)	$C^*=10^3$ $\mu g\ m^{-3}$ (d_1)
10^3 $\mu g\ m^{-3}$	0.000	0.310	1.000	0.000		0.195	0.000	0.863	0.000
10^4 $\mu g\ m^{-3}$	0.000	0.089	1.000	0.000		0.085	0.000	0.994	0.000
10^5 $\mu g\ m^{-3}$	0.000	0.000	0.302	0.000		0.000	0.000	0.938	0.000
10^6 $\mu g\ m^{-3}$	0.000	0.000	0.034	0.000		0.000	0.000	0.601	0.000
10^7 $\mu g\ m^{-3}$	0.000	0.000	0.001	0.000		0.000	0.000	0.370	0.000

Table 3.3 provides Hybrid-parameterizations determined in this work for aircraft emissions. They are suitable for use with the VBS framework in any box, plume, regional or global OA model in conjunction with the emissions data listed in Table 3.2. Although the emissions data are representative of specific engines, emissions data for another gas-turbine engine could be estimated by scaling the emissions (both VOC and POC) using a high-flux species like acetylene, propene or benzene. For different engine loads, we use the JP8 non-idle experiments to determine a mass yield matrix ($\alpha_{i,j}$) for JP8 non-idle emissions and the JP8 idle experiments to determine a mass yield matrix ($\alpha_{i,j}$) for JP8 idle emissions. Figure S.2 indicates reasonable model-measurement comparison when the JP8 non-idle mass yield matrix is used for the JP8 non-idle experiments and JP8 idle mass yield matrix is used for the JP8 idle experiments.

Future research is needed to extend the methods developed here to model SOA formation from other combustion sources.

3.6 Supplementary material

Table S.1: SAPRC07 lumping and reaction rate for each speciated precursor

	Species	**Lumping**	**k_{OH} (cm^3 $molecules^{-1}$ s^{-1})**
VOC	1-butene	OLE1	3.14E-11
	1-heptene	OLE1	3.34E-12
	1-hexene	OLE1	3.70E-11

	1-methylcyclohexene	OLE1	9.64E-12
	1-octene	OLE1	3.70E-11
	1-pentene	OLE1	3.14E-11
	1;2-butadiene	OLE1	2.60E-11
	1;2-diethylbenzene	ARO1	5.80E-12
	1;2;3-trimethylbenzene	ARO2	3.27E-11
	1;2;4-trimethylbenzene	ARO2	3.25E-11
	1;2;4;5-tetramethylbenzene	ARO2	3.25E-11
	1;3-butadiene	OLE2	6.66E-11
	1;3-diethylbenzene	ARO2	3.25E-11
	1;3;5-trimethylbenzene	ARO2	5.67E-11
	1;4-diethylbenzene	ARO2	3.25E-11
	2-ethyltoluene	ARO1	1.18E-11
	2-methyl-1-butene	OLE2	6.10E-11
	2-methyl-1-pentene	OLE2	6.30E-11
	2-methyl-2-butene	OLE2	8.69E-11
	2-methyl-2-pentene	OLE2	8.90E-11
	2-methylheptane	ALK4	4.77E-12
	2-methylhexane	ALK4	4.77E-12
	2-methylpentane	ALK4	5.20E-12
	2;2-dimethylbutane	NONE	2.23E-12
	2;3-dimethyl-2-pentene	OLE2	1.03E-10
	2;3-dimethylbutane	ALK4	5.78E-12
	2;3;4-trimethylpentane	ALK4	6.60E-12
	2;4-dimethylpentane	ALK4	6.75E-12
	3-ethyltoluene	ARO1	1.19E-11
	3-methyl-1-butene	OLE1	3.18E-11
	3-methylheptane	ALK4	5.20E-12
	3-methylhexane	ALK5	8.11E-12
	3-methylpentane	ALK4	5.20E-12
	4-ethyltoluene	ARO2	1.86E-11
	4-methyl-1-pentene	OLE2	6.30E-11
	4-methylheptane	ALK4	5.20E-12
	a-pinene	TERP	5.23E-11
	acetylene	NONE	8.15E-13
	benzene	ARO1	1.22E-12
	butane	NONE	2.36E-12
	butylbenzene	ARO1	4.50E-12
	c-1;3-dimethylcyclopentane	ALK5	9.64E-12
	c-2-butene	OLE2	5.64E-11
	c-2-hexene	OLE1	3.70E-11
	c-2-pentene	OLE2	6.50E-11
	c-3-hexene	OLE1	3.70E-11
	cyclohexane	ALK5	6.97E-12
	cyclohexene	OLE2	6.77E-11

	cyclopentane	ALK4	4.97E-12
	cyclopentene	OLE2	6.70E-11
	cyclopropane	NONE	8.15E-14
	decane	ALK5	1.10E-11
	dodecane	ALK5	1.32E-11
	ethane	NONE	2.48E-13
	ethene	NONE	8.52E-12
	ethylbenzene	ARO1	7.00E-12
	heptane	ALK4	6.76E-12
	hexane	ALK4	5.20E-12
	hexylbenzene	ARO2	1.13E-10
	i-butane	NONE	2.36E-12
	i-butene	OLE1	3.14E-11
	i-pentane	ALK4	3.80E-12
	isoprene	ISOP	1.01E-10
	i-propylbenzene	ARO1	6.30E-12
	limonene	TERP	1.64E-10
	m-xylene	ARO2	2.31E-11
	methylcyclohexane	ALK5	9.64E-12
	methylcyclopentane	ALK4	3.80E-12
	naphthalene	ARO2	2.30E-11
	nonane	ALK5	9.70E-12
	o-xylene	ARO2	1.36E-11
	octane	ALK5	8.11E-12
	p-xylene	ARO2	1.43E-11
	pentane	ALK4	3.80E-12
	propane	NONE	1.09E-12
	propene	NONE	2.63E-11
	propylbenzene	ARO1	5.80E-12
	propyne	NONE	7.13E-12
	sec-butylbenzene	ARO1	5.80E-12
	styrene	ARO2	5.80E-11
	tetradecane	ALK5	1.79E-11
	toluene	ARO1	5.63E-12
	1;3-hexadiene (trans)	OLE2	1.12E-10
	t-2-butene	OLE2	6.40E-11
	t-2-hexene	OLE1	3.70E-11
	t-2-pentene	OLE2	6.70E-11
	tridecane	ALK5	1.51E-11
	undecane	ALK5	1.23E-11

Table S.2: VBS yields for SAPRC07 lumped species

	High Nox (Low Yield)					Low Nox (High Yield)			
	C* (µg/m3)					C* (µg/m3)			
Group	1	10	100	1000		1	10	100	1000
ALK4	0.0000	0.0375	0.0000	0.0000		0.0000	0.0750	0.0000	0.0000
ALK5	0.0000	0.1500	0.0000	0.0000		0.0000	0.3000	0.0000	0.0000
OLE1	0.0008	0.0045	0.0375	0.1500		0.0045	0.0090	0.0600	0.2250
OLE2	0.0030	0.0255	0.0825	0.2700		0.0225	0.0435	0.1290	0.3750
ARO1	0.0107	0.2571	0.4821	0.7500		0.0107	0.2571	0.7500	0.9643
ARO2	0.0015	0.1950	0.3000	0.4350		0.0750	0.3000	0.3750	0.5250
ISOP	0.0003	0.0225	0.0150	0.0000		0.0090	0.0300	0.0150	0.0000
SESQ	0.0750	0.1500	0.7500	0.9000		0.0750	0.1500	0.7500	0.9000
TERP	0.0120	0.1215	0.2010	0.5070		0.1073	0.0918	0.3587	0.6075

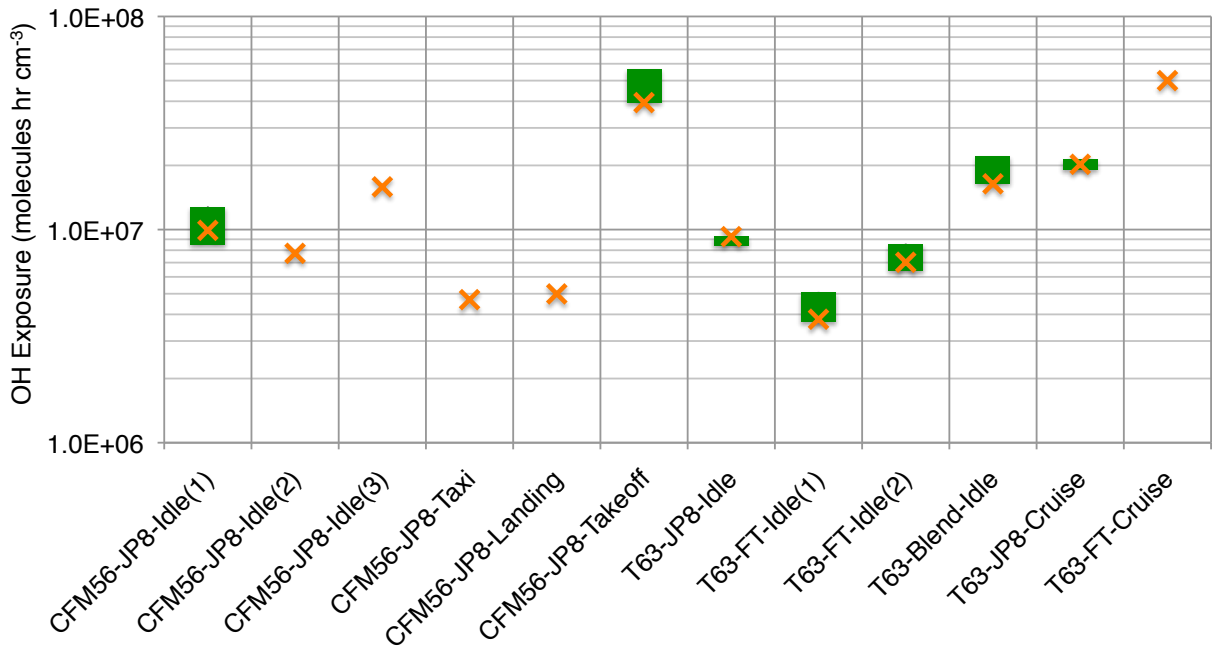

Figure S.1: Interpreted OH exposure range (molecules hr cm-3) for the twelve different experiments. The median value represented using the orange cross is what is used in our analysis.

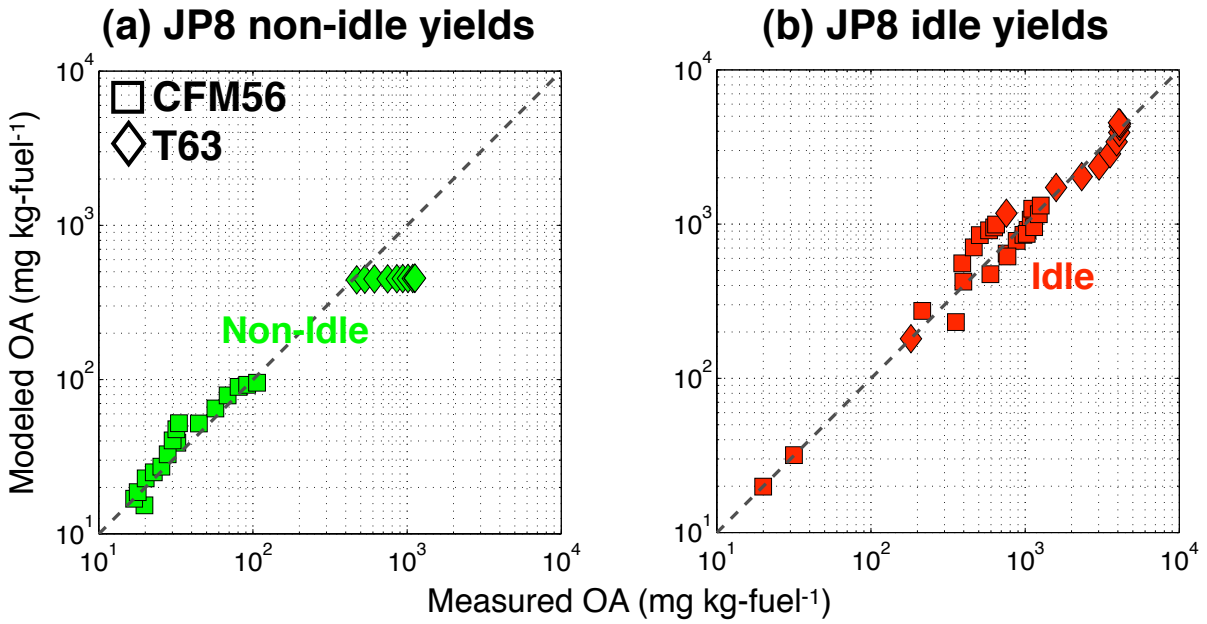

Figure S.2: Model-measurement comparison for the JP8 experiments using (a) NT-SOA yields derived from the non-idle experiments and (b) NT-SOA yields derived from the idle experiments.

3.7 Acknowledgements

Funding was provided by the U.S. Department of Defense Strategic Environmental Research and Development Program (SERDP) under project WP-1626. The views, opinions, and/or findings contained in this chapter are those of the authors and should not be construed as an official position of any of the funding agency.

3.8 References

Atkinson, R., and Arey, J.: Atmospheric degradation of volatile organic compounds, Chem. Rev., 103, 4605-4638, 2003.

Bernstein, J. A., Alexis, N., Barnes, C., Bernstein, I. L., Bernstein, J. A., Nel, A., Peden, D., Diaz-Sanchez, D., Tarlo, S. M., and Williams, P. B.: Health effects of air pollution, The Journal of Allergy and Clinical Immunology, 114, 1116-1123, 2004.

Chacon-Madrid, H., and Donahue, N.: Fragmentation vs. Functionalization: Chemical aging and organic aerosol formation, Atmos. Chem. Phys, 11, 10553-10563, doi:10.5194/acp-11-10553-2011 2011.

Chacon-Madrid, H. J., Presto, A. A., and Donahue, N. M.: Functionalization vs. Fragmentation: N-aldehyde oxidation mechanisms and secondary organic aerosol formation, Phys. Chem. Chem. Phys., 12, doi: 10.1039/c0cp00200c, 2010.

Corporan, E., Edwards, T., Shafer, L., DeWitt, M. J., Klingshirn, C., Zabarnick, S., West, Z., Striebich, R., Graham, J., and Klein, J.: Chemical, thermal stability, seal swell, and emissions studies of alternative jet fuels, Energy & Fuels, 25, 955-966, dx.doi.org/10.1021/ef101520v, 2011.

Donahue, N., Robinson, A., Stanier, C., and Pandis, S.: Coupled partitioning, dilution, and chemical aging of semivolatile organics, Environ. Sci. Technol, 40, 2635-2643, doi:10.1021/es052297c, 2006.

Drozd, G. T., Miracolo, M. A., Presto, A. A., Corporan, E., Lipsky, E. M., and Robinson, A. L.: Particulate and organic vapor emissions from an in-use helicopter engine., in prep.

Dzepina, K., Volkamer, R., Madronich, S., Tulet, P., Ulbrich, I., Zhang, Q., Cappa, C., Ziemann, P., and Jimenez, J.: Evaluation of recently-proposed secondary organic aerosol models for a case study in mexico city, Atmospheric Chemistry and Physics, 9, 5681-5709, doi:10.5194/acp-9-5681-2009, 2009.

Dzepina, K., Cappa, C. D., Volkamer, R. M., Madronich, S., DeCarlo, P. F., Zaveri, R. A., and Jimenez, J. L.: Modeling the multiday evolution and aging of secondary organic aerosol during milagro 2006, Environmental Science & Technology, 45, 3496-3503, doi: 10.1021/es103186f, 2010.

Farina, S. C., Adams, P. J., and Pandis, S. N.: Modeling global secondary organic aerosol formation and processing with the volatility basis set: Implications for anthropogenic secondary organic aerosol, Journal of Geophysical Research, 115, D09202, doi:10.1029/2009JD013046, 2010.

Goldstein, A. H., and Galbally, I. E.: Known and unexplored organic constituents in the earth's atmosphere, Environmental Science & Technology, 41, 1514-1521, doi:10.1021/es072476p, 2007.

Grieshop, A., Donahue, N., and Robinson, A.: Laboratory investigation of photochemical oxidation of organic aerosol from wood fires 2: Analysis of aerosol mass spectrometer data, Atmospheric Chemistry and Physics, 9, 2227-2240, 2009.

Heald, C. L., Jacob, D. J., Park, R. J., Russell, L. M., Huebert, B. J., Seinfeld, J. H., Liao, H., and Weber, R. J.: A large organic aerosol source in the free troposphere missing from current models, Geophys. Res. Lett., 32, doi:10.1029/2005GL023831, 2005.

Hildebrandt, L., Donahue, N., and Pandis, S.: High formation of secondary organic aerosol from the photo-oxidation of toluene, Atmospheric Chemistry and Physics, 9, 2973-2986, doi:10.5194/acp-9-2973-2009, 2009.

Hodzic, A., Jimenez, J., Madronich, S., Canagaratna, M., DeCarlo, P., Kleinman, L., and Fast, J.: Modeling organic aerosols in a megacity: Potential contribution of semi-volatile and intermediate volatility primary organic compounds to secondary organic aerosol formation, Atmospheric Chemistry and Physics, 10, 5491-5514, doi:10.5194/acp-10-5491-2010, 2010.

IPCC, W.: Climate change 2007: The physical science basis, Summary for Policy Makers, Contribution of Working Group I to the Fourth Assessment Report of the Intergovernmental Panel on Climate Change, 2007.

Jathar, S., Farina, S., Robinson, A., and Adams, P.: The influence of semi-volatile and reactive primary emissions on the abundance and properties of global organic aerosol, Atmospheric Chemistry and Physics, 11, 7727-7746, doi:10.5194/acp-11-7727-2011 2011.

Johnson, D., Utembe, S. R., Jenkin, M. E., Derwent, R. G., Hayman, G. D., Alfarra, M. R., Coe, H., and McFiggans, G.: Simulating regional scale secondary organic aerosol formation during the torch 2003 campaign in the southern uk, Atmos. Chem. Phys., 6, 403-418, 2006.

Kroll, J. H., and Seinfeld, J. H.: Chemistry of secondary organic aerosol: Formation and evolution of low-volatility organics in the atmosphere, Atmospheric Environment, 42, 3593-3624, 2008.

Kroll, J. H., Donahue, N. M., Jimenez, J. L., Kessler, S. H., Canagaratna, M. R., Wilson, K. R., Altieri, K. E., Mazzoleni, L. R., Wozniak, A. S., Bluhm, H., Mysak, E. R., Smith, J. D., Kolb, C. E., and Worsnop, D. R.: Carbon oxidation state as a metric for describing the chemistry of atmospheric organic aerosol, Nature Chemistry, 3, 133-139, 2011.

Lane, T. E., Donahue, N. M., and Pandis, S. N.: Simulating secondary organic aerosol formation using the volatility basis-set approach in a chemical transport model, Atmospheric Environment, 42, 7439-7451, 2008.

Lim, Y. B., and Ziemann, P. J.: Chemistry of secondary organic aerosol formation from oh radical-initiated reactions of linear, branched, and cyclic alkanes in the presence of no x, Aerosol Science and Technology, 43, 604-619, 2009.

Miracolo, M., Hennigan, C., Ranjan, M., Nguyen, N., Gordon, T., Lipsky, E., Presto, A., Donahue, N., and Robinson, A.: Secondary aerosol formation from photochemical aging of aircraft exhaust in a smog chamber, Atmos. Chem. Phys, 11, 4135-4147, doi:10.5194/acp-11-4135-2011, 2011.

Miracolo, M. A., Drozd, G. T., Jathar, S. H., Presto, A. A., Lipsky, E. M., Corporan, E., and Robinson, A. L.: Fuel composition and secondary organic aerosol formation: Gas-turbine exhaust and alternative aviation fuels, Environmental Science & Technology, submitted.

Morris, R. E., Koo, B., Guenther, A., Yarwood, G., McNally, D., Tesche, T. W., Tonnesen, G., Boylan, J., and Brewer, P.: Model sensitivity evaluation for organic carbon using two multi-pollutant air quality models that simulate regional haze in the southeastern united states, Atmos. Environ., 40, 4960-4972, 2006.

Murphy, B., and Pandis, S.: Simulating the formation of semivolatile primary and secondary organic aerosol in a regional chemical transport model., Environmental science & technology, 43, 4722-4728, doi:10.1021/es803168a, 2009.

Murphy, B. N., and Pandis, S. N.: Exploring summertime organic aerosol formation in the eastern united states using a regional-scale budget approach and ambient measurements, Journal of Geophysical Research, 115, D24216, doi:10.1029/2010JD014418, 2010.

Ng, N., Kroll, J., Chan, A., Chhabra, P., Flagan, R., and Seinfeld, J.: Secondary organic aerosol formation from m-xylene, toluene, and benzene, Atmos. Chem. Phys, 7, 3909-3922, doi:10.5194/acp-7-3909-2007, 2007.

Odum, J. R., Hoffmann, T., Bowman, F., Collins, D., Flagan, R. C., and Seinfeld, J. H.: Gas/particle partitioning and secondary organic aerosol yields, Environmental Science & Technology, 30, 2580-2585, 1996.

Pankow, J. F.: An absorption model of gas/particle partitioning of organic compounds in the atmosphere, Atmospheric Environment, 28, 185-188, 1994.

Presto, A. A., Miracolo, M. A., Donahue, N. M., and Robinson, A. L.: Secondary organic aerosol formation from high-no x photo-oxidation of low volatility precursors: N-alkanes, Environmental Science & Technology, 44, 2029-2034, 2010.

Presto, A. A., Nguyen, N. T., Ranjan, M., Reeder, A. J., Lipsky, E. M., Hennigan, C. J., Miracolo, M. A., Riemer, D. D., and Robinson, A. L.: Fine particle and organic vapor emissions from staged tests of an in-use aircraft engine, Atmospheric Environment, 45, 3603-3612, 2011.

Presto, A. A., Hennigan, C. J., Nguyen, N. T., and Robinson, A. L.: Determination of volatility distributions of primary organic aerosol emissions from combustion systems using thermal desorption gas chromatography mass spectrometry, Aerosol Science and Technology, submitted.

Pye, H., and Seinfeld, J.: A global perspective on aerosol from low-volatility organic compounds, Atmos. Chem. Phys, 10, 4377-4401, doi:10.5194/acp-10-4377-2010, 2010.

Robinson, A. L., Donahue, N. M., Shrivastava, M. K., Weitkamp, E. A., Sage, A. M., Grieshop, A. P., Lane, T. E., Pierce, J. R., and Pandis, S. N.: Rethinking organic aerosols: Semivolatile emissions and photochemical aging, Science, 315, 1259-1262, 2007.

Robinson, A. L., Grieshop, A. P., Donahue, N. M., and Hunt, S. W.: Updating the conceptual model for fine particle mass emissions from combustion systems, Journal of the Air & Waste management association, 60, 1204-1222, 2010.

Schauer, J. J., Kleeman, M. J., Cass, G. R., and Simoneit, B. R. T.: Measurement of emissions from air pollution sources. 2. C1 through c30 organic compounds from medium duty diesel trucks, Environ. Sci. Technol, 33, 1578-1587, 1999.

Schauer, J. J., Kleeman, M. J., Cass, G. R., and Simoneit, B. R. T.: Measurement of emissions from air pollution sources. 5. C1- c32 organic compounds from gasoline-powered motor vehicles, Environ. Sci. Technol, 36, 1169-1180, 2002.

Shakya, K. M., and Griffin, R. J.: Secondary organic aerosol from photooxidation of polycyclic aromatic hydrocarbons, Environmental Science & Technology, 44, 8134-8139, doi:10.1021/es1019417, 2010.

Shrivastava, M. K., Lane, T. E., Donahue, N. M., Pandis, S. N., and Robinson, A. L.: Effects of gas particle partitioning and aging of primary emissions on urban and regional organic aerosol concentrations, Journal of Geophysical Research-Atmospheres, 113, D18301, doi:10.1029/2007JD009735, 2008.

Tsimpidi, A., Karydis, V., Zavala, M., Lei, W., Molina, L., Ulbrich, I., Jimenez, J., and Pandis, S.: Evaluation of the volatility basis-set approach for the simulation of organic aerosol formation in the mexico city metropolitan area, Atmos. Chem. Phys, 10, 525-546, doi:10.5194/acp-10-525-2010, 2009.

Vutukuru, S., Griffin, R. J., and Dabdub, D.: Simulation and analysis of secondary organic aerosol dynamics in the south coast air basin of california, J. Geophys. Res., 111, doi:10.1029/2005JD006139, 2006.

Wey, C., Anderson, B., Hudgins, C., Wey, C., Li-Jones, X., Winstead, E., Thornhill, L., Lobo, P., Hagen, D., and Whitefield, P.: Aircraft particle emissions experiment (apex), NASA TM-2006, 2006.

Zhang, Q., Jimenez, J. L., Canagaratna, M. R., Allan, J. D., Coe, H., Ulbrich, I., Alfarra, M. R., Takami, A., Middlebrook, A. M., Sun, Y. L., Dzepina, K., Dunlea, E., Docherty, K., DeCarlo, P. F., Salcedo, D., Onasch, T., Jayne, J. T., Miyoshi, T., Shimono, A., Hatakeyama, S., Takegawa, N., Kondo, Y., Schneider, J., Drewnick, F., Borrmann, S., Weimer, S., Demerjian, K., Williams, P., Bower, K., Bahreini, R., Cottrell, L., Griffin, R. J., Rautiainen, J., Sun, J. Y., Zhang, Y. M., and Worsnop, D. R.: Ubiquity and dominance of oxygenated species in organic aerosols in anthropogenically-influenced northern hemisphere midlatitudes, Geophys. Res. Lett, 34, L13801, doi:10.1029/2007GL029979, 2007.

Chapter 4: Secondary organic aerosol formation from photo-oxidation of evaporated fuel: experimental results and implications for aerosol formation from combustion emissions*

Abstract

Photo-oxidation experiments were conducted using a smog chamber to investigate formation and properties of secondary organic aerosol (SOA) from evaporated fuel. We perform experiments on gasoline (commercial California Summer), three types of jet fuel (conventional JP-8 and two Fischer-Tropschs fuels derived from coal and natural gas) and six different diesels; the fuels span a modest range of volatility and molecular structure. We find that for a unit amount of fuel reacted, evaporated diesel forms the most SOA followed by JP-8, FT (natural gas), gasoline and FT (coal). Qualitatively, these trends are consistent with the differences in volatility and molecular structure of these fuels. Chemically, the SOA from our experiments is moderately oxygenated (O:C~0.2-0.4) and similar to semi-volatile oxygenated organic aerosol (SV-OOA). The dominant mass-to-charge ratios of 43 and 44 for JP-8 SOA are similar to those for *n*-alkane SOA and so is FT SOA similar to branched alkane SOA and gasoline SOA similar to aromatic SOA. When we compare the SOA yields for the evaporated fuels (SOA/Fuel reacted) to SOA yields from emissions experiments conducted on combustion sources that use those fuels (SOA/NMOG reacted; non-methane organic gas), we find that they compare within a factor of two for jet fuels and diesels. This implies that the observed differences in SOA formation from combustion emissions can partly be explained by differences in the fuel's composition. But for gasoline combustion emissions, the emission standard applicable to the engine plays a much more important role suggesting that other variables in a combustion system can also influence SOA formation. When results from this work and SOA work done on gasoline combustion

* To be submitted to Environmental Science and Technology

emissions are used to predict SOA formation from on-road gasoline vehicles in California and the US, we observe that tailpipe emissions form much more SOA than evaporative emissions (9:1) where the bulk of the tailpipe-related SOA (90%) arises from LEV-I and LEV-II vehicles.

4.1 Introduction

Atmospheric aerosols exert a large influence on climate and public health (Bernstein et al., 2004;IPCC, 2007). Secondary organic aerosol (SOA) is defined as the organic aerosol (OA) arising from the oxidation products of gas-phase organic species and accounts for a significant fraction of the submicron atmospheric aerosol mass or fine particulate matter (PM) (Zhang et al., 2007). Atmospheric SOA formation is a result of oxidation of organic emissions from both combustion- and non-combustion based, anthropogenic and natural sources. Examples of anthropogenic combustion sources are vehicles, fireplaces, ships, airplanes and prescribed burning while those for anthropogenic non-combustion sources are evaporated gasoline, solvent use and coatings. Examples of natural combustion sources are wildfires while those for natural non-combustion sources are biogenic emissions of isoprene, terpenes and sesquiterpenes. Of the four sources mentioned, anthropogenic combustion sources is the only classification that could be regulated to reduce total SOA formation because anthropogenic non-combustion sources mostly emit light volatile organic compounds (VOC) that do not form any SOA (Simon et al., 2010) and controlling the natural sources could lead to unintended consequences.

A novel approach to control anthropogenic combustion emissions is to control the fuel. In the past, amendments to the Clean Air Act in 1990 had required the use of reformulated gasoline to abate ozone production. Serving as motivation, Odum and coworkers (Odum et al., 1996;Odum et al., 1997a;Odum et al., 1997b) conducted photo-oxidation experiments on

evaporated gasoline and concluded that SOA formation from evaporated gasoline, and therefore possibly from emissions of gasoline engines, could be limited by controlling the fraction of single-ring aromatics in the fuel. The statement holds true for gasoline since single-ring aromatics form a lot more SOA compared to similar carbon-number alkanes and alkenes (C_5-C_9) but may not hold true for fuels like jet fuel and diesel that have higher carbon-number alkanes and alkenes (C_8-C_{18}) that are shown to form SOA (Lim and Ziemann, 2009a, b, 2005;Presto et al., 2010;Tkacik et al., submitted;Forstner et al., 1997;Na et al., 2006;Keywood et al., 2004). In fact, single component studies have demonstrated that SOA formation depends both on the precursor's carbon-number (or volatility) and molecular structure. For example, SOA formation increases for alkanes as the carbon number increases (or volatility decreases) (Tkacik et al., submitted;Lim and Ziemann, 2005, 2009b, a;Presto et al., 2010), cyclic alkanes form more SOA followed by straight alkanes than branched alkanes (Lim and Ziemann, 2005, 2009a, b), and single-ring aromatics (benzene, toluene and xylenes) form much more SOA than similar carbon-number (C_5-C_9) alkanes or alkenes (Chan et al., 2009;Ng et al., 2007;Song et al., 2007;Hildebrandt et al., 2009;Ng et al., 2006).

Odum and coworkers (Odum et al., 1996;Odum et al., 1997a;Odum et al., 1997b) hypothesized that SOA experiments on evaporated gasoline could serve as surrogates for SOA experiments on gasoline engine emissions. Presto et al. (Presto et al., 2011) and Miracolo et al. (Miracolo et al., submitted) have found evidence for that with aircraft engines, where emissions at low engine loads resemble a mixture of unburned fuel and oil. Jathar et al. (submitted) have gone further to show that the SOA formation from those emissions is similar to the SOA observed for C_{12} and C_{13} *n*-alkanes, carbon numbers representative of where most of the fuel resides. However, until recently (Gordon et al., in preparation-a), no SOA experiments have been

done on gasoline engine emissions and the hypothesis has remained unverified. Odum and coworkers (Odum et al., 1996;Odum et al., 1997a;Odum et al., 1997b) also hypothesized that single-ring aromatics would dominate SOA formation from gasoline emissions. But, Gordon et al. (in preparation-a) showed that single-ring aromatics and other light VOCs accounted for very little of the measured SOA formation. Earlier, Robinson et al. (2007), Grieshop et al. (2009) and Miracolo et al. (2011) have found the same pattern where single-ring aromatics and other light VOCs are unable to explain most of the SOA formation measured from diesel exhaust, woodstove emissions and aircraft exhaust respectively. It is suspected that the remainder of the SOA might be formed from compounds like substituted alkanes that are hard to speciate (unresolved complex mixture; UCM) (Schauer et al., 2002, 1999) and large enough (or low in volatility) to form plenty of SOA. Furthermore, SOA models developed using the Odum framework (i.e. models skewed towards single-ring aromatics) have under-predicted SOA formation in real-world environments (Vutukuru et al., 2006;Johnson et al., 2006;Morris et al., 2006;Dzepina et al., 2009;Dzepina et al., 2010;Grieshop et al., 2009).

Studying SOA formation from individual organic compounds is beneficial in understanding the fundamental chemical mechanisms of SOA formation but they are too simple to represent the complexity found in real-world emissions. On the other hand, the reason why there have been very few experiments to study SOA formation from combustion emissions is that they are very expensive and complicated to run. Also, emissions of other pollutants such as soot, inorganics and metals make it difficult to study the SOA system independently. In this work, we propose to study SOA formation in smog chamber experiments from different types of evaporated fuel that have different volatility distributions and molecular structures. The evaporated fuel-based SOA model system is less complex than the emissions-based system but

more complex than an individual species-based system. By doing so, we intend to meet several research needs. First, we will able to see for the first time how the formation and properties of SOA vary with the precursor's volatility and molecular structure in a complex mixture system. Second, the data collected in this work will be used in a follow-up paper to test and build SOA models that account for the precursor's volatility and structure (Jathar et al., in preparation). Third, for the first time, we will be able to compare SOA data from evaporated fuels with recently collected SOA data from emissions of engines using those fuels. And finally, we intend to use the fuel- and emissions-based SOA data to assess the importance of evaporative and tailpipe emissions from on-road gasoline vehicles in the state of California and the United States (US).

4.2. Materials and methods

4.2.1 Fuels

We conducted a total of twenty three, high-NO_x, photo-oxidation, smog chamber experiments on evaporated fuels; three on commercial California summer gasoline, two on Fischer-Tropsch made from coal (FT-coal), two on Fischer-Tropsch made from natural gas (FT-natural gas), six on two different JP-8s and ten on seven different diesels from the FACE fuel study commissioned by the Coordinating Research Council (CRC). The experiments are listed in Table 4.1.

The fuel composition data are presented in Tables S.1 through S.5. To compare the different fuels in terms of volatility and molecular structure, we represent the fuels using the volatility basis set (VBS) (Donahue et al., 2006). The VBS is a modeling framework that classifies organics into logarithmically spaced bins of effective saturation concentration (C^*). C^*

(inverse of the Pankow-type partitioning coefficient, K_p) is proportional to the saturation vapor pressure; it is a semi-empirical property that describes the gas-particle partitioning of an organic mixture (Pankow, 1994).

Table 4.1: List of experiments

Number	Date	Fuel	Fuel injected ($\mu g\ m^{-3}$)	OH exposure (molecules cm^{-3} hr)	VOC/NOx (ppbC/ppb)	Fuel reacted ($\mu g\ m^{-3}$)	SOA formed ($\mu g\ m^{-3}$)	Yield	O:C
1	1/14/11	JP8	476	1.50E+07*	0.6	215	12.6	6%	NA
2	1/17/11	JP8	476	1.50E+07*	0.6	215	17.0	8%	NA
3	6/16/11	JP8	635	1.50E+07*	0.8	287	71.7	25%	0.21
4	1/28/11	JP8	635	1.50E+07*	0.8	287	86.7	30%	NA
5	2/15/11	JP8	635	1.50E+07*	0.8	287	89.8	31%	NA
6	11/8/11	JP8	318	1.63E+07	0.4	152	9.6	6%	0.33
7	3/30/11	Gasoline	525	1.35E+07	1.5	184	2.4	1%	0.40
8	4/27/11	Gasoline	1050	1.50E+07*	3.1	394	11.3	3%	0.38
9	11/28/11	Gasoline	1973	1.20E+07	2.1	609	12.2	2%	NA
10	7/15/11	FT-natural gas	610	2.66E+07	0.8	373	2.3	1%	0.31
11	7/22/11	FT-natural gas	1128	1.90E+07	1.1	564	8.0	1%	0.13
12	10/20/11	FT-coal	1106	1.29E+07	2.1	418	73.2	18%	0.25
13	10/22/11	FT-coal	590	6.74E+06	0.8	131	14.8	11%	0.25
14	8/22/11	Diesel (1)	129	2.63E+07	0.1	99	1.6	2%	0.28
15	12/8/11	Diesel (2)	232	2.70E+07	0.3	174	32.9	19%	0.20
16	2/4/10	Diesel (3)	134	1.92E+07	0.2	86	16.6	19%	NA
17	2/15/10	Diesel (3)	184	1.77E+07	0.2	113	30.3	27%	NA
18	3/4/10	Diesel (5)	258	1.35E+07	0.3	134	17.3	13%	NA
19	12/21/11	Diesel (7)	304	9.84E+06	0.3	142	15.4	11%	0.28
20	10/24/11	Diesel (8)	138	1.50E+07*	0.2	98	6.7	7%	0.21
21	3/26/10	Diesel (9)	135	1.48E+07	0.1	85	23.8	28%	NA
22	4/1/10	Diesel (9)	135	1.86E+07	0.2	94	11.7	12%	NA
23	7/26/11	Diesel (9)	505	1.17E+07	0.5	280	79.6	28%	0.19

*estimate

To represent a fuel in the VBS, one needs to know the vapor pressure (or C*) of each individual species in the fuel. However, the granularity of the composition data varies a lot across the fuels. For gasoline, we have alkane and aromatic data by carbon number but no information about the specific species and no resolution in the alkene data. The FT-coal data are poorly resolved since FT-coal is mostly composed of iso-alkanes that are difficult to speciate. For FT-natural gas and JP-8, we have data for *n*-alkanes ranging from *n*-heptane to *n*-nonadecane but lumped data for branched alkanes, cyclic alkanes and aromatics. For diesels, we have finely-

resolved data both by organic class and carbon number. To translate the fuel composition data to the VBS, we develop a mathematical relationship to calculate C* based on the carbon number of a hydrocarbon. The relationship was derived using vapor pressure (C*) data from NIST for *n*-alkanes, pure cyclic alkanes, simple branched alkanes, single ring aromatics, naphthalene, straight and cyclic alkenes, isoprene, and common terpenes. Aromatics ($C^* = e^{(22.3\text{-carbon \#})/0.806}$) have a slightly different relationship than alkanes and alkenes ($C^* = e^{(24.5\text{-carbon \#})/0.899}$). For JP-8 and FT-natural gas where there is no information for branched and cyclic alkanes and aromatics by carbon number, we assume their distribution is similar to the distribution of *n*-alkanes in that fuel. For FT-coal, we assume that the distribution of branched and cyclic alkanes is similar to the distribution of *n*-alkanes in FT-natural gas since Corporan et al. (2011) suggest that the hydrocarbon distribution in vapor pressure (or C*) space is very similar for those two fuels.

Figure 4.1 plots a representation of the fuels in the VBS, color-coded by molecular structure. In terms of volatility, gasoline is the most volatile followed by FT, JP-8 and diesel; the mass-weighted average (avg $\log_{10}C^*$) of the volatility distribution is presented using the magenta arrows. In terms of molecular structure (shown by the inset pies), diesels generally have the largest aromatic fraction followed by gasoline and JP-8; the FT fuels have no aromatics. Further, the diesels also have a much wider volatility distribution compared to the other fuels with an alkane-dominated fraction in the $C^*=10^2$ to $C^*=10^6$ $\mu g\ m^{-3}$ space and an aromatic-dominated fraction in the $C^*=10^6$ to $C^*=10^9$ $\mu g\ m^{-3}$ space.

4.2.2 Experimental

We performed experiments in the Carnegie Mellon University smog chamber, a 10 m^3 Teflon bag suspended in a temperature-controlled room. Prior to an experiment, the chamber was

cleaned by heating, flushing with HEPA and activated carbon filtered air and irradiation with UV lights for a minimum of 12 hours.

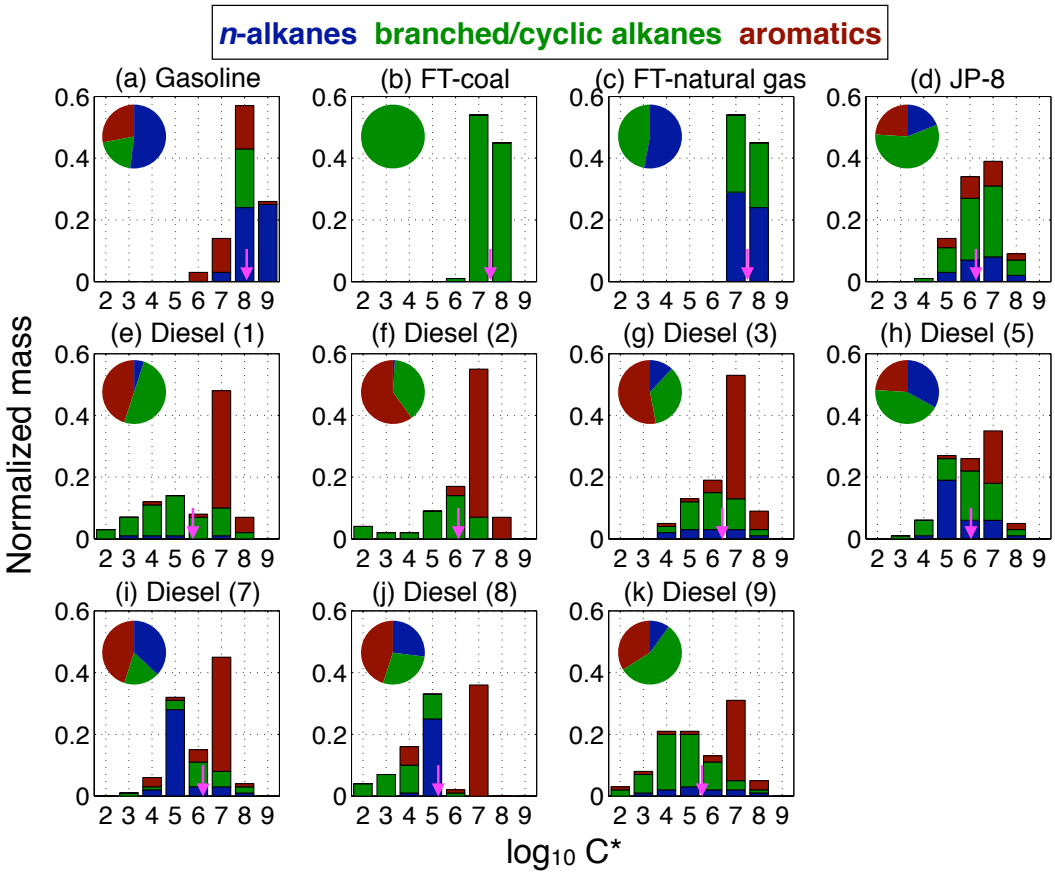

Figure 4.1: Volatility and molecular structure distributions for (a) gasoline, (b) FT-coal, (c) FT-natural gas, (d) JP-8 and (e-k) Diesel 1, 2, 3, 5, 7, 8 and 9 represented in the volatility basis set. For each plot, the bars sum up to one. The inset pie shows the relative fractions of n-alkanes, branched/cyclic alkanes and aromatics in the fuel. The magenta arrow shows the mass-weighted average of the volatility distribution.

A brief outline of the experimental procedure is presented. First, ammonium sulfate seed (7-25 μg m^{-3}) was added to the chamber to minimize losses of vapors to the walls and prevent nucleation of SOA products. Second, nitrous acid (HONO) was bubbled into the chamber. Third, the precursor (fuel) and, in some experiments, tracers (single-ring aromatics, 2-butanol (d9), acetonitrile) were introduced into the chamber by passing clean-filtered air through a heated septum into which the precursor/tracer was slowly injected using a syringe. Photo-oxidation was

initiated by turning on the chamber UV black lights (General Electric model 10526), which yield an NO_2 photolysis rate of 0.2 min^{-1}. The UV light photolyzed HONO to produce hydroxyl radicals (OH). NO and NO_2 formed as by-products of HONO irradiation resulted in a low VOC/NO_x ratio that was consistent with ratios found in urban polluted regions. The experiment was performed at low relative humidity (<5%) and a temperature of around 298 K.

Concentrations of gas-phase organic compounds (fuel species and their oxidation products) were tracked using a GC-MS (Logue et al., 2009) and a proton-transfer reaction mass spectrometer (PTR-MS, Ionicon Analytik). Between the two instruments, we were able to track the oxidation of single-ring aromatics such as benzene, toluene, xylenes, trimethylbenzenes, C_7 and higher n-alkanes and 2-butanol (d9) which were present in the precursor fuel and/or deliberately added as tracers, and the production of small oxygenated compounds like acetone and methyl ethyl ketone, which were oxidation products. Unfortunately, most of the gas-phase precursor mass and its products in the gas phase remain invisible to our instruments. We also tracked acetonitrile, which was used to check for smog chamber leakage. The OH concentration was interpreted by tracking the decay of either a detectable single-ring aromatic or 2-butanol (d9). In experiments without gas-phase data we estimated OH concentrations from the average of other experiments conducted using the same fuel. On average, the OH concentration was 1-3 x 10^7 molecules cm^{-3} in the first 30 to 60 minutes but dropped to less than 10^6 molecules cm^{-3} over the next few hours. The estimated OH exposure ranges from 7 to 27 hours of atmospheric oxidation at a typical OH concentration of 10^6 molecules cm^{-3}.

Particle-phase measurements were made using a scanning mobility particle sizer (SMPS, TSI Inc.) to measure the particle size distribution and a quadrupole or high resolution aerosol mass spectrometer (Q-AMS or HR-AMS, Aerodyne Research Inc.) to measure non-refractory

aerosol mass, size and composition. Both SMPS and Q-AMS/HR-AMS results were wall-loss corrected to calculate a lower and upper bound on the total SOA formation (Weitkamp et al., 2007;Hildebrandt et al., 2009). The wall-loss rates were estimated by characterizing the decay of ammonium sulfate before the lights were turned on. The lower bound was calculated assuming that the oxidation products only condense on the suspended particles while the upper bound was calculated assuming that the oxidation products could condense not only on the suspended particles but also on particles lost to the walls.

The SOA composition was determined from the Q-AMS and HR-AMS data. We use the toolkit Squirrel (version 1.51B) to obtain time series for various mass components (sulfate, nitrate, ammonium, organics) and mass spectra at unit mass resolution (UMR). We use the toolkit Pika (version 1.10B) to run an elemental analysis and determine molar ratios of H:C and O:C for SOA.

We are aware that experimental uncertainty could affect the quality of data from smog chamber experiments and therefore the conclusions from our analysis. The experimental uncertainty can be thought of as that associated with measurements, repeatability and atmospheric relevance. Of the three, the uncertainty in measurements is probably the lowest as the instruments and techniques used to characterize smog chamber data have evolved over the past two decades. In this work, measurement uncertainties are quantified and wherever possible, included in our analysis. Particularly for experiments used in this work, there is slightly more uncertainty associated with repeatability because there might be factors that have a larger than anticipated effect on the experiment (ambient temperature, relative humidity, VOC/NOx ratio). The uncertainty was kept to a minimum by undertaking tasks such as cleaning the chamber for 12 hours before use, ensuring a minimum background concentration and running a blank

experiment. But the largest uncertainty results from whether our static and controlled experiments are truly representative of the dynamic processes in the atmosphere. We ensure atmospheric relevance by diluting the emissions and maintaining VOC/NOx ratios to those found in the atmosphere.

4.2.3 SOA yields

To compare the SOA formation across fuels, we calculate an SOA yield for each experiment. The SOA yield is calculated as a ratio of the SOA formed to the mass of fuel reacted; the approach is the same as that employed by Odum and coworkers in describing SOA formation from gasoline vapors (Odum et al., 1996;Odum et al., 1997a;Odum et al., 1997b). We analyze the SMPS and AMS results independently and from that analysis estimate a minimum and maximum amount of SOA formed. For the SMPS results, we use an aerosol density of 1.4 g cm^{-3} to estimate the SOA mass from the volume measurement. In some experiments where some of the SOA mass nucleated, we did not use the AMS results because a significant fraction of the SOA mass was too small to be detected by the AMS. The amount of fuel reacted is calculated by assuming that each fuel species undergoes a first order decay due to reaction with the OH radical, as shown in equation (4.1):

$$\frac{d[X_i]}{dt} = -k_{OH,X_i}[OH][X_i]$$
$$\Delta Fuel\ reacted = \sum \Delta X_i \quad (4.1)$$

where $[X_i]$ is the fuel species concentration in μg m^{-3}, k is the reaction rate constant in cm^3 $molecules^{-1}$ s^{-1}, $[OH]$ is the OH radical concentration in molecules cm^{-3} and $\Delta Fuel\ reacted$ is the mass of fuel reacted in μg m^{-3}. The reaction rate constant used for each fuel species is listed in Tables S.1 through S.5. As mentioned earlier, the fuel composition data is incomplete and hence

we need to assume reaction rate constants for fuel constituents that are lumped, e.g. branched alkanes. We assign a surrogate compound to the lumped fuel constituent based on the average carbon number of the fuel and use its reaction rate constant to represent the reactivity of that entire fuel constituent. The initial concentration of a fuel species is calculated by multiplying the mass of fuel injected and its percentage mass listed in the fuel composition (Tables S.1 through S.5 in supplementary material). We assume a smog chamber volume of 10 m^3.

To address uncertainty in our assumptions and measurements, we estimate a low and high value for the SOA yield. The lower value is calculated using the minimum estimate of SOA formed and an injection efficiency of 100% while the higher value is calculated using the maximum estimate of SOA formed and an injection efficiency of 90%.

4.3 Experimental results

Figure 4.2 plots measured time series of particle- and gas-phase concentrations from an experiment performed on Diesel (2) on 12/8/11. Figure 4.1(a) plots the suspended $PM_{0.5}$ volume, suspended ammonium sulfate seed and the wall-loss corrected OA concentration as a function of time. After photo-oxidation is initiated (lights turned on), a lot of OA (or SOA) is formed in a short amount of time (~20-40 mins). Figure 4.2(a) shows both the lower (light green) and upper (dark green) bound estimates of wall-loss corrected OA. The difference between these two estimates is small because the SOA formation timescale is much shorter than the timescale associated with particle loss to the wall. Figure 4.2(b) shows the measured evolution of 1-butanol, m-xylene and trimethylbenzene with time. As soon as the lights are turned on, the compounds rapidly decay, which coincides with prompt SOA formation.

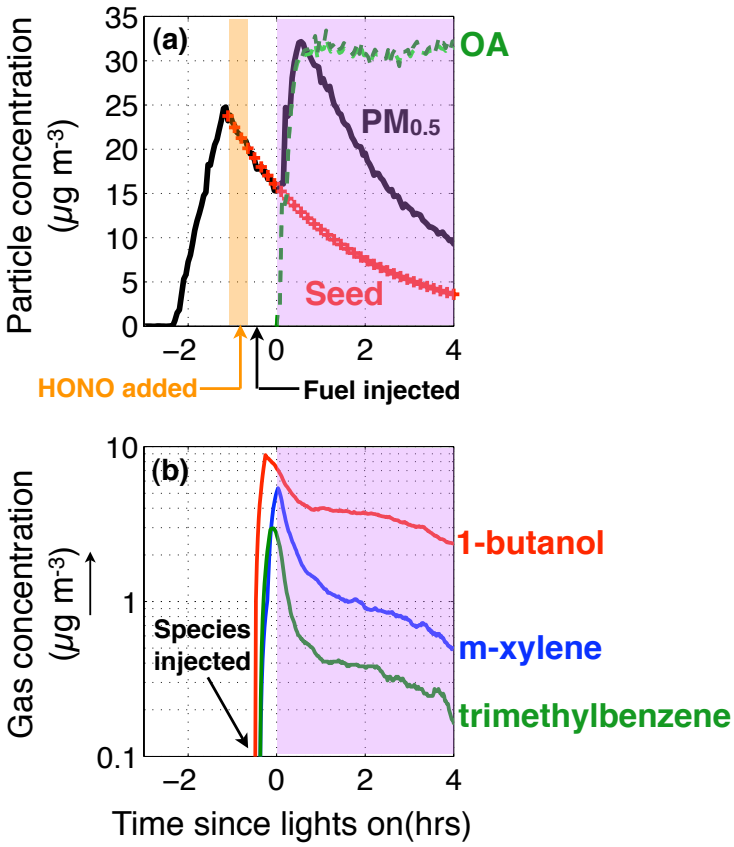

Figure 4.2: Particle-phase (top panel) and gas-phase (bottom panel) concentrations measured during the Diesel (2) experiment (12/08/11). The $PM_{0.5}$ and seed concentrations are as measured by the SMPS. The OA concentrations are wall-loss corrected.

4.3.1 SOA yield

Figure 4.3 plots the SOA yield as a function of the wall-loss corrected OA concentration (C_{OA}). Each point represents a six-minute average from an individual experiment. For each fuel, the SOA yield increases with increasing $C_{OA,}$ implying that the oxidation products are semi-volatile and are actively participating in gas-particle partitioning. Across all fuels, the SOA yield varies by an order of magnitude across the plotted C_{OA} range. Diesel has the highest SOA yield followed by JP-8/FT-natural gas, gasoline and FT-coal. Qualitatively, this trend agrees with our understanding of SOA formation being dependent on volatility and molecular structure. Diesel fuels form a lot of SOA because they have a lower volatility (avg $\log_{10}C^*$ = 5.2-6.4) and a

higher aromatic fraction (42%). JP-8 forms less SOA than diesel because it is slightly more volatile than diesel (avg $\log_{10}C^* = 6.2$) and has a significantly smaller aromatic fraction (24%). Surprisingly, FT-natural gas forms as much SOA as JP-8 even though it is more volatile (avg $\log_{10}C^* = 7.4$) and does not have any aromatics. Gasoline forms even less SOA because it is dominated by high volatility alkanes (avg $\log_{10}C^* = 8.1$) that do not form any SOA; most of the SOA it forms probably comes from single-ring aromatics (28%). The gasoline SOA yield is in-line with the results of Odum et al (1997a). FT-coal forms the least amount of SOA because it is very volatile ($\log_{10}C^* = 7.4$) and is mostly composed of branched alkanes (88%) that fragment during oxidation and form very little SOA.

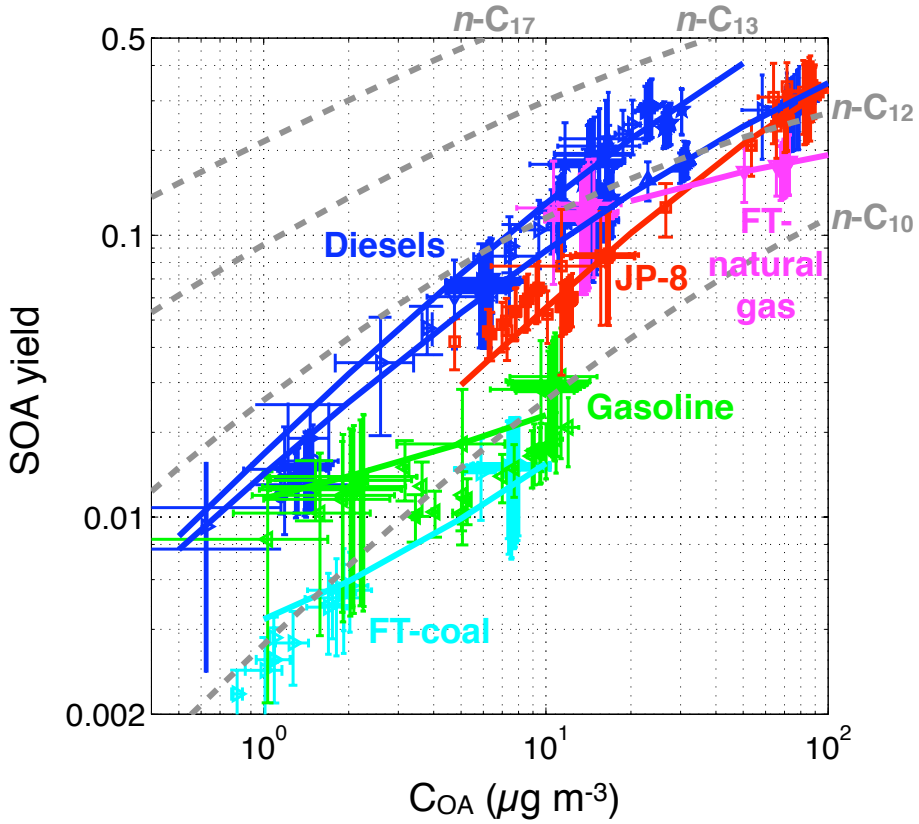

Figure 4.3: SOA Yield (SOA / Fuel reacted) plotted as a function of the OA concentration (COA). The solid lines represent fits for different fuels based on five bin VBS. For reference, we plot SOA yields for *n*-decane, *n*-dodecane, *n*-tridecane and *n*-heptadecane.

A simple approach to fit the SOA data is to assume that all species in a given fuel react with OH to form the same set of semi-volatile products, which can be represented using a five-bin VBS (C^*=0.1, 1, 10, 100 1000 μg m^{-3}) (Donahue et al., 2006;Pankow, 1994). Figure 4.3 shows that we need different curves (solid lines) to fit the SOA data for different fuels. Two curves are required to fit the diesel SOA data: one curve for diesels (1), (2), (5), (7) and (8) and another curve for diesels (3) and (9).

Even though the different diesels have a slightly different composition (similar volatility but different molecular structure), their SOA yield is quite similar. We suspect that the SOA yield for diesel is less sensitive to molecular structure because diesel is comprised of relatively low volatility alkanes, alkenes and aromatics, all of which form SOA. Therefore, substituting *n*-alkanes with branched alkanes, cyclic alkanes or single ring aromatics only marginally changes the SOA potential of diesel. In contrast, for FT-natural gas and FT-coal (that are much more volatile than diesel) that share the same volatility profile but have very different molecular structure (50:50 *n*-alkanes:branched alkanes versus 88% branched alkanes), the SOA yield is an order of magnitude different. This suggests that for lower volatility precursors, the SOA yield might have a lower sensitivity to molecular structure but for higher volatility precursors, molecular structure might become very important.

The emissions from a combustion system (exhaust) and therefore the SOA from it are partly a function of the composition of the fuel. To explore this relationship, we first analyze SOA data from experiments conducted on combustion emissions that used fuels considered in this work (Miracolo et al., 2011;Miracolo et al., submitted;Gordon et al., in preparation-a;Gordon et al., in preparation-b). For each system, we calculate an SOA yield which is defined as the ratio of the mass of SOA formed to the mass of precursor reacted; the precursor is the total non-

methane organic gas (NMOG). The mass of precursor reacted is calculated in the same way as we calculate the mass of fuel reacted in this work (equation (4.1)). Here, X_j is either a speciated VOC or lumped unspeciated mass. The reaction rate constants for speciated VOCs are based on literature and we assume that the lumped unspeciated mass has an OH reactivity of 1 x 10^{-11} cm^3 $molecules^{-1}$ s^{-1}.

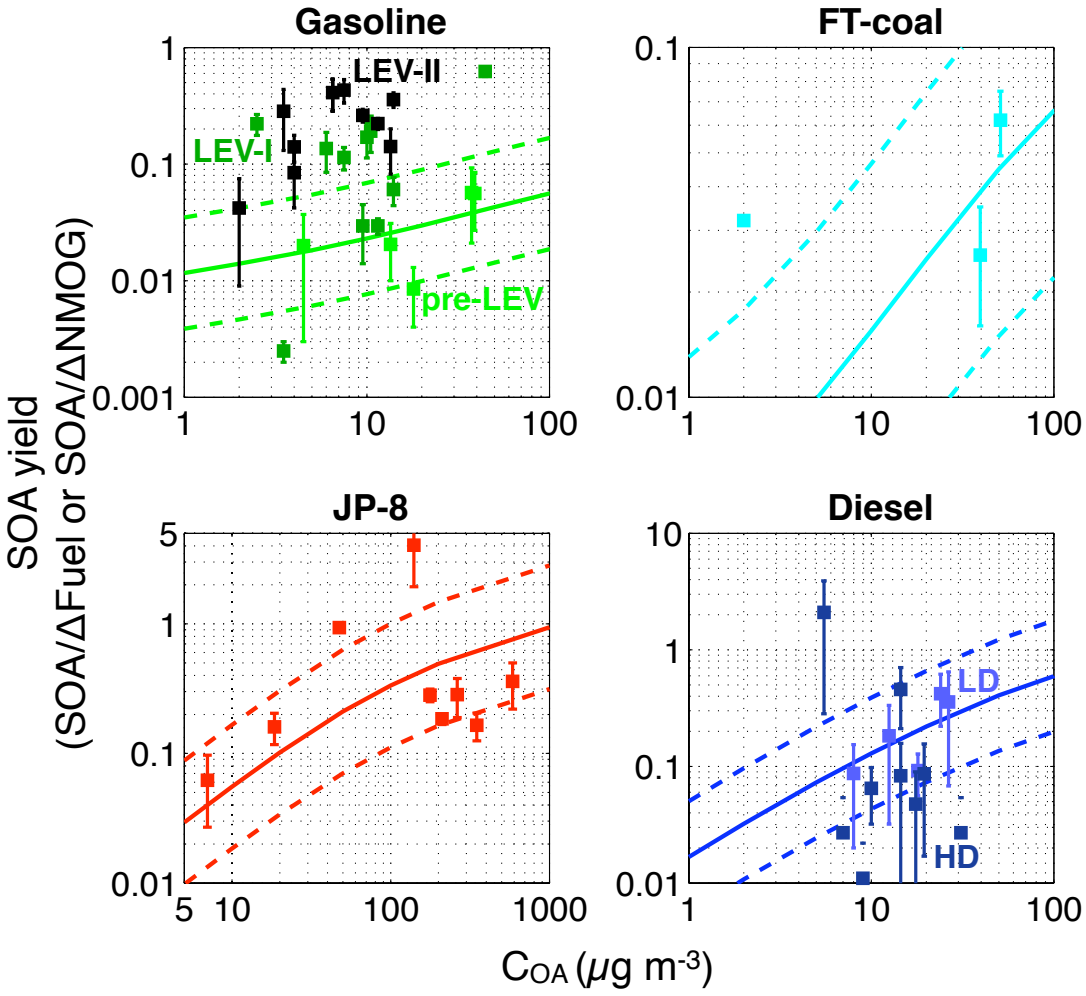

Figure 4.4: SOA yield plotted against the OA concentration. The solid lines represent the SOA yield calculated from the fuel SOA data (same as fits in Figure 4.3); dotted lines show a factor of two uncertainty. The points represent the SOA yield calculated from data measured from real exhaust. The SOA yield is expressed as the ratio of SOA formed to the amount of NMOG reacted.

Figure 4.4 plots SOA yields (symbols with error bars) for the exhaust experiments alongside SOA yield curves (SOA/Fuel reacted; solid lines from Figure 4.3) for evaporated fuel

from this work. For exhaust, most SOA yields range between 0.2 and 50%, which is similar to the SOA-yield range observed for evaporated fuel (0.4-40%) across the entire C_{OA} range. Despite the variability seen with the exhaust SOA yields, they appear to be more or less within a factor of two of the SOA yields for evaporated fuel, with the exception of the gasoline LEV-I and LEV-II data (LEV: Low Emissions Vehicle). This would imply that the observed differences in SOA formation between the different combustion sources can partly be explained by differences in the fuel composition. For gasoline exhaust, a lot of the variability can be explained if the experiments are also sorted by the emission standard applicable to the vehicle (pre-LEV, LEV-I and LEV-II). Hence, for gasoline, it seems like the emission standard on the engine has a much larger influence on the SOA yield than the fuel composition. Similar to gasoline exhaust, variability in the diesel exhaust data also seems to be weakly dependent on the engine size, i.e. light-duty has slightly higher SOA yields than heavy-duty. The comparison presents a much more complicated picture where the fuel-based SOA yields explain some of the variability in the exhaust-based SOA yields but other variables of the combustion source like engine type and size could also be influential in affecting SOA formation.

4.3.2 SOA composition

Previously, the AMS has been extensively used to characterize the chemical composition and thereby gain insight into the properties and sources of OA (Zhang et al., 2005;Ulbrich et al., 2009;Ng et al., 2010;Heald et al., 2010;Chhabra et al., 2010). We use the work of Ng et al. (2010), who have used the mass fraction at m/z=43 (f_{43}) and mass fraction at m/z=44 (f_{44}), to visualize and interpret the AMS data. The m/z=43 signal is a result of the $C_3H_7^+$ and $C_2H_3O^+$ ions, where $C_3H_7^+$ is believed to be part of the hydrocarbon signature and $C_2H_3O^+$ is thought to

represent non-acid oxygenates. The m/z=44 signal is dominated by the CO_2^+ ion and is thought to denote the presence of organic acids and peroxides and therefore a strong indicator of the extent of oxidation of OA. Ng et al. (2010) suggested that as OA (irrespective of their source or location) evolved (or aged) in the atmosphere (or laboratory), its f_{43} decreased and f_{44} increased, and eventually converged to an f_{43} of 0.02 and an f_{44} of 0.3. Using the same data and positive matrix factorization, they were also able to separate oxygenated organic aerosol (OOA) into two factors: a semi-volatile oxygenated organic aerosol (SV-OOA) that had a higher f_{43} intensity and a low-volatility oxygenated organic aerosol (LV-OOA) that had a higher f_{44} intensity.

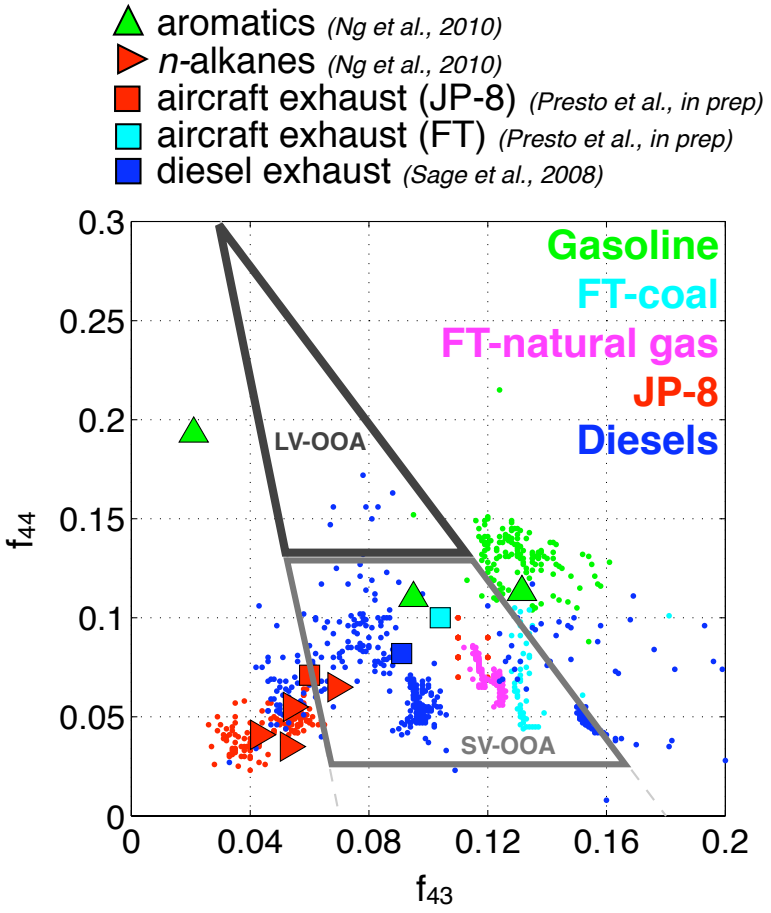

Figure 4.5: SOA aerosol mass spectrometer data presented using a triangle plot (Ng et al., ACP, 2010). The small dots show SOA data from this work. The colored symbols show SOA data from literature. SV-OOA and LV-OOA regions adapted from Ng et al., ACP, 2010.

Figure 4.5 plots f_{44} against f_{43} for all the experiments from this work. Each point represents a two- to four-minute average from an individual experiment. We excluded two JP-8 experiments (1/17/11 and 6/16/11) and one FT-natural gas (7/15/11) experiment because of poor AMS signal. Figure 4.5 also shows the triangular region occupied by SV-OOA and LV-OOA from Ng et al. (2010) and plots f_{43}-f_{44} data from single component and emissions studies using solid symbols (Sage et al., 2008;Ng et al., 2010).

The fuel data span a large range in the f_{43} and f_{44} space and lie near the base of the "triangle". SOA formed from FT-coal, FT-natural gas and most diesels lie in the SV-OOA region while the JP-8 and gasoline data lie just outside the SV-OOA region. This suggests that the SOA formed from photo-oxidation of evaporated fuel resembles ambient SV-OOA.

For FT-natural gas and FT-coal the f_{44} changes by a lot (0.05 to 0.1) implying that the SOA is becoming more oxidized. For gasoline, JP-8 and diesel (individual experiment) there is very little change in both f_{43} or f_{44} implying that, once formed, the SOA from gasoline, JP-8 and diesel does not evolve significantly. This might be because most of the SOA formation is driven by a short burst of OH (1-3 x 10^7 molecules cm^{-3}) in the first 30 to 60 minutes but there is very little OH (~ 10^6 molecules cm^{-3}) available after the first hour to interact with the SOA.

We notice several interesting trends when we compare SOA from this work to SOA from single-compounds and emissions experiments in f_{43}-f_{44} space. The SOA formed from an aircraft engine running on JP-8 (Presto et al., in preparation) has an f_{43} and f_{44} similar to that of SOA formed from evaporated JP-8 fuel. Similarly, in f_{43}-f_{44} space, the SOA formed from an aircraft engine running on FT-coal is close to SOA from evaporated FT-coal and SOA from diesel exhaust looks like the average SOA from evaporated diesel. Qualitatively, this suggests that, in terms of composition, the SOA from evaporated fuel is probably a reasonable surrogate for SOA

from emissions of engines that use those fuels. Furthermore, the SOA from *n*-decane, *n*-dodecane, *n*-pentadecane and *n*-heptadecane (Presto et al., 2010) have an f_{43} and f_{44} similar to that of SOA from evaporated JP-8 fuel and the SOA from two single-ring aromatics (toluene and m-xylene) (Ng et al., 2010) have an f_{43} and f_{44} similar to that of SOA from evaporated gasoline. This could mean that, not only is SOA from evaporated fuel similar to SOA from emissions of an engine that uses that fuel, but also that the SOA is probably dominated by a certain organic class.

Recently, Heald et al. (2010) and Ng et al. (2011) have used AMS data to determine molar ratios of H:C and O:C and plotted them against each other on a Van-Krevelen diagram. Both studies showed that H:C and O:C ratios for ambient and laboratory OA were inversely correlated (slope of -1 to -0.5), implying that as the OA aged in the atmosphere, the OA was on average being functionalized with a carbonyl and an alcohol group. When we plot our data on a Van-Krevelen diagram, most of our data lies in the SV-OOA region proposed by Ng et al. (2011) and the data have a slope of -0.87 (Figure S.1; supplementary material). The average end-of-experiment H:C and O:C ratios are listed in Table 4.1.

4.4. Summary and discussion

In this work, we conducted high-NOx photo-oxidation experiments on evaporated fuel to investigate the formation and properties of SOA arising from it. Diesel had the highest SOA potential followed by JP-8 and FT-natural gas, gasoline and FT-coal. The SOA potential can be qualitatively explained by differences in volatility and molecular structure of the precursor fuel. The f_{43} and f_{44} of the SOA from the evaporated fuel were similar to the SV-OOA factor estimated from ambient measurements. For FT-coal, JP-8 and diesel, there was additional proof

that the SOA from evaporated fuel, when compared in f_{43}-f_{44} space, was similar to the SOA from emissions of engines using that fuel.

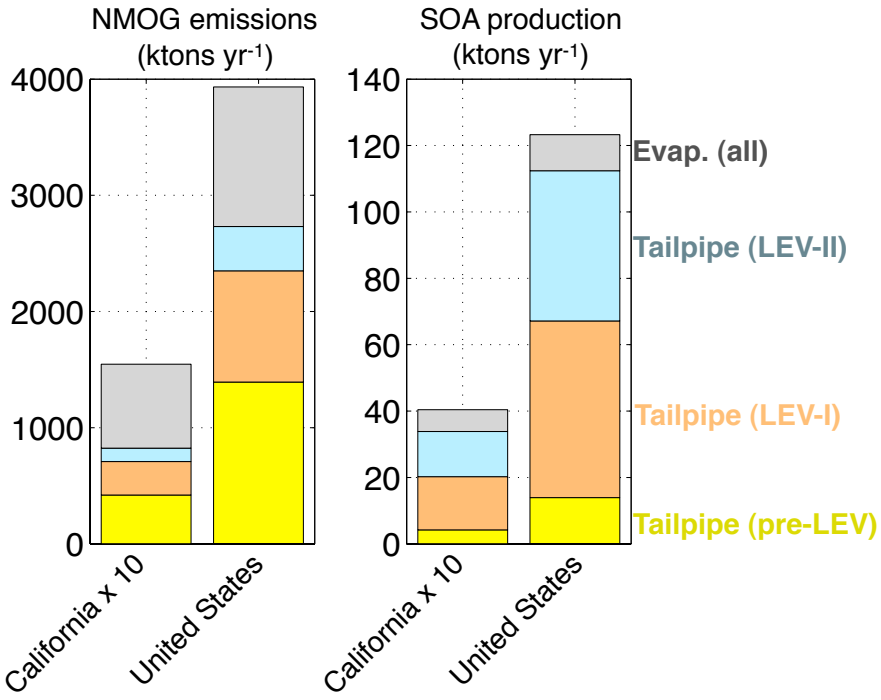

Figure 4.6: NMOG emissions and corresponding SOA production from on-road gasoline vehicles in California and the US after one day of atmospheric processing. The production is stacked according to the source type: tailpipe (pre-LEV), tailpipe (LEV-I), tailpipe (LEV-II) and evaporative.

The SOA yields for evaporated fuel are generally able to predict the value and ranking of SOA yields for combustion emissions except for SOA yields for gasoline exhaust from LEV-I and LEV-II vehicles. The comparison suggests that the fuel composition is able to explain some of the observed differences in SOA formation from combustion emissions but may not be the only variable influencing SOA formation. In the absence of any meaningful data, we propose that the SOA yield fits derived in this work could be used as reasonable estimates to model SOA formation from combustion emissions. Further, evaporated fuel SOA experiments are cheaper and more efficient to run. Therefore future work studying SOA formation from combustion

emissions might benefit by conducting SOA experiments on evaporated fuel instead. Additionally, it will help single out the influence of SOA from other pollutants that are present in real emissions (soot, inorganics, primary organic aerosol, metals).

On-road gasoline vehicles account for about a third of all NMOG (or VOC) emissions from combustion sources in the US (EPA, 2008) and therefore are an important source of SOA precursors. The NMOG emissions arise either as part of the exhaust from the tailpipe or from evaporative emissions. Nationally, the tailpipe-to-evaporative emissions ratio is slightly more than 2:1 (NRC, 2001) while in California the ratio is close to 1:1 (CARB, 2011). The evaporative gasoline results from this work and the tailpipe results from Gordon et al. (in preparation-a) can be used to estimate SOA formation from tailpipe and evaporative emissions from on-road gasoline vehicles in California and the US. We assume that the SOA yield for evaporated gasoline from this work can be used to model SOA formation from evaporative emissions. We assume that the median SOA yield for pre-LEV, LEV-I and LEV-II vehicles can be used to model SOA formation from the corresponding vehicles (median shown in Figure S.2 in supplementary material). NMOG estimates for tailpipe emissions from pre-LEV, LEV-I and LEV-II vehicles and total evaporative emissions for California are obtained from the online EMFAC database for 2011 (CARB, 2011). NMOG estimates for total tailpipe and evaporative emissions in the US are obtained from the National Emissions Inventory (NEI). Since the NEI inventory is not categorized by LEV type, we assume the same distribution of pre-LEV, LEV-I and LEV-II vehicles over the US as in California. The model is run to simulate one day of atmospheric processing (OH exposure = 10^6 molecules cm^{-3} x 24 hours). Figure 4.6 plots the NMOG emissions and SOA production (assuming a typical atmospheric C_{OA} of 5 μg m^{-3}) from tailpipe and evaporative NMOG emissions from on-road gasoline vehicles in California and the

US; 3900 ktons of NMOG form 120 ktons of SOA per year over the US and 150 ktons of NMOG form slightly less than 4 tons of SOA per year over California after one day of atmospheric processing. The figure indicates that tailpipe emissions dominate SOA production in both regions even when evaporative emissions represent 45% and 30% of total NMOG emissions from on-road gasoline vehicles. Further, LEV-I and LEV-II vehicles account for 26 to 35% of NMOG emissions but account for 73-80% of the SOA from on-road gasoline vehicles, making them a much important source than pre-LEV vehicles and all evaporative emissions together.

4.5 Supplementary material

Table S.1: Composition information and reactivity with OH for California summer gasoline

Species	Mass %	k_OH
C4 Paraffin	0.3	2.36E-12
C5 Paraffin	10.9	3.80E-12
C6 Paraffin	12.3	5.20E-12
C7 Paraffin	9.4	6.76E-12
C8 Paraffin	9.8	8.11E-12
C9 Paraffin	3.1	9.70E-12
C10 Paraffin	1.2	1.10E-11
C11+ Paraffin	0.7	1.23E-11
C6 Aromatic	0.6	1.22E-12
C7 Aromatic	5.8	5.63E-12
C8 Aromatic	9.3	1.43E-11
C9 Aromatic	8.8	1.43E-11
C10 Aromatic	2.7	1.43E-11
C11+ Aromatic	1.0	1.43E-11
Olefins	14.0	3.70E-11
C5 Cycloalkane	0.1	4.97E-12
C6 Cycloalkane	0.2	6.97E-12
C7 Cycloalkane	0.1	6.76E-12
C8 Cycloalkane	0.0	8.11E-12
C9 Cycloalkane	0.0	9.70E-12
poly-N	0.0	1.42E-11

Table S.2: Composition information and reactivity with OH for Fischer-Tropsch (coal)

Species	Mass %	k_OH
n-alkanes	0.2	1.10E-11
monoaromatics	0.5	1.43E-11
diaromatics	0.1	2.30E-11
Isoalkanes	84.9	1.10E-11
cycloalkanes	12.6	1.10E-11

Table S.3: Composition information and reactivity with OH for Fischer-Tropsch (natural gas)

Species	Mass %	k_OH
n-heptane	0.0	6.76E-12
n-octane	1.6	8.11E-12
n-nonane	22.4	9.70E-12
n-decane	25.1	1.10E-11
n-undecane	3.8	1.23E-11
n-dodecane	0.3	1.32E-11
n-tridecane	0.0	1.51E-11
n-tetradecane	0.0	1.79E-11
n-pentadecane	0.0	2.07E-11
n-hexadecane	0.0	2.32E-11
n-heptadecane	0.0	2.85E-11
n-octadecane	0.0	3.51E-11
n-nonadecane	0.0	4.32E-11
isoalkanes	46.8	1.10E-11

Table S.4: Composition information and reactivity with OH for JP-8

Species	Mass %	k_OH
n-heptane	0.1	6.76E-12
n-octane	0.3	8.11E-12
n-nonane	1.2	9.70E-12
n-decane	3.5	1.10E-11
n-undecane	4.2	1.23E-11
n-dodecane	3.7	1.32E-11
n-tridecane	2.8	1.51E-11
n-tetradecane	1.8	1.79E-11
n-pentadecane	0.9	2.07E-11
n-hexadecane	0.3	2.32E-11
n-heptadecane	0.1	2.85E-11
n-octadecane	0.0	3.51E-11
n-nonadecane	0.0	4.32E-11
monoaromatics	15.4	1.43E-11
diaromatics	1.7	2.30E-11

isoalkanes	23.1	1.23E-11
cycloalkanes	34.2	1.23E-11

Table S.5: Composition information and reactivity with OH for diesels

Species	Mass %							
	(1)	(2)	(3)	(5)	(7)	(8)	(9)	k_OH
C3 n-alkane	0.0	0.0	0.0	0.0	0.0	0.0	0.0	1.09E-12
C4 n-alkane	0.0	0.0	0.0	0.0	0.0	0.0	0.0	2.36E-12
C5 n-alkane	0.0	0.0	0.0	0.0	0.0	0.0	0.0	3.80E-12
C6 n-alkane	0.0	0.0	0.0	0.0	0.0	0.0	0.0	5.20E-12
C7 n-alkane	0.0	0.1	0.0	0.0	0.0	0.0	0.0	6.76E-12
C8 n-alkane	0.0	0.0	0.2	0.1	0.1	0.0	0.1	8.11E-12
C9 n-alkane	0.3	0.2	0.6	0.7	0.5	0.0	0.4	9.70E-12
C10 n-alkane	0.4	0.2	1.7	2.9	1.5	0.1	0.8	1.10E-11
C11 n-alkane	0.4	0.2	1.4	2.9	2.0	0.1	1.1	1.23E-11
C12 n-alkane	0.2	0.1	2.0	3.5	1.7	0.1	0.8	1.32E-11
C13 n-alkane	0.0	0.0	1.3	2.4	1.2	0.4	0.9	1.51E-11
C14 n-alkane	0.2	0.0	1.3	12.0	18.2	16.4	1.2	1.79E-11
C15 n-alkane	0.5	0.0	1.4	7.0	10.1	8.5	1.7	2.07E-11
C16 n-alkane	0.6	0.0	1.0	1.0	1.5	1.1	1.0	2.32E-11
C17 n-alkane	0.5	0.0	0.6	0.0	0.1	0.3	1.0	2.85E-11
C18 n-alkane	0.8	0.0	0.3	0.0	0.0	0.0	0.4	3.51E-11
C19 n-alkane	0.6	0.0	0.0	0.0	0.0	0.0	0.2	4.32E-11
C20 n-alkane	0.3	0.0	0.0	0.0	0.0	0.0	0.0	4.32E-11
C21 n-alkane	0.0	0.0	0.0	0.0	0.0	0.0	0.0	4.32E-11
C3 branched alkane	0.0	0.0	0.0	0.0	0.0	0.0	0.0	1.09E-12
C4 branched alkane	0.0	0.0	0.0	0.0	0.0	0.0	0.0	2.36E-12
C5 branched alkane	0.0	0.0	0.0	0.0	0.0	0.1	0.0	3.80E-12
C6 branched alkane	0.0	0.0	0.0	0.0	0.0	0.0	0.0	5.20E-12
C7 branched alkane	0.0	0.0	0.0	0.1	0.0	0.0	0.0	6.76E-12
C8 branched alkane	0.1	0.1	0.4	0.2	0.1	0.1	0.2	8.11E-12
C9 branched alkane	0.5	0.1	0.7	0.8	0.6	0.0	0.0	9.70E-12
C10 branched alkane	2.0	1.0	2.9	3.3	1.6	0.0	1.1	1.10E-11
C11 branched alkane	4.7	4.5	3.2	2.0	0.4	0.0	0.2	1.23E-11
C12 branched alkane	0.5	1.1	0.9	2.3	0.8	0.0	0.1	1.32E-11
C13 branched alkane	3.0	7.8	3.1	3.1	1.5	0.0	1.0	1.51E-11
C14 branched alkane	4.1	5.5	1.9	2.3	1.0	1.8	3.0	1.79E-11
C15 branched alkane	3.9	1.1	2.8	1.0	0.3	1.5	3.3	2.07E-11
C16 branched alkane	3.6	0.6	1.1	0.5	0.2	1.1	3.3	2.32E-11
C17 branched alkane	2.5	0.2	0.3	0.0	0.0	1.1	2.6	2.85E-11
C18 branched alkane	1.5	0.1	0.0	0.0	0.0	0.0	1.2	3.51E-11
C19 branched alkane	1.6	0.1	0.0	0.0	0.0	0.0	0.2	4.32E-11
C20 branched alkane	0.7	0.0	0.0	0.0	0.0	0.0	0.0	4.32E-11
C21 branched alkane	0.2	0.0	0.0	0.0	0.0	0.0	0.0	4.32E-11
C3 cycloalkane	0.0	0.0	0.0	0.0	0.0	0.0	0.0	1.09E-12
C4 cycloalkane	0.0	0.0	0.0	0.0	0.0	0.0	0.0	2.36E-12

C5 cycloalkane	0.0	0.0	0.0	0.0	0.0	0.0	0.0	3.80E-12
C6 cycloalkane	0.0	0.0	0.0	0.0	0.0	0.0	0.0	5.20E-12
C7 cycloalkane	0.0	0.0	0.1	0.0	0.0	0.0	0.0	6.76E-12
C8 cycloalkane	0.3	0.0	0.4	0.4	0.2	0.0	0.3	8.11E-12
C9 cycloalkane	0.6	0.1	0.8	1.0	0.8	0.0	0.9	9.70E-12
C10 cycloalkane	1.0	0.1	1.7	2.9	1.4	0.0	0.7	1.10E-11
C11 cycloalkane	1.4	0.7	2.1	3.3	1.1	0.0	0.7	1.23E-11
C12 cycloalkane	1.1	2.4	4.3	5.8	2.8	0.0	2.3	1.32E-11
C13 cycloalkane	1.8	2.1	4.0	4.6	2.5	1.0	5.9	1.51E-11
C14 cycloalkane	2.3	1.5	2.4	1.7	1.4	1.0	3.2	1.79E-11
C15 cycloalkane	2.9	0.9	1.4	1.6	0.6	3.3	7.9	2.07E-11
C16 cycloalkane	2.3	0.7	0.5	2.5	0.2	2.3	4.5	2.32E-11
C17 cycloalkane	1.9	0.7	0.1	2.0	0.5	4.1	7.2	2.85E-11
C18 cycloalkane	1.5	1.0	0.0	0.9	0.0	1.0	2.3	3.51E-11
C19 cycloalkane	1.4	1.3	0.0	0.5	0.5	6.1	1.9	4.32E-11
C20 cycloalkane	1.0	1.2	0.0	0.2	0.0	1.5	1.1	4.32E-11
C21 cycloalkane	0.7	2.5	0.0	0.0	0.0	2.0	0.5	4.32E-11
C3 aromatic	0.0	0.0	0.0	0.0	0.0	0.0	0.0	0.00E+00
C4 aromatic	0.0	0.0	0.0	0.0	0.0	0.0	0.0	0.00E+00
C5 aromatic	0.0	0.0	0.0	0.0	0.0	0.0	0.0	0.00E+00
C6 aromatic	0.1	0.0	0.0	0.0	0.0	0.0	0.0	1.22E-12
C7 aromatic	0.1	0.1	0.1	0.1	0.0	0.0	0.2	5.63E-12
C8 aromatic	5.0	7.1	5.4	1.8	0.5	0.1	3.1	1.43E-11
C9 aromatic	27.0	34.5	26.8	11.7	19.2	2.9	15.1	1.43E-11
C10 aromatic	4.4	5.6	0.8	0.7	0.9	0.0	0.3	1.43E-11
C11 aromatic	0.8	2.9	2.6	2.6	2.5	0.0	1.0	1.43E-11
C12 aromatic	0.3	0.4	1.5	1.6	1.3	1.4	0.6	1.43E-11
C13 aromatic	0.3	0.2	1.0	0.9	0.5	0.2	0.5	1.43E-11
C14 aromatic	0.3	0.2	1.0	0.4	2.9	6.1	0.8	1.43E-11
C15 aromatic	0.2	0.1	0.5	0.0	0.1	0.0	0.5	1.43E-11
C16 aromatic	0.2	0.1	0.3	0.0	0.0	0.1	0.4	1.43E-11
C17 aromatic	0.2	0.1	0.1	0.1	0.0	0.1	0.4	1.43E-11
C18 aromatic	0.1	0.1	0.0	0.1	0.0	0.1	0.4	1.43E-11
C19 aromatic	0.1	0.1	0.0	0.0	0.0	0.2	0.3	1.43E-11
C20 aromatic	0.1	0.2	0.0	0.0	0.0	0.3	0.2	1.43E-11
C21 aromatic	0.0	0.2	0.0	0.0	0.0	0.3	0.1	1.43E-11
benzocycloalkanes	3.9	3.3	8.1	3.6	4.9	6.3	6.4	4.09E-11
diaromatics	1.5	3.6	4.4	0.9	11.9	26.5	4.4	4.09E-11
triaromatics	0.0	0.0	0.0	0.0	0.0	0.1	0.0	4.09E-11
tetraaromatics	0.0	0.0	0.0	0.0	0.0	0.0	0.0	4.09E-11
olefins	1.8	2.5	0.1	0.2	0.1	0.0	0.1	5.00E-11

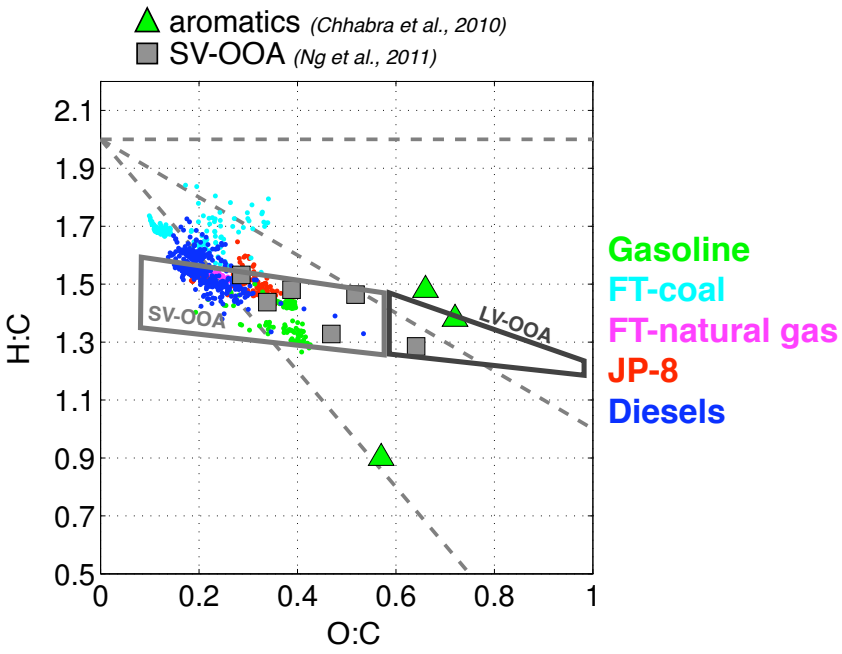

Figure S.1: SOA high resolution aerosol mass spectrometer data presented on a Van-Krevelen diagram (Heald et al., 2010). The small dots show SOA data from this work. The colored symbols show SOA data from literature. SV-OOA and LV-OOA regions adapted from Ng et al., ACP, 2011.

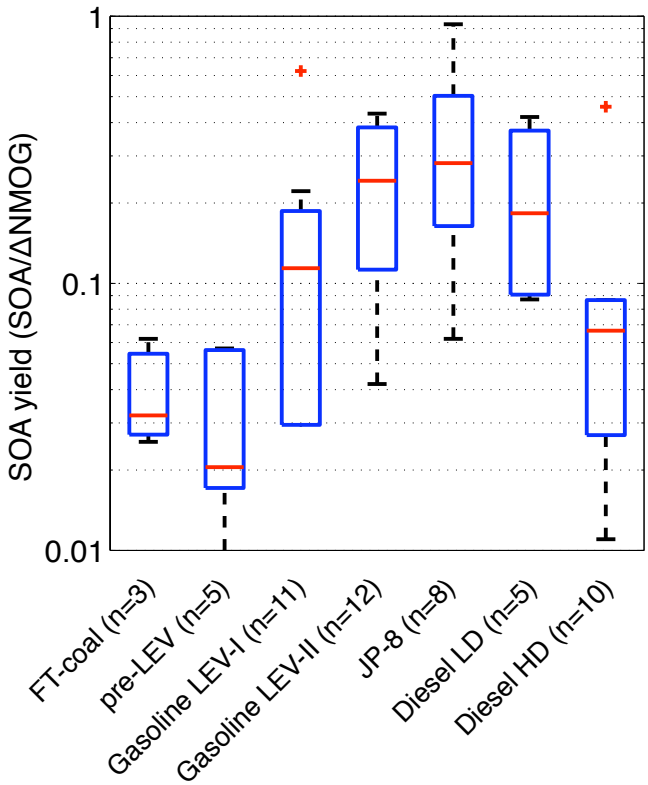

Figure S.2: SOA yield from emissions experiments shown using box-plots for different combustion sources. The SOA yield is expressed as the ratio of SOA formed to the amount of NMOG reacted.

4.6. Acknowledgements

Funding was provided by the U.S. Department of Defense Strategic Environmental Research and Development Program (SERDP) under project WP-1626 and by the U.S. Environmental Protection Agency National Center for Environmental Research (NCER) through the STAR program (R833748).

4.7. References

Bernstein, J. A., Alexis, N., Barnes, C., Bernstein, I. L., Bernstein, J. A., Nel, A., Peden, D., Diaz-Sanchez, D., Tarlo, S. M., and Williams, P. B.: Health effects of air pollution, The Journal of Allergy and Clinical Immunology, 114, 1116-1123, 2004.

CARB: Emfac (mobile source emission inventory), in, 2011.

Chhabra, P., Flagan, R., and Seinfeld, J.: Elemental analysis of chamber organic aerosol using an aerodyne high-resolution aerosol mass spectrometer, Atmospheric Chemistry and Physics, 10, 4111-4131, 2010.

Donahue, N., Robinson, A., Stanier, C., and Pandis, S.: Coupled partitioning, dilution, and chemical aging of semivolatile organics, Environ. Sci. Technol, 40, 2635-2643, doi:10.1021/es052297c, 2006.

Dzepina, K., Volkamer, R., Madronich, S., Tulet, P., Ulbrich, I., Zhang, Q., Cappa, C., Ziemann, P., and Jimenez, J.: Evaluation of recently-proposed secondary organic aerosol models for a case study in mexico city, Atmospheric Chemistry and Physics, 9, 5681-5709, doi:10.5194/acp-9-5681-2009, 2009.

Dzepina, K., Cappa, C. D., Volkamer, R. M., Madronich, S., DeCarlo, P. F., Zaveri, R. A., and Jimenez, J. L.: Modeling the multiday evolution and aging of secondary organic aerosol during milagro 2006, Environmental Science & Technology, 45, 3496-3503, doi: 10.1021/es103186f, 2010.

2005 national emissions inventory data & documentation: http://www.epa.gov/ttnchie1/net/2005inventory.html, 2008.

Forstner, H. J. L., Flagan, R. C., and Seinfeld, J. H.: Molecular speciation of secondary organic aerosol from photooxidation of the higher alkenes: 1-octene and 1-decene, Atmospheric Environment, 31, 1953-1964, 1997.

Gordon, T. D., Nguyen, N. T., May, A. A., Presto, A. A., Lipsky, E. M., Maldonado, S., Chattopadhyay, S., Gutierrez, A., Maricq, M., and Robinson, A. L.: Secondary organic aerosol formed from light duty gasoline vehicle exhaust dominates primary particulate matter emissions, Environ. Sci. Technol, in preparation-a.

Gordon, T. D., Nguyen, N. T., Presto, A. A., Lipsky, E. M., Maldonado, S., Maricq, M., and Robinson, A. L.: Impacts of aftertreatment, fuel chemistry and driving cycle on the production of secondary organic aerosol from diesel vehicle exhaust, Environ. Sci. Technol, in preparation-b.

Grieshop, A. P., Logue, J. M., Donahue, N. M., and Robinson, A. L.: Laboratory investigation of photochemical oxidation of organic aerosol from wood fires 1: Measurement and simulation of organic aerosol evolution, Atmospheric Chemistry and Physics, 9, 1263-1277, 10.5194/acp-9-1263-2009, 2009.

Heald, C., Kroll, J., Jimenez, J., Docherty, K., DeCarlo, P., Aiken, A., Chen, Q., Martin, S., Farmer, D., and Artaxo, P.: A simplified description of the evolution of organic aerosol composition in the atmosphere, Geophys. Res. Lett, 37, L08803, doi:10.1029/2010GL042737, 2010.

Hildebrandt, L., Donahue, N., and Pandis, S.: High formation of secondary organic aerosol from the photo-oxidation of toluene, Atmospheric Chemistry and Physics, 9, 2973-2986, doi:10.5194/acp-9-2973-2009, 2009.

IPCC, W.: Climate change 2007: The physical science basis, Summary for Policy Makers, Contribution of Working Group I to the Fourth Assessment Report of the Intergovernmental Panel on Climate Change, 2007.

Jathar, S. H., Adams, P. J., Donahue, N. M., and Robinson, A. L.: Modeling the influence of volatility and molecular structure on secondary organic aerosol formation, Environ. Sci. Technol, in preparation.

Johnson, D., Utembe, S. R., Jenkin, M. E., Derwent, R. G., Hayman, G. D., Alfarra, M. R., Coe, H., and McFiggans, G.: Simulating regional scale secondary organic aerosol formation during the torch 2003 campaign in the southern uk, Atmos. Chem. Phys., 6, 403-418, 2006.

Keywood, M., Varutbangkul, V., Bahreini, R., Flagan, R., and Seinfeld, J. H.: Secondary organic aerosol formation from the ozonolysis of cycloalkenes and related compounds, Environmental Science & Technology, 38, 4157-4164, 2004.

Lim, Y. B., and Ziemann, P. J.: Products and mechanism of secondary organic aerosol formation from reactions of n-alkanes with oh radicals in the presence of no x, Environmental Science & Technology, 39, 9229-9236, 2005.

Lim, Y. B., and Ziemann, P. J.: Chemistry of secondary organic aerosol formation from oh radical-initiated reactions of linear, branched, and cyclic alkanes in the presence of no x, Aerosol Science and Technology, 43, 604-619, 2009a.

Lim, Y. B., and Ziemann, P. J.: Effects of molecular structure on aerosol yields from oh radical-initiated reactions of linear, branched, and cyclic alkanes in the presence of no x, Environmental Science & Technology, 43, 2328-2334, 2009b.

Logue, J., Huff-Hartz, K., Lambe, A., Donahue, N., and Robinson, A.: High time-resolved measurements of organic air toxics in different source regimes, Atmospheric Environment, 43, 6205-6217, 2009.

Miracolo, M., Hennigan, C., Ranjan, M., Nguyen, N., Gordon, T., Lipsky, E., Presto, A., Donahue, N., and Robinson, A.: Secondary aerosol formation from photochemical aging of aircraft exhaust in a smog chamber, Atmos. Chem. Phys, 11, 4135-4147, doi:10.5194/acp-11-4135-2011, 2011.

Miracolo, M. A., Drozd, G. T., Jathar, S. H., Presto, A. A., Lipsky, E. M., Corporan, E., and Robinson, A. L.: Fuel composition and secondary organic aerosol formation: Gas-turbine exhaust and alternative aviation fuels, Environmental Science & Technology, submitted.

Morris, R. E., Koo, B., Guenther, A., Yarwood, G., McNally, D., Tesche, T. W., Tonnesen, G., Boylan, J., and Brewer, P.: Model sensitivity evaluation for organic carbon using two multi-pollutant air quality models that simulate regional haze in the southeastern united states, Atmos. Environ., 40, 4960-4972, 2006.

Na, K., Song, C., and Cocker, D. R.: Formation of secondary organic aerosol from the reaction of styrene with ozone in the presence and absence of ammonia and water, Atmospheric Environment, 40, 1889-1900, 2006.

Ng, N., Canagaratna, M., Zhang, Q., Jimenez, J., Tian, J., Ulbrich, I., Kroll, J., Docherty, K., Chhabra, P., and Bahreini, R.: Organic aerosol components observed in northern hemispheric datasets from aerosol mass spectrometry, Atmospheric Chemistry and Physics, 10, 4625-4641, 2010.

NRC: Evaluating vehicle emissions inspection and maintenance programs, Committee on vehicle emission inspection maintenance programs, National Academies Press, 2001.

Odum, J. R., Hoffmann, T., Bowman, F., Collins, D., Flagan, R. C., and Seinfeld, J. H.: Gas/particle partitioning and secondary organic aerosol yields, Environmental Science & Technology, 30, 2580-2585, 1996.

Odum, J. R., Jungkamp, T., Griffin, R., Flagan, R. C., and Seinfeld, J. H.: The atmospheric aerosol-forming potential of whole gasoline vapor, Science, 276, 96, 1997a.

Odum, J. R., Jungkamp, T., Griffin, R. J., Forstner, H., Flagan, R. C., and Seinfeld, J. H.: Aromatics, reformulated gasoline, and atmospheric organic aerosol formation, Environmental Science & Technology, 31, 1890-1897, 1997b.

Pankow, J. F.: An absorption model of gas/particle partitioning of organic compounds in the atmosphere, Atmospheric Environment, 28, 185-188, 1994.

Presto, A. A., Miracolo, M. A., Donahue, N. M., and Robinson, A. L.: Secondary organic aerosol formation from high-no x photo-oxidation of low volatility precursors: N-alkanes, Environmental Science & Technology, 44, 2029-2034, 2010.

Presto, A. A., Nguyen, N. T., Ranjan, M., Reeder, A. J., Lipsky, E. M., Hennigan, C. J., Miracolo, M. A., Riemer, D. D., and Robinson, A. L.: Fine particle and organic vapor emissions from staged tests of an in-use aircraft engine, Atmospheric Environment, 45, 3603-3612, 2011.

Presto, A. A., Gordon, T. D., Miracolo, M. A., Hennigan, C. J., and Robinson, A. L.: Primary to secondary organic aerosol: Evolution of emissions from combustion sources, in preparation.

Sage, A., Weitkamp, E., Robinson, A., and Donahue, N.: Evolving mass spectra of the oxidized component of organic aerosol: Results from aerosol mass spectrometer analyses of aged diesel emissions, Atmospheric Chemistry and Physics, 8, 1139--1152, 2008.

Schauer, J. J., Kleeman, M. J., Cass, G. R., and Simoneit, B. R. T.: Measurement of emissions from air pollution sources. 2. C1 through c30 organic compounds from medium duty diesel trucks, Environ. Sci. Technol, 33, 1578-1587, 1999.

Schauer, J. J., Kleeman, M. J., Cass, G. R., and Simoneit, B. R. T.: Measurement of emissions from air pollution sources. 5. C1- c32 organic compounds from gasoline-powered motor vehicles, Environ. Sci. Technol, 36, 1169-1180, 2002.

Simon, H., Beck, L., Bhave, P. V., Divita, F., Hsu, Y., Luecken, D., Mobley, J. D., Pouliot, G. A., Reff, A., Sarwar, G., and Strum, M.: The development and uses of epa's speciate database, Atmospheric Pollution Research, 1, 196-206, doi: 10.5094/APR.2010.026, 2010.

Tkacik, D. S., Presto, A. A., Donahue, N. M., and Robinson, A. L.: Secondary organic aerosol formation from intermediate-volatility organic compounds: Cyclic, linear, and branched alkanes, Environmental Science & Technology, submitted.

Ulbrich, I., Canagaratna, M., Zhang, Q., Worsnop, D., and Jimenez, J.: Interpretation of organic components from positive matrix factorization of aerosol mass spectrometric data, Atmospheric Chemistry and Physics, 9, 2891-2918, 2009.

Vutukuru, S., Griffin, R. J., and Dabdub, D.: Simulation and analysis of secondary organic aerosol dynamics in the south coast air basin of california, J. Geophys. Res., 111, doi:10.1029/2005JD006139, 2006.

Weitkamp, E. A., Amy, M., Pierce, J. R., Donahue, N. M., and Robinson, A. L.: Organic aerosol formation from photochemical oxidation of diesel exhaust in a smog chamber, Environmental Science & Technology, 41, 6969-6975, 2007.

Zhang, Q., Worsnop, D., Canagaratna, M., and Jimenez, J.: Hydrocarbon-like and oxygenated organic aerosols in pittsburgh: Insights into sources and processes of organic aerosols, Atmos. Chem. Phys, 5, 3289--3311, 2005.

Zhang, Q., Jimenez, J. L., Canagaratna, M. R., Allan, J. D., Coe, H., Ulbrich, I., Alfarra, M. R., Takami, A., Middlebrook, A. M., Sun, Y. L., Dzepina, K., Dunlea, E., Docherty, K., DeCarlo, P. F., Salcedo, D., Onasch, T., Jayne, J. T., Miyoshi, T., Shimono, A., Hatakeyama, S., Takegawa, N., Kondo, Y., Schneider, J., Drewnick, F., Borrmann, S., Weimer, S., Demerjian, K., Williams, P., Bower, K., Bahreini, R., Cottrell, L., Griffin, R. J., Rautiainen, J., Sun, J. Y., Zhang, Y. M., and Worsnop, D. R.: Ubiquity and dominance of oxygenated species in organic aerosols in anthropogenically-influenced northern hemisphere midlatitudes, Geophys. Res. Lett, 34, L13801, doi:10.1029/2007GL029979, 2007.

Chapter 5: Modeling the influence of the precursor's volatility and molecular structure on secondary organic aerosol formation*

Abstract

We use SOA data from smog chamber experiments conducted on evaporated fuel to better understand the influence of the precursor's volatility and molecular structure on secondary organic aerosol (SOA) formation. The goals are to test SOA models, identify problems (if any), propose modifications and build new models that are able to represent SOA formation better. SOA data from twenty-three experiments conducted on evaporated gasoline, jet fuel and diesels were used. A traditional (speciated) SOA model (SAPRC lumping, yields parameterized from chamber data, estimated oxidant concentrations, gas-particle partitioning using the volatility-basis set) severely under-predicts the SOA formation when compared to measurements (fractional error = -170%, fractional bias = -130%), mostly because the model includes only the precursor mass that would typically be speciated (volatile *n*-alkanes, single-ring aromatics, unsubstituted cycloalkanes). If we include all the precursor mass, the traditional (base) SOA model results in a much improved model-measurement comparison (fractional error = 76%, fractional bias = 26%) suggesting that the simple failure to account for all precursors results in a significant bias in traditional SOA models. The traditional (base) SOA model over-predicts SOA in the FT-coal experiments because it is not configured to account for branched alkanes, which have very low yields compared to straight/cyclic alkanes and which mostly constitute FT-coal. It over-predicts SOA in the gasoline experiments probably because published yields for single-ring aromatics are biased too high. When we add a branched alkane and multi-ring aromatic model species to the existing SAPRC scheme and "tune" yields for the traditional (base) SOA model,

* To be submitted to Environmental Science and Technology

we improve the model-measurement comparison significantly (fractional error = 54%, fractional bias=-2%). On using a volatility-based model that does not account for differences in the precursor's molecular structure, we find that the model (when fit) is marginally better than the traditional (base) SOA model when its predictions are compared to measurements (fractional error = 73%, fractional bias=13%). This implies that the SOA formation across these precursor fuels can be reasonably modeled using their volatility alone. Since the volatility-based model uses only four yield parameters compared to the traditional model's thirty six yield parameters, it would be much more efficient to use in computationally expensive regional and global aerosol models.

5.1 Introduction

Secondary organic aerosol (SOA) is defined as the aerosol mass formed by the atmospheric processing of gas-phase organic species emitted by natural and anthropogenic sources. Since it accounts for a significant fraction of the atmospheric fine dry aerosol mass (Zhang et al., 2007), it is believed to have a large impact on the earth's climate and public health (IPCC, 2007;Bernstein et al., 2004). However, most SOA models tend to under-predict SOA formation both in the laboratory and in the atmosphere (Heald et al., 2005;Vutukuru et al., 2006;Johnson et al., 2006;Morris et al., 2006;Dzepina et al., 2009;Dzepina et al., 2010;Grieshop et al., 2009;Miracolo et al., 2011). This is probably because there are large gaps in understanding the numerous precursors and pathways to SOA formation (gas-phase oxidation, multi-generational aging, heterogeneous chemistry, condensed-phase reactions, cloud processing), which have resulted in large uncertainties in SOA models. To build effective models, the

different precursors and pathways need to be independently studied, parameterized in models and rigorously tested before they are employed in chemical transport models (CTMs).

Gas-phase oxidation of organic compounds is believed to be the dominant source of SOA formation and hence, has been extensively studied using smog chamber experiments. However, most organic compounds have been studied independently and traditional SOA models based on those studies perform poorly when evaluated for real-world mixtures. Several studies have shown that traditional SOA models are able to explain only a small fraction of the SOA measured from gasoline, diesel and aircraft exhaust and woodsmoke (Gordon et al., in preparation-a;Gordon et al., in preparation-b;Robinson et al., 2007;Miracolo et al., 2011;Miracolo et al., submitted;Grieshop et al., 2009). Combustion emissions and their physico-chemical evolution is complex and the uncertainties mentioned above might be why traditional SOA models fail to perform well. Therefore, there is a research need to test traditional SOA models with realistic mixtures that are less complex than combustion emissions before they are applied to real-world emissions in the laboratory or in the atmosphere.

Single-component studies using smog chambers have demonstrated that SOA formation depends both on the precursor's volatility and molecular structure. Lim and Ziemann (2009a, b, 2005), Presto et al. (2010) and Tkacik et al. (submitted) showed that SOA formation from alkanes increased as the carbon-number increased or the volatility (vapor pressure) decreased. For the same carbon-number or volatility, Lim and Ziemann (2009a, b, 2005) and Tkacik et al. (submitted) showed that cyclic alkanes formed more SOA followed by straight alkanes and branched alkanes. Keywood et al. (2004) observed the same dependency for cycloalkenes and also found that the SOA formation was affected by the location of the double bond (endocyclic vs exocyclic). Experiments on single-ring aromatics (benzene, toluene and xylenes) have shown

that they form much more SOA than similar volatility (C_6 to C_9) *n*-alkanes or alkenes (Ng et al., 2007;Song et al., 2007;Hildebrandt et al., 2009). However, multi-ring aromatics are found to form as much SOA as similar volatility *n*-alkanes (Chan et al., 2009;Shakya and Griffin, 2010). Large biogenic compounds like sesquiterpenes (C_{15}) are extremely efficient in forming SOA (Ng et al., 2006) with yields as high as 50%. Monoterpenes like alpha-pinene (C_{10}) form much less SOA than sesquiterpenes but are comparable to equivalent volatility *n*-alkanes (Ng et al., 2006;Presto et al., 2010). Isoprene (C_5) forms less SOA than monoterpenes although it is much more efficient at forming SOA than any similar volatility organic compound (Ng et al., 2006). In general, SOA formation increases with decrease in volatility but has a complex dependence on molecular structure. Most SOA models have incorporated this influence of volatility and molecular structure. For example, the SAPRC lumping scheme has different model species to account for differences in volatility, i.e. ALK4 (C_5-C_7) versus ALK5 (C_{7+}) and molecular structure, i.e. alkanes (ALK) versus alkenes (OLE) versus aromatics (ARO).

Several studies have pointed out that evaporated primary organic aerosol (POA; also known as semi-volatile organic compounds or SVOC) and intermediate-volatility organic compounds (IVOC) form SOA similar to some of the speciated compounds mentioned above (Grieshop et al., 2009;Robinson et al., 2007;Shrivastava et al., 2008). However, SVOC and IVOC – especially from combustion emissions – are hard to speciate (Schauer et al., 2002a, 1999a, 2001, 1999b, 2002b) and therefore are not very well understood in terms of their SOA potential. Since most SVOC and IVOC cannot be speciated, many aerosol models have adopted a volatility-based approach to model SOA formation from them. For example, in Robinson et al. (2007), SVOC and IVOC react with the hydroxyl radical (OH) to form products that were one order of magnitude lower in volatility than their precursor. In contrast, Pye and Seinfeld (2010)

proposed a single-step mechanism for SVOC where the products of oxidation were two orders of magnitude lower in volatility than the precursor and used SOA yield-data for naphthalene as a surrogate to model IVOC in the traditional way. Jathar et al. (submitted) suggested that SVOC and IVOC reacted with the OH radical to form a distribution of products that were several orders of magnitude lower than their precursor. Although different, the various methods have provided insight and helped close large gaps between predicted and measured SOA concentrations (Shrivastava et al., 2008;Tsimpidi et al., 2009;Dzepina et al., 2010;Pye and Seinfeld, 2010;Jathar et al., 2011). These new generation of models use a lump-and-yield scheme to model SOA formation from speciated emissions and use a volatility-based scheme to model SOA formation from unspeciated emissions like SVOC and IVOC. However, given the success of volatility-based schemes, it could be worthwhile to explore their capabilities for modeling all of SOA.

In this work, we use data gathered from smog chamber experiments run on evaporated fuel to better understand the dependence of the precursor's volatility and molecular structure to form SOA. We test SOA models the way they are currently run in chemical transport or global aerosol models. Based on their performance, we suggest modifications or propose new frameworks to model SOA formation. Since smog chamber data typically capture only the first generation of oxidation, this work does not consider multigenerational aging of SOA products.

5.2 Materials and Methods

5.2.1 SOA experiments and data

Jathar et al. (in preparation) conducted twenty three high-NOx photo-oxidation experiments in the Carnegie Mellon University smog chamber to measure SOA formation from twelve different fuels (gasoline: 3 experiments, Fischer Tropsch-coal: 2 experiments, Fischer

Tropsch-natural gas: 2 experiments, JP-8: 6 experiments, Diesels: 10 experiments). The fuels modestly vary in volatility and molecular structure. In the previous work, we developed representations of the volatility and molecular structure for each fuel using the volatility basis set (VBS; Figure S.1).

We provide a brief outline of the experiments; details can be found in Jathar et al. (in preparation). First, ammonium sulfate seed was added to the chamber to facilitate condensation and prevent nucleation of SOA products. Second, nitrous acid (HONO) was bubbled into the chamber. Third, the precursor (fuel) was introduced into the chamber using a heated septum. Photo-oxidation was initiated by turning on the chamber UV black lights, which photolyzed HONO to produce hydroxyl radicals (OH). NO and NO_2 formed as by-products of HONO irradiation resulted in a low VOC/NO_x ratio that was consistent with ratios found in urban polluted regions. The experiment was performed at low relative humidity (<5%) and a temperature of around 298 K.

Concentrations of gas phase organic compounds were tracked using a GC-MS (Logue et al., 2009) and a proton-transfer reaction mass spectrometer (PTR-MS, Ionicon Analytik) and were used to calculate OH concentrations and OH exposure during the experiment. Particle-phase measurements were made using a scanning mobility particle sizer (SMPS, TSI Inc.) and a quadrupole or high resolution aerosol mass spectrometer (Q-AMS or HR-AMS, Aerodyne Research Inc.) to measure non-refractory aerosol mass, size and composition. Both SMPS and Q-AMS/HR-AMS results were wall-loss corrected to calculate a lower and upper bound on the total SOA formation (Weitkamp et al., 2007;Hildebrandt et al., 2009).

The initial concentration of a fuel species was calculated by multiplying the mass of fuel injected by its percentage mass listed in the fuel composition (Tables S.1 through S.5 in supplementary material). We assume a smog chamber volume of 10 m^3.

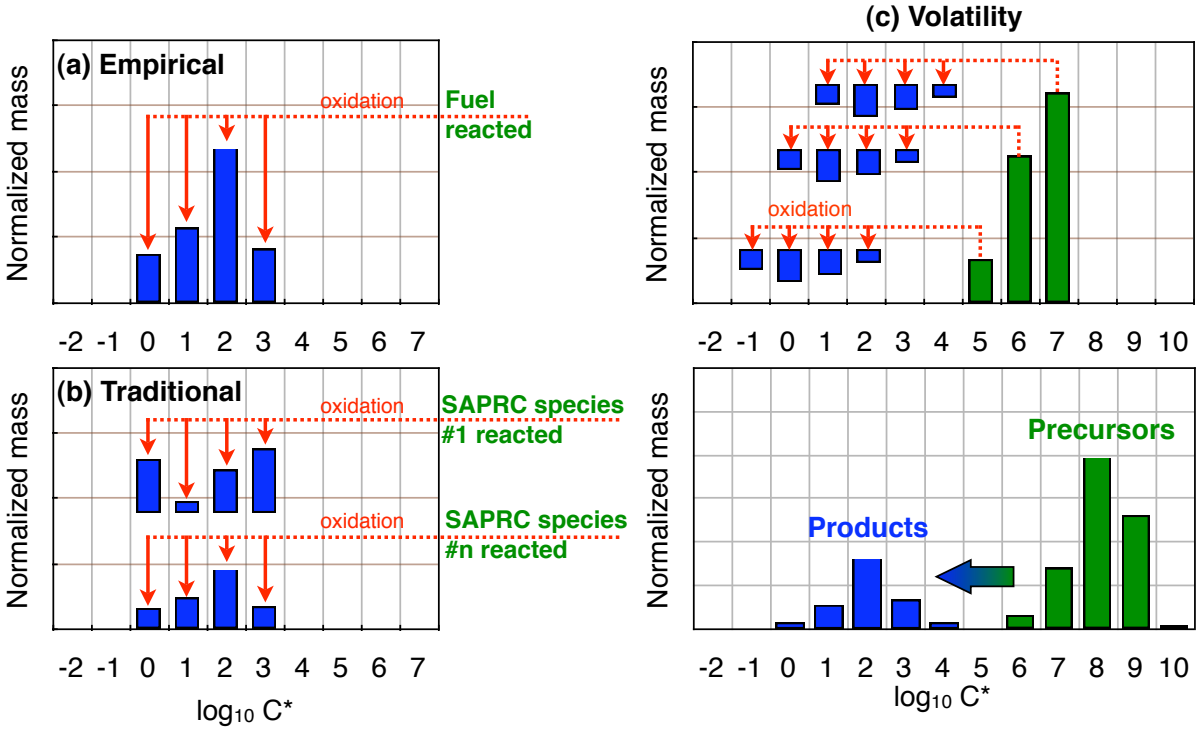

Figure 5.1: Schematics that demonstrate the (a) Empirical, (b) Traditional and (c) Volatility-Based SOA models.

We are aware that experimental uncertainty could affect the quality of data from smog chamber experiments and therefore the conclusions from our analysis. The experimental uncertainty can be thought of as that associated with measurements, repeatability and atmospheric relevance. Of the three, the uncertainty in measurements is probably the lowest as the instruments and techniques used to characterize smog chamber data have evolved over the past two decades. In this work, measurement uncertainties are quantified and wherever possible, included in our analysis. Particularly for experiments used in this work, there is slightly more uncertainty associated with repeatability partly because there might be factors that have a larger

than anticipated effect on the experiment (ambient temperature, relative humidity, VOC/NOx ratio). The uncertainty was kept to a minimum by undertaking tasks such as cleaning the chamber for 12 hours before use, ensuring a minimum background concentration and running a blank experiment. But the largest uncertainty results from whether our static and controlled experiments are truly representative of the dynamic processes in the atmosphere. Atmospheric relevance was ensured by diluting the emissions and maintaining VOC/NOx ratios to those found in the atmosphere.

5.2.2 SOA models

In this work, we model the SOA formed in the chamber using a set of semi-volatile surrogate products represented through the VBS framework (Donahue et al., 2006). The amount of SOA is defined by the gas-particle partitioning of these surrogate products. The VBS separates low-volatility organics into logarithmically spaced bins of effective saturation concentration (C*) between 10^{-2} to 10^{6} μg m^{-3} at 298 K. C* (inverse of the Pankow-type partitioning coefficient, K_p) is proportional to the saturation vapor pressure; it is a semi-empirical property that describes the gas-particle partitioning of an organic mixture (Pankow, 1994;Donahue et al., 2006). The gas-particle partitioning is calculated using absorptive partitioning theory:

$$\zeta_i = \left(1 + \frac{C_i^*}{C_{OA}}\right)^{-1}$$
$$C_{OA} = \sum_{i=1}^{N} \zeta_i \times M_i\big|_{g+p} \qquad (5.1)$$

where, ζ_i is the fraction of mass in volatility bin '*i*' in the particulate phase, C_i* is the effective saturation concentration of bin '*i*' in μg m^{-3}, C_{OA} is the total particulate OA concentration in μg

m^{-3}, M_i is the total organic concentration (gas+particle) in bin 'i' in μg m^{-3} and N is the number of basis set bins.

All models can be described using the following equations:

$$\frac{d[X_j]}{dt} = -k_{OH,X_j}[OH][X_j] \quad (5.2)$$

$$\frac{d[M_i|_{g+p}]}{dt} = \underbrace{\sum_j \alpha_{i,j} k_{OH,X_j}[OH][X_j]}_{first-generation\ products} \quad (5.3)$$

Equation (5.2) represents the first-generation oxidation of an SOA precursor where $k_{OH,Xj}$ is the reaction rate constant between the oxidant [OH] and SOA precursor [X_j]. The index j indicates different precursors, either fuel species or volatility bins of the fuel. The k_{OH} for each fuel species is listed in the supplementary material (Tables S.1-S.5). Equation (5.3) tracks the first-generation secondary organic mass formed in 'i'th bin as a result of the precursor oxidation where $\alpha_{i,j}$ is the mass yield for the first-generation oxidation reaction. $M_i|_{g+p}$ is the total gas+particle organic mass in the 'i'th bin of the VBS; its gas-particle partitioning is calculated using equation (5.1).

We do not consider the multi-generational aging of semi-volatile products because the smog chamber data only represents first-generation oxidation products.

5.2.2.1 Empirical

In the Empirical model, each fuel is modeled separately. For each fuel, we assume that every fuel species has the same mass yield or in other words $\alpha_{i,j} = \alpha_i$. We fit the SOA data to determine α's for each fuel. Figure 5.1(a) shows a schematic of the Empirical model. The empirical model represents a "best fit" to the experimental data, against which other theoretical models can be judged.

To implement the Empirical model in a CTM, one needs as many model precursors as there are source types. Here, we consider six model precursors for six different fuels. Each fuel is fit across a 5-bin VBS. Therefore, the Empirical model will have 30 free parameters.

5.2.2.2 Traditional

In the Traditional model, all fuels are modeled using the same methodology and parameters. Figure 5.1(b) shows a schematic of the Traditional model. We use the SAPRC scheme to lump fuel species into a model species, i.e. *n*-decane is lumped as ALK5, benzene is lumped as ARO1 and so on. The lumping used for each fuel species is listed in the supplementary material (Tables S.1-S.5). We use mass yields ($\alpha_{i,j}$) published by Murphy and Pandis (2010) for SAPRC model species to predict SOA formation; the mass yields are listed in Table S.6.

Due to the SAPRC lumping, the Traditional model accounts for differences in both the precursor's volatility and molecular structure to form SOA. The model treats different molecular structures, i.e. alkanes (ALK), alkenes (OLE), aromatics (ARO), isoprene (ISOP) and terpenes (TERP), separately. Since there are no terpenes or isoprene in the fuel, we do not discuss them in the rest of the chapter. Within each molecular structure (ALK, OLE and ARO), there are two or more model species that stand for different reactivities with the OH radical or also different volatilities, since reactivity within a molecular structure correlates well with the volatility of the species. SAPRC (or any other gas-phase mechanism) was initially designed to simulate hydrocarbon-NO_x-ozone photochemistry and the different reactivities were supposed to capture the efficiency with which a given species produced ozone. The Traditional model seems to be well-resolved in molecular structure but coarsely-resolved in volatility.

The Traditional model is run in three configurations:

Traditional (speciated): In this configuration, the model is run similar to contemporary SOA models. Contemporary SOA models only consider speciated organic compounds that are available as part of an emissions inventory. Therefore, in this configuration we only include *n*-alkanes, single-ring aromatics and smaller (<C_{12}) alkenes and branched and cyclic alkanes and ignore organics that typically remain unspeciated.

Traditional (base): In this configuration, the model includes both the speciated and unspeciated organics. The unspeciated organics are included in the model using engineering judgment.

Traditional (extended): The Traditional (extended) model is a modified version of the Traditional (base) model. With respect to lumping, we add a model species to represent all branched alkanes (BALK) and change the lumping for aromatics where all single-ring aromatics are lumped into ARO1 and all multi-ring aromatics are lumped into ARO2. The new lumping is listed in the supplementary material (Tables S.1-S.5). With respect to yields ($\alpha_{i,j}$), we use a genetic optimization technique to assign new yields to BALK, ARO1 and ARO2 and adjust the Murphy and Pandis (2010) yields for ALK4, ALK5, OLE1 and OLE2 so that there is better agreement between model predictions and measurements.

To implement the Traditional (speciated/base) models in a CTM, one would need 9 model precursors. Each model precursor would have a 5-bin VBS parameterization. Therefore, the Traditional (speciated/base) models would have 45 free parameters. To implement the Traditional (extended) model in a CTM, one would need 10 model precursors. Therefore, the Traditional (extended) model will have 50 free parameters.

5.2.2.3 Volatility-based

In the volatility-based model (VBM), we assume that SOA formation is a function of the precursor's volatility alone; the volatility is expressed using the VBS. Each precursor C* bin (corresponding to an X_j in equation (2)) forms a certain product distribution with mass yields $\alpha_{i,j}$. Each higher (or lower) precursor C* bin forms the same product distribution but shifted by one C* bin; we base this assumption on the work of Presto et al. (2010), who found that for *n*-alkanes, the addition of 2 carbon atoms to an *n*-alkane shifted its corresponding SOA product distribution, on average, by one C* bin. Figure 5.1(c) shows a schematic of the VBM. The top panel shows how each precursor C* bin forms products while the bottom panel illustrates how a 'precursor' volatility distribution transforms into a 'product' volatility distribution.

A key input to the VBM is the fuel's volatility distribution, which is constructed using fuel composition data; details are in Jathar et al. (in preparation). Figure S.1 shows the volatility distribution for each fuel. Another key input to the VBM is the precursor C* bin's reaction rate with the OH radical ($k_{OH,Xj}$). Using Atkinson and Arey (Atkinson and Arey, 2003), we develop a mathematical relationship between C* of a hydrocarbon and k_{OH}. We find that alkanes, alkenes and aromatics have very different relationships; alkanes: $k_{OH} = -1.84\text{x}10^{-12} \log(\text{C*}) + 4.27\text{x}10^{-11}$, alkenes: $k_{OH} = 4.0\text{x}10^{-11}$, aromatics: $k_{OH} = -5.7\text{x}10^{-12} \log(\text{C*}) + 1.14\text{x}10^{-10}$.

To implement the VBM in a CTM, one would need 8 model precursors. Each model precursor would have the same 5-bin VBS parameterization but shifted in volatility space. Therefore, the VBM will only have 5 free parameters.

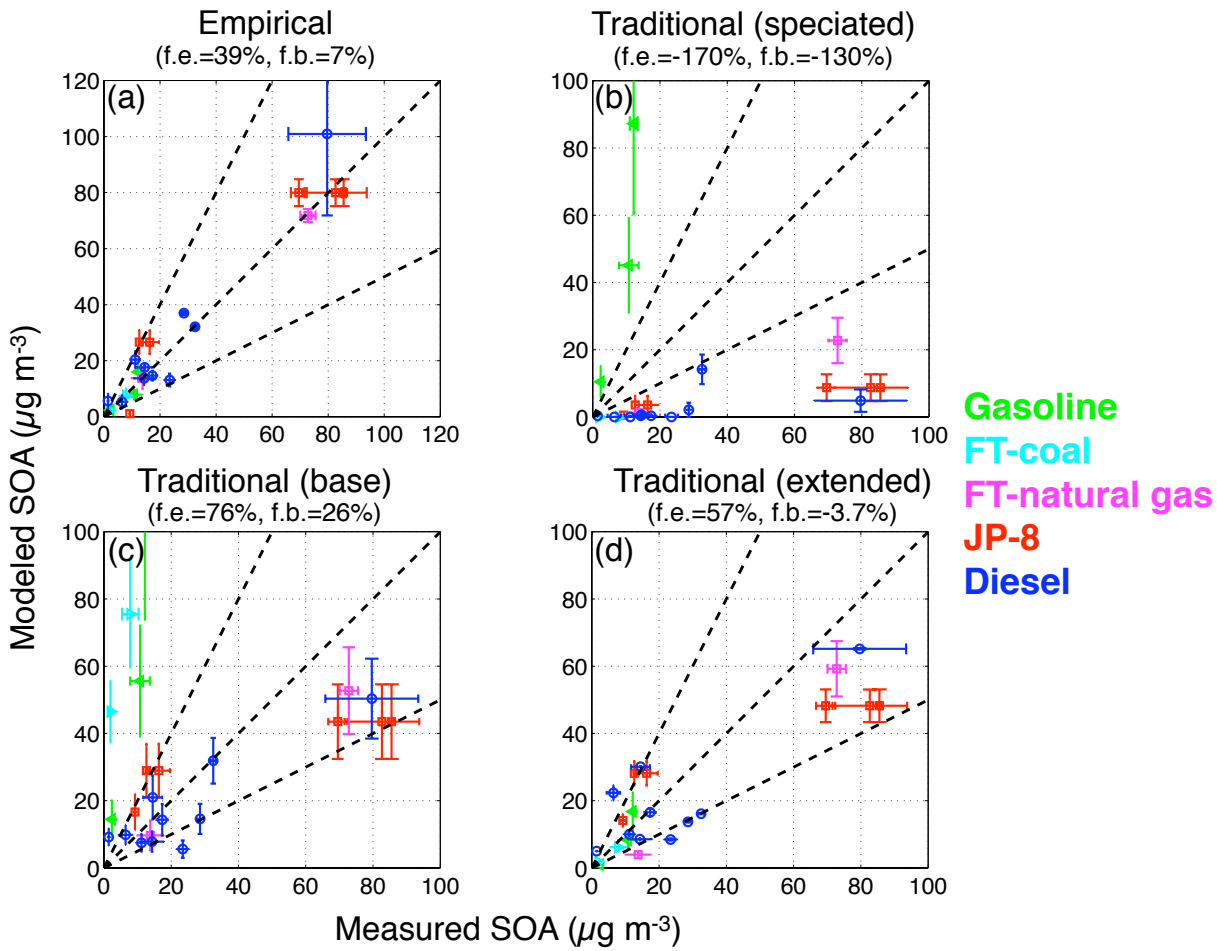

Figure 5.2: SOA predictions from the (a) Empirical, (b) Traditional (speciated), (c) Traditional (base) and (d) Traditional (extended) models compared to measurements. The fractional error (f.e.) and fractional bias (f.b.) are mentioned in parentheses.

5.3. Results

5.3.1 Empirical

The Empirical model uses α's, that were determined by fitting the SOA data for each fuel. Model predictions for the SOA mass concentration for the Empirical model are compared against measurements in Figure 5.2. For visual clarity, we only show end-of-experiment values for the comparison. We use statistical metrics of fractional error and fractional bias to quantitatively evaluate the model performance, which are calculated using all time-resolved data.

$$Fractional\ Error = \frac{1}{N}\sum_{i=1}^{N}\frac{P-M}{\frac{P+M}{2}} \quad (5.4)$$

$$Fractional\ Error = \frac{1}{N}\sum_{i=1}^{N}\frac{|P-M|}{\frac{P+M}{2}} \quad (5.5)$$

The Empirical model represents the best fit to the data and therefore its statistical metrics present an upper limit on the performance of other models. The Empirical model produces a good model-measurement comparison but still results in a high fractional error. The high fractional error is likely due, in part, to the experiment-to-experiment variability and uncertainty in the measurements. For example, fits to toluene SOA data collected from Hildebrandt et al. (2009) and Ng et al. (2007) imply an uncertainty of a factor of two. SOA data for similar experiments on naphthalene from Chan et al. (2009) and Shakya and Griffin (2010) vary by at least a factor of two. Across the experiments, it is possible that modest changes in the wall-loss rates, oxidant or radical concentrations and VOC to NO_x ratios result in a slightly different chamber environment that affects SOA formation. The fractional error and fractional bias for all models used in this work are plotted in Figure 5.6; the Empirical model is plotted using a red star.

5.3.2 Traditional

Figure 5.2(b) plots the model-measurement comparison for the Traditional (speciated) model. The model severely under-predicts the SOA formation when compared to measurements. The model results in both a high fractional error (-170%) and fractional bias (-130%).

When we include all the precursor mass in the Traditional (base) model, it does substantially better (fractional error = 76%, fractional bias = 26%) compared to the Traditional (speciated) model but does not do as well when compared to the Empirical model. The

improvement in performance of the Traditional (base) model (purple square) over the Traditional (speciated) model (blue circle) is substantial and can be clearly see in Figure 5.6. For the Traditional (base) model, the FT-natural gas, JP-8 and diesel data are predicted within a factor of two but the gasoline and FT-coal data are over-predicted. When we look closely at the Traditional (base) model's predictions by organic class, we find that for gasoline, most of the predicted SOA comes from aromatics. Given that published yields for precursors like toluene vary by more than a factor of two (Ng et al., 2007;Lane et al., 2008;Hildebrandt et al., 2009), it is possible that the SOA yields for aromatics in Murphy and Pandis (2010) are biased high. Further, SAPRC does not distinguish between different alkane structures and hence straight, branched and cyclic alkanes with similar volatility are assigned the same yields. But, previous work (Lim and Ziemann, 2009;Tkacik et al., submitted) has shown that branched alkanes have much smaller SOA yields than straight and cyclic alkanes. Hence, it is no surprise that the Traditional (base) model over-predicts SOA formation for FT-natural gas, which is dominated by branched alkanes (88%).

The performance of the Traditional (base) model can be further improved by making a few changes to the SAPRC model species and adjusting the Murphy and Pandis (2010) yields (see section 5.2.2.3 for more detail). If the model's prediction for FT-coal needs to be improved, branched alkanes would need to be modeled separately. Similarly, if the model's predictions for gasoline are to be improved, the single-ring aromatic yields would need to be lowered. But adding a branched alkane model species and lowering the single-ring aromatic yields would also change the model's predictions for FT-natural gas, JP-8 and diesels. To overcome the problem, we develop a genetic optimization algorithm where we try different lumping strategies for fuel species, determine a set of yields for the branched alkane model species, lower yields for single-

ring aromatics and adjust yields for the other model species (ALK4, AL5, OLE1, OLE2) all at the same time. The objective of the algorithm is to improve the model-measurement comparison by minimizing the fractional error. The optimum solution requires the Traditional (base) model to undergo two major changes: (1) addition of a branched alkane model species (BALK) that includes only branched alkanes with carbon-number 7 and higher and (2) single-ring aromatics will be lumped under ARO1 and multi-ring aromatics will be lumped under ARO2. New yields for BALK and extended yields for ARO1, ARO2, ALK4, AL5, OLE1 and OLE2 are listed in Table 5.1. We call this new model Traditional (extended).

Figure 5.2(c) compares model predictions from the Traditional (Extended) model to measurements. The Traditional (Extended) model performs better than the Traditional (base) model as most of its predictions lie within a factor of two of the measurements; the performance is also reflected through the improved statistical metrics and location in Figure 5.6 (green diamond). As expected, most of the improvement stems from better (lower) predicted yields from gasoline and FT-coal.

Table 5.1: SOA VBS yields for model precursors in Traditional (extended)

Group	C* (μg/m3)				
	0.1	1	10	100	1000
BALK	0.001	0.000	0.000	0.000	0.000
ALK4	0.001	0.039	0.042	0.040	0.977
ALK5	0.001	0.018	0.102	0.359	0.746
OLE1	0.000	0.001	0.005	0.038	0.150
OLE2	0.000	0.003	0.026	0.083	0.270
ARO1	0.001	0.015	0.089	0.034	0.404
ARO2	0.007	0.218	0.162	0.255	0.022
ISOP*	0.000	0.000	0.023	0.015	0.000
SESQ*	0.000	0.075	0.150	0.750	0.900
TERP*	0.000	0.012	0.122	0.201	0.507

*same as Murphy and Pandis (2010)

5.3.3 Volatility-based

Table 5.2: SOA VBS yields for model precursors in VBM

	Product C* ($\mu g\ m^{-3}$)				
Precursor C*	0.1	1	10	100	1000
$10^2\ \mu g\ m^{-3}$	0.431	0.000	0.000	0.000	0.000
$10^3\ \mu g\ m^{-3}$	0.210	0.191	0.029	0.000	0.000
$10^4\ \mu g\ m^{-3}$	0.142	0.000	0.271	0.018	0.000
$10^5\ \mu g\ m^{-3}$	0.097	0.023	0.013	0.290	0.008
$10^6\ \mu g\ m^{-3}$	0.011	0.078	0.034	0.006	0.297
$10^7\ \mu g\ m^{-3}$	0.000	0.011	0.080	0.028	0.060
$10^8\ \mu g\ m^{-3}$	0.000	0.000	0.011	0.078	0.041
$10^9\ \mu g\ m^{-3}$	0.000	0.000	0.000	0.011	0.085
$10^{10}\ \mu g\ m^{-3}$	0.000	0.000	0.000	0.000	0.022

For the VBM, all SOA data is fit to determine a mass yield matrix ($\alpha_{i,j}$) for the precursor C* bins; $\alpha_{i,j}$ is listed in Table 5.2. Figure 5.3(a) compares SOA model predictions from the VBM to measurements. The VBM is substantially better than the Traditional (speciated) model, marginally better than the Traditional (base) model but not as good as the Traditional (extended) or Empirical models. The VBM is plotted in Figure 5.6 using an orange triangle. The reasonable comparison implies that a model based on volatility alone can explain a lot of the variability in the measured SOA data. However, there are several instances where the VBM's performance is limited. For the diesel data at lower C_{OA}, the VBM predicts roughly the same SOA mass despite variability in the measured SOA mass because all the diesels have roughly the same volatility distribution. The VBM predicts the same SOA formation for FT-coal and FT-natural gas since they share the same volatility profile although they have different structures; FT-coal is mostly composed of branched alkanes while FT-natural gas is an equal mix of *n*-alkanes and branched alkanes. Therefore, the VBM over-predicts the FT-coal SOA and under-predicts the FT-natural gas SOA.

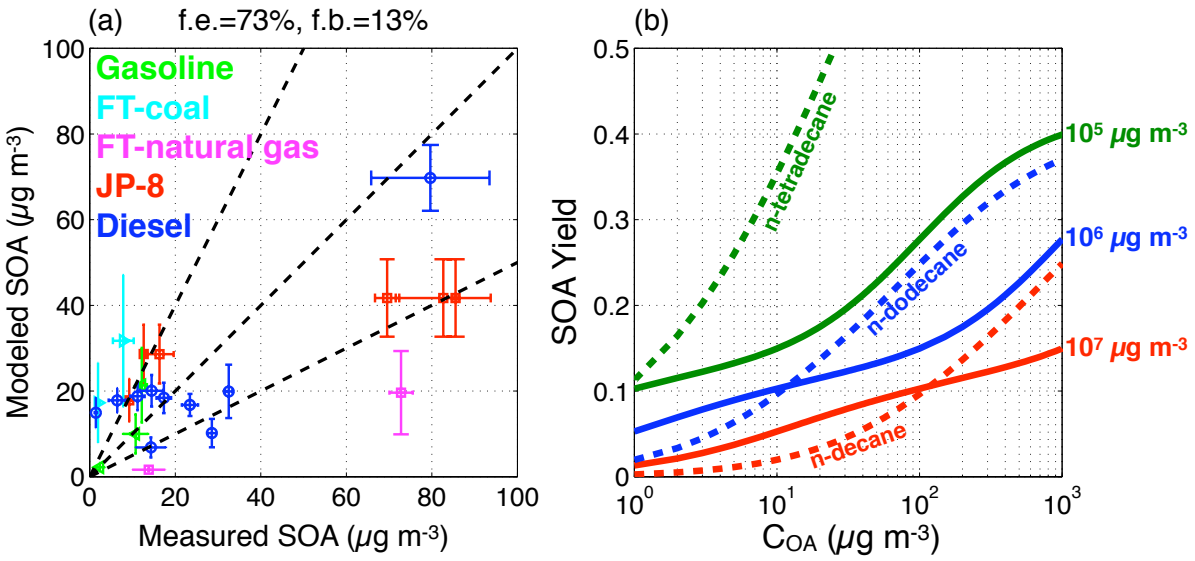

Figure 5.3: (a) SOA predictions from the Volatility-Based model compared to measurements and (b) SOA yield curves for C* precursors 10^5, 10^6 and 10^7 µg m^{-3} (solid lines). For comparison, we plot the SOA yield curves for n-decane (estimated), n-dodecane and n-tetradecane (dotted lines). The colors connect the solid lines to the dotted lines as the C* bins roughly correspond to the C* of the n-alkanes.

Figure 5.3(b) plots the SOA yields for the 10^5, 10^6 and 10^7 C* precursor bins. For reference, we also plot SOA yields for *n*-decane, *n*-dodecane and *n*-tetradecane. The colors are supposed to connect VBM's precursors to similar volatility *n*-alkanes. The SOA yields for the VBM precursors, on average, are lower than equivalent-volatility *n*-alkanes suggesting that the evaporated fuel emissions, on average, behave more like branched alkanes than *n*-alkanes, cycloalkanes or aromatics.

Figure 5.4 plots the SOA yield for various SOA precursors at a C_{OA} of 5 µg m^{-3}. The SOA yields for precursors from the VBM are plotted as a yellow band; the band captures uncertainty in the fit. We also plot SOA yields for various species based on published literature; the error bars represent an uncertainty of a factor of two. The SOA yields interpreted using the VBM compare reasonably well with those measured for the range of single species. This is despite the VBM using no *a-priori* information about what the SOA yields might be for species

in a given volatility range. The plot suggests that the parameters used in the VBM are able to modestly capture the variability in SOA yields observed with volatility.

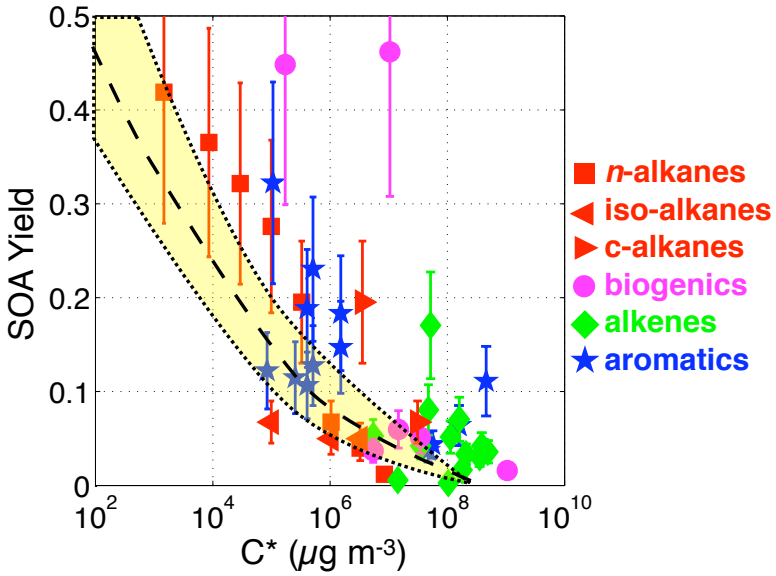

Figure 5.4: SOA yield presented as a function of precursor C* at a COA of 5 µg m^{-3}. The yellow band represents fits for the Volatility-based model. *n*-alkane data is from Presto et al. (2010), c-alkane and iso-alkane data is from Tkacik et al. (submitted), biogenic data is from Farina et al. (2010), alkene data is from Forstner et al. (1997), Na et al. (2006) and Keywood et al. (2004) and aromatic data is from Ng et al. (2007), Song et al. (2007), Hildebrandt et al. (2009), Chan et al. (2009) and Shakya et al. (2010). C* values are determined either from the NIST database or EPA's Estimation Program Interface suite.

Figure 5.5 plots the SOA production from gasoline, FT, JP-8 and diesel for unit precursor emissions assuming that all of the precursor is reacted. The SOA is stacked and color coded based on the C* of the precursor. Inline with our experimental results, Figure 5.5 shows that for unit precursor emissions, diesel forms the most SOA followed by JP-8, FT and gasoline. It also shows that, as one moves to lower volatility fuels (gasoline to FT to JP-8 to diesel), the contribution to total SOA from lower volatility species increases significantly. Traditional (speciated) SOA models have only included organic species that have a C* greater than 10^6 µg m^{-3}, an approximation that is appropriate for gasoline and Fischer-Tropschs fuels but not for JP-8 and diesel. If we assume that combustion emissions correlate with the fuel in terms of their

volatility, Figure 5.5 implies that these models may be able to capture the entire SOA formation from emissions of engines using gasoline and FT but might miss most of the SOA formed from the use of JP-8 and diesel.

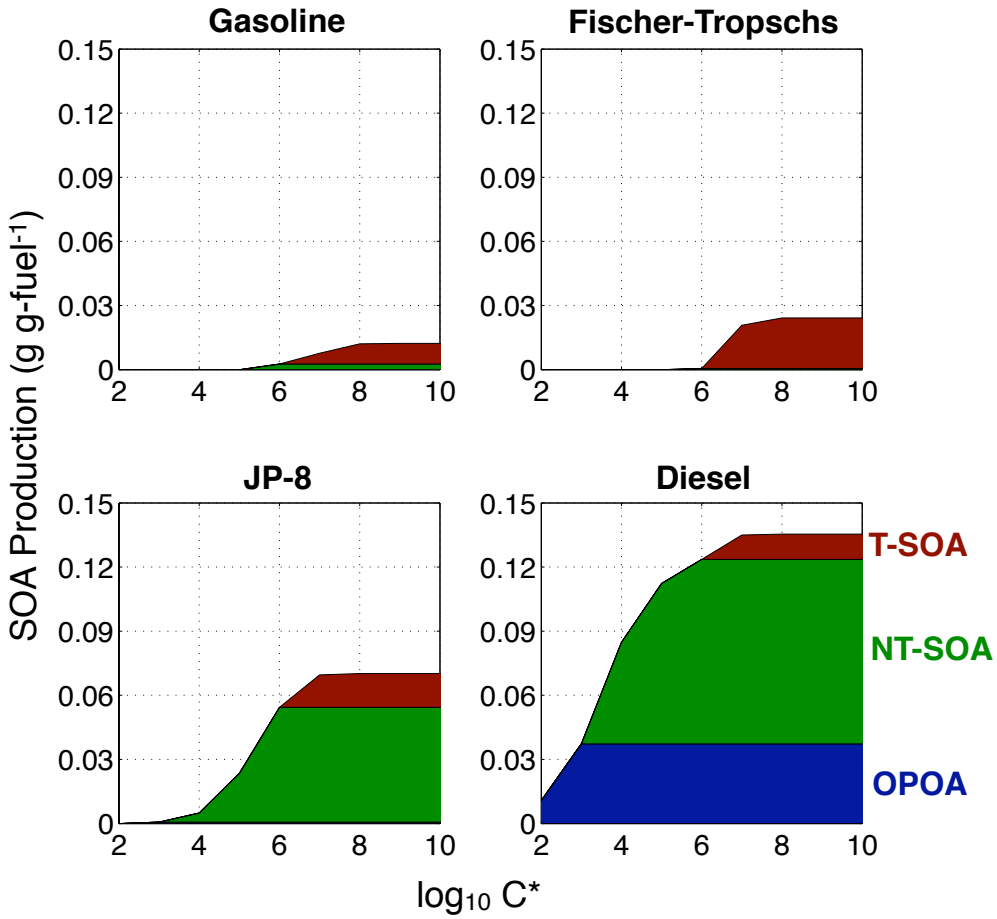

Figure 5.5: Cumulative SOA production as a function of C* for the four different fuels (see Fig S.2 for details). The different colors represent SOA arising from precursors with different C*s: OPOA (blue) is SOA from precursors in C* bins less than 10^3 µg m^{-3}, NT-SOA (green) is SOA from precursors in C* bins 10^4 to 10^6 µg m-3 and T-SOA (maroon) is from SOA from precursors in C* bins 10^7 µg m^{-3} and higher.

One could extend the VBM to also incorporate molecular structure by having a different set of yields for different molecular structures. However, SOA data used in this work are insufficient to determine a molecular structure-resolved VBM.

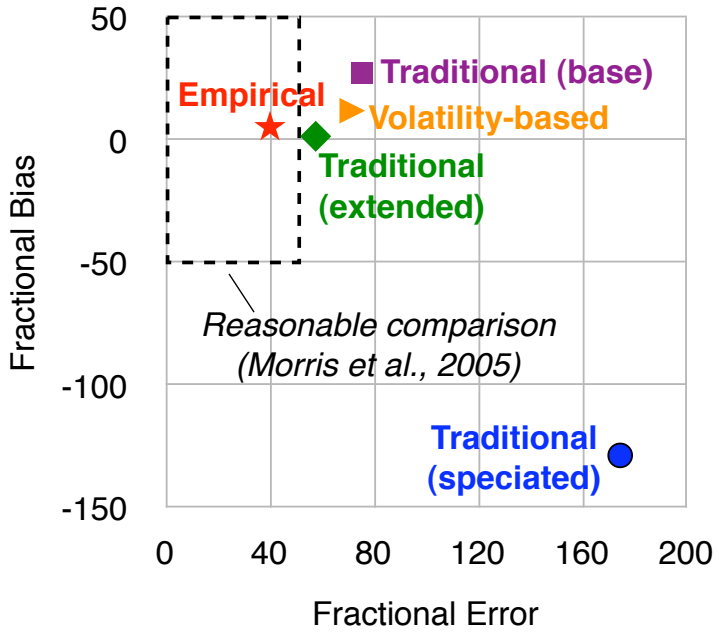

Figure 5.6: Fractional error and fractional bias plotted for different models used in this study.

5.4 Summary and Discussion

We use SOA data from smog chamber experiments conducted on evaporated fuel to parameterize and test SOA models that include the influence of the precursor's volatility and/or molecular structure. A Traditional (speciated) SOA model – run similar to contemporary SOA models where only the speciated mass is included in the model – severely under-predicts measured SOA formation. The Traditional (base) model reasonably predicts the measured SOA formation when all the precursor mass in included in the model. The performance of the Traditional (base) model can be improved somewhat by adding a model species to track branched alkanes and multi-ring aromatics and further tuning its SOA yields for straight/cyclic alkanes and single-ring aromatics. A volatility-based model (VBM) that models SOA as a function of the precursor's volatility alone is able to modestly fit the data and produce a model-measurement comparison slightly better than the Traditional (base) model.

Figure 5.6 plots the statistical metrics for different models (Empirical, Traditional, VBM) used in this study. From the figure, it is clear that the Traditional (speciated) model heavily under-predicts SOA formation. When contrasted with other models where all the precursor mass is included, we find that the models predict SOA formation substantially better than the Traditional (speciated) model. This suggests that simply including all the precursor mass in the models, would to some extent, correct the under-prediction seen with contemporary SOA models. Studies have found that precursor mass, especially from combustion processes, is hard to speciate, which makes it difficult to include explicitly in models (Schauer et al., 2002a, 1999a, 2001, 1999b, 2002b). There have been several efforts to speciate a larger fraction of complex organic mixtures using sophisticated chromatographic techniques (Edam et al., 2005;Isaacman et al.) but until those analyses reveal organic species that can be studied for their SOA potential, we will need alternative methods to incorporate the unspeciated mass in SOA models. Recently, Presto et al. (submitted, 2011) developed a technique to determine volatility mass distributions for emissions lower than a C* of 10^6 μg m^{-3} using a thermal desorption GC-MS; they very able to speciate very little of the emissions mass. The technique could provide the perfect input to the VBM which models SOA formation only based on the volatility of the precursor. So, although the model does not incorporate the influence of molecular structure, it becomes fairly easy to include all the precursor mass into the model.

The SOA models described in this work and used elsewhere in CTMs are semi-empirical because the organic compounds present in SOA and their interactions are currently too complex to be represented using first principles. So fundamentally, a model that is more finely resolved in terms of its precursors and (fit) parameters would do better than a less resolved model. The Empirical and Traditional (extended) models have many more parameters (30 and 50

respectively) than the VBM (5 parameters) but their performance is only marginally better than the VBM. This would imply that the VBM is a much simpler but more insightful method to represent SOA formation from gas-phase oxidation of organic emissions. Further, in a CTM where each precursor adds computational expense, one would like to keep the model precursors to a minimum. The Empirical model provides the best model-measurement comparison but would be computationally very expensive to implement in a CTM. Assuming different sources have different SOA potentials, each source would need a separate model precursor, i.e. for a CTM with 20 sources (conservative), using the Empirical model would mean 20 model precursors. In contrast, the Traditional (base/extended) models, which have a slightly poorer model-measurement comparison, would be much more computationally efficient since they would need 9/10 model precursors. This is assuming that the unspeciated mass can be well represented with the existing model precursors. Presently, SOA models in CTMs treat unspeciated SVOC and IVOC separately and hence add to the computational burden; Shrivastava et al. (2008), Jathar et al. (2011), Tsimpidi et al. (2009), Dzepina et al. (2009) used 9 model precursors while Pye and Seinfeld (2010) have used 3. The VBM produces a similar model-measurement comparison as the Traditional (base) model and would need 8 model precursors ($C^*=10^2$ to $C^*=10^9$ $\mu g\ m^{-3}$) for implementation in a CTM. Opposed to the Traditional models, the VBM also, offers the advantage of representing the SVOC and IVOC within the existing 9 model precursors. So, although molecular structure does influence SOA formation, SOA formation as a function of volatility alone (represented through the VBM) is probably sufficient for use in CTMs.

Based on this work, we make several recommendations for models simulating SOA formation from gas-phase oxidation of organic emissions. First, we propose that contemporary

SOA models critically review emission inventories for their unspeciated mass and find ways to include the mass in their models. Second, for SOA models that are currently using SAPRC-type schemes, we advise that they change their lumping schemes to account for branched alkanes and multi-ring aromatics and change their yields for alkanes and single-ring aromatics based on Table 5.1. Third, for modelers intent on adding or revising SOA schemes in regional or global models, we suggest that they consider the use of a volatility-based scheme. We recommend representing the precursor using the VBS and using the SOA yields in Table 5.2 to model SOA formation. And finally, for experimentalists working on characterizing combustion emissions, we would encourage them to pursue techniques to characterize the entire volatility spectrum of emissions for use in volatility-based models.

5.5 Supplementary material

Table S.1: Composition information for California summer gasoline

Species	Mass %	k_OH	Lumping		
			Traditional (speciated)	Traditional (base)	Traditional (extended)
C4 Paraffin	0.3	2.36E-12	NONE	NONE	NONE
C5 Paraffin	10.9	3.80E-12	ALK4	ALK4	NONE
C6 Paraffin	12.3	5.20E-12	ALK4	ALK4	NONE
C7 Paraffin	9.4	6.76E-12	ALK4	ALK4	BALK
C8 Paraffin	9.8	8.11E-12	ALK5	ALK5	BALK
C9 Paraffin	3.1	9.70E-12	ALK5	ALK5	BALK
C10 Paraffin	1.2	1.10E-11	ALK5	ALK5	BALK
C11+ Paraffin	0.7	1.23E-11	NONE	ALK5	BALK
C6 Aromatic	0.6	1.22E-12	ARO1	ARO1	ARO1
C7 Aromatic	5.8	5.63E-12	ARO1	ARO1	ARO1
C8 Aromatic	9.3	1.43E-11	ARO2	ARO2	ARO1
C9 Aromatic	8.8	1.43E-11	ARO2	ARO2	ARO1
C10 Aromatic	2.7	1.43E-11	ARO2	ARO2	ARO1
C11+ Aromatic	1.0	1.43E-11	ARO2	ARO2	ARO1
Olefins	14.0	3.70E-11	OLE1	OLE1	OLE1
C5 Cycloalkane	0.1	4.97E-12	ALK4	ALK4	ALK4
C6 Cycloalkane	0.2	6.97E-12	ALK5	ALK5	ALK5
C7 Cycloalkane	0.1	6.76E-12	ALK5	ALK5	ALK5

C8 Cycloalkane	0.0	8.11E-12	ALK5	ALK5	ALK5
C9 Cycloalkane	0.0	9.70E-12	ALK5	ALK5	ALK5
poly-N	0.0	1.42E-11	ALK5	ALK5	ALK5

Table S.2: Composition information for Fischer-Tropsch (coal)

Species	Mass %	k_OH	Lumping		
			Traditional (speciated)	Traditional (base)	Traditional (extended)
n-alkanes	0.2	1.10E-11	ALK5	ALK5	ALK5
monoaromatics	0.5	1.43E-11	ARO2	ARO2	ARO1
diaromatics	0.1	2.30E-11	NONE	ARO2	ARO2
Isoalkanes	84.9	1.10E-11	NONE	ALK5	BALK
cycloalkanes	12.6	1.10E-11	NONE	ALK5	ALK5

Table S.3: Composition information for Fischer-Tropsch (natural gas)

Species	Mass %	k_OH	Lumping		
			Traditional (speciated)	Traditional (base)	Traditional (extended)
n-heptane	0.0		ALK4	ALK4	ALK4
n-octane	1.6	6.76E-12	ALK5	ALK5	ALK5
n-nonane	22.4	8.11E-12	ALK5	ALK5	ALK5
n-decane	25.1	9.70E-12	ALK5	ALK5	ALK5
n-undecane	3.8	1.10E-11	ALK5	ALK5	ALK5
n-dodecane	0.3	1.23E-11	ALK5	ALK5	ALK5
n-tridecane	0.0	1.32E-11	NONE	ALK5	ALK5
n-tetradecane	0.0	1.51E-11	NONE	ALK5	ALK5
n-pentadecane	0.0	1.79E-11	NONE	ALK5	ALK5
n-hexadecane	0.0	2.07E-11	NONE	ALK5	ALK5
n-heptadecane	0.0	2.32E-11	NONE	ALK5	ALK5
n-octadecane	0.0	2.85E-11	NONE	ALK5	ALK5
n-nonadecane	0.0	3.51E-11	NONE	ALK5	ALK5
isoalkanes	46.8	4.32E-11	NONE	ALK5	BALK

Table S.4: Composition information for JP-8

Species	Mass %	k_OH	Lumping		
			Traditional (speciated)	Traditional (base)	Traditional (extended)
n-heptane	0.1	6.76E-12	ALK4	ALK4	ALK4
n-octane	0.3	8.11E-12	ALK5	ALK5	ALK5
n-nonane	1.2	9.70E-12	ALK5	ALK5	ALK5
n-decane	3.5	1.10E-11	ALK5	ALK5	ALK5
n-undecane	4.2	1.23E-11	ALK5	ALK5	ALK5
n-dodecane	3.7	1.32E-11	ALK5	ALK5	ALK5
n-tridecane	2.8	1.51E-11	NONE	ALK5	ALK5
n-tetradecane	1.8	1.79E-11	NONE	ALK5	ALK5
n-pentadecane	0.9	2.07E-11	NONE	ALK5	ALK5
n-hexadecane	0.3	2.32E-11	NONE	ALK5	ALK5

n-heptadecane	0.1	2.85E-11	NONE	ALK5	ALK5
n-octadecane	0.0	3.51E-11	NONE	ALK5	ALK5
n-nonadecane	0.0	4.32E-11	NONE	ALK5	ALK5
monoaromatics	15.4	1.43E-11	ARO2	ARO2	ARO1
diaromatics	1.7	2.30E-11	NONE	ARO2	ARO2
isoalkanes	23.1	1.23E-11	NONE	ALK5	BALK
cycloalkanes	34.2	1.23E-11	NONE	ALK5	ALK5

Table S.5: Composition information for diesels

Species	Mass %								Lumping		
	(1)	(2)	(3)	(5)	(7)	(8)	(9)	k_OH	Traditional (speciated)	Traditional (base)	Traditional (extended)
C3 n-alkane	0.0	0.0	0.0	0.0	0.0	0.0	0.0	1.09E-12	NONE	NONE	NONE
C4 n-alkane	0.0	0.0	0.0	0.0	0.0	0.0	0.0	2.36E-12	NONE	NONE	NONE
C5 n-alkane	0.0	0.0	0.0	0.0	0.0	0.0	0.0	3.80E-12	ALK4	ALK4	ALK4
C6 n-alkane	0.0	0.0	0.0	0.0	0.0	0.0	0.0	5.20E-12	ALK4	ALK4	ALK4
C7 n-alkane	0.0	0.1	0.0	0.0	0.0	0.0	0.0	6.76E-12	ALK4	ALK4	ALK4
C8 n-alkane	0.0	0.0	0.2	0.1	0.1	0.0	0.1	8.11E-12	ALK5	ALK5	ALK5
C9 n-alkane	0.3	0.2	0.6	0.7	0.5	0.0	0.4	9.70E-12	ALK5	ALK5	ALK5
C10 n-alkane	0.4	0.2	1.7	2.9	1.5	0.1	0.8	1.10E-11	ALK5	ALK5	ALK5
C11 n-alkane	0.4	0.2	1.4	2.9	2.0	0.1	1.1	1.23E-11	ALK5	ALK5	ALK5
C12 n-alkane	0.2	0.1	2.0	3.5	1.7	0.1	0.8	1.32E-11	ALK5	ALK5	ALK5
C13 n-alkane	0.0	0.0	1.3	2.4	1.2	0.4	0.9	1.51E-11	NONE	ALK5	ALK5
C14 n-alkane	0.2	0.0	1.3	12.0	18.2	16.4	1.2	1.79E-11	NONE	ALK5	ALK5
C15 n-alkane	0.5	0.0	1.4	7.0	10.1	8.5	1.7	2.07E-11	NONE	ALK5	ALK5
C16 n-alkane	0.6	0.0	1.0	1.0	1.5	1.1	1.0	2.32E-11	NONE	ALK5	ALK5
C17 n-alkane	0.5	0.0	0.6	0.0	0.1	0.3	1.0	2.85E-11	NONE	ALK5	ALK5
C18 n-alkane	0.8	0.0	0.3	0.0	0.0	0.0	0.4	3.51E-11	NONE	ALK5	ALK5
C19 n-alkane	0.6	0.0	0.0	0.0	0.0	0.0	0.2	4.32E-11	NONE	ALK5	ALK5
C20 n-alkane	0.3	0.0	0.0	0.0	0.0	0.0	0.0	4.32E-11	NONE	ALK5	ALK5
C21 n-alkane	0.0	0.0	0.0	0.0	0.0	0.0	0.0	4.32E-11	NONE	ALK5	ALK5
C3 branched alkane	0.0	0.0	0.0	0.0	0.0	0.0	0.0	1.09E-12	NONE	NONE	NONE
C4 branched alkane	0.0	0.0	0.0	0.0	0.0	0.0	0.0	2.36E-12	NONE	NONE	NONE
C5 branched alkane	0.0	0.0	0.0	0.0	0.0	0.1	0.0	3.80E-12	ALK4	ALK4	NONE
C6 branched alkane	0.0	0.0	0.0	0.0	0.0	0.0	0.0	5.20E-12	ALK4	ALK4	NONE
C7 branched alkane	0.0	0.0	0.0	0.1	0.0	0.0	0.0	6.76E-12	ALK4	ALK4	BALK
C8 branched alkane	0.1	0.1	0.4	0.2	0.1	0.1	0.2	8.11E-12	ALK5	ALK5	BALK
C9 branched alkane	0.5	0.1	0.7	0.8	0.6	0.0	0.0	9.70E-12	ALK5	ALK5	BALK
C10 branched alkane	2.0	1.0	2.9	3.3	1.6	0.0	1.1	1.10E-11	ALK5	ALK5	BALK

C11 branched alkane	4.7	4.5	3.2	2.0	0.4	0.0	0.2	1.23E-11	NONE	ALK5	BALK
C12 branched alkane	0.5	1.1	0.9	2.3	0.8	0.0	0.1	1.32E-11	NONE	ALK5	BALK
C13 branched alkane	3.0	7.8	3.1	3.1	1.5	0.0	1.0	1.51E-11	NONE	ALK5	BALK
C14 branched alkane	4.1	5.5	1.9	2.3	1.0	1.8	3.0	1.79E-11	NONE	ALK5	BALK
C15 branched alkane	3.9	1.1	2.8	1.0	0.3	1.5	3.3	2.07E-11	NONE	ALK5	BALK
C16 branched alkane	3.6	0.6	1.1	0.5	0.2	1.1	3.3	2.32E-11	NONE	ALK5	BALK
C17 branched alkane	2.5	0.2	0.3	0.0	0.0	1.1	2.6	2.85E-11	NONE	ALK5	BALK
C18 branched alkane	1.5	0.1	0.0	0.0	0.0	0.0	1.2	3.51E-11	NONE	ALK5	BALK
C19 branched alkane	1.6	0.1	0.0	0.0	0.0	0.0	0.2	4.32E-11	NONE	ALK5	BALK
C20 branched alkane	0.7	0.0	0.0	0.0	0.0	0.0	0.0	4.32E-11	NONE	ALK5	BALK
C21 branched alkane	0.2	0.0	0.0	0.0	0.0	0.0	0.0	4.32E-11	NONE	ALK5	BALK
C3 cycloalkane	0.0	0.0	0.0	0.0	0.0	0.0	0.0	1.09E-12	NONE	NONE	NONE
C4 cycloalkane	0.0	0.0	0.0	0.0	0.0	0.0	0.0	2.36E-12	NONE	NONE	NONE
C5 cycloalkane	0.0	0.0	0.0	0.0	0.0	0.0	0.0	3.80E-12	ALK4	ALK4	ALK4
C6 cycloalkane	0.0	0.0	0.0	0.0	0.0	0.0	0.0	5.20E-12	ALK4	ALK4	ALK4
C7 cycloalkane	0.0	0.0	0.1	0.0	0.0	0.0	0.0	6.76E-12	ALK4	ALK4	ALK4
C8 cycloalkane	0.3	0.0	0.4	0.4	0.2	0.0	0.3	8.11E-12	ALK5	ALK5	ALK5
C9 cycloalkane	0.6	0.1	0.8	1.0	0.8	0.0	0.9	9.70E-12	ALK5	ALK5	ALK5
C10 cycloalkane	1.0	0.1	1.7	2.9	1.4	0.0	0.7	1.10E-11	ALK5	ALK5	ALK5
C11 cycloalkane	1.4	0.7	2.1	3.3	1.1	0.0	0.7	1.23E-11	NONE	ALK5	ALK5
C12 cycloalkane	1.1	2.4	4.3	5.8	2.8	0.0	2.3	1.32E-11	NONE	ALK5	ALK5
C13 cycloalkane	1.8	2.1	4.0	4.6	2.5	1.0	5.9	1.51E-11	NONE	ALK5	ALK5
C14 cycloalkane	2.3	1.5	2.4	1.7	1.4	1.0	3.2	1.79E-11	NONE	ALK5	ALK5
C15 cycloalkane	2.9	0.9	1.4	1.6	0.6	3.3	7.9	2.07E-11	NONE	ALK5	ALK5
C16 cycloalkane	2.3	0.7	0.5	2.5	0.2	2.3	4.5	2.32E-11	NONE	ALK5	ALK5
C17 cycloalkane	1.9	0.7	0.1	2.0	0.5	4.1	7.2	2.85E-11	NONE	ALK5	ALK5
C18 cycloalkane	1.5	1.0	0.0	0.9	0.0	1.0	2.3	3.51E-11	NONE	ALK5	ALK5
C19 cycloalkane	1.4	1.3	0.0	0.5	0.5	6.1	1.9	4.32E-11	NONE	ALK5	ALK5
C20 cycloalkane	1.0	1.2	0.0	0.2	0.0	1.5	1.1	4.32E-11	NONE	ALK5	ALK5
C21 cycloalkane	0.7	2.5	0.0	0.0	0.0	2.0	0.5	4.32E-11	NONE	ALK5	ALK5
C3 aromatic	0.0	0.0	0.0	0.0	0.0	0.0	0.0	0.00E+00	NONE	NONE	NONE
C4 aromatic	0.0	0.0	0.0	0.0	0.0	0.0	0.0	0.00E+00	NONE	NONE	NONE
C5 aromatic	0.0	0.0	0.0	0.0	0.0	0.0	0.0	0.00E+00	NONE	NONE	NONE
C6 aromatic	0.1	0.0	0.0	0.0	0.0	0.0	0.0	1.22E-12	ARO1	ARO1	ARO1
C7 aromatic	0.1	0.1	0.1	0.1	0.0	0.0	0.2	5.63E-12	ARO1	ARO1	ARO1
C8 aromatic	5.0	7.1	5.4	1.8	0.5	0.1	3.1	1.43E-11	ARO2	ARO2	ARO1
C9 aromatic	27.0	34.5	26.8	11.7	19.2	2.9	15.1	1.43E-11	ARO2	ARO2	ARO1

C10 aromatic	4.4	5.6	0.8	0.7	0.9	0.0	0.3	1.43E-11	ARO2	ARO2	ARO1
C11 aromatic	0.8	2.9	2.6	2.6	2.5	0.0	1.0	1.43E-11	ARO2	ARO2	ARO1
C12 aromatic	0.3	0.4	1.5	1.6	1.3	1.4	0.6	1.43E-11	ARO2	ARO2	ARO1
C13 aromatic	0.3	0.2	1.0	0.9	0.5	0.2	0.5	1.43E-11	ARO2	ARO2	ARO1
C14 aromatic	0.3	0.2	1.0	0.4	2.9	6.1	0.8	1.43E-11	ARO2	ARO2	ARO1
C15 aromatic	0.2	0.1	0.5	0.0	0.1	0.0	0.5	1.43E-11	ARO2	ARO2	ARO1
C16 aromatic	0.2	0.1	0.3	0.0	0.0	0.1	0.4	1.43E-11	ARO2	ARO2	ARO1
C17 aromatic	0.2	0.1	0.1	0.1	0.0	0.1	0.4	1.43E-11	ARO2	ARO2	ARO1
C18 aromatic	0.1	0.1	0.0	0.1	0.0	0.1	0.4	1.43E-11	ARO2	ARO2	ARO1
C19 aromatic	0.1	0.1	0.0	0.0	0.0	0.2	0.3	1.43E-11	ARO2	ARO2	ARO1
C20 aromatic	0.1	0.2	0.0	0.0	0.0	0.3	0.2	1.43E-11	ARO2	ARO2	ARO1
C21 aromatic	0.0	0.2	0.0	0.0	0.0	0.3	0.1	1.43E-11	ARO2	ARO2	ARO1
benzocycloalkanes	3.9	3.3	8.1	3.6	4.9	6.3	6.4	4.09E-11	NONE	ARO2	ARO2
diaromatics	1.5	3.6	4.4	0.9	11.9	26.5	4.4	4.09E-11	NONE	ARO2	ARO2
triaromatics	0.0	0.0	0.0	0.0	0.0	0.1	0.0	4.09E-11	NONE	ARO2	ARO2
tetraaromatics	0.0	0.0	0.0	0.0	0.0	0.0	0.0	4.09E-11	NONE	ARO2	ARO2
olefins	1.8	2.5	0.1	0.2	0.1	0.0	0.1	5.00E-11	OLE2	OLE2	OLE2

Table S.6: VBS yields for SAPRC07 lumped species

	High Nox (Low Yield)					**Low Nox (High Yield)**			
	C* (µg/m3)					**C* (µg/m3)**			
Group	1	10	100	1000		1	10	100	1000
ALK4	0.0000	0.0375	0.0000	0.0000		0.0000	0.0750	0.0000	0.0000
ALK5	0.0000	0.1500	0.0000	0.0000		0.0000	0.3000	0.0000	0.0000
OLE1	0.0008	0.0045	0.0375	0.1500		0.0045	0.0090	0.0600	0.2250
OLE2	0.0030	0.0255	0.0825	0.2700		0.0225	0.0435	0.1290	0.3750
ARO1	0.0107	0.2571	0.4821	0.7500		0.0107	0.2571	0.7500	0.9643
ARO2	0.0015	0.1950	0.3000	0.4350		0.0750	0.3000	0.3750	0.5250
ISOP	0.0003	0.0225	0.0150	0.0000		0.0090	0.0300	0.0150	0.0000
SESQ	0.0750	0.1500	0.7500	0.9000		0.0750	0.1500	0.7500	0.9000
TERP	0.0120	0.1215	0.2010	0.5070		0.1073	0.0918	0.3587	0.6075

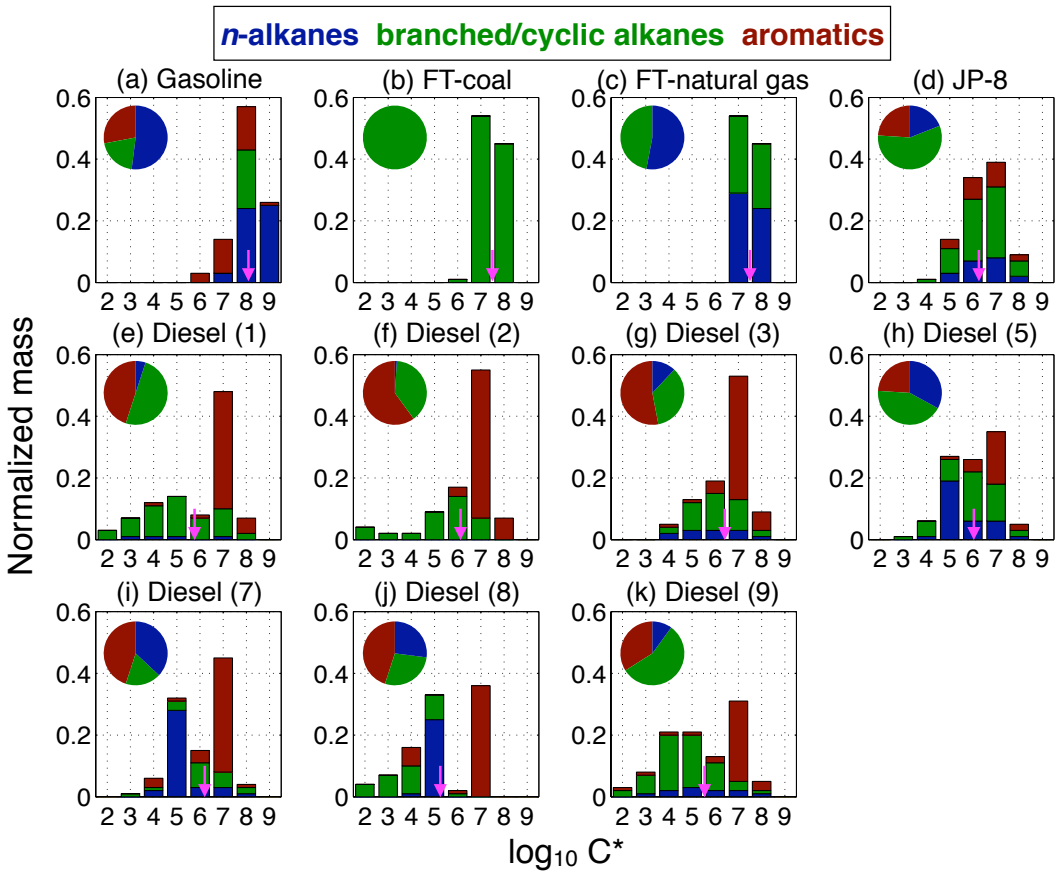

Figure S.1: Volatility and molecular structure distributions for unburned (a) gasoline, (b) FT-coal, (c) FT-natural gas, (d) JP-8 and (e-k) Diesel 1, 2, 3, 5, 7, 8 and 9 represented in the volatility basis set. For each plot, the bars sum up to one. The inset pie shows the relative fractions of n-alkanes, branched/cyclic alkanes and aromatics in the fuel. The magenta arrow shows the mass-weighted average of the volatility distribution.

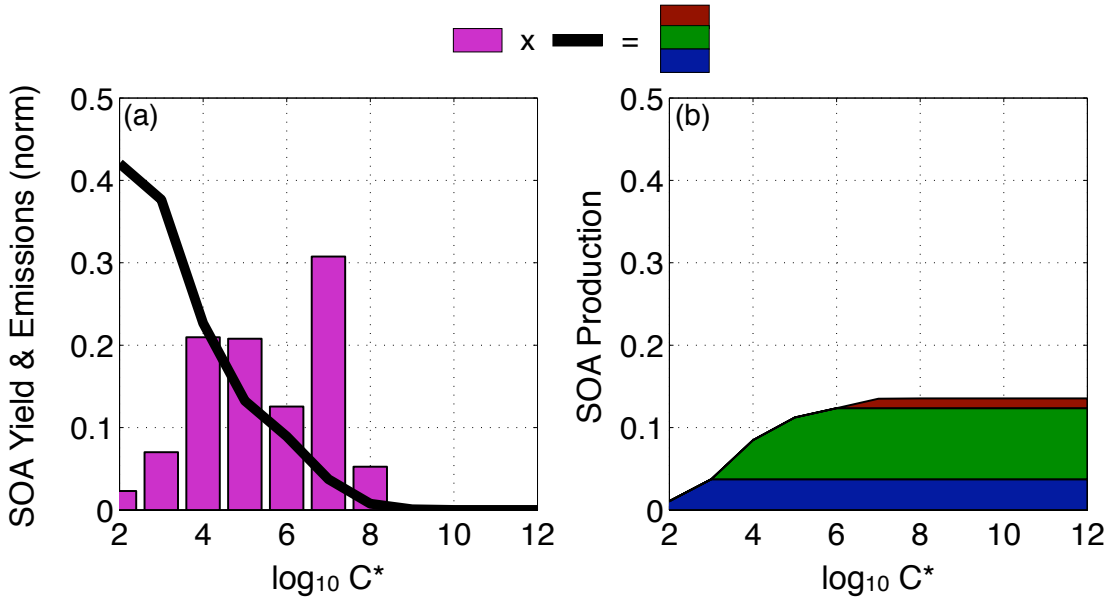

Figure S.2: (a) Average SOA yield for the Volatility-Based Model presented as a function of precursor C* at a COA of 5 μg m^{-3} and volatility distribution for diesel (9) (normalized). (b) Product of emissions and SOA yield presented as a cumulative distribution. The different colors represent SOA arising from precursors with different C*s: OPOA (blue) is SOA from precursors in C* bins less than 10^3 μg m-3, NT-SOA (green) is SOA from precursors in C* bins 10^4 to 10^6 μg m-3 and T-SOA (maroon) is from SOA from precursors in C* bins 10^7 μg m-3 and higher.

5.6 Acknowledgements

Funding was provided by the U.S. Department of Defense Strategic Environmental Research and Development Program (SERDP) under project WP-1626 and by the U.S. Environmental Protection Agency National Center for Environmental Research (NCER) through the STAR program (R833748).

5.7 References

Atkinson, R., and Arey, J.: Atmospheric degradation of volatile organic compounds, Chemical Reviews, 103, 4605-4638, 2003.

Bernstein, J. A., Alexis, N., Barnes, C., Bernstein, I. L., Bernstein, J. A., Nel, A., Peden, D., Diaz-Sanchez, D., Tarlo, S. M., and Williams, P. B.: Health effects of air pollution, The Journal of Allergy and Clinical Immunology, 114, 1116-1123, 2004.

Chan, A. W. H., Kautzman, K. E., Chhabra, P. S., Surratt, J. D., Chan, M. N., Crounse, J. D., Kurten, A., Wennberg, P. O., Flagan, R., and Seinfeld, J. H.: Secondary organic aerosol formation from photooxidation of naphthalene and alkylnaphthalenes: Implications for oxidation of intermediate volatility organic compounds (ivocs), Atmospheric Chemistry and Physics, 9, 3049-3060, 2009.

Donahue, N., Robinson, A., Stanier, C., and Pandis, S.: Coupled partitioning, dilution, and chemical aging of semivolatile organics, Environ. Sci. Technol, 40, 2635-2643, doi:10.1021/es052297c, 2006.

Dzepina, K., Volkamer, R., Madronich, S., Tulet, P., Ulbrich, I., Zhang, Q., Cappa, C., Ziemann, P., and Jimenez, J.: Evaluation of recently-proposed secondary organic aerosol models for a case study in mexico city, Atmospheric Chemistry and Physics, 9, 5681-5709, doi:10.5194/acp-9-5681-2009, 2009.

Dzepina, K., Cappa, C. D., Volkamer, R. M., Madronich, S., DeCarlo, P. F., Zaveri, R. A., and Jimenez, J. L.: Modeling the multiday evolution and aging of secondary organic aerosol during milagro 2006, Environmental Science & Technology, 45, 3496-3503, doi: 10.1021/es103186f, 2010.

Edam, R., Blomberg, J., Janssen, H. G., and Schoenmakers, P.: Comprehensive multi-dimensional chromatographic studies on the separation of saturated hydrocarbon ring structures in petrochemical samples, Journal of chromatography A, 1086, 12-20, 2005.

Gordon, T. D., Nguyen, N. T., May, A. A., Presto, A. A., Lipsky, E. M., Maldonado, S., Chattopadhyay, S., Gutierrez, A., Maricq, M., and Robinson, A. L.: Secondary organic aerosol formed from light duty gasoline vehicle exhaust dominates primary particulate matter emissions, Environ. Sci. Technol, in preparation-a.

Gordon, T. D., Nguyen, N. T., Presto, A. A., Lipsky, E. M., Maldonado, S., Maricq, M., and Robinson, A. L.: Impacts of aftertreatment, fuel chemistry and driving cycle on the production of secondary organic aerosol from diesel vehicle exhaust, Environ. Sci. Technol, in preparation-b.

Grieshop, A. P., Logue, J. M., Donahue, N. M., and Robinson, A. L.: Laboratory investigation of photochemical oxidation of organic aerosol from wood fires 1: Measurement and simulation of organic aerosol evolution, Atmospheric Chemistry and Physics, 9, 1263-1277, 10.5194/acp-9-1263-2009, 2009.

Heald, C. L., Jacob, D. J., Park, R. J., Russell, L. M., Huebert, B. J., Seinfeld, J. H., Liao, H., and Weber, R. J.: A large organic aerosol source in the free troposphere missing from current models, Geophys. Res. Lett., 32, doi:10.1029/2005GL023831, 2005.

Hildebrandt, L., Donahue, N., and Pandis, S.: High formation of secondary organic aerosol from the photo-oxidation of toluene, Atmospheric Chemistry and Physics, 9, 2973-2986, doi:10.5194/acp-9-2973-2009, 2009.

IPCC, W.: Climate change 2007: The physical science basis, Summary for Policy Makers, Contribution of Working Group I to the Fourth Assessment Report of the Intergovernmental Panel on Climate Change, 2007.

Isaacman, G., Wilson, K. R., Chan, A. W. H., Worton, D. R., Kimmel, J. R., Nah, T., Hohaus, T., Gonin, M., Kroll, J. H., and Worsnop, D. R.: Improved resolution of hydrocarbon structures and constitutional isomers in complex mixtures using gas chromatography-vacuum ultraviolet-mass spectrometry (gc-vuv-ms), Analytical Chemistry,

Jathar, S., Farina, S., Robinson, A., and Adams, P.: The influence of semi-volatile and reactive primary emissions on the abundance and properties of global organic aerosol, Atmospheric Chemistry and Physics, 11, 7727-7746, doi:10.5194/acp-11-7727-2011 2011.

Johnson, D., Utembe, S. R., Jenkin, M. E., Derwent, R. G., Hayman, G. D., Alfarra, M. R., Coe, H., and McFiggans, G.: Simulating regional scale secondary organic aerosol formation during the torch 2003 campaign in the southern uk, Atmos. Chem. Phys., 6, 403-418, 2006.

Lane, T. E., Donahue, N. M., and Pandis, S. N.: Simulating secondary organic aerosol formation using the volatility basis-set approach in a chemical transport model, Atmospheric Environment, 42, 7439-7451, 2008.

Lim, Y. B., and Ziemann, P. J.: Chemistry of secondary organic aerosol formation from oh radical-initiated reactions of linear, branched, and cyclic alkanes in the presence of no x, Aerosol Science and Technology, 43, 604-619, 2009.

Logue, J., Huff-Hartz, K., Lambe, A., Donahue, N., and Robinson, A.: High time-resolved measurements of organic air toxics in different source regimes, Atmospheric Environment, 43, 6205-6217, 2009.

Miracolo, M., Hennigan, C., Ranjan, M., Nguyen, N., Gordon, T., Lipsky, E., Presto, A., Donahue, N., and Robinson, A.: Secondary aerosol formation from photochemical aging of aircraft exhaust in a smog chamber, Atmos. Chem. Phys, 11, 4135-4147, doi:10.5194/acp-11-4135-2011, 2011.

Miracolo, M. A., Drozd, G. T., Jathar, S. H., Presto, A. A., Lipsky, E. M., Corporan, E., and Robinson, A. L.: Fuel composition and secondary organic aerosol formation: Gas-turbine exhaust and alternative aviation fuels, Environmental Science & Technology, submitted.

Morris, R. E., Koo, B., Guenther, A., Yarwood, G., McNally, D., Tesche, T. W., Tonnesen, G., Boylan, J., and Brewer, P.: Model sensitivity evaluation for organic carbon using two multi-pollutant air quality models that simulate regional haze in the southeastern united states, Atmos. Environ., 40, 4960-4972, 2006.

Ng, N., Kroll, J., Chan, A., Chhabra, P., Flagan, R., and Seinfeld, J.: Secondary organic aerosol formation from m-xylene, toluene, and benzene, Atmos. Chem. Phys, 7, 3909-3922, doi:10.5194/acp-7-3909-2007, 2007.

Ng, N. L., Kroll, J. H., Keywood, M. D., Bahreini, R., Varutbangkul, V., Flagan, R. C., Seinfeld, J. H., Lee, A., and Goldstein, A. H.: Contribution of first-versus second-generation products to secondary organic aerosols formed in the oxidation of biogenic hydrocarbons, Environmental Science & Technology, 40, 2283-2297, 2006.

Pankow, J. F.: An absorption model of gas/particle partitioning of organic compounds in the atmosphere, Atmospheric Environment, 28, 185-188, 1994.

Presto, A. A., Miracolo, M. A., Donahue, N. M., and Robinson, A. L.: Secondary organic aerosol formation from high-no x photo-oxidation of low volatility precursors: N-alkanes, Environmental Science & Technology, 44, 2029-2034, 2010.

Pye, H., and Seinfeld, J.: A global perspective on aerosol from low-volatility organic compounds, Atmos. Chem. Phys, 10, 4377-4401, doi:10.5194/acp-10-4377-2010, 2010.

Robinson, A. L., Donahue, N. M., Shrivastava, M. K., Weitkamp, E. A., Sage, A. M., Grieshop, A. P., Lane, T. E., Pierce, J. R., and Pandis, S. N.: Rethinking organic aerosols: Semivolatile emissions and photochemical aging, Science, 315, 1259-1262, 2007.

Schauer, J. J., Kleeman, M. J., Cass, G. R., and Simoneit, B. R. T.: Measurement of emissions from air pollution sources. 2. C1 through c30 organic compounds from medium duty diesel trucks, Environ. Sci. Technol, 33, 1578-1587, 1999a.

Schauer, J. J., Kleeman, M. J., Cass, G. R., and Simoneit, B. R. T.: Measurement of emissions from air pollution sources. 1. C1 through c29 organic compounds from meat charbroiling, Environmental Science & Technology, 33, 1566-1577, 1999b.

Schauer, J. J., Kleeman, M. J., Cass, G. R., and Simoneit, B. R. T.: Measurement of emissions from air pollution sources. 3. C1- c29 organic compounds from fireplace combustion of wood, Environ. Sci. Technol, 35, 1716--1728, 2001.

Schauer, J. J., Kleeman, M. J., Cass, G. R., and Simoneit, B. R. T.: Measurement of emissions from air pollution sources. 5. C1- c32 organic compounds from gasoline-powered motor vehicles, Environ. Sci. Technol, 36, 1169-1180, 2002a.

Schauer, J. J., Kleeman, M. J., Cass, G. R., and Simoneit, B. R. T.: Measurement of emissions from air pollution sources. 4. C1-c27 organic compounds from cooking with seed oils, Environmental Science & Technology, 36, 567-575, 2002b.

Shakya, K. M., and Griffin, R. J.: Secondary organic aerosol from photooxidation of polycyclic aromatic hydrocarbons, Environmental Science & Technology, 44, 8134-8139, doi:10.1021/es1019417, 2010.

Shrivastava, M. K., Lane, T. E., Donahue, N. M., Pandis, S. N., and Robinson, A. L.: Effects of gas particle partitioning and aging of primary emissions on urban and regional organic aerosol concentrations, Journal of Geophysical Research-Atmospheres, 113, D18301, doi:10.1029/2007JD009735, 2008.

Song, C., Na, K., Warren, B., Malloy, Q., and Cocker III, D. R.: Secondary organic aerosol formation from the photooxidation of p-and o-xylene, Environmental Science & Technology, 41, 7403-7408, 2007.

Tkacik, D. S., Presto, A. A., Donahue, N. M., and Robinson, A. L.: Secondary organic aerosol formation from intermediate-volatility organic compounds: Cyclic, linear, and branched alkanes, Environmental Science & Technology, submitted.

Tsimpidi, A., Karydis, V., Zavala, M., Lei, W., Molina, L., Ulbrich, I., Jimenez, J., and Pandis, S.: Evaluation of the volatility basis-set approach for the simulation of organic aerosol formation in the mexico city metropolitan area, Atmos. Chem. Phys, 10, 525-546, doi:10.5194/acp-10-525-2010, 2009.

Vutukuru, S., Griffin, R. J., and Dabdub, D.: Simulation and analysis of secondary organic aerosol dynamics in the south coast air basin of california, J. Geophys. Res., 111, doi:10.1029/2005JD006139, 2006.

Weitkamp, E. A., Amy, M., Pierce, J. R., Donahue, N. M., and Robinson, A. L.: Organic aerosol formation from photochemical oxidation of diesel exhaust in a smog chamber, Environmental Science & Technology, 41, 6969-6975, 2007.

Zhang, Q., Jimenez, J. L., Canagaratna, M. R., Allan, J. D., Coe, H., Ulbrich, I., Alfarra, M. R., Takami, A., Middlebrook, A. M., Sun, Y. L., Dzepina, K., Dunlea, E., Docherty, K., DeCarlo, P.

F., Salcedo, D., Onasch, T., Jayne, J. T., Miyoshi, T., Shimono, A., Hatakeyama, S., Takegawa, N., Kondo, Y., Schneider, J., Drewnick, F., Borrmann, S., Weimer, S., Demerjian, K., Williams, P., Bower, K., Bahreini, R., Cottrell, L., Griffin, R. J., Rautiainen, J., Sun, J. Y., Zhang, Y. M., and Worsnop, D. R.: Ubiquity and dominance of oxygenated species in organic aerosols in anthropogenically-influenced northern hemisphere midlatitudes, Geophys. Res. Lett, 34, L13801, doi:10.1029/2007GL029979, 2007.

Chapter 6: Unspeciated organic emissions from combustion sources and their influence on the secondary organic aerosol budget in the United States

Abstract

Combustion sources are a major source of organic emissions and therefore a potentially important source for secondary organic aerosol (SOA) formation in the atmosphere. Although speciated organic emissions from combustion sources are considered in models to form SOA, a large fraction of the organics are unspeciated. In this work, we analyze data from numerous smog chamber experiments, which photo-oxidized dilute emissions from different combustion sources (on-road gasoline vehicles, aircraft, on-road diesel vehicles, wood burning and open biomass burning), to determine the contribution that unspeciated emissions make to SOA formation. An SOA model based on speciated organics is able to explain, on average, 8-31% of the SOA measured in the experiments. We hypothesize that the remainder results from the gas-phase oxidation of unspeciated emissions, which account on average for 25-75% of the non-methane organic gas (NMOG) emissions. Using the SOA data, we develop, for the first time, source-specific parameterizations to model SOA from unspeciated emissions; all sources seem to have median SOA yields similar to large *n*-alkanes (C_{12+}). To assess the influence of unspeciated emissions on SOA formation regionally, we use the parameterization to predict SOA production in the United States. Using emissions data collected during the smog chamber experiments and data available in literature, we build a gross inventory for unspeciated emissions in the United States. We discover that unspeciated organics might be included in the current generation of SOA models but misallocated in terms of its SOA potential. The top six combustion sources (on- and off-road gasoline, on- and off-road diesel, open biomass and wood burning) emit 2.61 Tg yr^{-}

[1] of unspeciated emissions (20% of US anthropogenic VOC emissions from combustion sources) and are estimated to form a minimum of 0.68 Tg yr^{-1} of SOA; the estimate is a third of the biogenic SOA produced in the US. We predict that accounting for SOA from unspeciated emissions will double modeled SOA formation from anthropogenic combustion sources.

6.1 Introduction

Both natural and anthropogenic combustion sources such as wildfires, vehicles, aircraft, ships, electric generating units and fireplaces emit a complex mixture of gaseous and particulate pollutants (Turns, 1996) that influence the Earth's climate and ecology and human health (IPCC, 2007). While certain pollutants like carbon dioxide, methane, sulfur dioxide and nitrogen oxides have been well-studied and in some cases even regulated, the formation and evolution of secondary organic aerosol (SOA) from the atmospheric oxidation of non-methane organic gas (NMOG) emissions is still an open research question (Hallquist et al., 2009). SOA is the dominant fraction of organic (OA) aerosol and accounts for a third of the dry fine aerosol mass in the atmosphere (Zhang et al., 2007;Jimenez et al., 2009).

Over the past several years, Carnegie Mellon University's Center for Atmospheric Particle Studies (CAPS) has investigated SOA formation from diluted emissions from important combustion sources (aircraft: Miracolo et al. (2011), Miracolo et al. (submitted); gasoline light-duty vehicles: Gordon et al. (in preparation-a); diesel light- and heavy-duty vehicles: Gordon et al (in preparation-b); wood smoke: Grieshop et al. (2009a,b); open biomass burning: Hennigan et al. (2011)). For all sources, SOA accounts for a substantial fraction of the (primary+secondary) aerosol mass after a few hours of photochemical processing. Except for Henningan et al. (2011), the studies suggest that speciated organics are unable to explain the SOA formation measured

during the experiments. SOA from speciated organics is defined as traditional SOA (T-SOA). They hypothesize that the unexplained SOA arises from the oxidation of high molecular weight (C_6 and higher) and/or oxygenated compounds that are unspeciated by standard gas-chromatography mass spectrometry (GC-MS) techniques (Robinson et al., 2007). The unexplained SOA or the measured SOA minus the T-SOA has been defined as non-traditional SOA (NT-SOA) (Donahue et al., 2009).

Unspeciated emissions might comprise of two different types of species - unresolved: species that elute together through a GC column which makes it hard for them to be individually identified (e.g. iso-alkanes) and uneluted: species that do not pass through a GC column (e.g. substituted polar compounds while using a non-polar column). The unresolved species emissions often elute as an unresolved hump in a chromatogram and are referred to as an unresolved complex mixture (UCM). Over the years, numerous studies have found a significant amount of unresolved emissions while analyzing particle and gas-phase organic emissions from combustion sources (Fraser et al., 1997;Rogge et al., 1998, 1993, 1991;Schauer et al., 2002a, 1999a, 2001, 1999b, 2002b). Although detected, very rarely have they been quantified. Recently, Presto et al. (submitted) took a step forward and estimated the mass and volatility of unresolved emissions from aircraft exhaust using a thermal desorption GC-MS (TD-GC-MS). They estimated the mass and volatility by developing a calibration curve with the fuel and lubricating oil used by the aircraft. On average, these emissions were of a similar magnitude as the mass of speciated SOA precursors (Jathar et al., submitted). In a follow-up study, Jathar et al. (submitted) suggested that the unresolved emissions from aircraft exhaust were efficient in forming SOA and had SOA yields similar to large n-alkanes (C_{12}-C_{13}). Further, Nguyen et al. (in preparation) reported that unresolved emissions from gasoline and diesel engines accounted for less than 10% of the total

hydrocarbon mass and suspected that most of the unspeciated emissions did not elute. Semi-volatile organic compounds (SVOC) arising from the evaporation of directly emitted primary organic aerosol (POA) and intermediate-volatility organic compounds that have been defined using their volatility are probably a part of these unspeciated emissions.

At present, unspeciated emissions are poorly represented by the current generation of SOA models. Recently, a handful have modeled NT-SOA formation from the SVOC/IVOC fraction of unspeciated emissions (Tsimpidi et al., 2009;Pye and Seinfeld, 2010;Jathar et al., 2011;Shrivastava et al., 2008;Dzepina et al., 2009). Accounting for SVOC/IVOC has improved model performance but their inventories and SOA mechanisms still remain poorly constrained. For example, SVOC inventories were built only using gas-particle partitioning data for diesel exhaust and IVOC inventories were not based on direct measurements but estimated either using source test data from Schauer et al. (1999-2002) or using naphthalene as a surrogate. Further, the SOA mechanisms were based on very limited experimental data and assumed that different sources had the same potential to form NT-SOA. In turn, it follows that the OA budgets predicted by these models are not robust enough to answer important questions such as the contribution of NT-SOA to OA or source apportionment of OA. Also, no modeling study so far has explicitly accounted for the SOA formation from all unspeciated emissions.

Typically, SOA models use precursors that are already setup as model species in the gas-phase mechanism. Emission inventories are created by multiplying a total volatile organic compound (VOC) emissions rate by a normalized emissions profile (Simon et al., 2010). However, the source profiles in EPA's SPECIATE database (Simon et al., 2010) or used by models like CMAQ (Carlton et al., 2010) typically contain little or no unspeciated emissions. For example, in EPA SPECIATE, on-road gasoline vehicles, aircraft, woodstoves and open burning

have no unspeciated emissions while on-road and off-road diesel vehicles have 14% and 21% respectively of its VOC emissions allotted to a lumped unspeciated model-species. In CMAQ, on-road gasoline vehicles, aircraft, wood burning and on-road diesel vehicles have no unspeciated emissions while open burning has only 4% of its VOC emissions allotted to a lumped unspeciated model-species. This is in sharp contrast to the work of Rogge et al. (1991, 1993a, 1993b, 1998), Schauer et al. (1999a, 1999b, 2001, 2002a, 2002b) and the data presented in this work, where unspeciated emissions account for a substantial fraction of the NMOG. We suspect that most of the emissions profiles in EPA SPECIATE and CMAQ have been normalized to the sum of the speciated emissions instead of normalizing to the NMOG emissions and therefore have none to very little unspeciated emissions. Assuming that the total VOC emissions rate accounts for all NMOG from a source, the lack of unspeciated emissions in the emissions profile has resulted in the unspeciated emissions being under-represented and the speciated emissions being over-represented in models. For example, assume that source X emits 10 tons yr^{-1} of VOCs where X has an emissions profile of 33% ethane, 33% single-ring aromatics and 33% unspeciated. In CMAQ, the model would represent those emissions as 5 Tg yr^{-1} of ethane and 5 Tg yr^{-1} of single-ring aromatics instead of 3.3 Tg yr^{-1} each of ethane, single-ring aromatics and unspeciated i.e. the unspeciated are allocated to the speciated emissions. The misallocation might not have a large effect if the unspeciated organics on average have the same SOA potential as the speciated organics. However, as mentioned earlier, unspeciated organics possibly consist of higher molecular weight compounds that are likely to have higher SOA yields than speciated organics. The problem with emissions profiles is expected to propagate and potentially affect several components in a chemical transport model (CTM) and in the context of this work, both the gas-phase mechanism and the SOA model.

In this work, we use smog chamber data compiled from literature (Grieshop et al., 2009a;Grieshop et al., 2009b;Miracolo et al., 2011;Hennigan et al., 2011;Miracolo et al., submitted;Gordon et al., in preparation-b;Gordon et al., in preparation-a) to quantify the influence of unspeciated emissions to SOA formation in the United States (US). First, the data are used to determine what fraction of the SOA can be explained by speciated organics (T-SOA). Next, using the data, source-resolved parameterizations are developed to model residual SOA (NT-SOA) from the unspeciated fraction in combustion emissions. Then, we use smog chamber data and data from literature to build a gross inventory for unidentified emissions in the US. And finally, the new parameterizations are coupled with the gross inventory data to investigate the SOA budget in the US.

6.2. Methods

6.2.1 SOA data

In this work, we analyze POA and SOA data gathered from smog chamber experiments conducted on different combustion sources by Carnegie Mellon University's (CMU) Center for Atmospheric Particle Studies (CAPS) and Paul Scherrer Institute's (PSI) Laboratory of Atmospheric Chemistry. The PSI data are only used in Figure 6.1. Table 6.1 lists the campaign name and year, combustion sources tested, fuel(s) used, relevant references for each data set, notes and number of experiments used in this work.

Table 6.1: List of smog chamber experiment data used in this work

Campaign-Year	Source	Fuel(s) used	References	Notes	# of expts
CMU-2009	Woodstove	Logwoods	Grieshop et al., ACP, 2009a,b	Limited gas-phase organic data	6
PIT-2009	Commerical jet engine (CFM56)	JP-8	Miracolo et al., ACP, 2011	-	6
FLAME3-2009	Open burning	Trees, Pines, Grasses, Shrubs	Hennigan et al., ACP, 2011	-	18
CARB-2010	LEV-I and LEV-II light-duty vehicles	Gasoline, Diesel, Biodiesel	Gordon et al. (in prep)	-	14
WPAFB-2010	Helicopter gas turbine engine (T63)	JP-8, Fischer-Tropsch	Miracolo et al., ES&T, 2012	-	2
PSI-2010	Light-duty vehicles w/ and w/o aftertreatment	Diesel	Chirico et al., ACP, 2010	No gas-phase organic data	6
CARB-2011	Heavy-duty vehicles w/ and w/o aftertreatment	Diesel	Gordon et al. (in preparation-b)	-	15
CARB-2012	Light-duty vehicles, Off-road gasoline engines	Gasoline	Gordon et al. (in preparation-a)	-	21
PSI-2011	Woodstoves	Beech logwood, Pellets	Heringa et al., ACP, 2011	No gas-phase organic data	6

Here, we provide a brief overview of a typical smog chamber experiment. The experiments involved collecting emissions from the source and then transferring them through a heated transfer line into a portable Teflon smog chamber. The emissions were diluted with clean air to achieve particle concentrations in the smog chamber that were representative of those typically found in urban plumes. To initiate photo-oxidation, the smog chamber was exposed to natural or artificial sunlight; a suite of instruments tracked the evolution of the gas- and particle-

phase pollutants. In most experiments, gas-phase organic measurements were made online using a proton transfer reaction mass spectrometer (PTR-MS) and a flame ionization detector (FID) and offline using GCMS. The PTR-MS tracked the emission and decay of single-ring aromatics, which were then used to estimate OH concentrations in the smog chamber. Across the experiments (which typically lasted a few hours), the OH exposure ranged from $4x10^6$ to $5x10^7$ molecules-hr cm^{-3} with a median value of $1.1x10^7$ molecules-hr cm^{-3}, which corresponds to a range of 4 hours to 2 days of atmospheric processing at a typical OH concentration of 10^6 molecules cm^{-3}. The GC-MS was used to identify hydrocarbon and in some cases light-oxygenated species in the combustion emissions, which were then used in models to predict SOA formation. Typically, a GC-MS analysis is able to quantify straight-, branched- and cyclic-alkanes and alkenes, single-ring and double-ring aromatics and light carbonyls that have a carbon number less than or equal to 12. The number of species that can be quantified using the GC-MS can vary depending on the complexity of the emissions and the methods and internal standards used with the instrument. For FLAME3-2009, we were able to quantify 66 species while for CARB-2009/2010/2011 we were able to quantify 202 species. Particle-phase measurements were made online with a scanning mobility particle sizer (SMPS) and aerosol mass spectrometer (AMS). A combination of SMPS and AMS measurements were used to estimate SOA formed in the smog chamber.

The data are organized across five source categories: on-road gasoline, aircraft, on-road diesel, wood burning and open burning. The on-road gasoline source category includes data from twenty-eight experiments conducted on diluted emissions from five pre-LEV (Low Emission Vehicle), eleven LEV-I and twelve LEV-II light-duty gasoline vehicles from CARB-2010 and CARB-2012. The on-road diesel source category includes data from fifteen experiments

conducted on light duty and heavy-duty diesel vehicles from CARB-2010 and CARB-2011 and six experiments conducted on light duty diesel vehicles from PSI-2010. The aircraft source category includes data from eight experiments conducted on a commercial jet engine at idle, taxi, landing and takeoff loads and a helicopter engine at idle and cruise loads from PIT-2009 and WPAFB-2010. The wood burning source category includes data from twelve experiments conducted on woodstoves from CMU-2008 and PSI-2011. The open burning source category includes data from eighteen experiments conducted on open biomass burning from FLAME3-2009.

We are aware that experimental uncertainty could affect the quality of data from smog chamber experiments and therefore the conclusions from our analysis. The experimental uncertainty can be thought of as that associated with measurements, repeatability and atmospheric relevance. Of the three, the uncertainty in measurements is probably the lowest as the instruments and techniques used to characterize smog chamber data have evolved over the past two decades. In this work, measurement uncertainties are quantified and wherever possible, included in our analysis. Particularly for experiments used in this work, there is slightly more uncertainty associated with repeatability partly because it is too expensive to repeat every experiment and partly because there might be factors that have a larger than anticipated effect on the experiment (ambient temperature, relative humidity, VOC/NOx ratio). The uncertainty was kept to a minimum by undertaking tasks such as cleaning the chamber for 12 hours before use, ensuring a minimum background concentration and running a blank experiment. But the largest uncertainty results from whether our static and controlled experiments are truly representative of the dynamic processes in the atmosphere. Atmospheric relevance was ensured by diluting the

emissions and maintaining VOC/NOx ratios to those found in the atmosphere and in some cases exposing the chamber to natural sunlight than artificial UV light.

6.2.2 Terminology

Across the campaigns, several different instruments were used to measure the gas- and particle-phase mass, composition and properties of organics. To undertake a modeling effort, we need to ensure that the measurements map to a consistent set of definitions not only across the campaigns but also to definitions commonly used in the aerosol community. Figure 6.1 presents a schematic that shows the various instruments used and the measurements made that are relevant to this work. For simplicity and transparency, we describe the terms in light of the measurements and methods used to calculate them. We also note exceptions if any.

The FID was used to measure TOG for the on-road gasoline, on-road diesel and open burning experiments. FIDs detect functionalized carbon with lower efficiency (McNair et al., 1969). Therefore, depending on the extent of oxygenation of organic emissions, an FID would under-predict the TOG mass. For the aircraft experiments, we do not have a TOG measurement and therefore TOG is calculated as a sum of all the speciated and measured unspeciated organic gases. Further, the TOG is measured at a dilution level lower than the dilution level achieved in the smog chamber. So semi-volatile organic carbon (OC) measured along with the TOG would evaporate at the higher dilution levels found in the smog chamber, which might contribute to SOA formation. Hence, for each experiment the OC (CVS/tunnel) and POA (chamber) values are used to determine the evaporated OC and added to the TOG. The speciated organics are simply the sum of all the gas-phase organics that have been speciated using GC-MS. The SVOC and IVOC are organics measured and estimated using the TD-GC-MS. A very small fraction

(<10%) of the SVOC and IVOC mass is actually speciated and we assume that all of the SVOC and IVOC mass, for the purpose of this work, is unspeciated. The NMOG or VOC is defined as the methane mass subtracted from the TOG mass. The total unspeciated mass is defined as the speciated organics subtracted from the NMOG. By definition, the unspeciated mass includes the SVOC, IVOC and evaporated OC mass. The instruments and methods used to measure and estimate TOG, NMOG and unspeciated mass ensure that our values serve as a lower bound estimates. The TOG breakdown can be visualized using the schematic in Figure S.1.

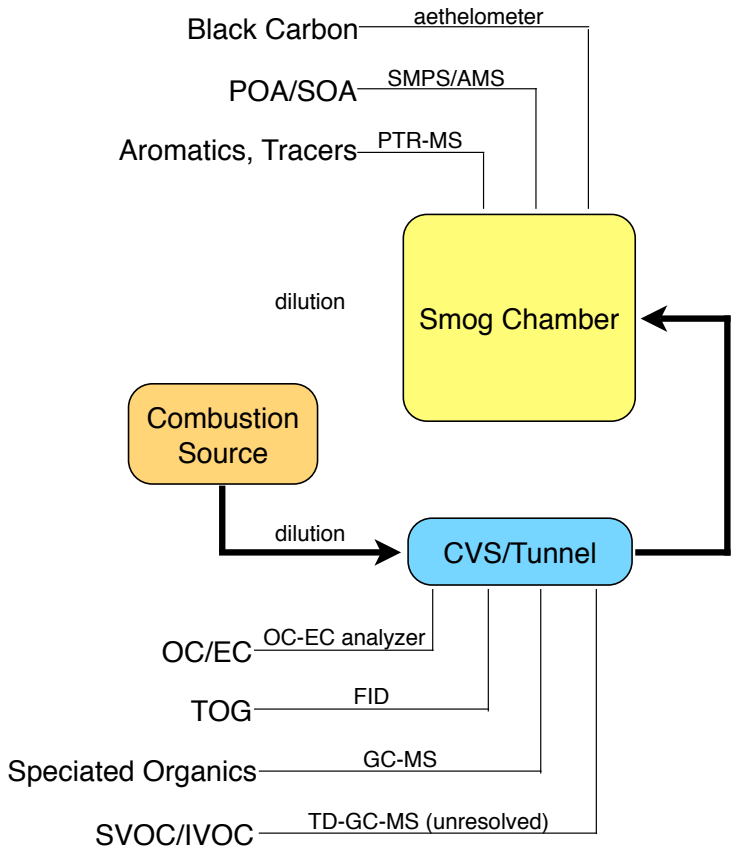

Figure 6.1: Schematic describing the instruments used to make measurements of gas- and particle-phase organics and elemental carbon during a typical experiment.

6.2.3 SOA model

A key objective of this work is to determine a way to represent SOA formation from unspeciated emissions. The first step is to predict T-SOA formation from speciated organics and subtract that from the measured SOA to calculate NT-SOA. The next step is to develop source-resolved parameters for NT-SOA by tying the estimated NT-SOA formation to the oxidation of unspeciated emissions.

We model all SOA formed in the smog chamber using a set of semi-volatile surrogate products represented using the volatility basis set (VBS) framework (Donahue et al., 2006). The VBS separates low-volatility organics into logarithmically spaced bins of effective saturation concentration (C*) between 10^{-1} to 10^{3} μg m^{-3} at 298 K. C* (inverse of the Pankow-type partitioning coefficient, K_p) is proportional to the saturation vapor pressure; it is a semi-empirical property that describes the gas-particle partitioning of an organic mixture (Pankow, 1994). The amount of SOA is defined by the gas-particle partitioning of these surrogate products calculated using absorptive partitioning theory:

$$\zeta_i = \left(1 + \frac{C_i^*}{C_{OA}}\right)^{-1}$$
$$C_{OA} = \sum_{i=1}^{N} \zeta_i \times M_i\big|_{g+p} \quad (6.1)$$

where, ζ_i is the fraction of mass in volatility bin '*i*' in the particulate phase, C_i* is the effective saturation concentration of bin '*i*' in μg m^{-3}, C_{OA} is the total particulate OA concentration in μg m^{-3} into which the organics partition, $M_i|_{g+p}$ is the total organic concentration (gas+particle) in bin '*i*' in μg m^{-3} and *N* is the number of VBS bins.

The production of semi volatile species is described by the following equations:

$$\frac{d[X_j]}{dt} = -k_{OH,X_j}[OH][X_j] \quad (6.2)$$

$$\frac{d[M_i|_{g+p}]}{dt} = \underbrace{\sum_j \alpha_{i,j} k_{OH,X_j}[OH][X_j]}_{\text{first-generation products}} + \underbrace{\underbrace{\sum_k^N \beta_{i,k} k_{OH,M_k}[OH][M_k|_g]}_{\text{production}} - \underbrace{k_{OH,M_i}[OH][M_i|_g]}_{\text{loss}}}_{\text{multi-generational oxidation}} \quad (6.3)$$

Equation (6.2) represents the first-generation oxidation of an SOA precursor where $k_{OH,Xj}$ is the reaction rate between the oxidant [*OH*] and SOA precursor [X_j]. The index *j* indicates different precursors, individual species and lumped precursors. The first term in equation (6.3) represents the production of first-generation products in the '*i*'th bin due to precursor oxidation (equation 6.2) where $\alpha_{i,j}$ is the stoichiometric mass yield for the first-generation oxidation reaction. The second and third terms in equation (6.3) account for the evolution of material in the VBS due to multi-generational oxidation; here we assume that only vapors in the VBS ($M|_g$) react. $\beta_{k,i}$ is the mass yield from multi-generational oxidation reactions in bin '*k*' and $k_{OH,M}$ is the oxidation rate of vapors in the VBS. $M_i|_{g+p}$ is the total gas+particle organic mass in the '*i*'th bin of the VBS; its gas-particle partitioning is calculated using equation (6.1).

6.2.3.1 Traditional SOA

We define T-SOA as the SOA mass formed through the oxidation of speciated organic emissions. Here, we use the speciated organics quantified using the GC-MS to predict T-SOA for all smog chamber experiments. To simulate T-SOA, X_j in equation (6.2) represents an individual precursor (e.g. benzene, toluene, n-dodecane, or cyclohexane) and OH is assumed to be the only oxidant. We use the SAPRC lumping and mass-yields ($\alpha_{i,j}$ in equation 6.2) proposed by Murphy and Pandis (2010) to model T-SOA. The mass yields for the lumped model species are listed in Table S.1.

The multi-generational oxidation of T-SOA is highly uncertain since it has not be constrained using experimental data. Here, we use the parameterizations recently applied to

anthropogenic SOA in regional and global models (Shrivastava et al., 2008;Murphy and Pandis, 2009;Murphy and Pandis, 2010;Farina et al., 2010;Jathar et al., 2011). T-SOA vapors reacts with the OH radical ($k_{Ox,M}$ = 1 x 10^{-11} cm^3 $molecules^{-1}$ s^{-1}) to form a product that is one order of magnitude lower in volatility than the precursor or shifted by one C^* bin relative to the precursor. To account for the addition of oxygen, 7.5% of the precursor's mass is added to the product. Hence, for T-SOA, $\beta_{i,k}$ in equation (6.4) takes the form:

$$\beta_{i,k} = \begin{cases} +1.075 & if\ k = i + 1; \\ 0 & otherwise \end{cases} \quad (6.4)$$

6.2.3.2 Unspeciated emissions and Non-Traditional SOA

Figure 6.2 shows the unspeciated emissions as a fraction of the NMOG emissions using a box-plot for the four sources; we are unable to plot the fraction for the wood burning source because very few gas-phase organics were measured for those experiments. Figure 6.2 suggests that a significant fraction of the NMOG is unspeciated; the median ranges from 25 to 65%. Qualitatively, the result agrees with the work of Schauer et al. (1999a, 2001, 2002a) who report that 43% of catalyst-equipped gasoline vehicle emissions, 15% of non-catalyst-equipped gasoline vehicle emissions, 20% of medium-duty diesel truck emissions and 7% of wood fireplace emissions are unspeciated.

We define NT-SOA as the SOA mass not explained by the T-SOA model or, based on our hypothesis, SOA mass arising from the gas-phase oxidation of unspeciated emissions. Prior work has represented the SVOC/IVOC fraction of unspeciated emissions using the VBS (Tsimpidi et al., 2009;Jathar et al., 2011;Shrivastava et al., 2008;Dzepina et al., 2009). But since the total unspeciated mass is calculated as a difference, we do not have complete information of its volatility distribution. Therefore, for our model, we use the approach used by Pye and

Seinfeld (2010) to model IVOC emissions, i.e. unspeciated emissions are represented using (three) lumped precursors: (1) unresolved emissions that have a C* less than or equal to 10^3 µg m^{-3} (semi-volatile organic compounds or SVOC), (2) unresolved emissions that have a C* greater than or equal to 10^3 µg m^{-3} (intermediate volatility organic compounds or IVOC) and (3) uneluted emissions defined by difference (remaining organic compounds or ROC). Hence, X_j in equation (6.2) is SVOC, IVOC or ROC. We assume that SVOC and IVOC have a OH reaction rate constant of 4 $x10^{-11}$ and $3x10^{-11}$ cm^3 $molecules^{-1}$ s^{-1} respectively based on Jathar et al. (2012). We assume that ROC have a OH reaction rate constant of $1x10^{-11}$ cm^3 $molecules^{-1}$ s^{-1} based on the range of OH reaction rates measured for alkanes, alkenes, aromatics and carbonyls (Figure S.2 plots OH reaction rate constants for compounds in Atkinson and Arey (2003)).

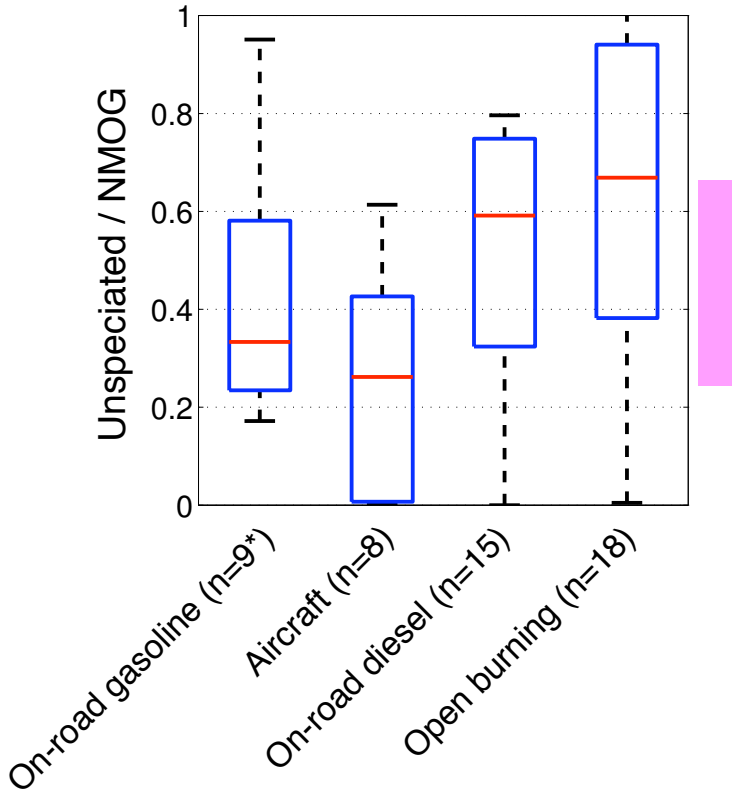

Figure 6.2: Unspeciated emissions as a fraction of the non-methane organic gas (NMOG) emissions. The colored bar on the right shows the median range for the four sources. *Currently, data available for only 9 experiments.

The goal is to determine an $\alpha_{i,j}$ for the unspeciated emissions. For simplicity and also due to the lack of data, we assume that SVOC, IVOC and ROC have the same $\alpha_{i,j}$. To determine $\alpha_{i,j}$, we first calculate an effective NT-SOA yield using the following equation:

$$NTSOA\ Yield = \frac{NTSOA\ formed}{\Delta SVOC + \Delta IVOC + \Delta ROC} \quad (6.5)$$

where Δ represents the mass reacted according to equation (6.2). Section 6.3.2.2 describes how the effective NT-SOA yields are used to determine $\alpha_{i,j}$.

6.3 Results

In this section, we summarize the POA and SOA data. Next, we present results from the T-SOA model and calculate the measured SOA fraction that is explained by T-SOA. Then we compare effective NT-SOA yields across combustion sources and describe how those yields can be used to parameterize NT-SOA formation in models.

6.3.1 POA emission factors and SOA production

Figure 6.3 compiles all POA and SOA data for the five source categories as box-plots. The box's edges represent the 25th and 75th percentiles of the data and the horizontal line through the box represents the median of the data. Across the five source categories, the median POA emission factor varies by slightly less than three orders of magnitude; it is highest for open burning and lowest for on-road gasoline vehicles. The POA emission factors are as measured in the smog chamber and are representative of atmospherically-relevant conditions (Robinson et al., 2010). Therefore, they are not directly comparable to literature data because the dilution factor in the smog chamber is 20 to 30 times higher than the dilution factors used in most source tests.

POA is semi-volatile and therefore a higher dilution factor results in substantial evaporation of the POA (Robinson et al., 2010). Except for open burning, the median SOA production is equal to or higher than the median POA emitted and therefore SOA would be an equal or majority component of ambient OA. In contrast to POA the median SOA production varies much less; by slightly more than an order of magnitude. This suggests that when considered together (OA=POA+SOA), there is much less variability in the total OA contribution from combustion sources, than if one only considers POA.

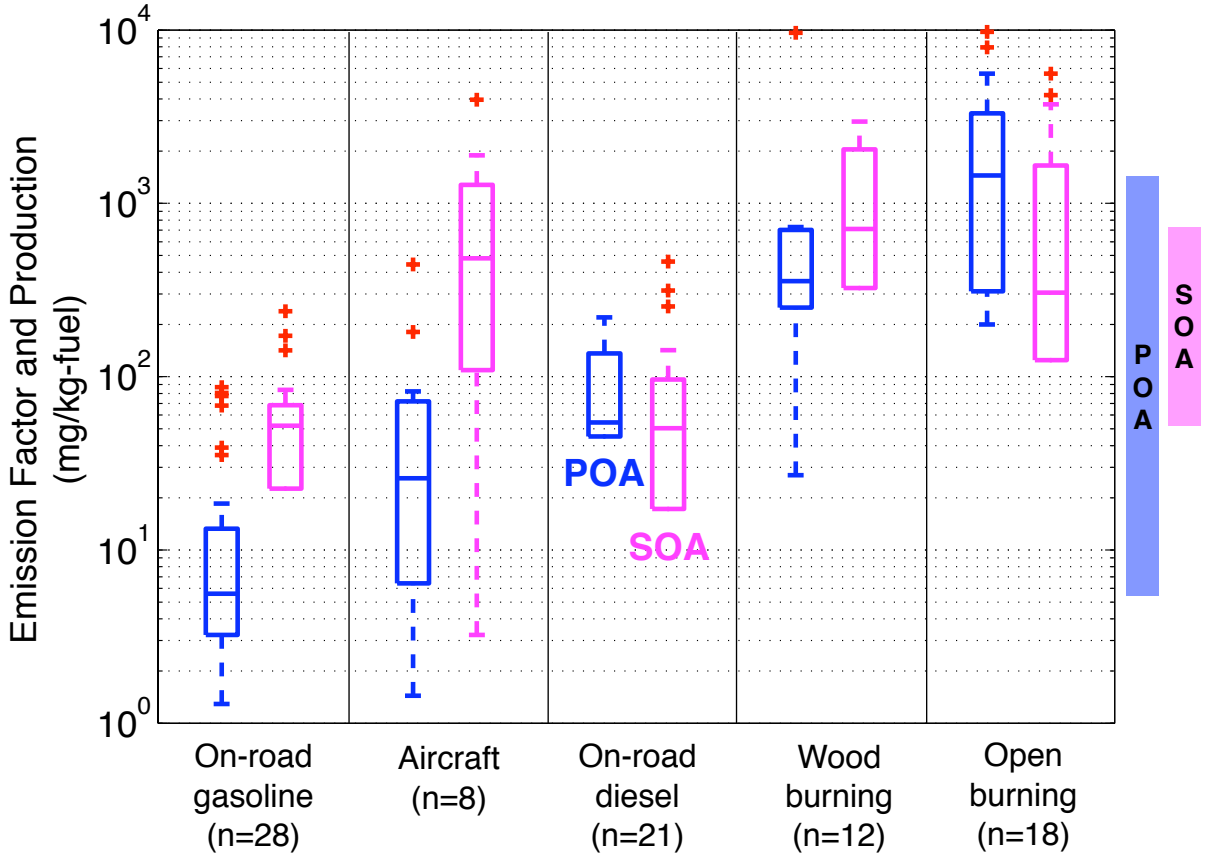

Figure 6.3: Smog chamber POA emission factors and SOA box-plots for five source categories. The edges of the box represent the 25th and 75th percentile and the solid line in the box represents the median of the data. Outliers are shown by the red '+' sign. The colored bars on the right show the median range for the entire data.

Based on Figure 6.2, we also make several other interesting observations. First, photo-oxidation of emissions from on-road gasoline produces a similar SOA range as emissions from on-road diesel when compared on a fuel-burned basis. Second, the total OA contribution (POA+SOA) from woodstoves and open burning is similar; woodstoves have a median total OA value of 1070 mg kg-fuel^{-1} versus 1750 mg kg-fuel^{-1} for open burning. However, these sources have very different POA-to-SOA ratios; woodstoves have a median POA-to-SOA ratio of 1:2 versus 5:1 for open burning. It is likely that woodstoves operating at slightly higher temperatures (flaming) have lower POA emissions but higher SOA precursor emissions which results in higher SOA formation while open burning at lower temperatures (smoldering) has higher POA emissions but lower SOA precursor emissions which results in lower SOA formation. This could imply that woodstoves and open burning are equivalent in terms of their total OA contribution.

6.3.2 Modeling smog chamber SOA

6.3.2.1 Traditional SOA

We use the SOA model, measured speciated organics data, and estimated OH concentrations to predict T-SOA formation. We assume that there is very little multigenerational oxidation since the SOA yields used in the model have been derived using similar smog chamber experiments, i.e. the second and third terms in equation (6.3) are set to zero. Figure 6.4 presents box plots of the ratio of T-SOA to measured SOA for the four sources (we are unable to model T-SOA for the wood burning source because very few organic precursors were measured for those experiments).

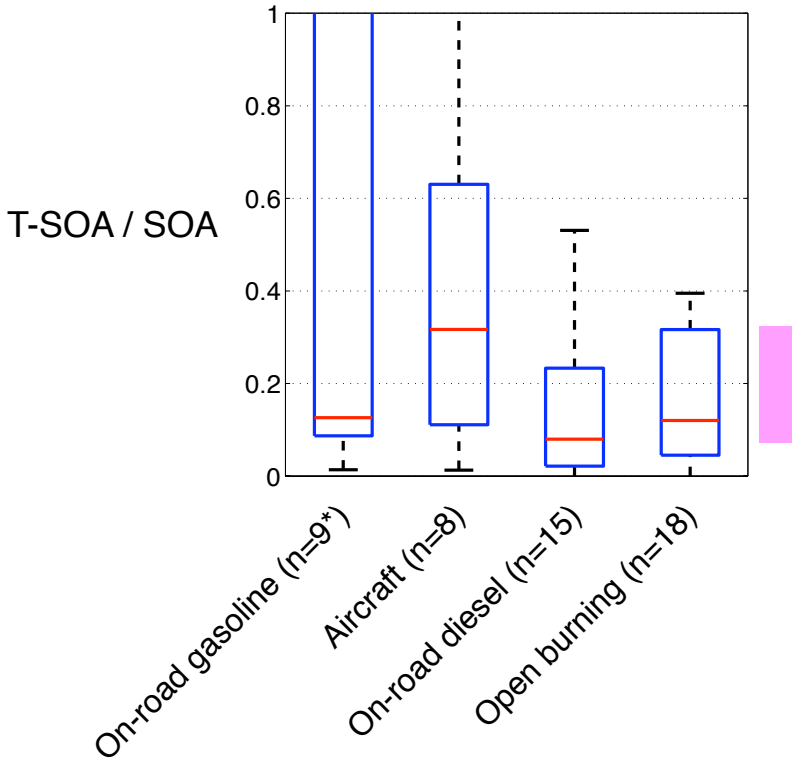

Figure 6.4: Ratio of predicted T-SOA to SOA measured during the smog chamber experiment. The colored bar on the right shows the median range. *Currently, data available for only 9 experiments.

Figure 6.4 shows that T-SOA only explains a small fraction of the SOA measured in the experiment. For example, the median T-SOA to SOA ratio ranges between 0.08 and 0.31 and about 80% of the data lies below a ratio of 0.5. The only exception to that conclusion are three experiments that were done on a high emitting 2003 Nissan Altima (on-road gasoline) where most of the SOA could be explained by emissions of single-ring aromatics. It is worth mentioning that the SAPRC-based lumping and the SOA yields of Murphy and Pandis (2010) likely predict an upper bound estimate for T-SOA because even small compounds like butene are assumed to form SOA.

6.3.2.2 Non-Traditional SOA

Figure 6.5(a) plots the effective NT-SOA yield for the four sources as a function of the organic aerosol mass loading (C_{OA}). Typically, this is how the SOA yield data from single-component studies is plotted and parameterized. We exclude data from four on-road gasoline experiments and four open burning experiments where the NT-SOA was negligible.

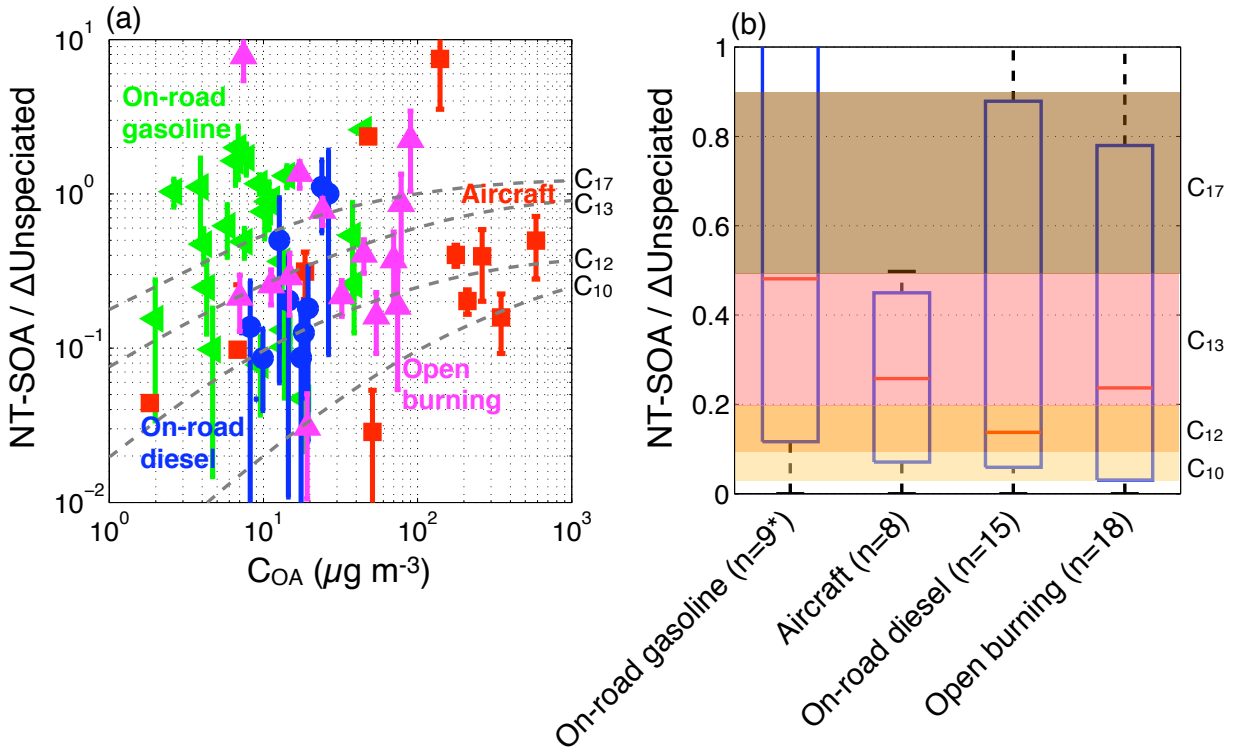

Figure 6.5: NT-SOA yield plotted (a) as a function of C_{OA} and (b) as a box-plot for the four sources.

The effective NT-SOA yield varies by two orders of magnitude and there is plenty of scatter within and across the sources. There is some evidence of the gas-particle partitioning effect (higher yields with higher C_{OA}), but clearly many other processes influence the effective NT-SOA yields. The scatter might be a realistic representation of real-world source-to-source variability but it may also reflect the large uncertainty in our effective NT-SOA yield estimate. The uncertainty might arise from our assumptions that the smog chamber experiments are equivalent and therefore comparable, the T-SOA model is correct, the method to calculate

unspeciated emissions includes all the unspeciated organic mass and that the unspeciated mass reacts with OH with a certain reaction rate. Future work directed towards characterizing the unspeciated emissions (Isaacman et al., 2012) and addressing those assumptions will help to constrain the estimates better.

Although the effective NT-SOA yields span more than two orders of magnitude, the median yield for the four sources varies between 14 and 48%. Over the C_{OA} ranges observed in our experiments, the median yields are comparable to high SOA-yield species such as toluene (12-41%) (Hildebrandt et al., 2009), naphthalene (18-40%) (Chan et al., 2009) and *n*-pentadecane (32-75%) (Presto et al., 2010).

The effective NT-SOA yield for on-road gasoline is higher than the other three sources. This is surprising because evaporated gasoline forms much less SOA than aircraft JP-8 fuel and diesel (Jathar et al., in preparation). The result holds even when we consider an effective SOA yield which is defined as the ratio of total SOA formed to total SOA precursors (speciated organics that form SOA, SVOC, IVOC, ROC) reacted. Also, some of the effective NT-SOA yields are greater than 100% implying that either the unspeciated emissions are extremely efficient in forming SOA or we are under-predicting the unspeciated emissions and the fraction that have reacted.

In a single-component study, one would fit the SOA yield data as function of C_{OA} to derive an α_i vector over a VBS. However, given the scatter, we seek to define the α_i vector to parameterize NT-SOA formation from unspeciated emissions by comparing the results to published yields of *n*-alkanes as parameterized by Presto et al. (2010). Figure 6.4(b) plots the NT-SOA yield using a box-plot for the four sources and super-imposes measured SOA yields for four *n*-alkanes: C_{10}, C_{12}, C_{13} and C_{17} (Presto et al., 2010). SOA yields for the *n*-alkanes are

shown as colored bands with bounds corresponding to yields at a C_{OA} of 5 and 50 μg m^{-3}, which spans the majority range of experimental C_{OA}. By assuming that the median represents the best estimate for the set of sources, we assign the unspeciated emissions to have SOA yields equal to the corresponding *n*-alkane (Presto et al., 2010). Table 6.2 lists how the unspeciated emissions can be mapped and modeled using *n*-alkanes. To assess the sensitivity of the parameterization in Section 6.4, we also consider the *n*-alkane corresponding to the 25th and 75th percentiles of the effective NT-SOA yield data.

Table 6.2: *n*-alkane surrogates for estimated NT-SOA yields

Source type	25th percentile	median	75th percentile
On-road gasoline	C_{12}	C_{13}	C_{17}
Aircraft	C_{10}	C_{13}	C_{13}
On-road diesel	C_{10}	C_{12}	C_{17}
Open burning	C_{10}	C_{13}	C_{17}

6.4 Modeling the US OA budget

In this section, the new source-resolved NT-SOA parameterizations are combined with activity data to assess the influence of unspeciated emissions on the OA budget in the US. It will be the first time when a semi-empirical and source-resolved parameterization will be used to model NT-SOA from directly measured unspeciated emissions.

6.4.1 Inventory of unspeciated organic emissions

Based on a literature review, there are no model-ready inventories available for unspeciated emissions from combustion sources that could be directly used to model NT-SOA formation. So first, we estimate emissions of unspeciated organics in the US. Our starting point is the 2005 National Emissions Inventory (NEI) for anthropogenic VOC emissions (EPA, 2008). The analysis focuses on emissions from six sources (on-road gasoline, off-road gasoline, open burning, wood burning, off-road diesel, on-road diesel). These sources account for almost 70%

of all combustion-based VOC emissions and slightly less than half of all anthropogenic VOC emissions in the US. Anthropogenic non-combustion sources (e.g. solvent utilization) are also important but are not included in the analysis because of lack of data (we assume that these non-combustion sources have smaller unspeciated fractions than combustion emissions). We also do not consider minor combustion sources (from the perspective of VOC emissions) such as natural gas plants, coal plants and petroleum refineries. Table 6.3 lists VOC emissions in columns 1-3 for the year 2005.

We use engineering judgment to estimate the fraction of VOC emissions that might be unspeciated (column 4 in Table 6.3) based on data from Schauer et al. (1999b, 2001, 2002b) , the recent CMU studies (Miracolo et al., 2011;Hennigan et al., 2011;Miracolo et al., submitted;Gordon et al., in preparation-b;Gordon et al., in preparation-a) and EPA SPECIATE data. The data are plotted in Figure S.3 (supplementary material). For on-road gasoline, an average unspeciated fraction of 34% is calculated using the Schauer et al. (2002b) estimate for catalyst-equipped gasoline vehicles (49%), CMU's median estimate for twenty eight experiments (25%) (Gordon et al., in preparation-a) and the Nakashima et al. (2010) estimate for gasoline vehicles (27%). For off-road gasoline, we assume an unspeciated fraction of 15% from Schauer et al. (2002b) for non-catalyst gasoline vehicles. For open burning, we use an unspeciated fraction of 65% based on CMU's median measurements for eighteen experiments during the FLAME-3 study (Hennigan et al., 2011). For residential wood burning, we assume an unspeciated fraction of 7% based on the Schauer et al. (2001) estimate for pine wood. For on-road diesel, an average unspeciated fraction of 27% is calculated using the Schauer et al. (1999b) estimate for medium-duty trucks (19%), CMU's median estimate for fifteen experiments (40%) (Gordon et al., in preparation-b) and EPA SPECIATE's estimate for the dominant on-road diesel

profile 4674. For off-road diesel, we use an unspeciated fraction of 14% based on profile 3161 in the EPA SPECIATE database.

Table 6.3: VOC and unspeciated emissions for anthropogenic combustion sources in the US.

Column 1	*Column 2*	*Column 3*	*Column 4*	*Column 5*	*Column 6*
Source	**VOC (Tg yr^{-1})**	**VOC as % of US anthro. emissions**	**Unspeciated (%)**	**Unspeciated (Tg yr^{-1})**	**EPA SPECIATE / CMAQ Profile #**
on-road gasoline	3.93	21%	34%	1.34	8750/8751
off-road gasoline	2.56	14%	15%	0.38	8750/8751
open burning	1.15	6%	65%	0.75	5560
wood burning	0.54	3%	8%	0.04	4642
off-road diesel	0.35	2%	14%	0.05	3161
on-road diesel	0.18	1%	27%	0.05	4674
other	4.04	22%	0%	0.00	-
non-combustion	5.76	31%	0%	0.00	-
Total	***18.51***	***100%***	**-**	***2.61***	**-**

Table 6.3 lists estimates for unspeciated emissions (column 5). The six sources emit 2.61 Tg yr^{-1} of unspeciated emissions, which is about 20% of all combustion-based VOC emissions and 14% of all anthropogenic VOC emissions in the US. Even though we only considered six sources, our estimate is a factor of five higher than the estimate of 0.47 Tg yr^{-1} of unidentified emissions in Simon et al. (2010). Simon et al. (2010) estimated unidentified emissions as a sum of 'unidentified VOCs', 'unidentified' and 'unknown' categories present in EPA's SPECIATE profiles. Their estimate is low because the EPA SPECIATE profiles – as shown in Figure S.3 – have little to none of the profile allotted to unidentified and unknown categories. We should note that our estimate is probably very conservative since we only consider six aggregated combustion sources. Further, we assume that the unspeciated emissions are included in the VOC emission rates provided by NEI.

6.4.2 POA emissions and SOA formation in the US

We use a box model to predict the US OA budget from POA emissions and SOA formed from the first-generation oxidation of speciated and unspeciated organic emissions. The analysis only considers the six sources discussed previously.

We calculate POA emissions for the six sources by multiplying the median POA emission factor (mg kg-fuel^{-1}; shown in Figure 6.1) by the activity (kg-fuel burned) for each source. Average fuel consumption data for gasoline, diesel and wood burning are from the Energy Information Administration (EIA) website for the years 2006-2011 (EIA, 2012). Average activity for open burning is from van der Werf et al. (2006) for the years 1997-2004. Gasoline consumption between on-road and off-road applications is split 96 to 4% based on Hwang and Davis (2009). Diesel consumption is split 50:50 between on-road and off-road applications based on Kean et al. (2000). Since we have not done any experiments on emissions from off-road vehicles, we estimate POA emission factors for off-road vehicles by scaling the on-road vehicle emission factors. Using the literature summarized in Bond et al. (2004), we assume that the POA emission factor for off-road gasoline is 10 times higher than that for on-road gasoline and that POA emission factor for off-road diesel is 4 times higher than on-road diesel.

We use equations (6.1-6.3) to model SOA in two model configurations: (1) Contemporary: POA and T-SOA only and (2) Updated: POA, T-SOA and NT-SOA. The POA treatment is the same between the two models. For the contemporary model, we use VOC emissions from Table 6.3 and emission profiles from CMAQ that are most representative of the source category (column 6 of Table 6.3) as inputs for the analysis. For the updated model, we modify the emissions profile by adding unspeciated emissions and renormalizing the profile. Since accounting for unspeciated organics reduces the emissions of speciated organics, the T-SOA needs to be modeled again. We use the unspeciated emissions from Table 6.3 and the 25th

percentile, median and 75th percentile parameterization in Table 6.2 to model NT-SOA. As we only have NT-SOA parameterizations for three out of the six source categories (on-road gasoline, on-road diesel, open burning), we assume that the on-road gasoline, on-road diesel and open burning parameterizations for NT-SOA applies to off-road gasoline, off-road diesel and wood burning respectively. In the box model, we assume a constant background OA concentration of 5 μg m^{-3} to determine gas-particle partitioning of the semi-volatile products. The model assumes that all emissions are reacted away and therefore the results signify the maximum OA that can be produced by the six sources due to first-generation oxidation.

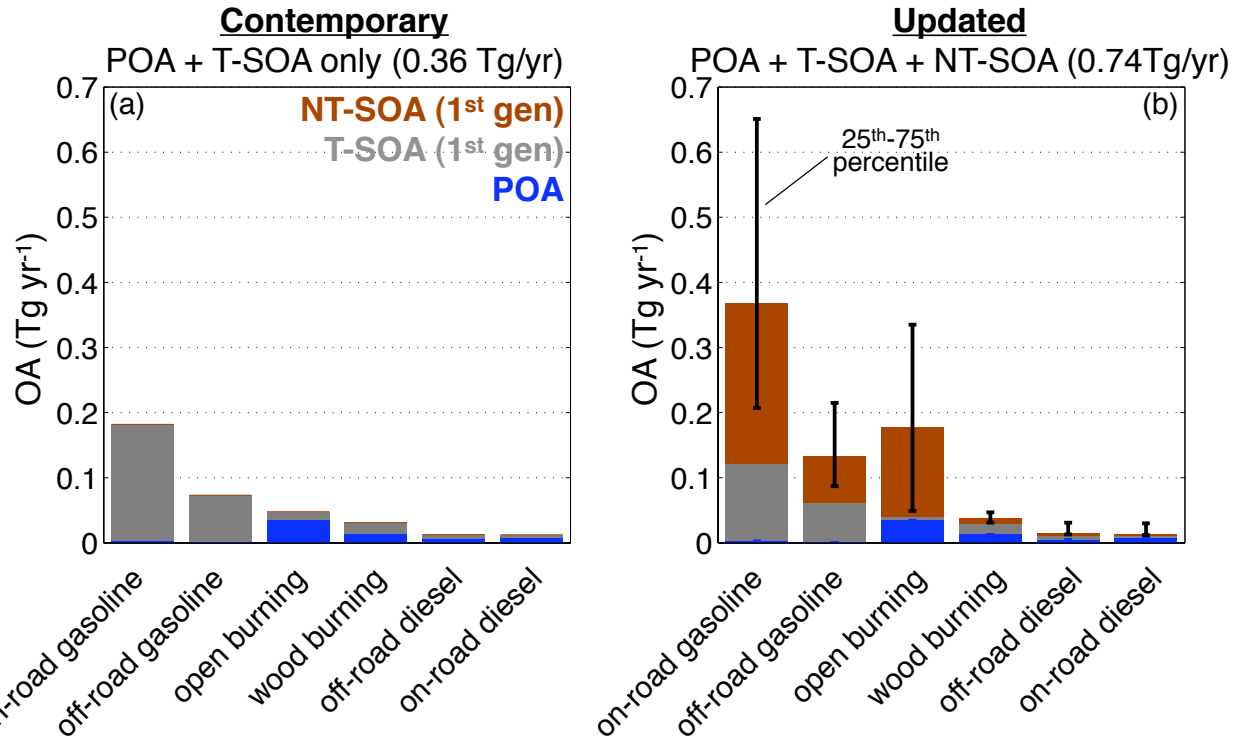

Figure 6.6: POA and first generation T-SOA and NT-SOA estimates for two model configurations for the top six combustion sources in the US.

Figure 6.6 plots the predicted OA for the two models. The updated model (with the median NT-SOA parameterization) predicts more than twice as much SOA than the contemporary model primarily because a larger fraction of the VOC emissions are now SOA

precursors. Based on Figure 6.2, one would expect that the addition of NT-SOA would triple or quadruple the net SOA formation. But the result is not as dramatic because in Figure 6.2 only directly measured and speciated VOC emissions are used to predict SOA while in Figure 6.6 the net VOC emissions remain the same between the two models; what changes is the emissions profile. So, the difference between the contemporary and updated models can be attributed to the inclusion of high yield SOA precursors (unspeciated) to the emissions profile. Based on the 25th and 75th percentile NT-SOA parameterizations, the updated model predicts a minimum SOA increase of 12% and a maximum of 325% over the contemporary model.

Across both models and amongst the sources considered, open burning is the dominant POA source and gasoline appears to be the dominant SOA source even after accounting for uncertainty. Also, SOA is a factor of 4 to 10 higher than POA, which is in-line with contemporary OA model results that have accounted for the semi-volatile and reactive nature of POA emissions (Jathar et al., 2011;Pye and Seinfeld, 2010;Shrivastava et al., 2008). Diesel emits three times as much POA than gasoline but gasoline dominates diesel in SOA by at least an order of magnitude because of the much higher VOC emissions. This is qualitatively similar to the conclusion made by Bahreini et al. (2012) for Los Angeles. The source apportionment is not very sensitive to the uncertainty in the NT-SOA parameterizations as it predicts that gasoline and open burning are the largest contributors to SOA formation in the US.

5. Summary and discussion

In this work, we analyzed SOA data from sixty nine (eighty seven for Figure 6.2) smog chamber experiments conducted on diluted emissions from four (five for Figure 6.2) types of combustion sources. First, we established that SOA is an equal or majority part of the OA

emitted and formed and varies much less than POA across the set of combustion sources studied. Second, we estimated that SOA from speciated organics (or T-SOA) explains, on average, only 8-31% of the SOA measured during the experiments. Third, we calculated that unspeciated organics had SOA yields similar to high SOA-yield species. And finally, we developed and employed a source-specific parameterization to model NT-SOA formation from combustion sources.

Although we have developed a parameterization to model NT-SOA, its implementation in CTMs is not straightforward because there are no model-ready inventories available for unspeciated emissions. We suspect that VOC or NMOG emission rates used to build inventories include unspeciated organics but are misallocated to speciated organics due to the absence of unspeciated organics in emissions profiles. Since, unspeciated emissions are much more efficient in forming SOA than all speciated emissions considered together, the inclusion of unspeciated emissions will surely increase SOA production in models. By building on the emissions characterization work done by Schauer et al. (Schauer et al., 2002a, 1999a, 2001), Carnegie Mellon and that available in the EPA SPECIATE database, we were able to build an inventory for the unspeciated emissions for six important combustion sources in the US. The inventory provides a conservative estimate of unspeciated emissions in the US because we assume that they arise only from combustion processes, the top six sources account for the bulk and NEI-supplied VOC emission rates include all NMOG emissions.

Our updated box-model predicts that the top six combustion sources produce a total of 0.68 Tg yr^{-1} of SOA. The estimate is about half to a third of the biogenic SOA production predicted by Murphy and Pandis (Murphy and Pandis, 2010) for the eastern US (1.9 Tg yr^{-1}; simulated using PMCAMx; extrapolated from summer production per day; likely to be an

overestimate of the annual values) and that predicted by Guenther et al. (1995) for the US (1.7 Tg yr^{-1}). The estimate is small when compared against the work of Murphy and Pandis (2010) that predicted a net SOA production of 5.1 Tg yr^{-1} (extrapolated from summer production per day) from all anthropogenic sources (combustion + non-combustion) over the eastern US and the work of deGouw et al. (2005) that predicted an SOA production of 2.1 Tg yr^{-1} from urban VOCs in the US. One reason the updated model estimate is significantly lower is that it does not model multigenerational oxidation. Unfortunately, the multigenerational oxidation mechanism described here (and used elsewhere) is not constrained experimentally. When we run the updated model using the multigenerational oxidation mechanism and parameters described in Section 6.3.2.1, the model predicts 1.6 Tg yr^{-1} of SOA production after one day of atmospheric processing, which is much more in line with the Murphy and Pandis (2010) and de Gouw et al. (2005) results. For gasoline, our updated model predicts 1.2 Tg yr^{-1} of SOA production after one day of atmospheric processing, which is close to the estimate of Bahreini et al. (2012) after we account for gasoline consumption in the US, i.e. 4 Tg yr^{-1} x 0.25 (fraction of global gasoline consumed by the US) ~ 1 Tg yr^{-1}. This would imply that without multi-generational oxidation, it would be hard for the smog chamber data alone to explain the measured formation (and presumably properties) of SOA in the atmosphere. However, if we run the multigenerational oxidation mechanism over a longer period the mechanism converts almost all of the first generation gas+particle mass into SOA making the SOA production more sensitive to the mechanism used to model multigenerational oxidation than the yields used to model first-generation oxidation products.

Unspeciated emissions from combustion sources are an efficient and important precursor of SOA formation in the atmosphere and we recommend that they be incorporated in future generations of SOA models.

6.6 Supplementary material

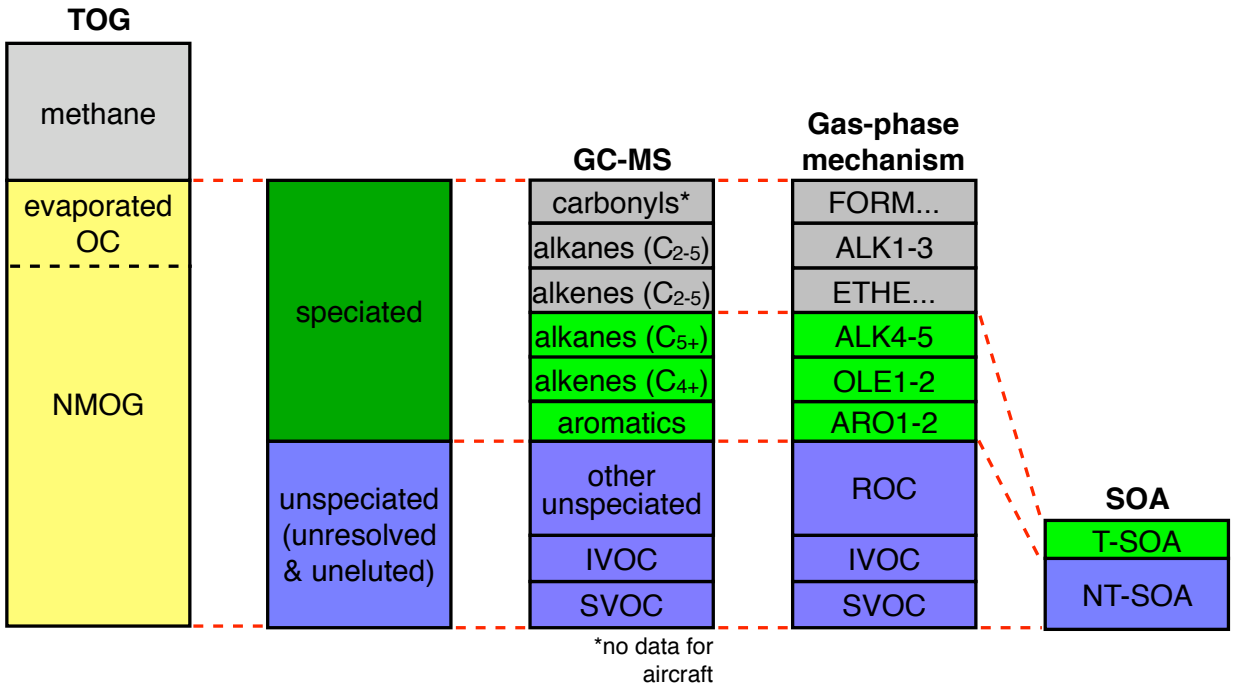

Figure S.1: Schematic showing breakdown of the total organic gas (TOG) mass emitted by a combustion source into different constituents and how those constituents are modeled in this work to form SOA.

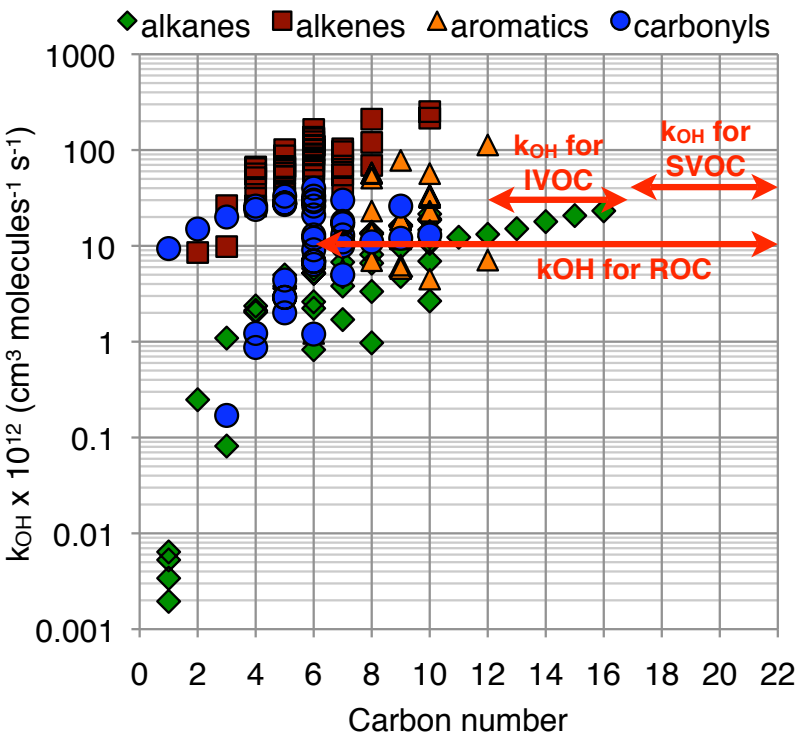

Figure S.2: OH reaction rate constants for alkanes, alkenes, aromatics and carbonyls described in Atkison and Arey (2003).

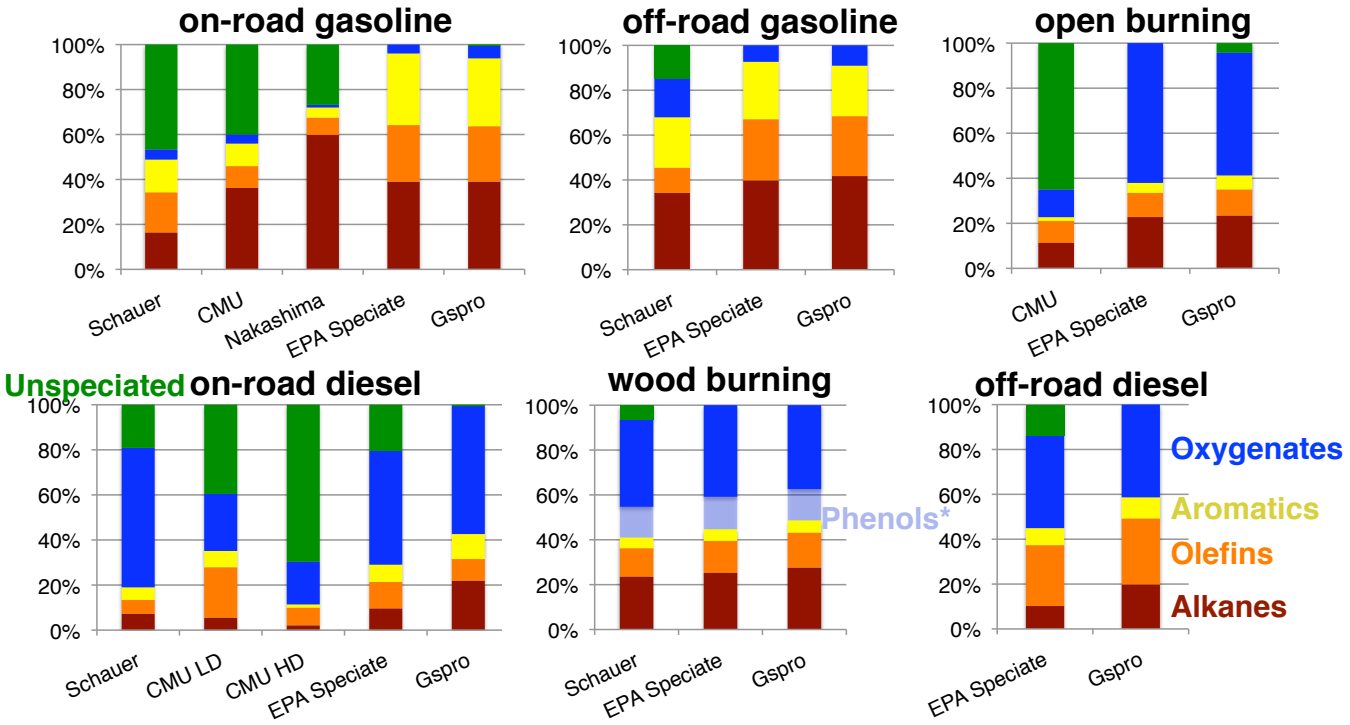

Figure S.3: Distribution of alkanes, alkenes, aromatics, oxygenates and unspeciated (calculated by difference) emissions from different combustion sources as quantified by different groups, organizations and models.

6.7 Acknowledgements

Funding was provided by the Coordinating Research Council under projects A74/E96.

6.8 References

Carlton, A. G., Bhave, P. V., Napelenok, S. L., Edney, E. O., Sarwar, G., Pinder, R. W., Pouliot, G. A., and Houyoux, M.: Model representation of secondary organic aerosol in cmaqv4. 7, Environmental Science & Technology, 44, 8553-8560, 2010.

Chan, H., Kautzman, K., Chhabra, P., Surratt, J., Chan, M., Crounse, J., Kurten, A., Wennberg, P., Flagan, R., and Seinfeld, J.: Secondary organic aerosol formation from photooxidation of naphthalene and alkylnaphthalenes: Implications for oxidation of intermediate volatility organic compounds(ivocs), Atmospheric Chemistry and Physics Discussions, 9, 1873--1905, 2009.

Donahue, N., Robinson, A., Stanier, C., and Pandis, S.: Coupled partitioning, dilution, and chemical aging of semivolatile organics, Environ. Sci. Technol, 40, 2635-2643, doi:10.1021/es052297c, 2006.

Donahue, N. M., Robinson, A. L., and Pandis, S. N.: Atmospheric organic particulate matter: From smoke to secondary organic aerosol, Atmospheric Environment, 43, 94--106, 2009.

Dzepina, K., Volkamer, R., Madronich, S., Tulet, P., Ulbrich, I., Zhang, Q., Cappa, C., Ziemann, P., and Jimenez, J.: Evaluation of recently-proposed secondary organic aerosol models for a case study in mexico city, Atmospheric Chemistry and Physics, 9, 5681-5709, doi:10.5194/acp-9-5681-2009, 2009.

EIA: Data tools and models, in, Department of Energy, 2012.

2005 national emissions inventory data & documentation: http://www.epa.gov/ttnchie1/net/2005inventory.html, 2008.

Farina, S. C., Adams, P. J., and Pandis, S. N.: Modeling global secondary organic aerosol formation and processing with the volatility basis set: Implications for anthropogenic secondary organic aerosol, Journal of Geophysical Research, 115, D09202, doi:10.1029/2009JD013046, 2010.

Fraser, M. P., Cass, G. R., Simoneit, B. R. T., and Rasmussen, R.: Air quality model evaluation data for organics. 4. C2-c36 non-aromatic hydrocarbons, Environmental Science & Technology, 31, 2356-2367, 1997.

Gordon, T. D., Nguyen, N. T., May, A. A., Presto, A. A., Lipsky, E. M., Maldonado, S., Chattopadhyay, S., Gutierrez, A., Maricq, M., and Robinson, A. L.: Secondary organic aerosol formed from light duty gasoline vehicle exhaust dominates primary particulate matter emissions, Environ. Sci. Technol, in preparation-a.

Gordon, T. D., Nguyen, N. T., Presto, A. A., Lipsky, E. M., Maldonado, S., Maricq, M., and Robinson, A. L.: Impacts of aftertreatment, fuel chemistry and driving cycle on the production of secondary organic aerosol from diesel vehicle exhaust, Environ. Sci. Technol, in preparation-b.

Grieshop, A., Donahue, N., and Robinson, A.: Laboratory investigation of photochemical oxidation of organic aerosol from wood fires 2: Analysis of aerosol mass spectrometer data, Atmospheric Chemistry and Physics, 9, 2227-2240, 2009a.

Grieshop, A. P., Logue, J. M., Donahue, N. M., and Robinson, A. L.: Laboratory investigation of photochemical oxidation of organic aerosol from wood fires 1: Measurement and simulation of organic aerosol evolution, Atmospheric Chemistry and Physics, 9, 1263-1277, 10.5194/acp-9-1263-2009, 2009b.

Hallquist, M., Wenger, J., Baltensperger, U., Rudich, Y., Simpson, D., Claeys, M., Dommen, J., Donahue, N., George, C., and Goldstein, A.: The formation, properties and impact of secondary organic aerosol: Current and emerging issues, Atmospheric Chemistry and Physics, 9, 5155-5236, 2009.

Hennigan, C., Miracolo, M., Engelhart, G., May, A., Presto, A., Lee, T., Sullivan, A., McMeeking, G., Coe, H., and Wold, C.: Chemical and physical transformations of organic aerosol from the photo-oxidation of open biomass burning emissions in an environmental chamber, Atmospheric Chemistry and Physics, 11, 7669-7686, doi:10.5194/acp-11-7669-2011 2011.

Hildebrandt, L., Donahue, N., and Pandis, S.: High formation of secondary organic aerosol from the photo-oxidation of toluene, Atmospheric Chemistry and Physics, 9, 2973-2986, doi:10.5194/acp-9-2973-2009, 2009.

IPCC, W.: Climate change 2007: The physical science basis, Summary for Policy Makers, Contribution of Working Group I to the Fourth Assessment Report of the Intergovernmental Panel on Climate Change, 2007.

Isaacman, G., Wilson, K. R., Chan, A. W. H., Worton, D. R., Kimmel, J. R., Nah, T., Hohaus, T., Gonin, M., Kroll, J. H., and Worsnop, D. R.: Improved resolution of hydrocarbon structures and constitutional isomers in complex mixtures using gas chromatography-vacuum ultraviolet-mass spectrometry (gc-vuv-ms), Analytical Chemistry, 2012.

Jathar, S., Farina, S., Robinson, A., and Adams, P.: The influence of semi-volatile and reactive primary emissions on the abundance and properties of global organic aerosol, Atmospheric Chemistry and Physics, 11, 7727-7746, doi:10.5194/acp-11-7727-2011 2011.

Jathar, S. H., Miracolo, M. A., Tkacik, D. S., Adams, P. J., and Robinson, A. L.: Secondary organic aerosol from photo-oxidation of evaporated fuel: Experimental results and implications for aerosol formation from combustion emissions, Environ. Sci. Technol, in preparation.

Jathar, S. H., Miracolo, M. A., Presto, A. A., Adams, P. J., and Robinson, A. L.: Modeling the formation and properties of traditional and non-traditional secondary organic aerosol: Problem formulation and application to aircraft exhaust, Atmospheric Chemistry & Physics Discussions, submitted.

Jimenez, J., Canagaratna, M., Donahue, N., Prevot, A., Zhang, Q., Kroll, J., DeCarlo, P., Allan, J., Coe, H., Ng, N., and others: Evolution of organic aerosols in the atmosphere, Science, 326, 1525, 2009.

McNair, H. M., Miller, J. M., and MyiLibrary: Basic gas chromatography, Wiley Online Library, 1969.

Miracolo, M., Hennigan, C., Ranjan, M., Nguyen, N., Gordon, T., Lipsky, E., Presto, A., Donahue, N., and Robinson, A.: Secondary aerosol formation from photochemical aging of aircraft exhaust in a smog chamber, Atmos. Chem. Phys, 11, 4135-4147, doi:10.5194/acp-11-4135-2011, 2011.

Miracolo, M. A., Drozd, G. T., Jathar, S. H., Presto, A. A., Lipsky, E. M., Corporan, E., and Robinson, A. L.: Fuel composition and secondary organic aerosol formation: Gas-turbine exhaust and alternative aviation fuels, Environmental Science & Technology, submitted.

Murphy, B., and Pandis, S.: Simulating the formation of semivolatile primary and secondary organic aerosol in a regional chemical transport model., Environmental science & technology, 43, 4722-4728, doi:10.1021/es803168a, 2009.

Murphy, B. N., and Pandis, S. N.: Exploring summertime organic aerosol formation in the eastern united states using a regional-scale budget approach and ambient measurements, Journal of Geophysical Research, 115, D24216, doi:10.1029/2010JD014418, 2010.

Pankow, J. F.: An absorption model of gas/particle partitioning of organic compounds in the atmosphere, Atmospheric Environment, 28, 185-188, 1994.

Presto, A. A., Miracolo, M. A., Donahue, N. M., and Robinson, A. L.: Secondary organic aerosol formation from high-no x photo-oxidation of low volatility precursors: N-alkanes, Environmental Science & Technology, 44, 2029-2034, 2010.

Pye, H., and Seinfeld, J.: A global perspective on aerosol from low-volatility organic compounds, Atmos. Chem. Phys, 10, 4377-4401, doi:10.5194/acp-10-4377-2010, 2010.

Robinson, A. L., Donahue, N. M., Shrivastava, M. K., Weitkamp, E. A., Sage, A. M., Grieshop, A. P., Lane, T. E., Pierce, J. R., and Pandis, S. N.: Rethinking organic aerosols: Semivolatile emissions and photochemical aging, Science, 315, 1259-1262, 2007.

Robinson, A. L., Grieshop, A. P., Donahue, N. M., and Hunt, S. W.: Updating the conceptual model for fine particle mass emissions from combustion systems, Journal of the Air & Waste management association, 60, 1204-1222, 2010.

Rogge, W. F., Hildemann, L. M., Mazurek, M. A., Cass, G. R., and Simoneit, B. R. T.: Sources of fine organic aerosol. 1. Charbroilers and meat cooking operations, Environmental Science & Technology, 25, 1112-1125, 1991.

Rogge, W. F., Hildemann, L. M., Mazurek, M. A., Cass, G. R., and Simoneit, B. R. T.: Sources of fine organic aerosol. 2. Noncatalyst and catalyst-equipped automobiles and heavy-duty diesel trucks, Environmental Science & Technology, 27, 636-651, 1993.

Rogge, W. F., Hildemann, L. M., Mazurek, M. A., Cass, G. R., and Simoneit, B. R. T.: Sources of fine organic aerosol. 9. Pine, oak, and synthetic log combustion in residential fireplaces, Environmental Science & Technology, 32, 13-22, 1998.

Schauer, J. J., Kleeman, M. J., Cass, G. R., and Simoneit, B. R. T.: Measurement of emissions from air pollution sources. 2. C1 through c30 organic compounds from medium duty diesel trucks, Environ. Sci. Technol, 33, 1578-1587, 1999a.

Schauer, J. J., Kleeman, M. J., Cass, G. R., and Simoneit, B. R. T.: Measurement of emissions from air pollution sources. 1. C1 through c29 organic compounds from meat charbroiling, Environmental Science & Technology, 33, 1566-1577, 1999b.

Schauer, J. J., Kleeman, M. J., Cass, G. R., and Simoneit, B. R. T.: Measurement of emissions from air pollution sources. 3. C1- c29 organic compounds from fireplace combustion of wood, Environ. Sci. Technol, 35, 1716--1728, 2001.

Schauer, J. J., Kleeman, M. J., Cass, G. R., and Simoneit, B. R. T.: Measurement of emissions from air pollution sources. 5. C1- c32 organic compounds from gasoline-powered motor vehicles, Environ. Sci. Technol, 36, 1169-1180, 2002a.

Schauer, J. J., Kleeman, M. J., Cass, G. R., and Simoneit, B. R. T.: Measurement of emissions from air pollution sources. 4. C1-c27 organic compounds from cooking with seed oils, Environmental Science & Technology, 36, 567-575, 2002b.

Shrivastava, M. K., Lane, T. E., Donahue, N. M., Pandis, S. N., and Robinson, A. L.: Effects of gas particle partitioning and aging of primary emissions on urban and regional organic aerosol concentrations, Journal of Geophysical Research-Atmospheres, 113, D18301, doi:10.1029/2007JD009735, 2008.

Simon, H., Beck, L., Bhave, P. V., Divita, F., Hsu, Y., Luecken, D., Mobley, J. D., Pouliot, G. A., Reff, A., Sarwar, G., and Strum, M.: The development and uses of epa's speciate database, Atmospheric Pollution Research, 1, 196-206, doi: 10.5094/APR.2010.026, 2010.

Tsimpidi, A., Karydis, V., Zavala, M., Lei, W., Molina, L., Ulbrich, I., Jimenez, J., and Pandis, S.: Evaluation of the volatility basis-set approach for the simulation of organic aerosol formation

in the mexico city metropolitan area, Atmos. Chem. Phys, 10, 525-546, doi:10.5194/acp-10-525-2010, 2009.

Turns, S. R.: An introduction to combustion: Concepts and applications, McGraw-hill New York, 1996.

Zhang, Q., Jimenez, J. L., Canagaratna, M. R., Allan, J. D., Coe, H., Ulbrich, I., Alfarra, M. R., Takami, A., Middlebrook, A. M., Sun, Y. L., Dzepina, K., Dunlea, E., Docherty, K., DeCarlo, P. F., Salcedo, D., Onasch, T., Jayne, J. T., Miyoshi, T., Shimono, A., Hatakeyama, S., Takegawa, N., Kondo, Y., Schneider, J., Drewnick, F., Borrmann, S., Weimer, S., Demerjian, K., Williams, P., Bower, K., Bahreini, R., Cottrell, L., Griffin, R. J., Rautiainen, J., Sun, J. Y., Zhang, Y. M., and Worsnop, D. R.: Ubiquity and dominance of oxygenated species in organic aerosols in anthropogenically-influenced northern hemisphere midlatitudes, Geophys. Res. Lett, 34, L13801, doi:10.1029/2007GL029979, 2007.

Chapter 7: Conclusions

7.1 Summary of science findings

The research presented in this thesis improves our understanding about the formation of secondary organic aerosol (SOA) from semi-volatile and intermediate-volatility organic compounds (SVOC and IVOC). Below, key results and conclusions from each chapter are summarized.

In chapter 2, a volatility-based method is used to model non-traditional SOA (NT-SOA) from SVOC/IVOC and used in a climate model to make predictions globally. Model-predictions suggested that SVOC/IVOC accounted for slightly more than half of the global organic aerosol (OA) in the atmosphere. When predictions of the POA-SOA (POA: primary organic aerosol) split and OA's surface concentrations, degree-of-oxygenation, volatility and modern carbon were compared to various measurement sets across the globe, the inclusion of SVOC/IVOC seemed to improve model performance. Further, model-predictions suggested that inventories might be under-predicting emissions from residential wood combustion in the United States. The work highlighted the need for aerosol models to incorporate NT-SOA formation from SVOC/IVOC if they were to reasonably predict the abundance and properties of aerosols.

In chapter 3, an SOA dataset of experiments run on aircraft exhaust was used to test an existing method and update it to describe NT-SOA formation from SVOC/IVOC. Speciated (traditional) precursors explained less than half of the SOA measured during the experiments. With the existing method to model NT-SOA formation (used in chapter 2), the model could not reproduce the measured SOA formation. An updated method to model NT-SOA formation was developed, which was physically more realistic in its representation and was able to fit the data better. Using the updated method, it could be concluded that SOA formation from aircraft

exhaust was (a) higher for petroleum-based than synthetically derived jet fuel and (b) higher at lower engine loads than at higher engine loads.

In chapter 4, smog chamber experiments were conducted to determine the formation and properties of SOA from photo-oxidation of evaporated fuels. The work used evaporated fuels because they are well characterized and they serve as reasonable surrogates for real combustion emissions. For a unit amount of fuel reacted, diesel formed the most SOA, followed by JP-8/Fischer-Tropsch fuel (derived from natural gas), gasoline and Fischer-Tropsch (derived from coal). Qualitatively, the trends were consistent with differences in volatility and molecular structure of these fuels. When compared against SOA data from experiments conducted on combustion emissions, the observed variability in SOA formation from combustion emissions could be partly explained by the composition of the fuel, although other variables such as engine size and type could also be influential. Using SOA data for evaporated gasoline and on-road gasoline exhaust, the work showed that in California and the United States (a) evaporative emissions accounted for less than 10% of the SOA arising from on-road gasoline vehicles despite accounting for 30-45% of the non-methane organic gas (NMOG) emissions and (b) relatively newer vehicles (LEV-I and LEV-II) accounted for three-quarters of the SOA from on-road gasoline vehicles although they only contributed a quarter to a third to the NMOG emissions.

In chapter 5, SOA data collected in chapter 4 was used to assess the ability of models to capture SOA formation as a function of the fuel constituent's volatility and molecular structure. If SVOC/IVOC-like constituents in the fuel were not included in the SOA model, the model severely under-predicted SOA formation. By including them and adjusting the lumping schemes and parameters used in the SOA model, the model-predictions were brought to within a factor of two of measurements. Further, a model based only the volatility of the fuel's constituents was as

good as an unadjusted traditional SOA model in terms of its predictions. This implied that differences in the volatility of the constituents were able to explain most of the variability observed in the SOA formation. If used, volatility-based models would be much simpler and efficient to use in modeling SOA formation in aerosol models.

In chapter 6, we used SOA data from six campaigns (sixty nine experiments) to develop source-resolved parameterizations for NT-SOA. The sources on-road gasoline, aircraft, open burning and on-road diesel were considered. For the experiments, NT-SOA accounted for three quarters of the measured SOA, which meant that NT-SOA precursors (SVOC/IVOC and other unspeciated emissions) were extremely efficient in forming SOA. Literature data suggested that combustion sources in the United States were emitting 2.61 Tg yr^{-1} of NT-SOA precursors (one-sixth of the total anthropogenic organic emissions), which were not currently included in OA models. Box-model predictions suggested that these NT-SOA precursors would be expected to double SOA production from combustion sources in the United States. The model also predicted that gasoline usage and open biomass burning would be the two largest sources of SOA in the United States.

This thesis shows that SVOC/IVOC and possibly other unspeciated organics (as described in chapter 6) emitted by combustion sources are very important precursors of SOA (chapter 2, 6) because they consistently account for a bulk of SOA production in laboratory experiments conducted on real (chapter 2,6) or surrogate (chapter 4) emissions of different combustion sources and evaporated fuels. Since they cannot be speciated using traditional techniques, it has been challenging to study them in detail and represent them in models. In the absence of speciated data, they can be reasonably represented in models either using a simple lumped approach (chapter 6) or on the basis of their volatility (chapter 2, 5). Box and global

models that have included SOA formation from SVOC/IVOC and/or other unspeciated emissions seem to predict a significant enhancement in SOA production in the atmosphere (chapter 1,6) and bring model-predictions in better agreement with measurements (chapter 1,6).

7.2 Recommendations for policy-makers

SOA formation in the atmosphere is a result of oxidation of organic emissions from both combustion- and non-combustion based, anthropogenic and natural sources. Of the four classifications, 'anthropogenic combustion sources' is the only classification that can be regulated to reduce SOA formation because anthropogenic non-combustion sources mostly emit light volatile organic compounds (VOC) that form very little SOA (Simon et al., 2010) and controlling the natural sources could lead to unintended consequences. Results from this thesis are used to offer recommendations to policy-makers interested in mitigating the adverse effects of aerosols on climate and public health.

SOA might need to be controlled to bring $PM_{2.5}$ mass levels into attainment, especially in counties like Los Angeles that are not in compliance (EPA, 2012) and where $PM_{2.5}$ is dominated by OA. The National Emissions Inventory (NEI) for 2005 estimates that 12.3 Tg yr^{-1} of NMOG emissions are emitted by anthropogenic combustion sources. In chapter 6, six amongst those accounted for a majority (70%) of the NMOG emissions and only three (on-road gasoline, off-road gasoline and open biomass burning) accounted for majority of the SOA formation. Therefore, any exercise to reduce the $PM_{2.5}$ burden at the local or regional level where it is dominated by OA would need to consider these sources as prime targets for regulation.

Recently, there has been a renewed interest within the aviation industry to assess the viability of synthetic fuels over conventional petroleum-based fuels for reasons ranging from

environmental concerns to energy security. The methods developed in chapter 3 suggest that the use of synthetically-derived Fischer Tropsch fuels in aircraft engines results in much less SOA formation than through the use of conventional JP-8 fuel. Considering that SOA accounts for the significant fraction of $PM_{2.5}$ emitted or formed from aircraft exhaust, the use of synthetic fuels could reduce the aviation industry's net impact on the environment.

On-road gasoline vehicles account for about a third of all NMOG emissions from combustion sources in the US (EPA, 2008) and therefore are an important source of SOA and $PM_{2.5}$. Newer vehicles with stricter emission standards (Low Emissions Vehicle (LEV) – I/II) make up 90% of the on-road fleet but account for slightly less than 50% of the NMOG emissions. However, their NMOG emissions are more efficient in forming SOA than those from pre-LEV vehicles, which results in their contributing to three-quarters of the SOA from on-road gasoline vehicles. So although newer vehicles emit very low NMOG (two orders of magnitude) compared to pre-LEV vehicles, the emission standard on NMOG has not ensured a corresponding reduction in SOA (one only order of magnitude).

On-road gasoline vehicles emit NMOG either as part of the exhaust from the tailpipe or from evaporative losses. Using the work in chapter 4, Gordon et al. (in preparation-a) and the EMFAC database, the average SOA production for the vehicle fleet can be inter-compared and assessed against current and future emissions standards in California. Pre-LEV, LEV-I and LEV-II vehicles would expect to produce a minimum of 65, 30 and 6 mg mi^{-1} of SOA respectively due to atmospheric oxidation of NMOG emissions. Therefore, replacing a pre-LEV vehicle with a newer LEV-II vehicle would expect to reduce the absolute SOA production by an order of magnitude and the net $PM_{2.5}$ emitted and formed by roughly the same amount. So, it is important

that benefit-cost analyses that evaluate programs to scrap, trade-in, repair or retrofit older vehicles consider the benefit associated with the large reduction in the vehicle's $PM_{2.5}$ burden.

7.3 Future work

SVOC/IVOC and other unspeciated organics account for a substantial fraction of the NMOG emissions from combustion sources and, as this thesis shows, appear to be responsible for a lot of the OA in the atmosphere. Based on our findings in this thesis, we propose a few directions for future work.

The biggest challenge currently in modeling SVOC/IVOC and other unspeciated organics is that they cannot be well characterized in terms of their mass, composition and properties using traditional instruments and techniques. Recent work at Carnegie Mellon University (Presto et al., submitted;Presto et al., 2011) and the University of California at Berkeley (Isaacman et al., 2012) have made some progress in developing the instrumentation and techniques to characterize emissions in terms of their carbon number (or volatility) and polarity (or base molecular structure). But, a much larger effort is needed if we intend to understand more about the species present in those emissions and study their reaction pathways that lead to SOA formation. It is quite likely that traditional speciation becomes impossible and therefore the emissions would need to be characterized using other gross dimensions. Based on the findings in this thesis, as a first step to building a better model, it would be useful to characterize these emissions by volatility, molecular structure (alkanes versus alkenes versus aromatics…) and degree-of-oxygenation.

In chapter 5, the thesis proposed an extended traditional SOA model and developed a volatility-based model to represent SOA formation from organic emissions. The extended SOA

model needs the entire organic-emission's mass to be speciated or at least crudely characterized by carbon number and organic class. The volatility-based model, however, only needs to know the volatility of the organic emissions, which appears to be an easier task than speciation. If the volatility of all emissions can be measured, estimated or guessed, its implementation to model SOA would be trivial. As future work, an effort needs to be made to create an emission inventory of organic emissions that is volatility-resolved, which can then be used with parameterizations in chapter 5 to model and evaluate SOA formation in chemical transport models and climate models. If found to be better, the volatility-based SOA model would be computationally cheaper and therefore an attractive substitute for future use in aerosol models.

In chapter 6, we developed source-resolved parameterizations to model NT-SOA from SVOC/IVOC and other unspeciated emissions, which were used in a simplified model. They are an improvement over those used in chapter 1, where the emissions and parameterizations were not source resolved, i.e. SVOC/IVOC from all sources were assumed to have the same potential to form SOA. Hence, chapter 6 provides us with source-resolved, model-ready parameterizations to be employed in chemical transport models and climate models to assess the influence of various combustion sources on the abundance and properties of OA.

7.4 References

2005 national emissions inventory data & documentation: http://www.epa.gov/ttnchie1/net/2005inventory.html, 2008.

EPA: Our nation's air: Status and trends through 2010, Environmental Protection Agency, 2012.

Isaacman, G., Wilson, K. R., Chan, A. W. H., Worton, D. R., Kimmel, J. R., Nah, T., Hohaus, T., Gonin, M., Kroll, J. H., and Worsnop, D. R.: Improved resolution of hydrocarbon structures and constitutional isomers in complex mixtures using gas chromatography-vacuum ultraviolet-mass spectrometry (gc-vuv-ms), Analytical Chemistry, 2012.

Presto, A. A., Nguyen, N. T., Ranjan, M., Reeder, A. J., Lipsky, E. M., Hennigan, C. J., Miracolo, M. A., Riemer, D. D., and Robinson, A. L.: Fine particle and organic vapor emissions from staged tests of an in-use aircraft engine, Atmospheric Environment, 45, 3603-3612, 2011.

Presto, A. A., Hennigan, C. J., Nguyen, N. T., and Robinson, A. L.: Determination of volatility distributions of primary organic aerosol emissions from combustion systems using thermal desorption gas chromatography mass spectrometry, Aerosol Science and Technology, submitted.

Simon, H., Beck, L., Bhave, P. V., Divita, F., Hsu, Y., Luecken, D., Mobley, J. D., Pouliot, G. A., Reff, A., Sarwar, G., and Strum, M.: The development and uses of epa's speciate database, Atmospheric Pollution Research, 1, 196-206, doi: 10.5094/APR.2010.026, 2010.